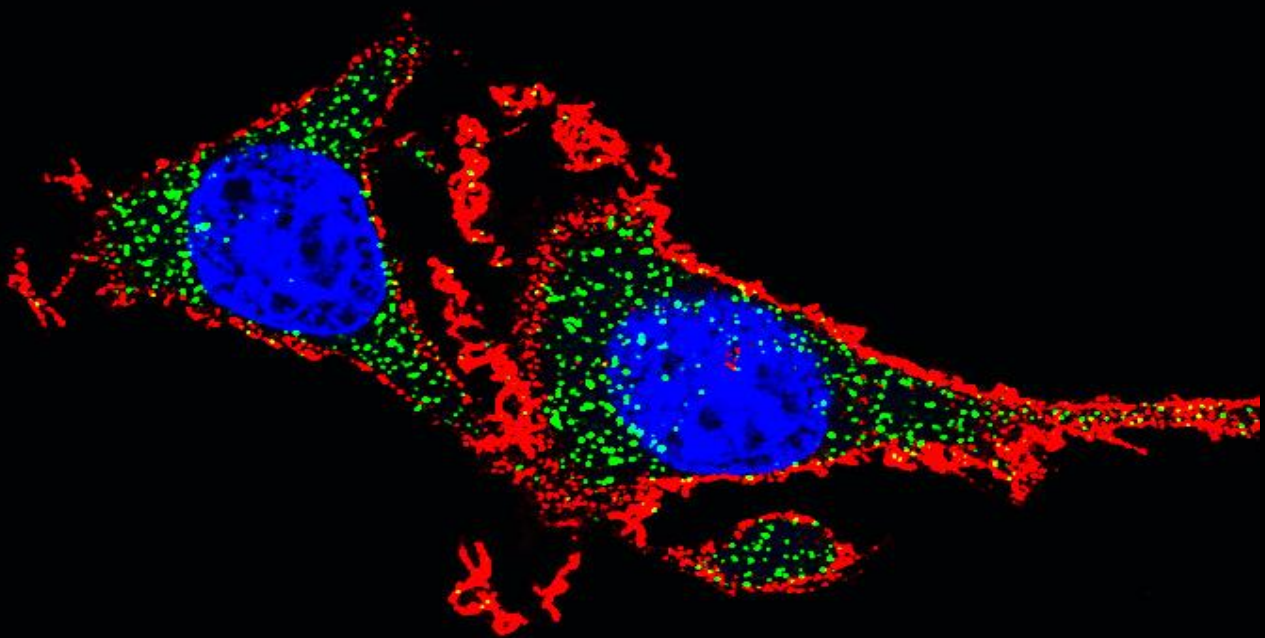




Universidad de Valladolid

The insulin-degrading enzyme:
from molecular evolution and
subcellular localization to new
roles in microglial physiology



PhD Thesis

Miriam Corraliza Gómez



Universidad de Valladolid



PhD PROGRAM IN BIOMEDICAL RESEARCH

DOCTORAL THESIS

**The insulin-degrading enzyme: from molecular
evolution and subcellular localization to new
roles in microglial physiology**

By Miriam Corraliza Gómez

To apply for PhD degree at the

University of Valladolid

Supervised by:

María Dolores Ganfornina Álvarez, PhD

Irene Cózar Castellano, PhD

Eduardo Arranz Sanz, PhD



DEFENCE AUTHORIZATION BY THE DOCTORAL THESIS SUPERVISOR

(As required by Section 7.2. of the Regulation concerning doctoral thesis defence at UVa)

TO THE CHAIRMAN OF THE DOCTORAL COMMISSION OF THE UNIVERSIDAD DE
VALLADOLID

Full name: MARIA DOLORES GANFORNINA ÁLVAREZ
ID or passport number: 28873307G
Department: BIOQUÍMICA Y BIOLOGÍA MOLECULAR Y FISIOLÓGIA.....
University or Research Institution: UNIVERSIDAD DE VALLADOLID - IBGM
Postal address: Calle SANZ Y FORÉS 3, 47003 VALLADOLID.....
E-mail opabinia@ibgm.uva.es

Full name: IRENE CÓZAR CASTELLANO.....
ID or passport number: 43799205Y
Department: BIOQUÍMICA Y BIOLOGÍA MOLECULAR Y FISIOLÓGIA.....
University or Research Institution: UNIVERSIDAD DE VALLADOLID - IBGM
Postal address: Calle SANZ Y FORÉS 3, 47003 VALLADOLID.....
E-mail irene.cozar@uva.es.....

Full name: EDUARDO ARRANZ SANZ.....
ID or passport number: 12240983S.....
Department: Pediatría, Inmunología, Ginecología-Obst., Nutrición-Brom., Psiquiatría e Hª de la
Ciencia
University or Research Institution: UNIVERSIDAD DE VALLADOLID - IBGM
Postal address: Calle Ramón y Cajal 7, 47005 VALLADOLID.....
E-mail earranz@uva.es



Universidad de Valladolid

We hereby authorize the defence of the doctoral thesis entitled THE INSULIN-DEGRADING ENZYME: FROM MOLECULAR EVOLUTION AND SUBCELLULAR LOCALIZATION TO NEW ROLES IN MICROGLIAL PHYSIOLOGY

Written by Mrs. MIRIAM CORRALIZA GÓMEZ

under our supervision, within the doctoral programme¹ DOCTORADO EN INVESTIGACIÓN BIOMÉDICA, under the modality of INTERNATIONAL DOCTOR MENTION, after taking into account the following considerations²:

The candidate has fulfilled all the requirements and the level of training necessary to aspire to the Doctor's Degree with International Mention by the University of Valladolid, by performing an original research project. She has significantly contributed to the design of the scientific questions to be solved, framed at the interface of several disciplines, has designed, executed and analysed the experiments, and has performed data presentations in different formats (writing published work and presenting at scientific meetings), contributing to the dissemination of her results to the scientific community.

The three supervisors listed above³

Declare that they fulfil the requirements to be able to direct doctoral theses as established in the Royal Decree RD 99/2011 (modified by the Royal Decree RD 195/2016) and the Agreement of the Directors' Committee of the Doctoral School of the University of Valladolid of February 17th, 2014, that is, that they possess at least a recognized period of research activity in accordance with the provisions set out in the Royal Decree RD 1086/1989 of August 28th⁴.

Place and date: Valladolid, 2 October, 2021.

GANFORNINA ALVAREZ MARIA DOLORES - 28873307G
Firmado digitalmente por GANFORNINA ALVAREZ MARIA DOLORES - 28873307G
Nombre de reconocimiento (DN): c=ES, serialNumber=IDCES-28873307G, givenName=MARIA DOLORES, sn=GANFORNINA ALVAREZ MARIA DOLORES - 28873307G
Fecha: 2021.10.02 10:25:22 +02'00'

María D Ganfornina Álvarez

COZAR CASTELLANO IRENE - 43799205Y
Firmado digitalmente por COZAR CASTELLANO IRENE - 43799205Y
Nombre de reconocimiento (DN): c=ES, serialNumber=IDCES-43799205Y, givenName=IRENE, sn=COZAR CASTELLANO IRENE - 43799205Y
Fecha: 2021.10.03 12:37:03 +02'00'

Irene Cózar Castellano

ARRANZ SANZ EDUARDO - DNI 12240983S
Firmado digitalmente por ARRANZ SANZ EDUARDO - DNI 12240983S
Nombre de reconocimiento (DN): c=ES, ou=UNIVERSIDAD DE VALLADOLID, ou=CERTIFICADO ELECTRONICO DE EMPLEADO PUBLICO, serialNumber=IDCES-12240983S, sn=ARRANZ SANZ EDUARDO, cn=ARRANZ SANZ EDUARDO - DNI 12240983S
Fecha: 2021.10.04 08:49:12 +02'00'

Eduardo Arranz Sanz

¹ Name of the doctoral programme in which the student is registered at the Universidad de Valladolid (you may cut and paste it in Spanish).

² Please briefly summarize the reasons that lead you to consider that the thesis is suitable for defence.

³ The document can be modified if there is more than one supervisor.

⁴ Should the contractual figure not be evaluable by periods of research activity or if the professor were from a foreign university, the Academic Commission of the Doctoral Programme should be provided with a CV or other supporting document to prove that she/he possesses the merits equivalent to one period of research activity.

This thesis has been carried out under the supervision of Prof. Maria Dolores Ganfornina Álvarez, Dr. Irene Cózar Castellano and Prof. Eduardo Arranz Sanz at the Instituto de Biología y Genética Molecular (Universidad de Valladolid-CSIC), Valladolid. It has been possible thanks to the following funding:

- Mechanism of action of lipoproteins on cell membrane homeostasis and repair: therapeutic targets for neurodegenerative diseases (PID-2019-110911-RB-I00). Ministerio de Economía y Competitividad/FEDER.
- Role of the insulin degrading enzyme in microglial behavior during Alzheimer's disease in the context of type 2 diabetes mellitus (VA086G18). Consejería de Educación, Junta de Castilla y León.
- Role of the insulin degrading enzyme (IDE) in hyperglucagonemia (SAF2016-77871-C2-1-R). Ministerio de Economía y Competitividad/FEDER.
- Role of lipoproteins in cell membrane homeostasis: target therapies for neurodegenerative and demyelinating diseases (BF2015-68149-R). Ministerio de Economía y Competitividad/FEDER.

Some of the original results exposed in this Thesis have been compiled in the following scientific publications:

- **Corraliza-Gómez M**, Gallardo AB, Díaz-Marrero AR, de la Rosa JM, D'Croz L, Darias J, Arranz E, Cózar-Castellano I, Ganfornina MD, Cueto M. Modulation of Glial Responses by Furanocembranolides: Leptolide Diminishes Microglial Inflammation in Vitro and Ameliorates Gliosis In Vivo in a Mouse Model of Obesity and Insulin Resistance. (2020) *Marine Drugs*. 22;18(8):378. Doi: 10.1016/j.nbd.2020.105046.
- **Corraliza-Gomez M**, Lillo C, Cozar-Castellano I, Arranz E, Sanchez D, Ganfornina MD. Evolutionary origin of Insulin-Degrading Enzyme and its subcellular localization and secretion mechanism: A study in microglial cells. *Submitted to Cells*.

Additionally, within the framework of this Thesis, results were obtained for other projects that have resulted in the participation of the doctoral student in the following publications:

- Pascua-Maestro R, **Corraliza-Gomez M**, Diez-Hermano S, Perez-Segurado C, Ganfornina MD, Sanchez D. The MTT-formazan assay: Complementary technical approaches and in vivo validation in *Drosophila* larvae. (2018) *Acta Histochemica*. Doi: 10.1016/j.acthis.2018.01.006.
- **Corraliza-Gomez M**, Sanchez D, Ganfornina MD. Lipid-Binding Proteins in Brain Health and Disease. (2019) *Frontiers in Neurology*. Doi: 10.3389/fneur.2019.01152.

- Pascua-Maestro R, **Corraliza-Gomez M**, Fadrique-Rojo C, Ledesma MD, Schuchman EH, Sanchez D, Ganfornina MD. Apolipoprotein D-mediated preservation of lysosomal function promotes cell survival and delays motor impairment in Niemann-Pick type A disease. *Neurobiology of Disease*. (2020) Doi: 10.1016/j.nbd.2020.105046.
- **Corraliza-Gomez M***, del Caño-Espinel M*, Sanchez D, Ganfornina MD. The neuroprotective lipocalin Apolipoprotein D stably interacts with specific subtypes of detergent-resistant membrane domains in a Basigin-independent manner. *Submitted*.

Communications have also been presented at the following conferences:

- **Corraliza-Gomez, M**; Sanchez, D; Arranz, E; Cózar-Castellano, I; Ganfornina, MD. Role of insulin degrading enzyme (IDE) in microglial cells challenged with pathological conditions at the confluence of Alzheimer's disease and type 2 diabetes. XIV European Meeting on Glial Cells in Health and Disease. Porto 2019. Poster.
- **Corraliza-Gomez, M**; Sanchez, D; Arranz, E; Cózar-Castellano, I; Ganfornina, MD. Role of insulin degrading enzyme (IDE) in microglial cells at the confluence of Alzheimer's disease (AD) and type 2 diabetes (T2D). X Meeting of the Spanish Glial Network. Santiago de Compostela 2019. Oral communication.
- **Corraliza-Gomez, M**; Sanchez, D; Arranz, E; Cózar-Castellano, I; Ganfornina, MD. Role of insulin degrading enzyme (IDE) in microglial cells at the confluence of Alzheimer's disease (AD) and type 2 diabetes (T2D). 18th Meeting of the Spanish Society of Neuroscience. Santiago de Compostela 2019. Poster.
- **Corraliza-Gomez, M**; Bermejo, T; Rodriguez-Iglesias, N; Valero, J; Sanchez, D; Arranz, E; Cozar-Castellano, I; Ganfornina, MD. In vivo and in vitro studies reveal a sex-specific role for the insulin-degrading enzyme (IDE) in memory tasks and in microglial cells. 19th Meeting of the Spanish Society of Neuroscience. Lleida 2021. Poster.

TABLE OF CONTENTS

ABBREVIATIONS	VII
ABSTRACT	XIII
SUMMARY	XV
RESUMEN	XVII
GRAPHICAL ABSTRACT	XIX
INTRODUCTION	1
1. ALZHEIMER'S DISEASE	3
1.1. A β : A KEY MOLECULE IN AD	4
1.2. THE HALLMARKS OF ALZHEIMER'S DISEASE.....	7
2. MICROGLIA	12
2.1 MICROGLIA ONTOGENY: A UNIQUE CELL POPULATION	12
2.2. FACTORS THAT PROMOTE MICROGLIA DEVELOPMENT AND HOMEOSTASIS	13
2.3. MICROGLIAL ACTIVATION STATES	13
2.4. HOMEOSTATIC MICROGLIAL FUNCTIONS.....	15
2.5. MICROGLIAL DYSFUNCTION IN AD	23
3. DIABETES MELLITUS	23
3.1. INSULIN DEREGULATION IN PRE-DIABETES AND T2DM.....	24
3.2. INSULIN SIGNALING.....	25
4. INSULIN-DEGRADING ENZYME	26
4.1. MOLECULAR CHARACTERISTICS OF IDE	27
4.2. IDE FUNCTIONS.....	28
4.3. SUBCELLULAR LOCALIZATION OF IDE.....	29
4.4. GENETIC LINKAGE OF <i>IDE</i> WITH DISEASE	30
5. "TYPE 3 DIABETES"	30
5.1. EVIDENCE LINKING ALZHEIMER'S DISEASE AND DIABETES	31
5.2. TRANSPORT OF GLUCOSE AND INSULIN INTO THE BRAIN	31
5.3. IDE AS CANDIDATE PATHOPHYSIOLOGICAL LINK BETWEEN AD AND DM.....	32
5.4. CANDIDATE DRUGS TO SIMULTANEOUSLY TREAT AD AND DM	32
HYPOTHESIS AND OBJECTIVES	37
MATERIALS AND METHODS	41
1. EXPERIMENTAL ANIMALS	43
2. CELL CULTURES.....	50
3. MTT ASSAYS	56
4. RNA ISOLATION, cDNA SYNTHESIS AND RT-QPCR.....	57
5. POLYACRYLAMIDE GEL ELECTROPHORESIS AND IMMUNOBLOTTING	60

6. LUMINEX AND ELISA ASSAYS FROM PRIMARY MICROGLIAL CULTURE SUPERNATANTS	62
7. AMYLOID β_{1-42} ($A\beta_{1-42}$) OLIGOMERS PREPARATION	64
8. IMMUNOCYTOCHEMISTRY	66
9. ELECTRON MICROSCOPY	68
10. IMMUNOHISTOCHEMISTRY	68
11. BIOCHEMICAL MEMBRANE PREPARATIONS	69
12. EXTRACELLULAR VESICLES ISOLATION	72
13. MYELIN PREPARATIONS	72
14. FLOW CYTOMETRY	73
15. BIOINFORMATIC ANALYSES.....	75
16. RNA SEQUENCING (RNA-SEQ).....	77
17. STATISTICAL ANALYSES	78
18. REAGENTS AND RESOURCES.....	79

RESULTS **83**

CHAPTER 1. EFFECTS OF DM- AND AD-RELATED STIMULI ON MICROGLIAL FUNCTIONS AND REGULATION OF IDE EXPRESSION IN A CELL-LINE PARADIGM **85**

1.1. CHRONIC HIGH D-GLUCOSE STIMULATES METABOLIC ACTIVITY SPECIFICALLY ON MICROGLIAL CELLS	85
1.2. CHRONIC HIGH D-GLUCOSE AND OSMOLARITY POLARIZE MICROGLIAL CELLS TOWARDS A MILD PRO-INFLAMMATORY PHENOTYPE	86
1.3. CHRONIC HIGH D-GLUCOSE INDUCES CHANGES IN MICROGLIAL GLYCOCALYX.....	87
1.4. IDE EXPRESSION IS NOT REGULATED BY CHRONIC HIGH D-GLUCOSE	88
1.5. IDE EXPRESSION IS DIFFERENTIALLY REGULATED IN MICROGLIA AND MACROPHAGES, AND CHANGES ALONG WITH THE POLARIZATION STATE	89
1.6. D-GLUCOSE COMBINED WITH $A\beta$ OLIGOMERS REGULATES IDE INTRACELLULAR AND EXTRACELLULAR DISTRIBUTION	92

CHAPTER 2. IDE MOLECULAR EVOLUTION AND SUBCELLULAR LOCALIZATION AND TRAFFIC IN MICROGLIAL CELLS..... **95**

2.1. MOLECULAR PHYLOGENY ON CLAN ME METALLOPEPTIDASES	95
2.2. IDE EVOLUTION AND MOLECULAR PHYLOGENY: FROM <i>ARCHAEA</i> TO <i>EUKARYA</i>	96
2.3. BIOINFORMATIC PREDICTIONS OF SIGNAL PEPTIDE ON IDE'S HOMOLOGOUS PROTEINS REVEAL A SHIFT IN EXPORTATION BETWEEN PROKARYOTES AND EUKARYOTES.....	99
2.4. BIOINFORMATIC SUBCELLULAR LOCALIZATION PREDICTION INDICATES THAT IDE IS PRIMARILY CYTOSOLIC IN ALL KINGDOMS	100
2.5. IDE IS MAINLY CYTOSOLIC, BUT IT ALSO ASSOCIATES TO MEMBRANES IN GLIAL CELLS	102
2.6. IDE INTERACTS WITH PARTICULAR LIPID RAFTS IN MICROGLIAL CELLS	103
2.7. IDE ASSOCIATES TO MICROGLIAL MEMBRANES BY THEIR CYTOSOLIC SIDE.....	104
2.8. IDE IS FOUND IN MULTIVESICULAR BODIES AND THEIR MICROVESICLES IN SECRETORY STATE MICROGLIA	105
2.9. IDE EXPORTATION IN EXTRACELLULAR VESICLES IS REGULATED BY THE ACTIVATION STATE OF MICROGLIAL CELLS.....	107

CHAPTER 3. ROLE OF IDE <i>IN VIVO</i> IN A CONSTITUTIVE KNOCK-OUT MOUSE PARADIGM	109
3.1. PROGENY PRODUCED BY <i>IDE</i> HETEROZYGOUS BREEDING DOES NOT FOLLOW MENDELIAN INHERITANCE	109
3.2. <i>IDE</i> GENE DOSE GENERATES SUBTLE EFFECTS IN METABOLIC PARAMETERS OF 12-MONTH-OLD MICE	110
3.3. BEHAVIORAL ANALYSES REVEAL SEX- AND GENOTYPE-DEPENDENT EFFECTS OF <i>IDE</i> DEFICIENCY ON BEHAVIORAL AND MEMORY TASKS	111
3.4. EXPRESSION OF <i>IDE</i> , INSULIN RECEPTOR, AND <i>AKT1</i> ARE SEX-DEPENDENT IN THE OLFACTORY BULB, AN INSULIN SIGNALING HIGH-EXPRESSION SITE IN THE BRAIN	115
3.5. GLIOSIS MARKERS <i>CD11b</i> AND <i>GFAP</i> , GLIAL-DERIVED NEUROPROTECTOR <i>ApoD</i> , AND <i>Aβ</i> OLIGOMERS, ALSO SHOW SEX-DEPENDENT CHANGES	118
3.6. MULTIVARIATE ANALYSIS HELPS TO VISUALIZE <i>IDE</i> -DEPENDENT EFFECTS ON BRAIN-RELATED VARIABLES	120
CHAPTER 4. ROLE OF IDE SPECIFICALLY IN PRIMARY MICROGLIAL CELLS	127
4.1. <i>IDE</i> ABSENCE SLIGHTLY AFFECTS MICROGLIAL CELL VIABILITY	127
4.2. <i>IDE</i> -KO MICROGLIAL CELLS PROLIFERATE LESS AND PRESENT A DELAYED RESPONSE TO THE CYTOKINE <i>M-CSF</i>	128
4.3. <i>IDE</i> DOES NOT REGULATE INSULIN SIGNALING IN MICROGLIAL CELLS	129
4.4. MICROGLIAL POLARIZATION IS ALTERED IN THE ABSENCE OF <i>IDE</i>	130
4.5. MYELIN PHAGOCYTOSIS BY MICROGLIAL CELLS SHOWS SEX- AND <i>IDE</i> -DEPENDENT EFFECTS, WHILE MYELIN DEGRADATION REMAINS UNALTERED	134
4.6. LACK OF <i>IDE</i> ALTERS <i>Aβ</i> OLIGOMER INTERNALIZATION DYNAMICS AND IMPAIRS <i>Aβ</i> OLIGOMER DEGRADATION IN MALE MICROGLIA	135
4.7. TRANSCRIPTOMIC ANALYSES REVEAL THAT ABSENCE OF <i>IDE</i> ALTERS PATHWAYS SUCH AS RESPONSE TO CYTOKINES, IMMUNE SYSTEM PROCESSES AND REGULATION OF RESPONSE TO STRESS	137
CHAPTER 5. NOVEL THERAPEUTICS FOR NEURODEGENERATIVE PROCESSES: MODULATION OF GLIAL RESPONSES BY FURANOCEMBRANOLIDES	141
5.1. <i>IN VITRO</i> SCREENING OF FURANOCEMBRANOLIDES WITH ANTI-INFLAMMATORY PROPERTIES ON MICROGLIAL CELLS	141
5.2. LEPTOLIDE TREATMENT <i>IN VIVO</i> AMELIORATES MICROGLIOSIS IN A MOUSE MODEL OF OBESITY AND INSULIN RESISTANCE	144
5.3. LEPTOLIDE TREATMENT <i>IN VIVO</i> ALSO REDUCES ASTROGLIOSIS	145
DISCUSSION	147
CONCLUSIONS	161
REFERENCES	165
ANNEX	197
ACKNOWLEDGEMENTS	209
NOTES	213

LIST OF FIGURES

FIGURE 1. PREVALENCE AND WORLDWIDE DISTRIBUTION OF DEMENTIA CASES IN 2015 AND ESTIMATED GROWTH BY 2050.	3
FIGURE 2. ALTERNATIVE PROTEOLYTIC PROCESSING OF APP.	5
FIGURE 3. THE HALLMARKS OF ALZHEIMER'S DISEASE.	7
FIGURE 4. INFLAMMATORY RESPONSE IN ALZHEIMER'S DISEASE.	9
FIGURE 5. EVOLUTION OF THE CONCEPT OF MICROGLIAL ACTIVATION PHENOTYPES.	15
FIGURE 6. MICROGLIAL KEY FUNCTIONS.	16
FIGURE 7. A β MANAGING BY MICROGLIAL CELLS.	23
FIGURE 8. PREVALENCE AND WORLDWIDE DISTRIBUTION OF DIABETES IN 2019 AND ESTIMATED PREVALENCE FOR THE YEARS 2030 AND 2045.	24
FIGURE 9. PATHOGENESIS OF TYPE 2 DIABETES.	25
FIGURE 10. CRITICAL NODES IN THE INSULIN-SIGNALING NETWORK.	26
FIGURE 11. STRUCTURE AND FUNCTIONAL MECHANISM OF IDE.	28
FIGURE 12. CHEMICAL STRUCTURES OF NOVEL FURANOCEMBRANOLIDES (1-6) AND LEPTOLIDE.	34
FIGURE 13. GENETIC MAP OF MUTANT IDE-KO ALLELE.	43
FIGURE 14. GENOTYPING OF MICE FROM THE IDE-NULL COHORT.	45
FIGURE 15. EXPERIMENTAL PARADIGM FOR METABOLIC, BEHAVIORAL AND MOLECULAR BIOLOGY STUDIES.	45
FIGURE 16. BEHAVIORAL TESTS PROTOCOL.	47
FIGURE 17. PROLIFERATION KINETICS IN BV-2 CELL LINE.	51
FIGURE 18. PROTOCOL TO PREPARE PRIMARY MICROGLIAL CULTURES.	53
FIGURE 19. PRINCIPLE OF THE EdU 'CLICK' REACTION.	55
FIGURE 20. RNA QUANTIFICATION AND QUALITY ASSESSMENT.	57
FIGURE 21. LUMINEX ASSAY PRINCIPLE.	63
FIGURE 22. PROTOCOL TO PREPARE A β OLIGOMERS.	65
FIGURE 23. PROTEIN QUANTIFICATION IN MEMBRANE PREPARATION SAMPLES.	70
FIGURE 24. PRINCIPLE OF THE LIVE/DEAD™ FIXABLE DEAD CELL STAIN KITS.	73
FIGURE 25. TECHNIQUE TO QUENCH THE FLUORESCENCE OF EXTRACELLULAR, MICROGLIAL-ATTACHED, FAM-AB OLIGOMERS.	75
FIGURE 26. TRANSCRIPTOME ANALYSIS PIPELINE.	78
FIGURE 27. METABOLIC ACTIVITY PER CELL IN MICROGLIAL AND MACROPHAGES CELL LINES EXPOSED TO DIFFERENT D-GLUCOSE CONCENTRATIONS FOR 72 HOURS.	86
FIGURE 28. PRO-INFLAMMATORY RESPONSE IN MICROGLIA AND MACROPHAGES EXPOSED TO DIFFERENT D-GLUCOSE CONCENTRATIONS FOR 72 HOURS.	87
FIGURE 29. HYPERSIALYLATION OF MICROGLIAL CELLS CHRONICALLY EXPOSED TO HIGH D-GLUCOSE CONCENTRATIONS.	88
FIGURE 30. IDE PROTEIN EXPRESSION IN BV-2 AND RAW264.7 CELLS EXPOSED TO DIFFERENT D-GLUCOSE CONCENTRATIONS FOR 72 HOURS.	89
FIGURE 31. CELL VIABILITY ASSAYS IN BV-2 TO SELECT THE DOSE FOR EACH STIMULUS.	89
FIGURE 32. LPS-INDUCED PRO-INFLAMMATORY POLARIZATION OF MICROGLIA AND MACROPHAGES AND EFFECTS ON IDE mRNA AND PROTEIN EXPRESSION.	90
FIGURE 33. IL-4+IL-13-INDUCED ANTI-INFLAMMATORY POLARIZATION OF MICROGLIA AND MACROPHAGES AND EFFECTS ON IDE mRNA AND PROTEIN EXPRESSION.	91
FIGURE 34. IDE PROTEIN EXPRESSION IN MICROGLIA AND MACROPHAGES UPON PQ-INDUCED OXIDATIVE STRESS.	92
FIGURE 35. TIME-COURSE OF IDE DISTRIBUTION AFTER AMYLOID- β OLIGOMERS TREATMENT.	93

FIGURE 36. PHYLOGENETIC ANALYSIS OF CLAN ME METALLOPEPTIDASES.....	96
FIGURE 37. GLOBAL PHYLOGENY OF IDE-LIKE PROTEINS.	98
FIGURE 38. EVOLUTION TIMESCALE AND IDE PHYLOGENY.	99
FIGURE 39. SIGNAL PEPTIDE PREDICTIONS IN PROKARYOTIC AND EUKARYOTIC SEQUENCES.	100
FIGURE 40. SUBCELLULAR LOCALIZATION PREDICTIONS FOR IDE-LIKE EUKARYOTIC PROTEINS.....	101
FIGURE 41. IDE IS STABLY ASSOCIATED TO MEMBRANES OF GLIAL CELLS.	102
FIGURE 42. IDE IS ASSOCIATED TO MEMBRANE MICRODOMAINS WITH SPECIFIC PROPERTIES IN THE MICROGLIAL CELL LINE BV-2.....	103
FIGURE 43. IDE ASSOCIATES TO MEMBRANES ONLY AT THE CYTOPLASMATIC SIDE.....	104
FIGURE 44. IMMUNOELECTRON MICROSCOPY MICROGRAPHS OF THE SUBCELLULAR LOCALIZATION OF IDE IN BV-2 MICROGLIAL CELLS.	106
FIGURE 45. EXTRACELLULAR IDE PROTEIN FROM PRIMARY MICROGLIAL CULTURES EXPOSED TO DIFFERENT STIMULI.....	107
FIGURE 46. IMMUNOBLOT ANALYSES OF IDE, CD81 AND ACTIN IN EXTRACELLULAR VESICLES PREPARATIONS.....	108
FIGURE 47. PROGENY RESULTANT FROM IDE HETEROZYGOUS BREEDING.	109
FIGURE 48. BODY WEIGHT OF WT, IDE-HET AND IDE-KO MICE AT 12 MONTHS.....	110
FIGURE 49. BLOOD GLUCOSE AND PLASMA INSULIN LEVELS AFTER SIX HOURS FASTING.	111
FIGURE 50. OPEN FIELD RESULTS.	112
FIGURE 51. OBJECT RECOGNITION TESTS RESULTS.	114
FIGURE 52. IMMUNOBLOTS OF INSULIN SIGNALING IN THE BRAIN.	116
FIGURE 53. RESULTS FROM IMMUNOBLOTS OF INSULIN SIGNALING-RELATED PROTEINS.	117
FIGURE 54. RESULTS FROM IMMUNOBLOTS OF “INFLAMMAGING” MARKERS.	119
FIGURE 55. CORRELATION PLOT WITH ALL THE VARIABLES ANALYZED IN THE 12-MONTH-OLD MICE COHORT.	121
FIGURE 56. PRINCIPAL COMPONENT ANALYSIS ON THE IDE-NULL COHORT.....	122
FIGURE 57. PRINCIPAL COMPONENT ANALYSES OF THE IDE-NULL COHORT, SEPARATED BY SEX.....	123
FIGURE 58. MULTINOMIAL LOGISTIC REGRESSION MODEL RESULTS.....	125
FIGURE 59. COMPARISON OF CELL VIABILITY IN WT AND IDE-KO PRIMARY MICROGLIA UPON DIFFERENT STRESSFUL STIMULI.	128
FIGURE 60. QUANTIFICATION OF CELL PROLIFERATION IN WT AND IDE-KO PRIMARY MICROGLIA BY EdU ASSAY.	129
FIGURE 61. COMPARISON OF INSULIN SIGNALING IN WT VS IDE-KO MICROGLIA.	130
FIGURE 62. HEATMAP SHOWING THE RESULTS OF THE CYTOKINE PROFILING.....	132
FIGURE 63. CYTOKINE PROFILES SEPARATED INTO PRO-/ANTI-INFLAMMATORY TREATMENTS AND OXIDATIVE AND AMYLOID STRESSES.	133
FIGURE 64. MYELIN-DII PHAGOCYTOSIS AND DEGRADATION IN WT AND IDE-KO MICROGLIA.....	135
FIGURE 65. FAM-A β OLIGOMERS INTERNALIZATION IN WT AND IDE-KO MICROGLIA.	136
FIGURE 66. FAM-A β OLIGOMERS DEGRADATION IN WT AND IDE-KO MICROGLIA.....	137
FIGURE 67. TRANSCRIPTOMIC PROFILING OF WT AND IDE-KO MICROGLIA.	138
FIGURE 68. GENE ENRICHMENT ANALYSIS ON DIFFERENTIALLY EXPRESSED GENES BETWEEN WT AND IDE- KO MICROGLIA.....	139
FIGURE 69. FURANOCEMBRANOLIDE TREATMENTS AND EFFECTS ON BV-2 VIABILITY.	142
FIGURE 70. EXPRESSION OF IL-1 β mRNA IN VITRO AFTER LPS STIMULATION AND/OR FURANOCEMBRANOLIDE TREATMENT.	143
FIGURE 71. LEPTOLIDE TREATMENT AMELIORATES MICROGLIOSIS TRIGGERED BY HFD.	144
FIGURE 72. LEPTOLIDE TREATMENT AMELIORATES ASTROGLIOSIS TRIGGERED BY HFD.	145

LIST OF TABLES

TABLE 1. PRIMER SEQUENCES USED FOR IDE-KO MICE GENOTYPING.....	44
TABLE 2. COMPOSITION OF DISSECTION AND DIGESTION MEDIA USED IN PRIMARY GLIAL CULTURES.....	52
TABLE 3. REACTION MIX FOR RT-PCR.....	58
TABLE 4. RT-QPCR PROGRAM.....	58
TABLE 5. GENES ANALYZED BY RT-QPCR.....	59
TABLE 6. PRIMARY ANTIBODIES FOR IMMUNOBLOTTING.....	61
TABLE 7. SECONDARY ANTIBODIES FOR IMMUNOBLOTTING.....	61
TABLE 8. PRIMARY ANTIBODIES USED IN IMMUNOCYTOCHEMISTRY.....	67
TABLE 9. SECONDARY ANTIBODIES USED IN IMMUNOCYTOCHEMISTRY.....	67
TABLE 10. REAGENTS AND RESOURCES USED DURING THIS THESIS.....	79
TABLE 11. CLAN ME METALLOPEPTIDASES.....	95
TABLE 12. SUMMARY OF THE DATABASE OF IDE HOMOLOGS.....	97
TABLE 13. OLT AND NORT RESULTS ANALYZED BY CATEGORICAL VARIABLES.....	115
TABLE 14. MULTINOMIAL LOGISTIC REGRESSION MODEL.....	124
TABLE 15. CYTOKINE PROFILING IN WT AND IDE-KO PRIMARY MICROGLIA SUBJECTED TO DIFFERENT STIMULI.....	131
TABLE A1. SEQUENCES USED FOR GLOBAL IDE PHYLOGENY.....	199
TABLE A2. GENES UPREGULATED IN IDE-KO MICROGLIA VS WT MICROGLIA.....	202
TABLE A3. GENES DOWNREGULATED IN IDE-KO MICROGLIA VS WT MICROGLIA.....	206

ABBREVIATIONS

%	Percentage
a.m.	<i>Ante meridiem</i> (before midday)
a.u.	Arbitrary units
AD	Alzheimer's disease
AGEs	Advanced glycation end products
AIC	Akaike Information Criterion
AICD	APP intracellular domain
ANOVA	Analysis of variance
ApoD	Apolipoprotein D
ApoE	Apolipoprotein E
ApoE-ε4	Apolipoprotein E epsilon 4 allele
APP	Amyloid precursor protein
Arg-1	Arginase 1
ATCC	American Type Culture Collection
ATP	Adenosine triphosphate
Aβ	Amyloid-β
BBB	Blood-brain barrier
BIC	Bayesian inference criterion
BLAST	Basic Local Alignment Search Tool
BLOSUM	Blocks of amino acid substitution matrix
BP	Band pass filter
bp	Base pairs
BSA	Bovine serum albumin
CCD	Charged-coupled device
CCL	Chemokine ligand
CCR	Chemokine receptor
CD	Cluster of differentiation
cDNA	Complementary deoxyribonucleic acid
cm	Centimeter
CNS	Central nervous system
COX-2	Cyclooxygenase-2
CSF	Cerebrospinal fluid
CSF1R	Colony-stimulating factor 1 receptor
Ct	Threshold cycle
CTF	C-terminal fragment
DAPI	4',6-diamino-2-phenylindol
DEGs	Differentially expressed genes
DiI	1,1'-Dioctadecyl-3,3,3',3'-Tetramethylindocarbocyanine perchlorate
DIV	Days <i>in vitro</i>
DM	Diabetes mellitus
DMEM	Dulbecco's Modified Eagle's Medium
DMSO	Dimethyl sulfoxide
DNA	Deoxyribonucleic acid
DNase I	Deoxyribonuclease I
DRM	Detergent-resistant membrane
DTT	Dithiothreitol
EBSS	Earle's Balanced Salt Solution
ECL	Enhanced Chemoluminescence
EdU	5-ethynyl-2'-deoxyuridine
ELISA	Enzyme-linked immunosorbent assay

EM	Electron microscopy
EOAD	Early-onset Alzheimer's disease
ERK	Extracellular signal-regulated kinase
EVs	Extracellular vesicles
FAM-Aβ	Fluorescein-labeled β -amyloid peptide
FBS	Fetal bovine serum
FBS-CHST	Charcoal-stripped FBS
FC	Fold change
FL	Fluorescent channel
FPR	Formyl peptide receptor
FS	Forward scatter
Fwd	Forward
g	Universal gravitational force
GFAP	Glial fibrillary acidic protein
GLP-1	Glucagon-like peptide-1
GO	Gene Ontology
GOI	Gene of interest
h	hour
HAB	Habituation
HET	Heterozygous
HFD	High-fat diet
HIV-1	Human immunodeficiency virus type 1
HKG	Housekeeping gene
HOMA	Homeostatic Model Assessment
HRP	Horseradish peroxidase
Iba-1	Ionized calcium-binding adapter molecule 1
ICC	Immunocytochemistry
IDE	Insulin-degrading enzyme
IDE-C	C-terminal portion of IDE
IDE-N	N-terminal portion of IDE
IGF	Insulin-like growth factor
IGF1R	Insulin-like growth factor-1 receptor
IgG	Immunoglobulin G
IL-10	Interleukin 10
IL-13	Interleukin 13
IL-1β	Interleukin 1 beta
IL-4	Interleukin 4
IL-6	Interleukin 6
InsR	Insulin receptor
IRF	Interferon regulatory factor
IRS	Insulin receptor substrate
JAK	Janus kinase
JNK	C-Jun N-terminal kinase
kDa	Kilodalton
Km	Michaelis constant
KO	Knockout
LDL	Low-density lipoprotein
LOAD	Late-onset Alzheimer's disease
LP	Long pass filter
LPS	Lipopolysaccharide

LRP1	Low-density lipoprotein receptor-related protein 1
M-CSF	Macrophage colony-stimulating factor
MAA	Maackia amurensis
MAPK	Mitogen-activated protein kinase
MCI	Mild cognitive impairment
MCP-1	Monocyte chemoattractant protein-1
MetOH	Methanol
MFI	Mean fluorescence intensity
MGI	Mouse Genome Informatics
min	minute
MIP-1A	Macrophage inflammatory protein 1-alpha
miR (miRNA)	Micro-Ribonucleic acid
ML	Maximum likelihood
MPP	Mitochondrial processing peptidase
mRNA	Messenger ribonucleic acid
MSA	Multiple sequence alignment
mTOR	Mammalian target of rapamycin
MTT	3-(4,5-dimethylthiazol-2-yl)-2,5-diphenyltetrazolium bromide
MVBs	Multivesicular bodies
MW	Molecular weight
MyD88	Myeloid differentiation primary response 88
NCBI	National Center for Biotechnology Information
NF-kB	Nuclear factor kappa light chain enhancer of activated B cells
NGS	Next-generation sequencing
NIRKO	Neuron-specific insulin receptor knockout
NLRP3	Nod-like receptor family, pyrin domain containing 3
NLS	Nuclear Localization Signal
NORT	Novel object recognition test
NRD	Nardilysin
O.D.	Optical density
°C	Degree Celsius (originally known as centigrade)
OF	Open field
OFT	Object familiarization trial
OLT	Object location test
OS	Oxidative stress
P/S	Penicillin-Streptomycin
P/S/A	Penicillin-Streptomycin-Amphoterycin B
PAGE	Polyacrylamide gel electrophoresis
PBS	Phosphate-buffered saline
PCA	Principal component analysis
PCR	Polymerase chain reaction
PDB	Protein Data Bank
PI3K	Phosphatidylinositol 3-kinase
PMSF	Phenylmethylsulfonyl fluoride
PPAR-γ	Peroxisome proliferator-activated receptor gamma
PQ	N,N'-dimethyl-4,4'-bipyridinium dichloride (paraquat)
PreP1	Presequence protease 1
PRR	Pattern recognition receptor
PSI-BLAST	Position-Specific Iterated BLAST
PSSM	Position-Specific Scoring Matrix

PTEN	Phosphatase and tensin homolog deleted on chromosome 10
PVDF	Polyvinylidene fluoride
qPCR	Quantitative PCR
RAGE	Receptor for advanced glycation end products
Rev	Reverse
RIN	RNA Integrity Number
RNA	Ribonucleic acid
ROS	Reactive oxygen species
rpm	Revolutions per minute
RPMI	Roswell Park Memorial Institute Medium
RT	Room temperature
RT-PCR	Reverse transcription PCR
RT-qPCR	Reverse transcription quantitative real-time PCR
s	second
SD	Standard diet
SDS	Sodium dodecyl sulfate
SEM	Standard error of the mean
SMADs	Suppressor of Mothers Against Decapentaplegic
SOCS-3	Suppressor of cytokine signaling 3
SPP	Stromal processing peptidase
SR-A	Scavenger receptor type A
SS	Side scatter
STAT	Signal transducer and activator of transcription
T1DM	Type 1 diabetes mellitus
T2DM	Type 2 diabetes mellitus
TBS	Tris-buffered saline
TGF-β	Transforming growth factor beta
TLR	Toll-like receptor
T_m	Melting temperature
TMB	3,3',5,5'-Tetramethylbenzidine
TNF-α	Tumor necrosis factor alpha
TREM2	Triggering receptor expressed on myeloid cells 2
Tyk2	Tyrosine kinase 2
vs	<i>Versus</i>
WT	Wild-type
λ	Wavelength

ABSTRACT

Summary

Alzheimer's disease (AD) and diabetes mellitus (DM) are two chronic progressive pathologies with an alarming increase in their incidence worldwide. During the recent years, the term "type 3 diabetes" has been proposed to describe the hypothesis that AD is triggered by a type of insulin resistance that occurs specifically in the brain. Insulin-degrading enzyme (IDE) is a metalloprotease markedly expressed in the brain that has been described to cleave not only insulin but also amyloid-beta ($A\beta$) peptides, which makes this enzyme a good target to study type 3 diabetes.

Here, we demonstrated that chronic high D-glucose exposure stimulates metabolic activity and triggers a mild pro-inflammatory state in microglial cells but does not regulate IDE expression. Instead, we found a link between IDE expression and the polarization state of microglia. Furthermore, we observed that $A\beta$ treatment increased IDE exportation to the extracellular media in a time-dependent manner, and this process was reduced under high D-glucose conditions.

To address IDE subcellular localization, we constructed a molecular phylogeny and found homologous proteins from *Archaea* to *Eukarya*. Bioinformatic analyses revealed that a shift in subcellular localization took place between prokaryotic (with signal peptide) and eukaryotic cells (without it). Our experiments in microglia indicate that IDE is mostly cytoplasmatic, is not found inside any membranous organelle, and partitions between soluble and membrane fractions. IDE association to membranes only occurs at the cytosolic side, and membrane-associated IDE further partitions between raft and non-raft fractions. Moreover, IDE secretion is mediated by extracellular vesicles originating from multivesicular bodies. This mechanism of IDE exportation is modulated by the polarization of microglial cells.

To address the role of IDE *in vivo* we performed a comprehensive analysis of metabolic, behavioral and molecular parameters on a cohort of 12-month-old wild-type, heterozygous and mice with genetic deletion of the *Ide* gene. The effects of IDE ablation on metabolic parameters were very subtle; however, memory tests revealed sex- and genotype-dependent differences. In the brain, insulin signaling-related proteins and gliosis markers were differentially expressed between males and females but showed no significant differences across genotypes. Nevertheless, a multivariate analysis revealed correlations between IDE and brain-related variables such as gliosis and $A\beta$ managing.

In vitro studies in primary microglial cells demonstrated that *Ide* deletion significantly decreases microglial proliferation and delays its response to M-CSF (macrophage colony-stimulating factor, an important mitogen for microglia). Cytokine profiling assays revealed that IDE knockout (IDE-KO) microglia have impaired polarization under both pro- and anti-inflammatory stimuli, are more sensitive to oxidative stress, and exhibit a sex-specific pro-inflammatory response to $A\beta$ oligomers. Furthermore, lack of IDE alters $A\beta$ internalization dynamics and impairs $A\beta$ oligomer degradation.

A transcriptomic profiling of wild-type and IDE-KO microglia revealed that differentially expressed genes were particularly associated with response to stimuli and stress, regulation of immune processes and signaling pathways, confirming prominent roles for IDE in microglial physiology.

Finally, we performed a drug screening of natural products to search for new therapeutic approaches to treat type 3 diabetes. Among the compounds that showed anti-inflammatory properties in microglia *in vitro*, we chose leptolide and appraised its anti-glioinflammatory potential *in vivo*, demonstrating that leptolide represents a feasible therapeutic approach to reduce neuroinflammation when concurring with metabolic impairment.

The results presented in this PhD Thesis reveal previously unknown biological properties and physiological functions of IDE in the nervous system, particularly in microglial cells, where it modulates their multidimensional response to various damaging conditions relevant to the pathogenesis of AD and DM.

Resumen

La enfermedad de Alzheimer (EA) y la diabetes mellitus (DM) son dos patologías crónicas progresivas con un aumento alarmante de su incidencia a nivel mundial. Durante los últimos años, se ha propuesto el término “diabetes tipo 3” para describir la hipótesis de que la EA se desencadena por un tipo de resistencia a la insulina que se produce específicamente en el cerebro. La enzima degradadora de insulina (IDE) es una metaloproteasa fuertemente expresada en el cerebro que, según se ha descrito, degrada no sólo la insulina sino también los péptidos beta-amiloides ($A\beta$), lo cual convierte a esta enzima en una buena diana para estudiar la diabetes tipo 3.

En este trabajo demostramos que la exposición crónica a altas concentraciones de D-glucosa estimula la actividad metabólica y desencadena un estado pro-inflamatorio leve en las células microgliales, pero no regula la expresión de IDE. En cambio, encontramos una relación entre la expresión de IDE y el estado de polarización de la microglía. Además, observamos que el tratamiento con $A\beta$ incrementa la exportación de IDE al medio extracelular de manera tiempo-dependiente, y este proceso es reducido en condiciones de alta D-glucosa.

Para abordar la localización subcelular de IDE, construimos una filogenia molecular y encontramos proteínas homólogas desde *Archaea* hasta *Eukarya*. Los análisis bioinformáticos revelaron que se produjo un cambio en la localización subcelular entre células procariotas (con péptido señal) y eucariotas (sin él). Nuestros experimentos en microglía indican que IDE es principalmente citoplasmática, no se encuentra dentro de ningún orgánulo membranoso y se reparte entre fracciones solubles y de membrana. La asociación de IDE a las membranas sólo ocurre en el lado citosólico, y la proteína IDE asociada a membrana se divide entre fracciones de balsas lipídicas y de no balsas. Además, la secreción de IDE está mediada por vesículas extracelulares que se originan en cuerpos multivesiculares. Este mecanismo de exportación de IDE está modulado por la polarización de las células microgliales.

Para abordar el papel de IDE *in vivo*, realizamos un análisis exhaustivo de parámetros metabólicos, de comportamiento y moleculares en una cohorte de ratones de 12 meses de edad silvestres, heterocigotos y con una deleción genética del gen *Ide*. Los efectos de la ablación de IDE sobre los parámetros metabólicos fueron muy sutiles; sin embargo, las pruebas de memoria revelaron diferencias dependientes del sexo y del genotipo. En el cerebro, las proteínas relacionadas con la señalización de la insulina y los marcadores de XVIIurface se expresaron diferencialmente entre machos y hembras, pero no mostraron diferencias significativas entre los genotipos. Sin embargo, un análisis multivariante reveló correlaciones entre IDE y variables relacionadas con el cerebro tales como la XVIIurface y el manejo de $A\beta$.

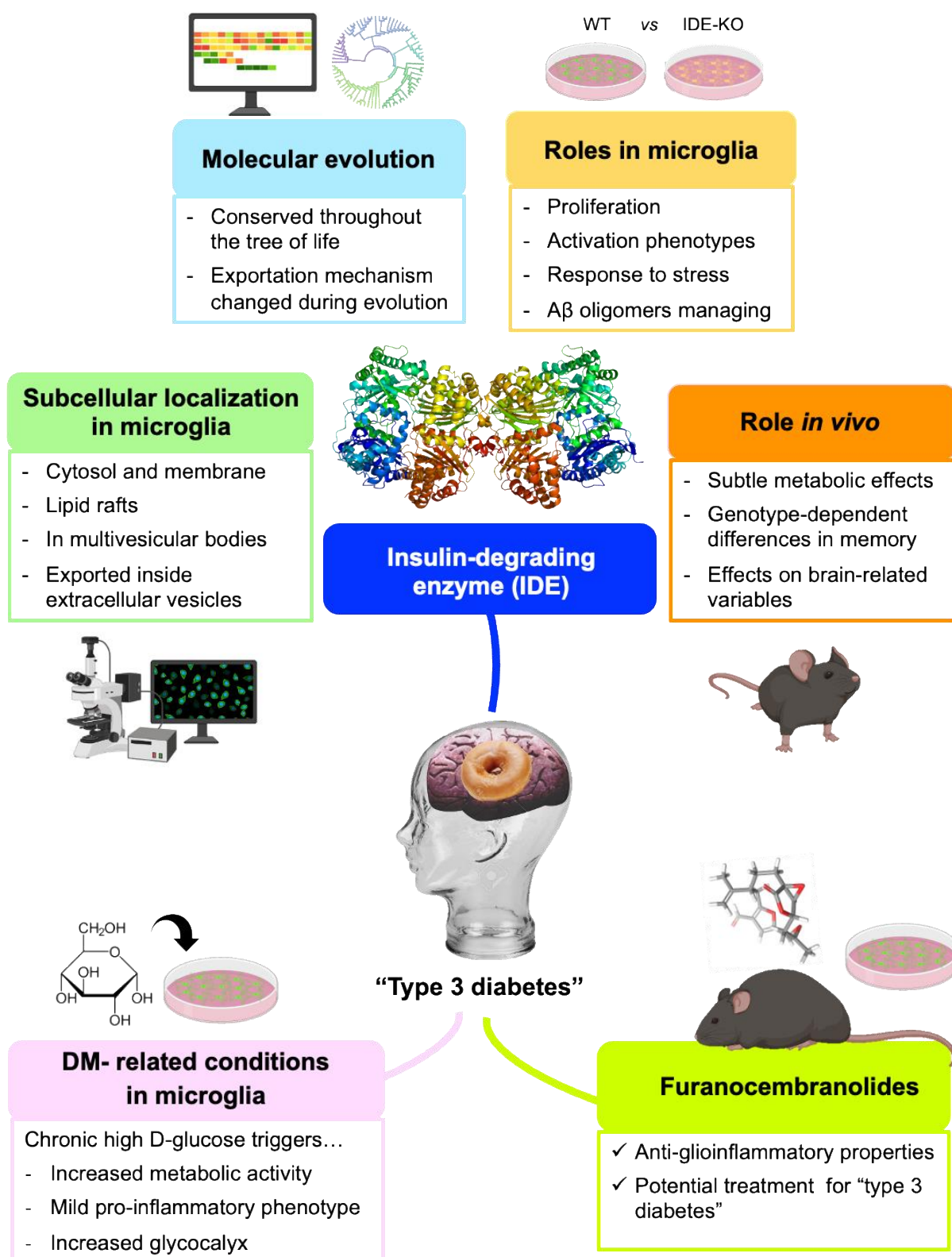
Los estudios *in vitro* en células microgliales primarias demostraron que la deleción de *Ide* disminuye significativamente la proliferación microglial y retrasa su respuesta a M-CSF (factor

estimulante de colonias de macrófagos, un importante mitógeno para la microglía). Los análisis de perfiles de citoquinas revelaron que la microglía *knockout* para IDE (IDE-KO) tiene una polarización alterada tanto bajo estímulos pro-inflamatorios como anti-inflamatorios, es más sensible al estrés oxidativo y exhibe una respuesta pro-inflamatoria específica de sexo a los oligómeros de A β . Además, la falta de IDE altera la dinámica de internalización de A β y perjudica la degradación de los oligómeros de A β . El perfil transcriptómico de la microglía de tipo silvestre e IDE-KO reveló que los genes expresados diferencialmente se asocian particularmente con la respuesta a estímulos y estrés, la regulación de los procesos inmunes y las vías de señalización, lo que confirma roles prominentes de IDE en la fisiología microglial.

Finalmente, realizamos un cribado farmacológico de productos naturales para buscar nuevos enfoques terapéuticos para tratar la diabetes tipo 3. Entre los compuestos que mostraron propiedades anti-inflamatorias en microglía *in vitro*, elegimos el leptolide y evaluamos su potencial anti-glioinflamatorio *in vivo*, demostrando que el leptolide representa una aproximación terapéutica factible para reducir la neuroinflamación concurrente con deterioro metabólico.

Los resultados presentados en esta Tesis Doctoral revelan propiedades biológicas y funciones fisiológicas previamente desconocidas de IDE en el sistema nervioso, particularmente en las células microgliales, donde modula su respuesta multidimensional a diversas condiciones dañinas relevantes para la patogénesis de la EA y la DM.

Graphical Abstract



INTRODUCTION

The main objective of this thesis is to characterize the physiological roles of the insulin-degrading enzyme (IDE) in microglial cells in the context of Alzheimer's disease and diabetes mellitus. For this reason, this introduction will initially describe the main pathological hallmarks of Alzheimer's disease. Next, the most relevant aspects related to microglial homeostatic functions will be displayed. On the other hand, the main concepts regarding to diabetes mellitus will be briefly described. Then, the structural, molecular, and functional characteristics of IDE, as well as its genetic association with Alzheimer's disease and diabetes mellitus, will be reviewed. Finally, the concept of "type 3 diabetes" will be introduced, and a brief review of candidate drugs to simultaneously treat Alzheimer's disease and diabetes mellitus will be shown.

1. Alzheimer's disease

Alzheimer's disease (AD) is a progressive, unremitting, neurodegenerative disorder and the most common cause of dementia, constituting one of the great health-care challenges of the 21st century. AD is characterized by a progressive death of neuronal cells and synapses, especially in brain areas responsible for learning and memory such as the cerebral cortex and the hippocampus, triggering deficits in memory, cognition, orientation and language. It has been estimated that more than 40 million people, mostly older than 60 years, have dementia worldwide, and these data are predicted to double every 20 years until at least 2050 (Scheltens et al., 2016) (**Figure 1**).

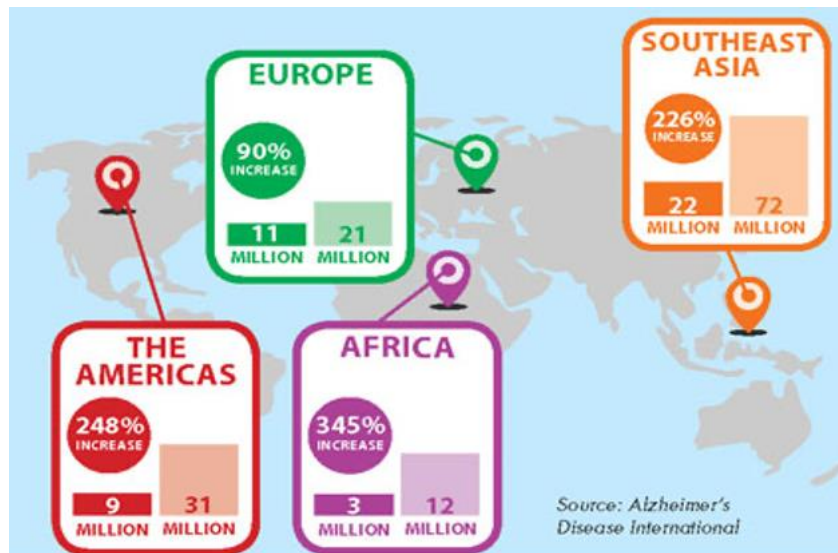


Figure 1. Prevalence and worldwide distribution of dementia cases in 2015 and estimated growth by 2050. Taken from (NIH's National Institute on Aging, 2015).

The pathognomonic traits of AD were described by Alois Alzheimer more than one century ago (Alzheimer, 1907), and consisted in two aberrant structures that accumulate within the patient's brain, namely intraneuronal neurofibrillary tangles and extracellular senile plaques. The main component of neurofibrillary tangles and senile plaques are hyperphosphorylated tau proteins and amyloid-beta ($A\beta$) peptides, respectively (Scheltens et al., 2016). AD can be classified into two

groups, according to the age of onset: the “late-onset AD” (LOAD), occurring after the age of 65 years and representing the majority of cases (around 95%), and the “early-onset AD” (EOAD), based on dominant inheritance, with an onset prior to the age of 65 (1-5% of all AD cases).

1.1. A β : a key molecule in AD

The A β molecule, a 4-kDa peptide composed of 39-43 amino acids, is synthesized and detectable throughout the body under physiological circumstances, although its role remains uncertain (Masters et al., 1985; Seubert et al., 1992). A β is formed as a result of the proteolytic cleavage of a larger protein, the amyloid precursor protein (APP), and is normally cleared quickly; however, during pathological processes such as AD, there is an imbalance between A β production and clearance (Savage et al., 1998; Selkoe, 2001), leading to the accumulation of A β in the brain. Multiple lines of evidence propose that a change of conformation of A β , to forms with a high content of β -sheet structures, is crucial in AD pathogenesis (Gandy, 2005; Karran et al., 2011; Naslund et al., 2000). Since A β is highly hydrophobic and fibrillogenic, aggregation and deposition of amyloid fibrils occur in the brain in the form of senile plaques and diffuse aggregates (Selkoe and Hardy, 2016; Suzuki et al., 1994).

In the EOAD, autosomal dominant mutations in either presenilin 1, presenilin 2 or APP genes lead to increased levels of A β ; while for the remaining cases of LOAD the cause is less clear, although aging and the possession of the apolipoprotein E epsilon 4 (ApoE- ϵ 4) allele are the most important risk factors (Bolós et al., 2017). In contrast to the inherited EOAD, where an increase in overall A β production or an increased aggregation propensity of A β seem to be the main causes, in sporadic LOAD rather a decreased degradation rate of A β is considered to cause the neurodegeneration (Mawuenyega et al., 2010; Miners et al., 2011; Selkoe, 2001). Based on these observations, the amyloid cascade hypothesis posits that AD pathology is initiated by increased levels of A β , which lead to A β deposition and aggregation in the brain parenchyma, triggering a cascade of events that ultimately result in neuronal loss and AD dementia (Hardy and Higgins, 1992). However, several A β -centric approaches intended to reduce A β production or aggregation have failed in Phase III clinical trials (Karran et al., 2011), questioning the suitability of A β as a pharmacological target for the treatment of AD.

1.1.1. A β production from the amyloid precursor protein (APP)

A β peptides originate from the multi-step proteolytic processing of APP, a ubiquitously expressed type I transmembrane protein that traffics between the plasma membrane and acidic intracellular compartments. There are two alternative APP processing pathways, summarized in **Figure 2**. The non-amyloidogenic pathway is predominant in the healthy brain and takes place at the cell surface, where the α -secretase initiates APP processing. The amyloidogenic pathway, which results in the synthesis of A β peptides, requires internalization of APP into acidic compartments where β -secretase is at its optimal pH. In both pathways, membrane-anchored C-terminal fragments (CTFs) are

subsequently processed by γ -secretase to generate either p3 or A β peptides, concomitantly with the release of an APP intracellular domain (AICD) into the cytosol. Soluble APP metabolites play their own roles in brain function: sAPP β seems to be involved in synaptic pruning and apoptosis, while sAPP α is considered neuroprotective. The AICD resulting from the amyloidogenic pathway is known to translocate to the nucleus and regulate gene transcription, with APP, β -secretase, neprilysin and several enzymes involved in lipid metabolism as target genes. In contrast, the AICD generated by the non-amyloidogenic pathway is rapidly degraded in the cytosol (Corraliza-Gomez et al., 2019).

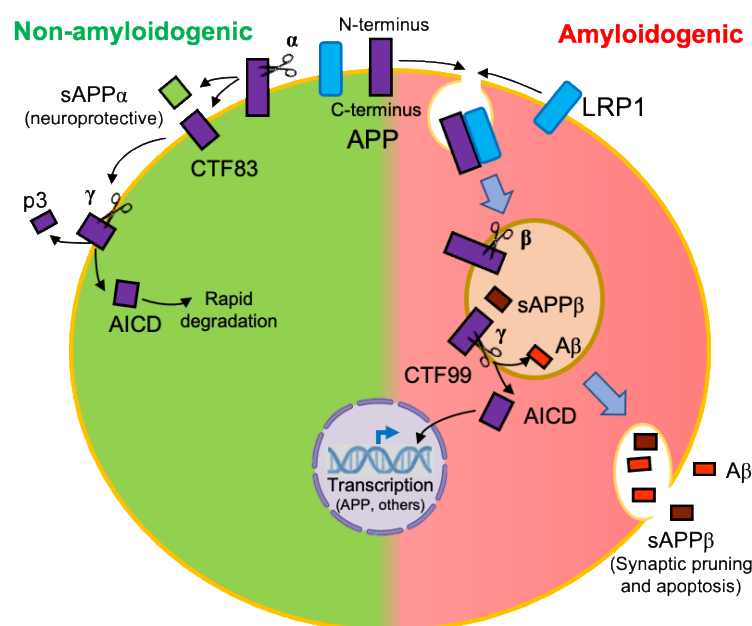


Figure 2. Alternative proteolytic processing of APP. Plasma membrane α -secretase initiates the non-amyloidogenic pathway, releasing a soluble ectodomain (sAPP α) and generating a membrane-anchored CTF of 83 amino acids. In contrast, the amyloidogenic pathway is initiated by β -secretase in intracellular acidic organelles. Its processing results in a 99-amino-acid CTF and a soluble extracellular sAPP β . CTFs are subsequently processed by γ -secretases generating p3 or A β peptides and releasing an AICD. The AICD resulting from the amyloidogenic pathway translocates to the nucleus and regulates amyloidogenic and lipid metabolism gene transcription. The AICD generated by the non-amyloidogenic pathway is rapidly degraded in the cytosol. Taken from (Corraliza-Gomez et al., 2019). Abbreviations: APP = amyloid precursor protein, CTF = C-terminal fragment, AICD = APP intracellular domain, LRP1 = LDL receptor-related protein 1.

1.1.2. A β toxicity in AD

Monomers of A β peptides self-associate to form oligomers and subsequently fibrils, which appear to be associated with the level of toxicity and neurodegeneration (Pike et al., 1993). Early studies suggested that the neurotoxicity of A β could be attributed to the insoluble amyloid fibrils present in senile plaques, so plaque numbers would be directly related to quantitative measures of cognitive decline in aged patients (Roth et al., 1966). However, further research suggested that plaques are relatively inert and proposed that pre-fibrillar, soluble small A β oligomers are more relevant than plaques in neuronal injury (Stine et al., 2003; Walsh and Selkoe, 2007; Yankner and Lu, 2009). Today, A β oligomers (A β o) are widely regarded as the most toxic and pathogenic form of A β (Cline

et al., 2018; Selkoe and Hardy, 2016). Interestingly, A β has been described to have neurotrophic properties *in vitro*, dependent on low peptide concentration and reduced exposure time (Pike et al., 1993, 1991; Yankner et al., 1990). In the same way, oligomer and fibril formation, as well as the neurotoxicity of these aggregates, have been demonstrated to be concentration- and time-dependent, aside from dependent on certain metal ions such as zinc or copper (Hartley et al., 1999; Stine et al., 2003).

1.1.3. Mechanisms of A β clearance

Once A β is generated by amyloidogenic processing of APP, it is released to the interstitial fluid, where clearance takes place by different mechanisms.

1.1.3.1. A β exportation through blood-brain barrier and the glymphatic system

According to the “peripheral sink hypothesis”, brain A β has been demonstrated to be transported across the blood-brain barrier (BBB) into the peripheral circulation (de Matos et al., 2018; Shibata et al., 2000). This transport, facilitated by the low density lipoprotein (LDL) receptor-related protein 1 (LRP1), takes place by transcytosis across endothelial cells (Pflanzner et al., 2011), which involves that A β crosses the cell inside vesicles, bypassing the cytoplasm. Once in the periphery, A β binding agents, such as the soluble circulating LRP1, bind to the amyloid peptide and prevent its return to the central nervous system (CNS) (Sagare et al., 2007; Takata et al., 2007).

Another mechanism for brain A β clearance is by transport through perivascular drainage pathways into the cerebrospinal fluid (CSF) and subsequently into the peripheral circulation via the glymphatic system, a glial-dependent waste clearance pathway in the brain which efficiently eliminates potentially neurotoxic waste-products (Benveniste et al., 2019). Age-related decline in glymphatic clearance has been described to contribute to the accumulation of aggregated proteins, such as A β , in the CNS (Jessen et al., 2015). Furthermore, vascular and parenchymal A β deposition might be related to the development of cerebral amyloid angiopathy, frequently found in AD (Thal et al., 2008).

1.1.3.2. A β degradation by proteases

Besides the exportation mechanisms described above, the clearance of A β from the CNS can also occur via proteolytic degradation by both neurons and glial cells. Multiple proteases have been reported with the capability to cleave A β at either a single or multiple sites, generating cleavage products less prone to aggregate and less neurotoxic than A β itself. These include IDE, neprilysin, endothelin-converting enzyme, angiotensin-converting enzyme, cathepsin B and D, gelatinases A and B and matrix metalloproteinases 2 and 9 (Miners et al., 2011; Wang et al., 2006). These proteases are particularly involved in the degradation of monomeric A β species, although neprilysin can also hydrolyze oligomeric forms (Ries and Sastre, 2016).

1.1.3.3. Cellular degradation pathways involved in A β removal

The endo-lysosomal system, autophagy and the ubiquitin proteasome system are cellular degradation pathways that play a critical role in the removal and the prevention of accumulation of misfolded proteins (Ji et al., 2018). In fact, alterations in these systems are widely involved in protein aggregation and toxicity occurring in neurodegenerative disorders (Limanaqi et al., 2020). Both *in vitro* and *in vivo*, autophagy and the proteasome remove oligomeric A β , while monomeric A β species are preferentially cleared via the endo-lysosomal system (Ji et al., 2018; Limanaqi et al., 2020).

In conclusion, steady-state A β levels in the brain are maintained by an equilibrium between amyloidogenic processing of APP and the elimination of soluble A β by clearance routes and protease-mediated degradation. Either increased activity of amyloidogenic enzymes (β - and γ -secretases) or decreased activity of A β -degrading enzymes results in A β accumulation. This probably triggers compensatory upregulation of A β -degrading proteases, increased A β degradation and reduced A β accumulation. However, an impairment in the activity of A β -degrading enzymes as a result of aging, genetic and environmental factors, and also a decline in the efficiency of other A β clearance pathways, result in an excessive accumulation of A β , plaque formation and deposition of A β within and around vessel walls, causing cerebral amyloid angiopathy.

1.2. The hallmarks of Alzheimer's disease

Aside from senile plaques and neurofibrillary tangles, the main diagnostic criteria for AD, there are some other major abnormalities contributing to the neurodegenerative processes that must be considered, including neuronal loss, neuroinflammation, gliosis, oxidative stress, white matter degeneration, vascular damage, blood-brain barrier disruption and impairments in brain metabolism (Nakabeppu and Ninomiya, 2019) (**Figure 3**).

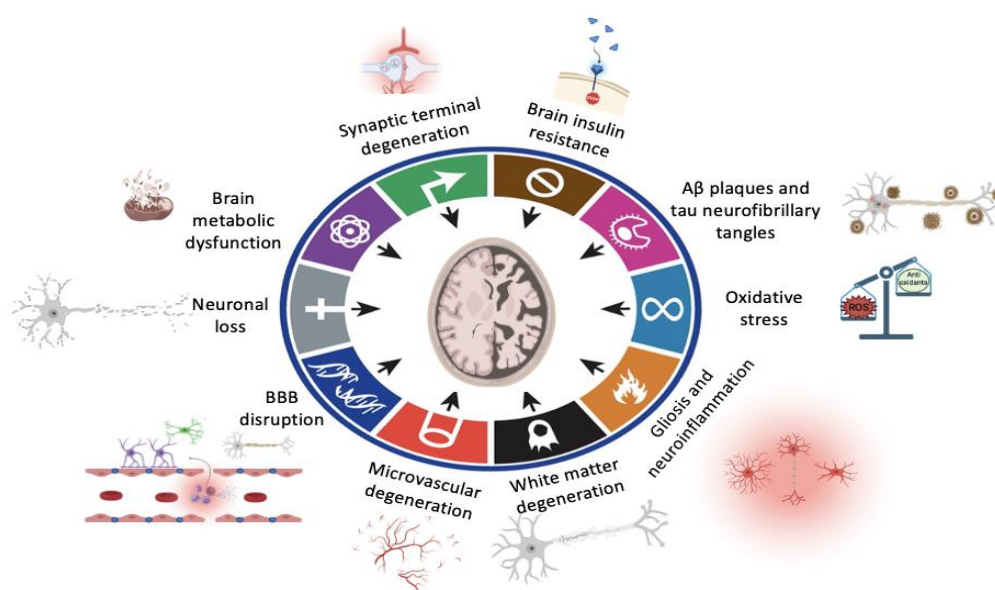


Figure 3. The hallmarks of Alzheimer's disease. Summary of the major brain abnormalities that occur in AD and contribute to the neurodegenerative process. Inspired from (Hanahan and Weinberg, 2011).

1.2.1. Neuronal loss and neurofibrillary tangles

Neurodegeneration in AD is associated with loss of neurons beginning in the hippocampus, entorhinal cortex and medial temporal structures (Mizutani et al., 1990). However, the main feature which distinguishes AD from other neurodegenerative processes is that neuronal loss is accompanied by progressive accumulation of neurofibrillary tangles, dystrophic neurites, neuritic plaques and neuropil threads (De la Monte et al., 2018). Neurofibrillary tangles are composed of aggregated twisted insoluble fibrillar proteins whose main component is the hyperphosphorylated tau protein, a microtubule-associated molecule (De la Monte, 2019).

1.2.2. Synaptic terminal degeneration

Synaptic disconnection due to degeneration is accompanied by loss of neuronal and neuritic sprouting in AD. Dystrophic neurites are often found around the periphery of A β ₁₋₄₂ plaques, which could be linked to the presence of trophic factors within plaques (Cummings et al., 1993). Experimental models of AD suggest that the neurotoxic effects of A β ₁₋₄₂ species have causal roles in the loss of cortical synapses and the impairment of synaptic plasticity (Buttini, 2005; Eleuteri et al., 2015).

1.2.3. Gliosis

Gliosis is a non-specific reactive switch of glial cells in response to CNS damage, and involves the proliferation or hypertrophy of glial cells (Bronzuoli et al., 2016). Data from animal models and human post-mortem brains revealed that both senile plaques and neurofibrillary tangles cause an immune response in the brain and co-localize close to activated glial cells (De la Monte, 2019). In response to AD-triggered neuronal death, astrocytes and microglia acquire a reactive phenotype and rapidly undergo important changes in their morphology and function, producing a protective response aimed at removing injurious stimuli and repair the damaged tissue. However, when sustained glial activation goes beyond physiological control, glial cells foster a neuroinflammatory response and synthesize pro-inflammatory mediators, promoting oxidative stress and tissue injury, thereby worsening neurodegeneration (Bronzuoli et al., 2016).

1.2.4. Neuroinflammation

Neuroinflammation is a complex inflammatory process in the CNS, which is sought to play an important defensive role against pathogens, toxins and other factors that induce neurodegeneration (Tohidpour et al., 2017). It is orchestrated by glial cells, mainly microglia and astrocytes, and is a symptom of perturbed brain homeostasis. Microglia constitute the brain's innate immune system and are the first cells that respond to inflammatory stimuli. In addition, when the situation is resolved, microglia counteract inflammation, driving astrocytes to an anti-inflammatory profile by the secretion of IL-10, which triggers TGF- β production. TGF- β is a neuroprotective molecule that restrains inflammation, reinforcing the anti-inflammatory microglial phenotype. However, if the situation is not resolved or under chronic inflammation, microglial cells proliferate and switch to a

reactive phenotype, known as microgliosis, and produce and release IL-1 β and TNF- α into the brain milieu (Kettenmann et al., 2011). These pro-inflammatory cytokines are detected by astrocytes as inflammation inducers, triggering astrogliosis. The abnormal increase in the number of astrocytes causes secretion of even more pro-inflammatory stimuli, initiating a reactive loop (Bernaus et al., 2020). In AD brains the A β aggregates, especially their oligomeric or fibrillar forms, act as damage-associated molecular patterns activating the NLRP3 inflammasome in microglia, among other effects (Halle et al., 2008), as well as in astrocytes (Couturier et al., 2016), enhancing the release of pro-inflammatory cytokines (**Figure 4**).

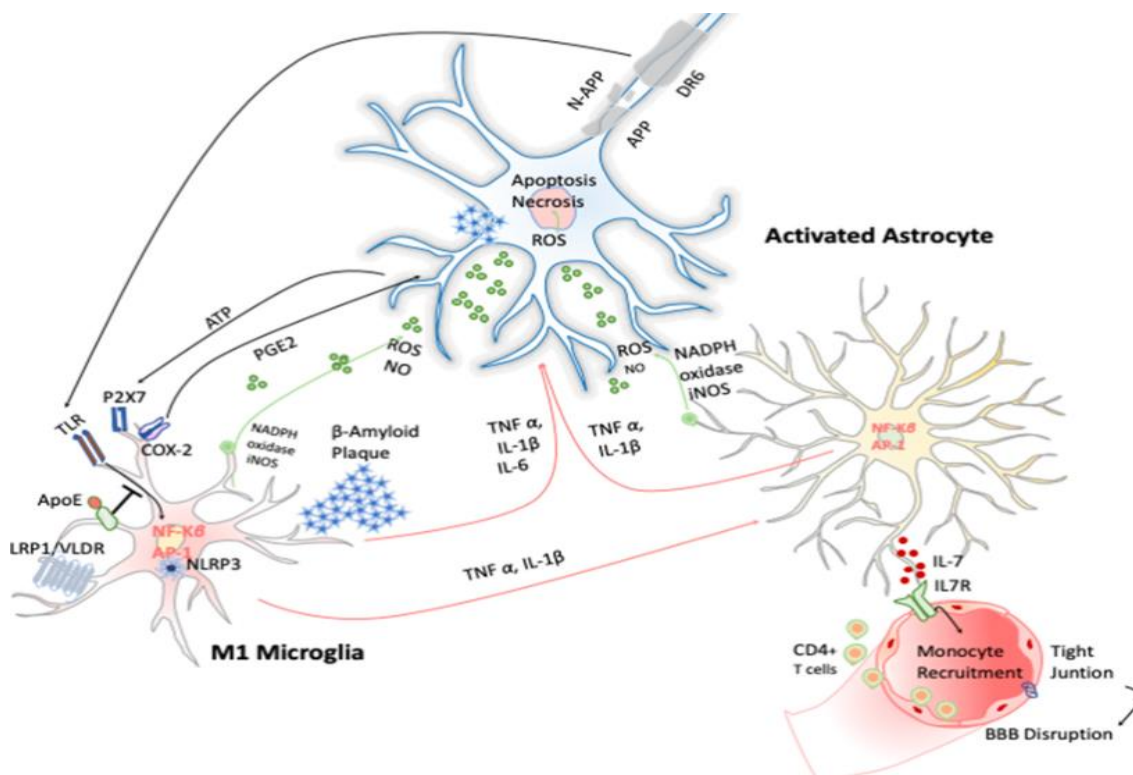


Figure 4. Inflammatory response in Alzheimer's disease. Amyloidogenic processing of APP produces A β peptides, which activate microglial cells, triggering the production of reactive oxygen species (ROS) and inflammatory cytokines. These molecules amplify the pro-inflammatory response by the stimulation of astrocytes, which produce more pro-inflammatory cytokines, starting a reactive loop. Moreover, astrocytes act directly on the neuronal population inducing neuronal death. Apoptosis of neurons results in the release of ATP, which further activates microglia through purinergic P2X7 receptors. This inflammatory environment has also a direct effect on the BBB endothelial cells by downregulating the tight junctions between these cells, which triggers BBB disruption and allows the entrance of the components of the adaptive immune response. Taken from (Bernaus et al., 2020).

1.2.5. Oxidative stress

Oxidative stress (OS) is a phenomenon caused by an imbalance between production and accumulation of reactive oxygen species (ROS) and reactive nitrogen species in cells and tissues, and the ability of a biological system to detoxify these noxious products by using antioxidant defenses (Pizzino et al., 2017). OS has been shown to contribute significantly to the pathogenesis

and progression of AD. Levels of oxidative damage to a wide range of biomolecules are increased in the brains of individuals with mild cognitive impairment (MCI), preclinical AD and AD. Interestingly, oxidative damage has been described to be intimately related with inefficient brain glucose utilization, another trait of AD, which can be explained by the oxidative modification, and subsequent decrease in activity, of the enzymes involved in glucose metabolism (Butterfield and Halliwell, 2019).

When reducing sugars react with the side chain amino groups of lysine residues on proteins, advanced glycation end products (AGEs) are generated, accompanied by oxidative damage to the proteins, in a process known as glycoxidation. These AGEs are ligands for receptors for AGEs (RAGEs) and result highly relevant to AD, in part because extracellular fibrillar A β aggregates have characteristics of AGEs and bind to RAGEs in neurons and brain endothelial cells, leading to further OS that contributes to neuronal death and vascular dementia in AD. Moreover, glycation may slow the conversion of A β to fibrils, keeping them longer in the toxic oligomeric forms (Butterfield and Halliwell, 2019).

1.2.6. White matter degeneration and demyelination

In addition to neuronal loss, white matter degeneration and demyelination are also important pathophysiological features involved in AD (Nasrabad et al., 2018). White matter consists of myelinated axons along with glial cells (oligodendrocytes and astrocytes) and vascular elements. Axons are long cytoplasmic extensions of neuronal cell bodies, whose structure is maintained by a cytoskeleton rich in neurofilament proteins and microtubule-associated proteins such as tau. CNS myelin is composed of lipid-rich oligodendrocyte membranes that wrap around axons to provide insulation and ensure efficient conductivity (De la Monte, 2019). Neuroinflammation triggers injury and degeneration of myelin and axons, and such white matter degeneration has been demonstrated to occur early in the preclinical stages of AD (De la Monte, 2019), especially in the later-myelinated areas such as the cortex and hippocampus (Bartzokis et al., 2007).

1.2.7. Microvascular degeneration

Progressive deficits in cerebral blood flow have been described in AD brains. Two types of vascular pathology are present in AD: A β -associated and A β -unassociated. In cerebral amyloid angiopathy, which affects cortical and leptomeningeal vessels (Vinters et al., 1990; Joachim and Selkoe, 1992), microvessels contain A β deposits in their walls and in the adjacent perivascular parenchyma (Vinters, 2015). Non-amyloid vascular degeneration, which occurs in the cerebral cortex, white matter and subcortical nuclei, is characterized by microvessels exhibiting thickened basement membranes and attrition of perivascular tissue (Scheibel et al., 1989).

1.2.8. Blood-brain barrier disruption

The BBB is a continuous endothelial structure within brain microvessels that has sealed cell-to-cell contacts and is covered by mural cells (pericytes in capillaries and vascular smooth muscle cells

in arterioles and arteries) and perivascular astrocyte end-feet. The BBB protects neurons from factors present in the systemic circulation and maintains the highly regulated chemical composition of brain interstitial fluid. BBB disruption allows influx into the brain of neurotoxic blood-derived molecules, cells and microbial pathogens and is associated with inflammatory and immune responses, which can initiate neurodegeneration (Sweeney et al., 2018) (see **Figure 4**).

Cerebral amyloid angiopathy and vascular pathology contribute to cognitive decline in AD, and vascular degeneration also weakens vessels and make them leaky, enabling circulating toxins and inflammatory mediators to enter the brain. According to the “two-hit vascular hypothesis of AD”, damage to blood vessels is the initial insult, causing BBB dysfunction and diminished brain perfusion that, in turn, lead to neuronal injury and A β accumulation in the brain (Sweeney et al., 2018).

1.2.9. Brain metabolic dysfunction

The brain composes only 2% of total body mass, yet 50% of the glucose utilized in the body supplies the brain. Thus, the brain is an energy-demanding organ which depends on efficient ATP production via glycolysis, the Krebs cycle and oxidative phosphorylation (Butterfield and Halliwell, 2019). Glucose metabolism is critical for most brain functions, but especially those related to cognition, behavior and plasticity, which are most significantly impaired in AD.

In the last few years, numerous studies have provided compelling evidence that AD is a metabolic disease whereby the brain loses its ability to efficiently utilize glucose to produce energy (De la Monte, 2014), which results in global reductions in brain glucose metabolism in comparison with healthy control brains (Waldron et al., 2015; Wurtman, 2015). These findings postulate mitochondrial dysfunction as an early feature of AD. Mitochondria are dynamic ATP-generating organelles involved in many cellular functions including bioenergetics processes, intracellular calcium regulation and free radical scavenging. Mitochondrial functions can be impaired by A β peptides, which are imported into both isolated mitochondria and SH-SY5Y (human neuroblastoma cells) by the translocase of the outer membrane complex and progressively accumulate inside these organelles, inducing mitotoxicity (Hansson Petersen et al., 2008; Picone et al., 2014).

1.2.10. Brain insulin resistance

Brain insulin resistance is a common hallmark of AD (Arnold et al., 2018; Neth and Craft, 2017). Although peripheral hyperinsulinemia and insulin resistance are risk factors for AD, it has been shown that insulin levels in the brain are lower in AD patients, suggesting that a deficiency in insulin and its action underlies AD pathology (Banks et al., 2012). However, it is still unclear whether insulin resistance in the brain might contribute to neuronal glucose metabolism impairment. The mainstay model of dysregulated brain insulin signaling, the neuron-specific insulin receptor knockout (NIRKO) mouse, had only a mild phenotype with elevated phosphorylated tau protein. Nevertheless, the mouse was able to perform normally in spatial learning and memory tasks and exhibited normal brain glucose metabolism, suggesting that the regulation of brain glucose metabolism is insulin

receptor-independent (Schubert et al., 2004; Gandy and Huffman, 2019). One of the mechanisms by which insulin resistance can develop is the activation of the mammalian target of rapamycin (mTOR), involved in many functions such as autophagy and insulin signaling, and is also crucially linked to glucose metabolism (Butterfield and Halliwell, 2019). Inhibition of autophagy following activation of mTOR in AD causes accumulation of aggregated proteins and damaged organelles, which can lead to inhibition of normal cellular processes. This important mediator of neuronal death is present in the early stages of AD, and impaired autophagy is also found in MCI and AD brains (Di Domenico et al., 2018; Nixon, 2017).

The multifactorial hypothesis for AD proposes that onset of sporadic AD results from the collective effects of multiple factors (Gong et al., 2018). Consequently, AD must be considered as a complex neurodegenerative disorder caused by several different pathological features contributing to its etiology (**Figure 3**).

2. Microglia

Microglia are the resident macrophages of the CNS, acting as professional phagocytes and orchestrators of the innate immune response to protect the brain against all kind of pathogenic factors (Sierra et al., 2013). Microglial cells were first described by the Spanish researcher Pio del Río-Hortega in 1919 as the “third element” of the neural centers (Rio-Hortega, 1919a), and they account for 5-12% of the total number of glial cells in the brain (Gomez-Nicola and Perry, 2015).

2.1 Microglia ontogeny: a unique cell population

Rio-Hortega had rightly proposed that microglial cells are of mesodermal origin, whereas the other glial cells originate from the neuroectoderm, which makes microglia a unique brain cell population (Rio-Hortega, 1919b). This hypothesis was recently confirmed by *in vivo* lineage tracing studies that demonstrated that microglia originate from the primitive hematopoietic wave of early myeloid progenitors at embryonic day 7.5 (E7.5) in the yolk sac, in a process dependent on the transcription factors Pu.1 and Irf8 (Ginhoux et al., 2013, 2010). These primitive macrophages migrate via the bloodstream into the developing CNS before birth, as early as E9.5, to colonize the developing neuroepithelium and finally become microglia (Prinz and Priller, 2014; Ginhoux and Prinz, 2015).

Different stages of microglia development have been described in mice. During neonatal development microglial progenitors do not possess highly ramified processes and closely resemble macrophages. However, after birth microglia undergo a developmental program that includes proliferation and subsequent acquisition of ramified processes, converting into the microglia commonly observed in the adult CNS. Once ramified, microglia spread evenly over the whole neural tissue (Nayak et al., 2014).

2.2. Factors that promote microglia development and homeostasis

During neonatal development, committed myeloid precursors differentiate into microglia following a developmental program controlled by various molecules including transcription factors, growth factors, chemokines and microRNAs (reviewed by (Nayak et al., 2014)).

- **Runx1:** Runx1 is a transcription factor that binds directly to the enhancer elements of several genes crucial for microglial development, such as *Pu.1* and *Csf1r*.
- **PU.1:** PU.1 is a transcription factor constitutively expressed in both resting and activated microglia. It is considered a master regulator for the myeloid lineage, involved in the maturation of yolk-sac derived myeloid progenitors.
- **CSF1R:** colony-stimulating factor 1 receptor (CSF1R) is a tyrosine kinase transmembrane receptor originally identified as a growth factor receptor, but also involved in cell survival, differentiation, development and chemotaxis.
- **IRF-8:** interferon regulatory factor 8 (IRF-8) is a transcription factor involved in maintaining both microglial embryonic development and microglial homeostasis in the adult brain.
- **miR-124:** microRNA-124 is one of the most abundantly expressed miRNAs in the CNS. Besides from regulating adult neurogenesis and neuronal differentiation, miR-124 is also highly expressed in microglia, where it has been reported to be involved in maintaining microglial quiescence.
- **M-CSF:** macrophage colony-stimulating factor (M-CSF) is a cytokine that exerts its effects by signaling through the CSF1R pathway. M-CSF has critical roles in microglia such as promoting cell proliferation and differentiation, and also controlling microglial activity, impairing the release of pro-inflammatory and toxic mediators while favoring the release of mediators promoting tissue repair (Pons and Rivest, 2018).

Unlike macrophages, the adult population of microglia does not renew from bone-marrow circulating progenitors. In contrast, microglia are renewed from local proliferation of brain resident cells, coupling apoptosis and mitosis (Askew et al., 2017). The turnover of microglial population has been described as a highly dynamic process, with an estimated renewal rate of 96 hours for the entire rodent microglia (Askew et al., 2017).

2.3. Microglial activation states

The concept of “microglial activation” is an umbrella term commonly used to describe a wide variety of functional and morphological responses of microglia toward different stimuli, including stress or homeostatic imbalance, inflammation or chronic neurodegenerative conditions. While this concept seems to imply that microglia are in a dormant or quiescent state under healthy conditions (previously called “resting state”), it has been demonstrated that under homeostatic conditions microglia are constantly surveying the brain environment with their highly motile protrusions (Davalos et al., 2005; Nimmerjahn et al., 2005).

Microglia in a healthy brain are characterized by a small soma from which ramified processes are extending, a morphology evolutionarily conserved across different species (Walker et al., 2014). Classically, microglial activation was associated with an amoeboid-like morphology that enables microglia motility and phagocytic function. However, morphological transformation is not a uniform process, with microglial morphologies ranging from amoeboid-like under inflammatory conditions (Beynon and Walker, 2012) to hyper-ramification in response to stress (Hellwig et al., 2016) and accelerated aging (Raj et al., 2014), with many intermediate morphologies in between. Thus, microglial morphology does not seem to be a clear criterion to classify microglial activation states.

2.3.1. The M1/M2 dichotomic states: an outdated concept

In an attempt to categorize the complexity of microglial activation, the dichotomic concept of M1 (classical activation) and M2 (alternative activation) states, initially postulated for peripheral macrophages (Mills et al., 2000), was applied to microglia. According to this concept, the M1 microglial phenotype is characterized by the production of pro-inflammatory cytokines (TNF- α , IL-1 β and IL-6), chemokines and ROS, leading to an acute immune response, while the M2 microglial phenotype is characterized by the production of anti-inflammatory cytokines (IL-4, IL-10, IL-13 and TGF- β) and promotes debris clearance, wound healing and restoration of brain homeostasis. It was assumed that microglia react to a stimulus with an M1 phenotype to address damage, followed by transition to an M2 phenotype to restore brain homeostasis. However, further research on this field demonstrated that the M1/M2 concept is an oversimplification of microglial activation states, which are highly diverse and exhibit many intermediate states between M1 and M2 mutually exclusive polarization phenotypes (Cherry et al., 2014). In fact, recent studies have led to the abandonment of the static and outdated M1/M2 concept of microglial activation states (Ransohoff, 2016).

2.3.2. Microglial changes during aging

During aging, microglia undergo several phenotypic changes in morphology and function. Overall, aging seems to induce a phagocytic and antigen-presentation gene expression profile, characterized by upregulation of genes involved in phagocytosis, antigen processing and presentation, interferon and cytokine signaling, as well as lipid homeostasis. Moreover, age-associated changes in murine microglia occur in a brain region-specific manner, with gene expression changes taking place during early aging in cortical and cerebellar microglia (Spittau, 2017; Dubbelaar et al., 2018).

2.3.3. Microglial sexual dimorphism

Recent data from rodents indicate significant differences in microglia between males and females (Habib and Beyer, 2015; Wolf et al., 2017). There is a sex bias in the number of microglia in the developing rodent brain, with males having more microglia than females across the neonatal period. It is currently unknown whether more microglial progenitors are recruited into the male brain early in life, whether more proliferation occurs, or whether more cells survive in males than females (Lenz and McCarthy, 2015). Besides, a developmentally more mature state, marked by upregulation of

genes involved in immune processes, is identified in female microglia compared to male microglia at 2 months of age (Hanamsagar and Bilbo, 2016). In addition, sex-specific transcriptomic signatures have been described when comparing adult male and female mice. A higher gene expression level of pro-inflammatory genes such as *Ccl2*, *Tnf*, *Irf1*, *Cxcl10* and *Il1b* is found in female mice, indicating a more immune-activated state of female microglia (Dubbelaar et al., 2018).

2.3.4. The kaleidoscope of microglial phenotypes

The diversity of microglial phenotypes led to Town and colleagues to propose that microglial “activation” is not just one phenotypic manifestation, but a *continuum* of responses (Town et al., 2005). Traditionally, this concept has been understood as two-dimensional activation states, with the most well characterized pro-/anti-inflammatory states at the extremes of this *continuum* (**Figure 5A**). However, a comprehensive transcriptomic analysis of human macrophages exposed to 29 different stimuli *in vitro* revealed that each stimulus triggered the expression of a different transcriptomic profile (Xue et al., 2014). Recently, Dubbelaar and coworkers suggested that microglial polarization is a multidimensional concept, and thus microglial activation phenotypes can be metaphorically imagined as the manifold compositions of colorful crystals seen in a kaleidoscope, whereby a change in microenvironment is functionally equivalent to a rotation of the kaleidoscope (Dubbelaar et al., 2018) (**Figure 5B**).

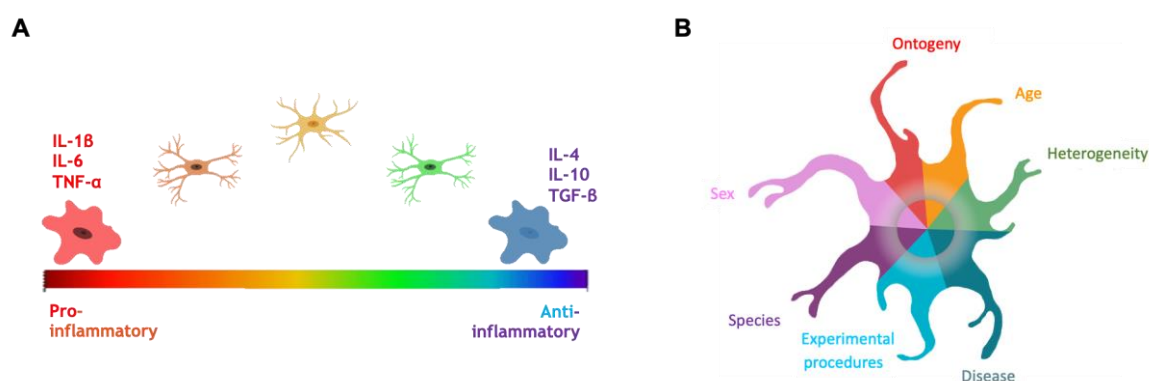


Figure 5. Evolution of the concept of microglial activation phenotypes. **A)** *Continuum of microglial activation states, where each cell represents an individual stimulus and/or environment. Note that this 2D graph must be interpreted as a multidimensional matrix, and classical and alternative polarization states do not have to be the extremes but have been represented in these positions since are the most well characterized microglial phenotypes.* **B)** *The kaleidoscope of microglial phenotypes: examples of factors that impinge on the microglia epigenome and transcriptome. The influence of these factors on the transcriptome converges in the center of the gray rim. Taken from (Dubbelaar et al., 2018).*

2.4. Homeostatic microglial functions

Microglia are the main sensor cells in the brain tissue. The two principal abilities of microglia, which highlight their relevance in the CNS, are the control of the inflammatory response and the phagocytosis of debris. Microglial cells possess a unique surveillance capacity, supported by the high motility of their fine processes, which allows them to perform parenchymal surveillance tasks and

continuously monitor the brain microenvironment (Nimmerjahn et al., 2005). Microglia are able to respond to many changes of their surrounding milieu by modifying their morphology and gene expression (Kettenmann et al., 2013). This feature allows microglia to play important roles in physiology and pathology, performing a wide range of functions (**Figure 6**).

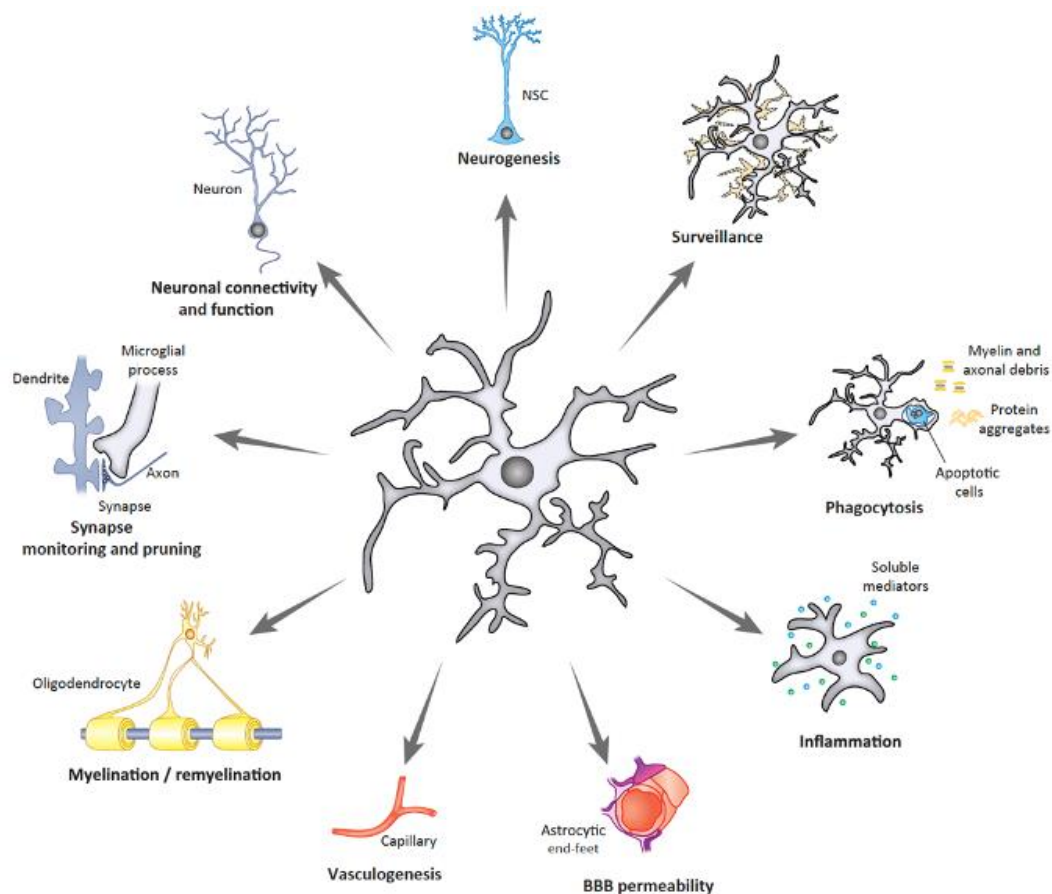


Figure 6. Microglial key functions. Microglia carry out several functions that are to some extent altered in pathological conditions, such as synapse monitoring and pruning, and also interact with other brain cells, impacting on their functions: neurons and their connectivity, neural stem cells and neurogenesis, oligodendrocytes and myelination/remyelination, endothelial cells and vasculogenesis, and astrocytes and blood-brain barrier permeability. Moreover, under pathological situations microglia perform classical immune functions such as release of inflammatory mediators and phagocytosis of cellular debris (apoptotic cells, axonal debris and myelin waste). Taken from (Sierra et al., 2019).

2.4.1. Synaptic homeostasis

Microglia are indispensable for normal brain development and synaptic homeostasis. During CNS development, more synapses are produced than are finally required, thus a remodeling of neuronal circuits is needed. Microglia play an important role eliminating the immature synapses and strengthening the mature ones (Katz and Shatz, 1996; Paolicelli et al., 2011). During postnatal development, microglia have a prominent role in synapse pruning by engulfing presynaptic elements (Schafer et al., 2012). Moreover, in the adult brain microglia have been involved in reshaping neuronal circuits via trogocytosis or partial phagocytosis of presynaptic elements (Weinhard et al.,

2018). However, excessive microglial synaptic pruning, especially neurophagy, may contribute to pathology in AD (Vilalta and Brown, 2018).

2.4.2. Neurogenesis

During adulthood, microglia have been demonstrated to regulate neurogenesis through the phagocytosis of apoptotic newborn neurons in the hippocampus and in the subventricular zone (Sierra et al., 2010; Fourgeaud et al., 2016). However, under pathological conditions, aging or neurodegenerative disorders, microglial activation triggers the release of pro-inflammatory cytokines, which has negative consequences for neurogenesis (Sierra et al., 2014).

2.4.3. Neuronal survival and death

Microglial immune function is controlled by neurons by producing two classes of signals, called 'On' and 'Off' signals. Off signals are constitutively expressed by neurons in the healthy brain and maintain microglia in a surveillant phenotype, while the disappearance of these Off signals causes microglial responses. Conversely, On signals are expressed in damaged neurons to activate either supportive or neurotoxic microglial functions (Biber et al., 2007). Examples of Off signals are CD200 and fractalkine, constitutively expressed by neurons. When these molecules are recognized by their microglial receptors (CD200R and CX3CR1, respectively), neurotoxic microglia activity is suppressed (Biber et al., 2007). On signals, expressed by damaged neurons, include purines such as ATP and UTP, for which microglia express the corresponding receptors (mainly P2X4 and P2X7); glutamate, which activates microglial glutamate receptors, triggering the release of TNF- α ; or apoptotic bodies, which activate the TREM2-DAP12 signaling in microglial cells, increasing non-inflammatory phagocytic activity of microglia (Biber et al., 2007; Nayak et al., 2014).

2.4.4. Myelination

Microglia are also involved in the myelination process through the production of growth factors that regulate the proliferation and survival of oligodendrocytes (Park et al., 2001). Furthermore, microglial phagocytic activity is crucial for remyelination after myelin injury, since the removal of damaged myelin is required to avoid further lesions and also facilitates the recruitment and differentiation of oligodendrocyte precursor cells (Kotter, 2006; Domingues et al., 2021).

2.4.5. Vasculogenesis

It has been suggested that microglia also play a role in embryonic vasculogenesis, since microglial cells have been observed in close association with developing vessels (Rezaie et al., 2005) and the lack of microglia is linked to a decrease in the developing vasculature (Kubota et al., 2009). In the adult brain, microglia have been described to physically interact with the neurovasculature and to promote angiogenesis, participating in the formation of new blood vessels (Zhao et al., 2018). In addition, in neurodegenerative contexts such as AD microglia are thought to promote vascular pathology, including a breakdown of the BBB (Zhao et al., 2018).

2.4.6. The immune response

Microglia are the main immune cells in the CNS (Kettenmann et al., 2011). Microglia modulate the innate immune response and also participate in the adaptative immune response. Innate immunity is the immediate response of the organism against any harmful stimulus, such as pathogens or apoptosis, by triggering an inflammatory response (Ferrero-Miliani et al., 2006). In response to CNS injury or neurodegenerative conditions, microglia undergo phenotypic change and, concomitantly, other immune cells from the peripheral blood infiltrate into the brain to protect this tissue by mounting an inflammatory response (Garden and Möller, 2006). Once infection is contained, microglia switch to a phagocytic phenotype and remove infective agents and debris. Phagocytosis constitutes, along with inflammation, the fundamental component of the innate immune response. Moreover, microglia engulf cell debris and pathogens and present them to T cells to develop an adaptative immune response (Garden and Möller, 2006). Interestingly, experimental models of AD revealed that microglial innate immunity can be activated by fibrillar A β , which is recognized by microglial pattern recognition receptors (PRRs), present both on the cell surface, such as Toll-like receptors (TLRs) TLR2 and TLR4, and intracellularly, such as the NLRP3 inflammasome. Such activation leads to the production of pro-inflammatory cytokines (Cisbani and Rivest, 2021).

2.4.7. Inflammatory response

Inflammation, a mechanism triggered by the immune system in response to harmful stimuli such as pathogens or excessive cell death, has been reported in all neurodegenerative disorders (Amor et al., 2010; Matejuk et al., 2021). Upon an inflammatory stimulus, microglia respond by releasing cytokines, chemokines and complemental proteins (Nayak et al., 2014).

2.4.7.1. Cytokines

Cytokines, the major orchestrators of the microglial inflammatory response, are proteins that coordinate the immune response by triggering cell proliferation, differentiation, apoptosis or release of other cytokines (Zhang et al., 2009). Remarkably, microglia are not the only source of these molecules, since they are also produced by astrocytes, oligodendrocytes, neurons and endothelial cells (Benveniste, 1992). Several cytokines have been described with either pro-inflammatory or anti-inflammatory effects, including interleukins (ILs), which help to activate several immune cells and facilitate their migration towards the affected tissue (Brocker et al., 2010); interferons, crucial during the innate immune response to viruses (Fensterl and Sen, 2009); colony-stimulating factors (CSFs), which stimulate the proliferation and differentiation of immune cells and are also related to the production of other cytokines (Jeannin et al., 2018); and tumor necrosis factors (TNFs), relevant during the initiation of the inflammatory response and involved in proliferation and apoptosis (Sun and Fink, 2007).

Pro-inflammatory cytokines

Pro-inflammatory cytokines are essential for the initiation of the inflammatory response. Although their main role is to defend the organism, an excessive and continuous release of pro-inflammatory cytokines results detrimental in pathological conditions, aggravating several neurodegenerative disorders (Amor et al., 2010). High amounts of pro-inflammatory cytokines in the brain milieu increase the permeability of the BBB, which results in infiltration of peripheral immune cells into the CNS and neuronal damage through the increase of neurotoxic factors such as ROS or nitric oxide (Sastre et al., 2006; Smith et al., 2012).

- **Interleukin 1 β (IL-1 β):** inducible cytokine involved in the regulation of the innate immune response. IL-1 β has been also implicated in perpetuating immune responses and contributing to disease severity in many CNS diseases, including neurodegenerative disorders (Mendiola and Cardona, 2018). Following microglial stimulation, IL-1 β mRNA is transcribed and translated to produce the IL-1 β precursor, which accumulates inactive in the cytosol. Then, microglial activation results in the assembly of the NLRP3 inflammasome, which activates caspase-1. Active caspase-1 processes the IL-1 β precursor, resulting in the production of mature IL-1 β , which is released to the extracellular space. IL-1 β exerts its biological effects via IL-1 receptor. Among IL-1 β 's downstream targets are the adaptor protein MyD88 and NF- κ B, which promote the expression of many inflammatory genes, including IL-1 β itself (Dinarello, 2009).
- **Tumor necrosis factor alpha (TNF- α):** strong pro-inflammatory cytokine that plays important roles in the immune system during inflammation, cell proliferation, differentiation and apoptosis (Baud and Karin, 2001). A negative feedback has been described to control TNF- α production, by which TNF- α itself increases the synthesis of anti-inflammatory factors, such as IL-10, that negatively regulate TNF- α expression (Zelová and Hošek, 2013). Activation of TNF- α receptors triggers different signaling pathways such as NF- κ B, ERK, JNK and p38 MAPK, which produce downstream cellular responses that lead to apoptosis, necrosis, proliferation, survival and generation of pro-inflammatory mediators (Al-Lamki and Mayadas, 2015).
- **Interleukin 6 (IL-6):** pleiotropic cytokine that not only regulates the immune and inflammatory responses but also is a potent mediator of cellular communication. Although IL-6 is widely produced by many CNS-resident cells, the IL-6 receptor, required for cellular responses, is only found on microglia surface (West et al., 2019). IL-6 binding to its receptor can simultaneously elicit distinct or even contradictory physiopathological processes, which are likely discriminated by the cascades of downstream signaling pathways, termed classical and trans-signaling. The classical pathway has been linked with anti-inflammatory effects, while the alternative trans-signaling pathway has been shown to be rather pro-inflammatory (Rothaug et al., 2016).

Anti-inflammatory cytokines

Anti-inflammatory cytokines act as a mechanism to control the duration of the inflammatory response, determining the resolution of inflammatory processes to avoid complications linked to

chronic inflammation (Vezzani et al., 2013). In contrast to the rapid production of pro-inflammatory mediators, immunosuppressive cytokines are typically produced at peripheral sites in a delayed manner to promote tissue repair.

- **Interleukin 4 (IL-4) and interleukin 13 (IL-13):** IL-4, considered the quintessential regulatory cytokine, is structurally and functionally related to another immunomodulatory cytokine, IL-13. Both cytokines are secreted proteins typically considered as anti-inflammatory cytokines due to their ability to downregulate the synthesis of T-helper type 1 pro-inflammatory cytokines. IL-4 can signal through two distinct cell surface receptors, namely type I and type II IL-4 receptors (IL-4R), while IL-13 can only signal through the type II IL-4R (Quarta et al., 2020). Following the correct dimerization of the IL-4 and IL-13 receptor subunits, JAKs kinases are activated. While the type I IL-4 receptor can activate both signal transducer and activator of transcription 6 (STAT6) and insulin receptor substrate (IRS), the type II IL-4 receptor is limited to the STAT6 pathway (Junttila, 2018).
- **Interleukin 10 (IL-10):** immunosuppressive cytokine which acts as an anti-inflammatory modulator of glial activation. IL-10 has multiple immunomodulatory effects, particularly important during the resolution phase of the inflammatory process. When IL-10 binds to its receptors, it triggers the recruitment of Jak1 and Tyk2. Tyk 2 stimulates the PI3K/AKT and p38 pathways, while Jak1 phosphorylates STAT3, which translocates into the nucleus and promotes the expression of many genes that, among others, include SOCS-3. SOCS-3 inhibits the expression of both pro-inflammatory cytokines genes and antigen presentation related genes, resulting in a strong anti-inflammatory response (Porro et al., 2020).
- **Transforming growth factor beta 1 (TGF- β):** pivotal regulator of immune responses, it has been revealed as an essential immune suppressor by controlling the development, differentiation, activation and homeostasis of immune cells (Sheng et al., 2015). Within the CNS, TGF- β and its signaling are indispensable for postnatal microglia maturation, adult microglia homeostasis, and the control of microglia activation in neurodegenerative pathologies. TGF- β is secreted as an inactive dimer bound in a latent complex, preventing TGF- β immediate biological effects. SMADs are regarded as the main downstream effectors of TGF- β signaling, but TGF- β receptors also activate signaling mediators including the ERK, PI3K, AKT, mTOR, JNK and p38 MAPK pathways (Spittau et al., 2020).

2.4.7.2. Chemokines

Chemokines are molecules secreted during the inflammatory response whose main function is mediating the motility of immune cells towards the infection site in a process named chemotaxis (Hughes and Nibbs, 2018). During the inflammatory challenge, microglia secrete several chemokines such as macrophage inflammatory protein 1-alpha (MIP-1A), monocyte chemoattractant protein-1 (MCP-1) and chemokine ligand 5 (CCL5). Furthermore, chemokines are involved in other immune processes such as phagocytosis, as is the case of fractalkine (Lehnardt, 2009).

2.4.8. Phagocytosis

Phagocytosis is the cellular process of engulfment and digestion of large (>0.5 μm) extracellular particles, including other cells or parts of cells (Vilalta and Brown, 2018). It is a dynamic process that consists of various steps: first, the targets of phagocytosis are either recognized by phagocytic receptors or endocytosed through non-specific mechanisms; next, the ingested targets are encapsulated and incorporated into the early endosome, where they are sorted either for degradation or recycling pathways. Finally, in the degradation pathway early endosomes mature into late endosomes, which fuse with lysosomes, acidic vesicles containing proteases, and the phagocytosed targets are degraded (Kono et al., 2021).

Microglia, the main professional phagocytes in the brain, have been described to phagocytose a wide variety of materials during both physiological and pathological conditions, including synapses, microbes, axonal and myelin debris, pathogenesis-related proteins such as $\text{A}\beta$, living cells and also apoptotic cells (Wolf et al., 2017).

2.4.8.1. Axonal and myelin debris

Microglial cells play an important role in removing debris resultant from white matter degeneration, such as axons and myelin corpses, main obstacles for axonal outgrowth after nerve injury in the CNS. This function is important not only to facilitate the start of remyelination processes by oligodendrocytes, but also to quickly remove harmful stimuli that could trigger an exacerbated neuroinflammatory response (Jin and Yamashita, 2016; Safaiyan et al., 2016).

2.4.8.2. Apoptotic cells

Apoptosis or programmed cell death is a frequent event that occurs throughout life in almost any tissue, including brain, as a normal part of development. Apoptosis can be initiated by two different mechanisms: the extrinsic pathway, activated by death signals and mediated by death receptor ligands; and the intrinsic pathway, activated by cell stress, leading to the release of cytochrome C from mitochondria via Bcl-2 proteins (Taylor et al., 2008). Phagocytosis of apoptotic neurons is mediated by neuronal exposure of phosphatidylserine, which is detected by microglial phagocytic receptors (Vilalta and Brown, 2018).

2.4.8.3. Living cells (phagoptosis)

Phagoptosis is a type of cell death in which a living cell dies as a result of being phagocytosed by another cell. This process is triggered when phosphatidylserine and other considered “eat me” signals such as calreticulin are reversibly exposed on the surface of viable cells, causing its engulfment (Brown and Neher, 2012). Some studies have reported that living neurons are phagocytosed by microglia activated with lipopolysaccharide (LPS) or $\text{A}\beta$ (Neher et al., 2011; Neniskyte et al., 2011).

2.4.9. A β internalization

One of the most important functions of microglial cells in AD is the regulation of A β levels in the brain. A β can be internalized by microglia by different mechanisms:

- ❖ **Pinocytosis:** soluble A β can be cleared through fluid phase pinocytosis, with spontaneous formation and internalization of pinosomes from membrane ruffles (Mandrekar et al., 2009). Furthermore, soluble A β is able to induce its pinocytic self-uptake by stimulating the P2Y4 receptor and the PI3K/AKT cascade through autocrine ATP signaling (Li et al., 2013).
- ❖ **Phagocytosis:** uptake of fibrillar A β is modulated by other molecules, being increased when bound by the C3b complement system (Lee and Landreth, 2010) and attenuated by oligomeric A β (Pan et al., 2011).
- ❖ **Receptor-mediated endocytosis:** oligomeric and fibrillar A β are primarily internalized through receptor-mediated endocytosis, via surface receptors (Ries and Sastre, 2016):
 - Scavenger receptors, such as the scavenger receptor A and the glycoprotein CD36;
 - Toll-like receptors, such as TLR2 and TLR4;
 - RAGEs, which mediate the inflammatory cascade in activated microglia;
 - Formyl peptide receptors (FPRs), which bind to A β_{1-42} and activate its internalization, and also interact with RAGEs to initiate microglial signaling cascades in response to A β ;
 - LRP1, involved in lipid homeostasis and also a large endocytic receptor for more than 40 ligands including ApoE and A β ;
 - Triggering receptor expressed on myeloid cells 2 (TREM2), which enhances microglial phagocytic capacity and reduces TLR-mediated signaling, promoting anti-inflammatory cytokine expression.

A β internalization by microglia induces a variety of changes that include the release of cytokines and the production of ROS (Mosher and Wyss-Coray, 2014). But what happens to A β after being endocytosed by microglial cells? In addition to the A β clearance mechanisms described in Section 1.1.3, partially degraded A β peptides have also been found in microvesicles and exosomes, which suggests that internalization is not the ultimate step of A β removal (Kono et al., 2021).

A summary of the managing of A β by microglial cells can be found in **Figure 7**.

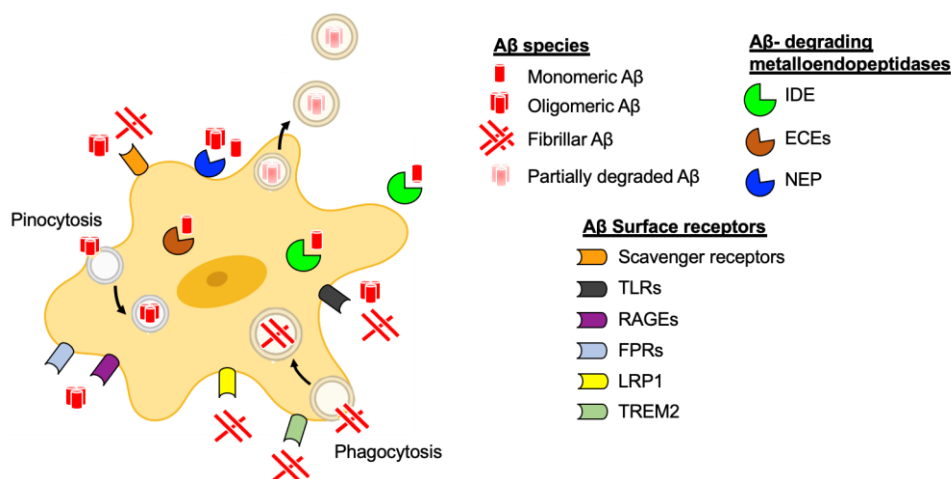


Figure 7. A β managing by microglial cells. Microglia can internalize A β by three different mechanisms: pinocytosis (oligomeric A β), phagocytosis (fibrillar A β) and receptor-mediated endocytosis (both oligomeric and fibrillar A β). Once internalized, A β can be degraded by different cellular degradation pathways, cleaved by metalloendopeptidases, or exported outside the cells in extracellular vesicles.

2.5. Microglial dysfunction in AD

Because of the close relationship between microglia and neurons, microglia respond to and can sometimes exacerbate neurodegenerative conditions, contributing to a chronic neuroinflammatory state in the CNS, although their initial role is neuroprotective.

The precise function of microglia during the course of AD remains controversial, although there is no doubt that microglia play an active role (either beneficial or detrimental). Numerous studies suggest that microglia play an important early role in slowing the toxic effects of A β and hence the progression of neurodegeneration, but are less involved later in the disease as their phagocytic function declines and their neuroprotective function wanes over time. In fact, a transition from phagocytosis to pro-inflammatory cytokine production with minimal phagocytic activity could position microglia as late-stage exacerbators of AD (Nayak et al., 2014).

3. Diabetes mellitus

The term “diabetes mellitus” (DM) describes a group of metabolic disorders characterized by the presence of hyperglycemia in the absence of treatment. They are chronic diseases that occur either when the pancreas does not produce enough of the hormone insulin, or when the body cannot effectively use the insulin it produces (Geneva: World Health Organization, 2019).

The prevalence of diabetes has exponentially increased in the recent years. In 2019, 463 million people had diabetes, which represents a 9.3% of the global population at the time. Without sufficient action to address this global health problem, it has been predicted that 578 million people (10.2% of the population) will have diabetes by 2030, and that number will jump to 700 million (10.9%) by 2045 (International Diabetes Federation, 2019), as depicted in **Figure 8**.

Number of adults (20–79 years) with diabetes worldwide

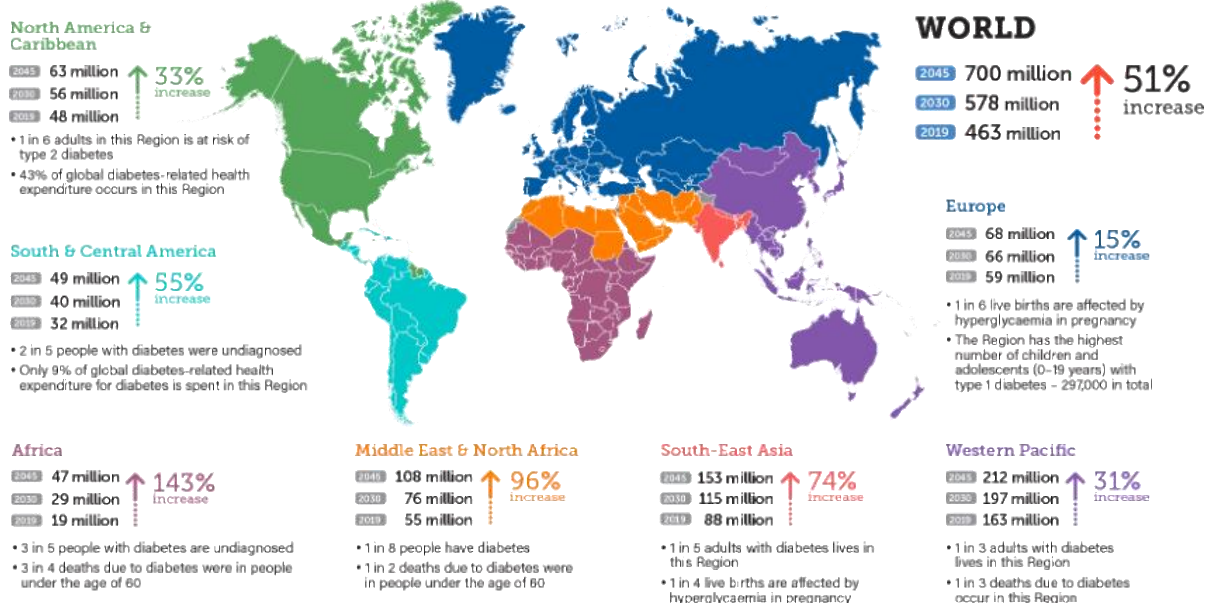


Figure 8. Prevalence and worldwide distribution of diabetes in 2019 and estimated prevalence for the years 2030 and 2045. Taken from (*International Diabetes Federation, 2019*).

The main categories of diabetes are type 1 and type 2 diabetes mellitus (Sociedad Española de Diabetes, 2017).

- Type 1 diabetes mellitus (T1DM) is an autoimmune disease that causes specific destruction of pancreatic β -cells, the main insulin-producing cells in the body. This destruction leads to low or no insulin secretion into the bloodstream, with the consequent increase in blood glucose levels (Bach, 1994). T1DM represents 5-10% of the total cases of the disease.
- Type 2 diabetes mellitus (T2DM) is characterized by an insufficient response to insulin by the peripheral tissues of the body (insulin resistance) (Kahn et al., 2014). T2DM accounts for the vast majority of diabetes cases worldwide (around 90-95%).

3.1. Insulin deregulation in pre-diabetes and T2DM

In healthy individuals, their digestive system breaks down the food they eat into glucose, and insulin, produced by pancreatic β -cells, activates glucose transport into the cells to produce energy. Conversely, in people with insulin resistance the cells do not respond normally to insulin and glucose cannot enter the cells so easily, which leads to increased insulin demand. Initially, pancreatic β -cells display an enhanced insulin secretion, producing high amounts of insulin to try to lower glycemia (compensatory mechanism for insulin resistance); but this insulin hypersecretion leads to eventual β -cell failure, with a decreased functional β -cell mass, resulting in a decreased insulin secretion, hyperglycemia and diabetes onset (Kahn et al., 2014) (**Figure 9**).

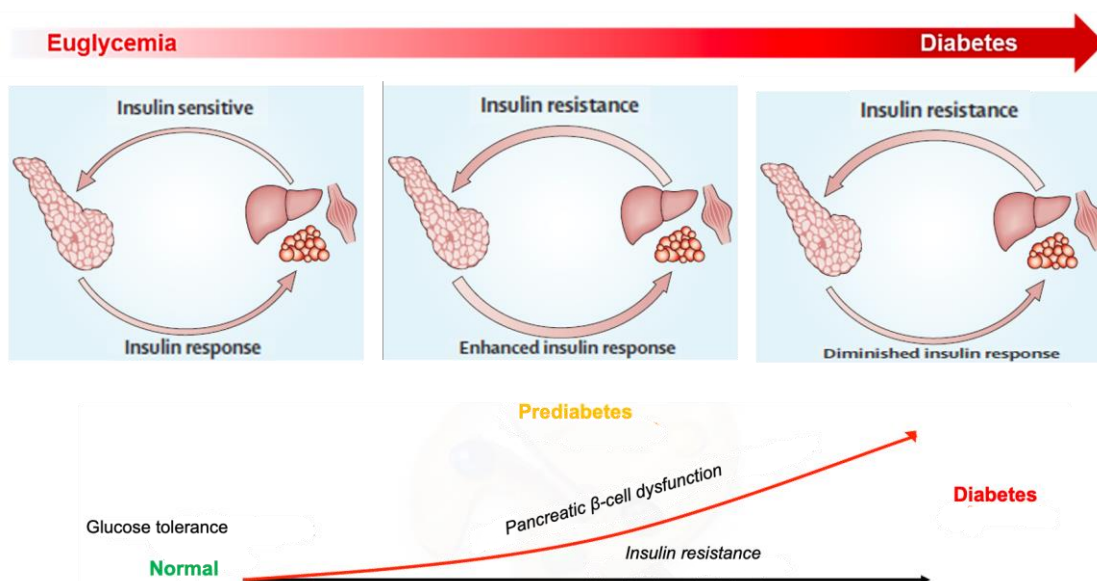


Figure 9. Pathogenesis of type 2 diabetes. Sequence of events in the development of type 2 diabetes, involving a feedback loop between pancreatic β -cells and insulin-sensitive tissues. Image adapted from (Kahn et al., 2014).

3.2. Insulin signaling

Insulin is the major regulator of peripheral glucose levels. In response to elevated blood glucose levels, pancreatic β -cells secrete insulin (packaged and co-secreted with amylin), which stimulates the uptake of glucose by liver, muscle and adipose tissue (Boucher et al., 2014).

Insulin signaling starts when insulin binds to the insulin receptor (InsR), which is formed by two extracellular alpha subunits and two transmembrane beta subunits, the latter contain a tyrosine kinase domain which is auto phosphorylated when insulin binds to InsR. Downstream, InsR activation induces the recruitment and phosphorylation of insulin receptor substrates (IRSs). Activated IRSs are responsible for the activation of the two major insulin signaling pathways: the MAPK pathway, involved in cellular growth and development; and the PI3K/AKT pathway, crucial for metabolic functions. Interestingly, signaling pathways activated by pro-inflammatory cytokines such as $\text{TNF}\alpha$ and IL-6 have crosstalks with insulin signaling (Taniguchi et al., 2006), as shown in **Figure 10**.

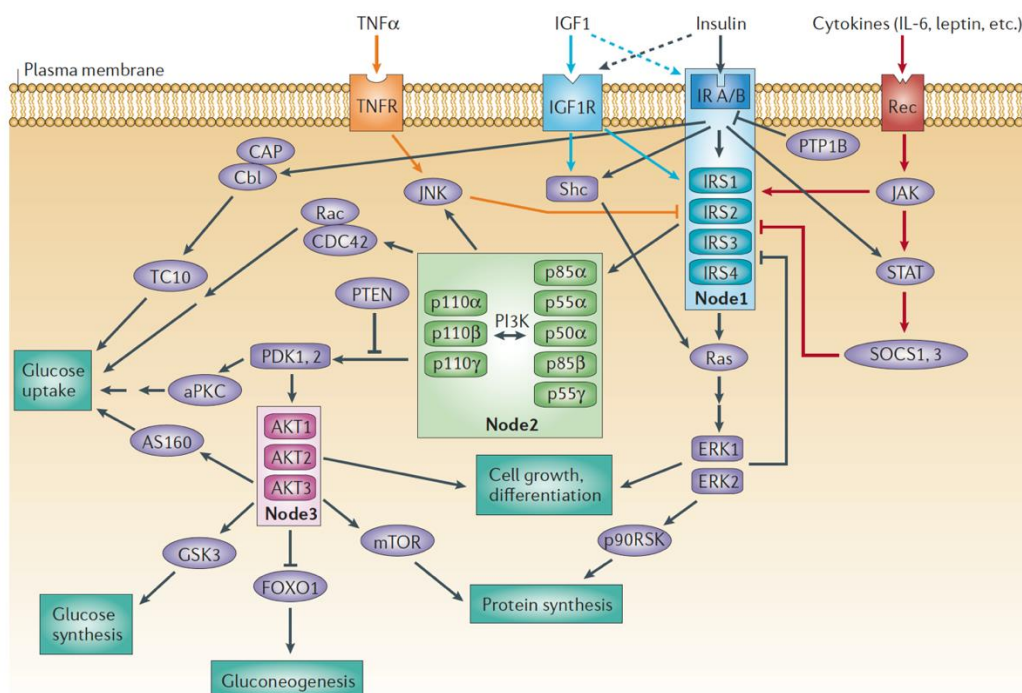


Figure 10. Critical nodes in the insulin-signaling network. Critical nodes form an important part of the signaling network that functions downstream of the insulin receptor (*InsR*) and the insulin growth factor-1 receptor (*IGF1R*). Signaling pathways that are activated by cytokines such as *TNF α* , *IL-6* and leptin interfere with insulin signaling through crosstalk (orange and red arrows). Three important nodes in the insulin pathway are the *InsR* substrates (*IRS*), the *PI3K* with its several regulatory and catalytic subunits, and the three *AKT* isoforms. Taken from (Taniguchi et al., 2006).

4. Insulin-degrading enzyme

Insulin-degrading enzyme (IDE; EC 3.4.24.56, also known as insulysin, insulin protease or insulinase) was discovered more than 70 years ago by Mirsky and Broh-Kahn in several tissue extracts and was named after its ability to strongly bind and degrade insulin (Broh-Kahn and Mirsky, 1949). IDE is a 110-kDa zinc-metalloendopeptidase that belongs to the clan ME, family M16A of metalloproteases, also known as “inverzincins” because they are characterized by a zinc-binding consensus motif (HxxEH, where “x” means any amino acid) that is inverted with regard to the sequence in the majority of conventional M16 peptidases (HexxH) (Hooper, 1994). M16A proteases are typically large proteins (>100 kDa) related by primary sequence, whose zinc-metalloprotease core motif is located within around 200 residues of the N-terminal. In addition, these proteases also have a pair of glutamate residues located 70 and 77 amino acids distal to the core motif, constituting an extended metalloprotease motif (HXXEHX₆₉EX₆E) (Becker and Roth, 1992).

IDE is ubiquitously expressed in multiple tissues (Shen et al., 2006). Although liver, kidney and muscle are major tissues involved in insulin metabolism, the highest levels of IDE expression in rats are found in testes, brain and tongue, which suggests that IDE may have other functions besides degrading insulin (Kuo et al., 1993). The expression of IDE is also developmentally regulated in

some tissues such as the brain, indicating that IDE might play a significant role in regulating cell growth and development (Kuo et al., 1993). Furthermore, IDE expression is affected by aging, with IDE activity significantly decreased in both muscles and liver of old animals compared to young ones (Runyan et al., 1979).

IDE has a high degree of evolutionary conservation. In eukaryotic organisms, IDE exhibits homology in both exonic and intronic regions, suggesting a functional relevance of the enzyme in cellular function (Affholter et al., 1988; Fujita et al., 1994; Kuo et al., 1990; Qiu and Folstein, 2006).

4.1. Molecular characteristics of IDE

The *Ide* gene is located on human chromosome 10 and mouse chromosome 19, respectively, and produces a single polypeptide with a molecular weight of ~110 kDa (Affholter et al., 1990).

The IDE enzyme assembles as a stable homodimer, and each monomer can be divided into two roughly equal sized subunits (~55 kDa), the N-terminal portion (IDE-N) and the C-terminal part (IDE-C), which are joined by a 28 amino acid residue loop (Shen et al., 2006). IDE can also be further subdivided into four domains, with domains 1 and 2 comprising IDE-N, and domains 3 and 4 comprising IDE-C (**Figure 11A**). The overall structure of IDE resembles a clamshell, with IDE-N and IDE-C comprising bowl-shaped domains with their interiors facing one another, connected by a hinge. When the two halves come together, an internal triangular crypt is formed, enclosing its substrates and preventing them to escape (Hulse et al., 2009; Leissring et al., 2021). Due to its dimensions, the crypt limits the size of the substrates to less than 70 amino acids, favoring small substrates which are less than 6 kDa with few positively charged residues at their C-terminus (Malito et al., 2008). The catalytic site is located inside the crypt in IDE domain 1, also known as insulinase domain, and it consists on a catalytic tetramer, HxxEHx₇₆E, in which the binding of the Zn²⁺ ion is coordinated by two histidine residues (H108 and H112) and a glutamate (E189), while a second glutamate (E111) has been demonstrated to be crucial for the activity of the enzyme (Shen et al., 2006). This catalytic site is rich in charged, polar and hydrophobic patches, which facilitate interaction with both IDE-C and substrates. IDE-N also has an exosite, which is approximately 30 Å away from the catalytic site, where the N-termini of ligands are anchored. This exosite may play a role in the positioning of substrates for cleavage, and might also contribute to the unique cleavage patterns of IDE's substrates (Shen et al., 2006).

The IDE-N and IDE-C subunits can pivot on the hinge, adopting “open” and “closed” conformations (Hulse et al., 2009). IDE needs to undergo a significant conformational change from the open state, which can incorporate the substrate, to the closed conformation, enabling precise substrate recognition and hydrolysis of the peptide, and also preventing the binding of another substrate (**Figure 11B**). The switch between open and closed conformations of IDE is crucial for the proteolytic activity; in fact, mutations that prevent or facilitate the open conformation inhibit or increase, respectively, the catalytic rate of the enzyme (Shen et al., 2006). IDE has been found to

exist as a mixture of monomers, dimers and tetramers in equilibrium, with dimers being the dominant form (Song et al., 2003). The aggregation status of IDE is important in regulating its function: dimers are reported to be the most active form, while in tetrameric structures the interaction of two IDE dimers potentiates the closed conformation of the enzyme and therefore decreases its catalytic activity (Shen et al., 2006; Song et al., 2003).

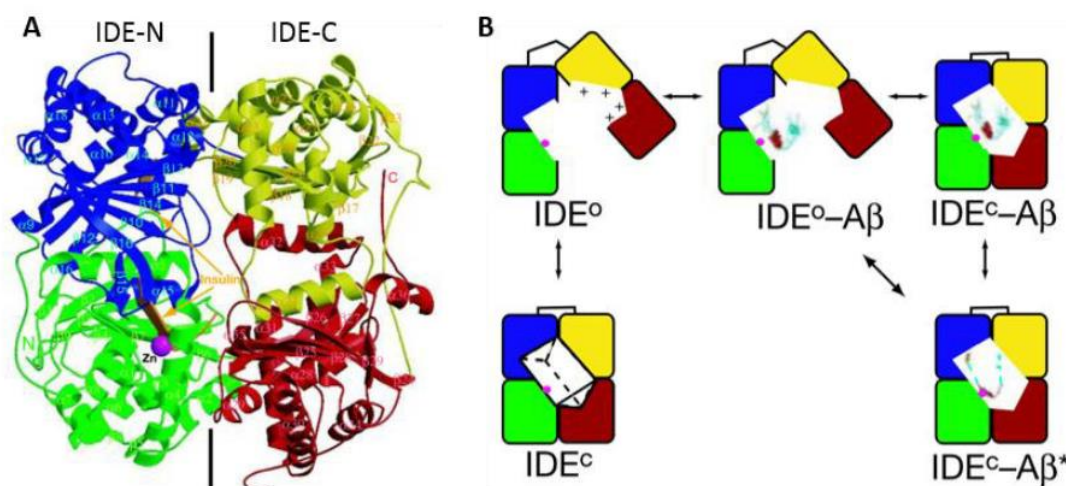


Figure 11. Structure and functional mechanism of IDE. **A)** Secondary structure of human IDE-E111Q in complex with the B chain of insulin after X-ray crystallography. Glutamate 111 is replaced with glutamine to prevent the catalysis of substrates. The insulin B chain is colored in orange, and the Zn^{2+} ion is represented in magenta. **B)** Model of the IDE mechanism of substrate binding and recognition including a conformational switch from an open (IDE°) to a closed (IDE^c) conformation. Binding of $A\beta$ is shown as an example. The binding of $A\beta$ occurs in the open state, while proper recognition, conformational changes in the substrates and cleavage occur in the closed state of IDE. Taken from (Shen et al., 2006).

4.2. IDE functions

IDE was first characterized in 1949 by its ability to degrade insulin *in vitro*. Since then, many proteolytic and non-proteolytic functions have been proposed for this enzyme.

4.2.1. Proteolytic functions of IDE

During the last decades, several short peptides with molecular weights of 3-10 kDa have been shown to be putative substrates of IDE, including insulin, insulin-like growth factors I and II, glucagon, somatostatin, amylin, $A\beta$, amyloid Bri and amyloid Dan, amyloid precursor protein intracellular domain, atrial natriuretic peptide, bradykinin and kallidin, calcitonin and β -endorphin, growth hormone-release factor, transforming growth factor- α , oxidized hemoglobin, cytochrome c, chemokine ligand (CCL)-3 and CCL4 and human immunodeficiency virus type 1 (HIV-1)-p6 protein (reviewed at (González-Casimiro et al., 2021)). These substrates share little to no homology of primary amino acid sequence, but possess a 7-13 amino acid sequence that contains a large hydrophobic group and have similar secondary structure and amyloidogenic character, prone to form

β -sheets (Kurochkin, 2001; Qiu and Folstein, 2006). Therefore, IDE could perform a housekeeping task as a scavenger for amyloid- β forming peptides.

4.2.2. Non-proteolytic functions of IDE

IDE has been described to directly interact with androgen and glucocorticoid receptors (Kupfer et al., 1994), suggesting a relevant role for this enzyme in steroid hormone action and metabolism. Other work described colocalization of IDE with the cytoplasmic tail of the scavenger receptor type A in macrophages (Caravaggio et al., 2013), while others described co-immunoprecipitation of IDE with the mitochondrial ADP-ribosyltransferase sirtuin 4 (Ahuja et al., 2007) and with the tumor suppressor PTEN (Liu et al., 2019). IDE has also been described to interact with intermediate filaments, specifically with disassembled and soluble vimentin/nestin complexes during mitosis (Chou et al., 2009). In line with this, Tundo and colleagues reported that IDE downregulation impairs SH-SY5Y proliferation and viability (Tundo et al., 2013).

Focusing on metabolism, emerging evidence has identified several non-proteolytic functions of IDE that might be perturbed in T2DM, implying that IDE's functional role is more complex than it was initially believed (González-Casimiro et al., 2021). For instance, although pancellular genetic deletion of *Ide* in mice consistently produces a pronounced diabetic phenotype (Abdul-Hay et al., 2011; Steneberg et al., 2013), this phenotype has variously been associated with hyperinsulinemia (Abdul-Hay et al., 2011) or hypoinsulinemia (Steneberg et al., 2013) in different studies. Liver-specific deletion of IDE, meanwhile, results in decreased insulin sensitivity but —notably— does not impair insulin clearance (Villa-Pérez et al., 2018; Merino et al., 2020). Of special interest, in studies of *Ide*-null mice, Steneberg and colleagues identified a key role for IDE in the regulation of insulin secretion from pancreatic β -cells (Steneberg et al., 2013). Genetic deletion of IDE exclusively in β -cells produced impaired glucose-stimulated insulin secretion, along with elevated basal constitutive insulin secretion, decreased cell surface-associated levels of the glucose transporter GLUT2, and a phenotype of β -cell functional immaturity (Fernández-Díaz et al., 2019). These findings, among many others (González-Casimiro et al., 2021), suggest that IDE is a pleiotropic protein whose involvement in the pathogenesis of T2DM is likely to be complex and multifaceted.

4.3. Subcellular localization of IDE

The discovery of IDE as insulin-degrading enzyme (Broh-Kahn and Mirsky, 1949) and as an A β -degrading enzyme (Kurochkin and Goto, 1994) raised questions about precisely where IDE interacts with these substrates. Since then, the subcellular localization of IDE has been extensively studied; however, it remains controversial. The majority of IDE is unquestionably present in the cytosol (Akiyama et al., 1988; Duckworth, 1988; Leissring, 2021), but it has been reported in many other subcellular compartments, including mitochondria (Leissring et al., 2004), endosomes (Hamel et al., 1991; Seabright and Smith, 1996; Song et al., 2017), peroxisomes (Authier et al., 1995), multivesicular bodies (Bulloj et al., 2010; Tamboli et al., 2010), plasma membrane (Duckworth,

1979; Yokono et al., 1979; Vekrellis et al., 2000), on the cell surface (Bulloj et al., 2010; Yokono et al., 1982; Goldfine et al., 1984), at the extracellular space (Qiu et al., 1997), in exosomes (Tamboli et al., 2010; Bulloj et al., 2010; Glebov et al., 2015) and even in human cerebrospinal fluid (Qiu et al., 1998).

These contradictory antecedents reflect the need to address IDE subcellular localization as a paramount point to understanding how IDE can perform its proposed functions.

4.4. Genetic linkage of *IDE* with disease

Various genetic studies have shown that chromosome 10 contains potentially important novel genes for AD as well as T2DM (reviewed at (Qiu and Folstein, 2006)). Since *IDE* gene is located on chromosome 10q23-q25 (Affholter et al., 1990), and IDE has been demonstrated to degrade insulin, amylin and A β , it is reasonable to hypothesize that *IDE* is a candidate gene for both T2DM and AD.

There is compelling evidence that the region in and/or around *IDE* might be genetically associated with both AD (Kehoe et al., 1999; Myers, 2000; Bertram, 2000; Bian et al., 2004; Liu et al., 2007; Hamshere et al., 2007; Muller et al., 2007; Vepsalainen et al., 2007; Björk et al., 2007; Zuo and Jia, 2009; Carrasquillo et al., 2010) and T2DM (Duggirala et al., 1999; Wiltshire et al., 2001; Karamohamed et al., 2003; Furukawa et al., 2008). Furthermore, *IDE* has been linked to other quantitative indices of AD, such as plasma A β levels, memory and cognitive function, CSF levels of tau protein, cerebral A β and neurofibrillary tangles load (Liu et al., 2007; Muller et al., 2007; Prince et al., 2003). Quantitative indices of T2DM such as elevated fasting plasma glucose levels (Karamohamed et al., 2003; Meigs et al., 2002), plasma insulin levels (Gu et al., 2004; Marlowe et al., 2006) and age of onset (Duggirala et al., 1999) have also been associated with the chromosomal region encompassing *IDE* gene, and even a study discovered an association between human life span and *IDE* (Hong et al., 2008).

5. “Type 3 diabetes”

AD and DM fall into the category of chronic degenerative diseases and have various overlapping features. Between 2005 and 2006, de la Monte’s group demonstrated brain insulin resistance and insulin deficiency in AD, with an AD Braak-stage dependent decline in insulin and insulin-like growth factor (IGF) signaling, expression and function in the brain. Moreover, they provided evidence about the colocalization of insulin and IGF signaling networks with the brain regions typically affected in AD, suggesting potential adverse consequences of impaired insulin signaling in the brain (De la Monte and Wands, 2005; Steen et al., 2005). The main concept that emerged from these publications was that AD is associated with chronic deficits in insulin/IGF signaling, and therefore AD is in fact a neuroendocrine disorder that shares features with both T1DM (insulin deficiency) and T2DM (insulin resistance). To consolidate this concept, de la Monte proposed that

AD should be referred to as “type 3 diabetes” to better conceptualize its underlying nature (De la Monte and Wands, 2005; Steen et al., 2005).

5.1. Evidence linking Alzheimer’s disease and diabetes

Cross-sectional studies have demonstrated the association between AD and DM in a bidirectional manner: T2DM is considerably over-represented in AD patients in comparison with non-AD controls (Kuusisto et al., 1997; Ott et al., 1996; Stewart and Liolitsa, 1999), and on the other hand large population-based longitudinal studies have shown that T2DM may significantly increase the risk of AD (Ott et al., 1999; Leibson et al., 1997; Xu et al., 2004; Arvanitakis et al., 2004). Furthermore, both AD and T2DM have an increased prevalence with age (Davidson, 1979; Von Strauss et al., 1999), which suggests that a common pathological mechanism related with aging might be involved in both diseases.

There are some pathological similarities between AD and T2DM. Both diseases are characterized by cytotoxic deposit of amyloid peptides: A β in the brain of AD patients and amylin in the islets of Langerhans in the pancreas of most T2DM patients (De la Monte and Wands, 2005). Moreover, AD patients are more prone to have islet amyloid deposits than non-AD controls, which constitutes further evidence linking AD to T2DM (Janson et al., 2004). Conversely, T2DM patients have been shown to be more susceptible to cognitive impairment (Sinclair et al., 2000; Grodstein et al., 2001; Arvanitakis et al., 2004).

5.2. Transport of glucose and insulin into the brain

Glucose uptake by the brain is independent of insulin but regulated by the insulin-insensitive glucose transporter GLUT1. In most cases, glucose levels are about twice as high in blood as in the brain, thus driving the glucose transport in the blood-to-brain direction. The non-insulin sensitive glucose transporters GLUT1 (astrocytes), GLUT3 (neurons) and GLUT5 (microglia) account for the majority of glucose uptake by the CNS (Banks et al., 2012).

Insulin belongs to a superfamily that includes IGF-I and IGF-II. In humans, insulin is mainly secreted from the pancreas when blood glucose levels are sensed to be high, while IGF-I secretion from the liver is stimulated by growth hormone. The ancestral insulin-like peptide is postulated to have functioned as a mitogenic growth factor. In mammals, the IGFs have assumed the mitogenic role while insulin evolved to be a metabolic regulatory hormone (Chan and Steiner, 2000). The brain endothelial cells that form the BBB possess insulin-binding sites, which are thought to perform two functions: some of them transport insulin across the barriers and others act as classic receptor sites (reviewed at (Banks et al., 2012)). Insulin crosses the BBB by a saturable mechanism, in a rate averaging about 0.5-0.6 $\mu\text{l/g-min}$, in a process mediated by an insulin transporter (Banks et al., 2012). This insulin transport is affected by different factors, including obesity, inflammation, glycemia, diabetes mellitus and levels of circulating triglycerides. In humans, the CSF:serum ratio of insulin

levels is reported to be reduced in the presence of whole-body insulin resistance, as well as with increasing age and in AD (Arnold et al., 2018). Broadly speaking, insulin effects on the brain are mainly related to food intake regulation and cognition. Remarkably, CNS insulin has the opposite effects of peripheral insulin, increasing blood glucose levels, decreasing feeding and body weight and even decreasing blood levels of insulin (Banks et al., 2012).

5.3. IDE as candidate pathophysiological link between AD and DM

Insulin has been demonstrated to regulate A β levels both in the CNS and in the periphery, although the mechanisms controlling A β levels are unclear. *In vivo* studies demonstrated that AD patients respond differently to insulin treatment in comparison with healthy controls: while levels of plasma A β decreased in healthy controls after receiving a peripheral insulin infusion, the AD patients showed an increase in A β levels in a dose-dependent manner (Kulstad et al., 2005). Since IDE degrades insulin with higher affinity than A β [$K_m \sim 100$ nM *vs* >2 μ M, respectively (Hoyer, 2006)], a widely-used hypothesis postulates that high insulin concentrations decrease IDE-mediated A β degradation due to competitive inhibition (Qiu and Folstein, 2006). Nevertheless, insulin levels in the brain are ~ 3.8 pM (Geijselaers et al., 2017), much lower than the insulin K_m , and thus unlikely to competitively inhibit A β degradation. Therefore, the hypothesis about competitive inhibition needs to be reformulated (Pivovarova et al., 2016). Nonetheless, insulin is known to increase A β via other mechanisms, such as upregulation of APP trafficking, favoring the amyloidogenic pathway and also increasing A β secretion in the N2a neuroblastoma cell line (Gasparini et al., 2001), or inhibiting A β degradation *in vitro* in conditioned media produced by the BV-2 microglial cell line (Qiu et al., 1998). Because insulin increases IDE expression through the PI3K pathway (Zhao, 2004), brain insulin resistance might lower IDE expression, which consequently would decrease IDE-mediated A β degradation. These antecedents postulate IDE as a pathophysiological link between AD and T2DM (Pivovarova et al., 2016).

The levels of IDE have been found to decline as a result of aging in certain brain areas susceptible to AD pathology, such as the hippocampal regions (Caccamo et al., 2005). Clinical evidence also supports the notion that IDE may be integral to the development and progression of AD, since the activity of IDE was significantly lower in AD brains compared with controls (Pérez et al., 2000). These findings were supported by a larger study that found decreased levels of IDE mRNA and protein in hippocampal regions of AD brains compared with healthy brains (Cook et al., 2003). This aging-induced regional decrease in IDE supports the concept that insulin and IDE are relevant molecules in AD pathogenesis.

5.4. Candidate drugs to simultaneously treat AD and DM

AD and DM have traditionally been treated individually as independent disorders. However, given their epidemiological associations and some common pathophysiological mechanisms, common pharmacotherapy should be effective and helpful to manage both diseases together.

5.4.1. Clinical trials

- **Intranasal insulin:** given the insulin deficiency in the pathogenesis of AD, the most obvious therapy is intranasal insulin administration, which can quickly deliver insulin to the CNS avoiding some potential side effects produced by intravenous insulin infusion, such as hypoglycemia. Some studies have shown promising results suggesting that intranasal insulin treatment improves cognitive function in AD and MCI patients. Nevertheless, the sample size of clinical trials exploring insulin administration seems to be relatively low, with a short treatment period. Therefore, longer trials are needed (Li et al., 2015).
- **Metformin:** metformin is an orally active biguanide used to decrease blood glucose levels by increasing insulin-mediated glucose disposal and intestinal glucose use, decreasing fatty acid oxidation and suppressing hepatic glucose output. In this case, two studies showed the beneficial outcome of metformin treatment on cognitive function, either lowering the rate of cognitive impairment in patients with both T2DM and AD in comparison with untreated patients (Domínguez et al., 2012) or decreasing the risk of dementia in patients with T2DM (Hsu et al., 2011). However, another large epidemiological trial including individuals above 65 years old showed that T2DM patients long term-treated with metformin had a slightly higher risk of AD than those who were not treated (Imfeld et al., 2012).
- **Thiazolidinediones:** thiazolidinediones are peroxisome proliferator-activated receptor-gamma (PPAR- γ) agonists and potent insulin sensitizers, whose mechanism involves stimulation of the action of PPAR- γ in response to changes in insulin, triggering a drop in blood glucose. Two studies on AD patients showed that thiazolidinediones had beneficial effects on cognition (Risner et al., 2006; Watson et al., 2005), while a phase III clinical trial in mild to moderate AD found no benefit (Gold et al., 2010). However, the major limitation of thiazolidinediones is the side effects of edema and congestive heart failure, which has caused a restriction in their use as antidiabetic drugs (Li et al., 2015).
- **GLP-1 receptor agonists:** glucagon-like peptide 1 (GLP-1) is a gut-derived incretin hormone that enhances glucose-stimulated insulin secretion and suppresses glucagon secretion. Animal studies have demonstrated that exendin-4 and liraglutide, two GLP-1 receptor agonists, restored impaired insulin signaling, exerting neuroprotective effects, improving cognition and decreasing brain A β accumulation in a mouse model of AD (Bomfim et al., 2012; McClean et al., 2011).
- **Apomorphine:** apomorphine is a drug that promotes intracellular A β degradation and enhanced memory function *in vivo* in an AD mouse model. More recently, this drug has been described to improve neuronal insulin resistance and to activate IDE in mice (Ohyagi et al., 2019).

In summary, although there are some promising candidates to simultaneously treat systemic insulin resistance and AD-related neurodegeneration, none of these drugs has been demonstrated to be totally effective in clinical trials. Therefore, the search for new therapeutic targets is urgently needed.

5.4.2. A novel approach: natural compounds

The marine world is a huge reservoir of a great variety of bioactive compounds. Due to exposure to exceptionally different oceanic environments, marine organisms have the capacity to produce unique natural products with tremendous potential as human medicines. In this context, marine biotechnology is the most powerful tool to discover the many interesting properties of marine organisms (Kim, 2015). Many bioactive and therapeutical compounds highly effective and safe to the human body have been developed from natural compounds. The uppermost focus in natural substance bioactivity has been on antioxidation, anti-inflammation, antitumoral, cytotoxic, antibacterial, antifungal and antiviral effects (Kim, 2019).

Soft corals (octocorals: *phylum Cnidaria*, class *Anthozoa*, subclass *Octocorallia*) are multicellular marine animals, most of which form colonies, mainly in tropical waters, composed of hundreds or thousands of polyps, which cover a soft skeleton composed of a protein/calcium carbonate material. Using allelopathic secondary metabolites, soft corals compete for space and protect themselves against predators, infections and injuries. Thus, these organisms produce a wide variety of structurally diverse compounds, including diterpenes, sesquiterpenes, prostaglandins and steroids, which makes soft corals a rich source of natural compounds (Kim, 2015).

Dr. Mercedes Cueto's group (Instituto de Productos Naturales y Agrobiología (IPNA-CSIC), La Laguna, Spain) recently obtained and characterized new furanocembranolides, highly oxygenated diterpenes into which a γ -lactone subunit is embedded, from extracts of octocorals of the genus *Leptogorgia* (Corraliza-Gómez et al., 2020) (**Figure 12**).

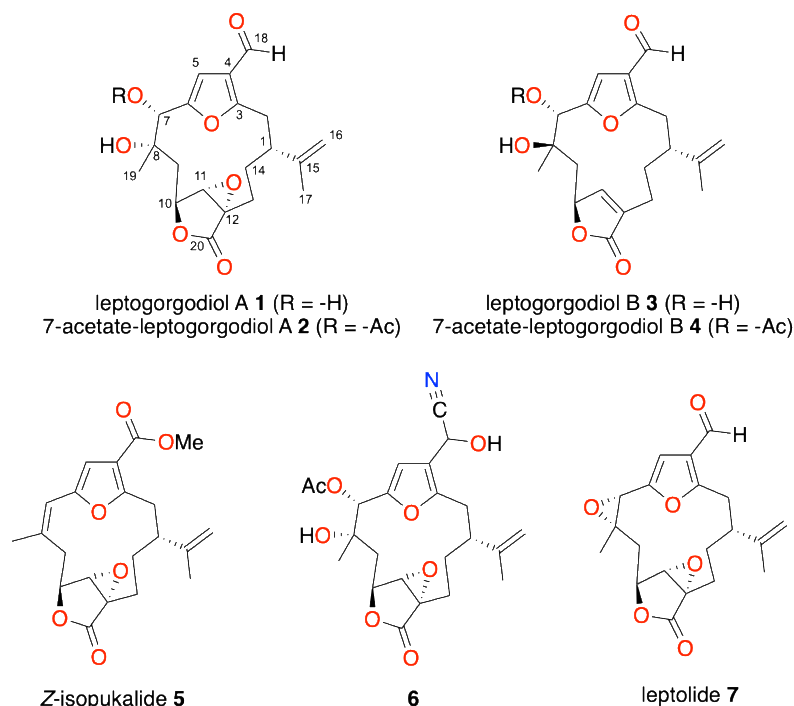


Figure 12. Chemical structures of novel furanocembranolides (**1-6**) and leptolide. These natural products were isolated and characterized by Mercedes Cueto's group (IPNA-CSIC). Taken from (Corraliza-Gómez et al., 2020).

Previous studies in octocorals from the coast of Panama showed that furanocembranolides exert protective effects on pancreatic β -cells, inducing proliferation and protecting them from cytokine-mediated apoptosis both *in vitro* (López-Acosta et al., 2013) and in streptozotocin-induced diabetic mice (López-Acosta et al., 2015). Furthermore, *in vivo* treatment with leptolide, a member of the furanocembranolide family, was shown to act as an insulin sensitizer, enhancing insulin signaling and sensitivity in the liver and muscle of high-fat diet-induced obese mice (Villa-Pérez et al., 2017). Collectively, these results postulate furanocembranolides as feasible treatments for T2DM.

Regarding AD treatment, the amyloid cascade hypothesis has been dominating drug discovery for AD for the last two decades. However, the failure of the development of effective drugs for AD and the multifactorial nature of neurodegenerative disorders urge a paradigm shift in AD drug development from a single target to multiple targets (Gong et al., 2018). Although the pharmacological potential of furanocembranolides remains largely unexplored, two examples of anti-inflammatory activity have been reported in the Raw264.7 macrophage cell line (Chao et al., 2011; Lin et al., 2015). These antecedents suggest that furanocembranolides might be an experimental treatment to be considered to target neuroinflammation concomitant with metabolic impairment and, hence, a good therapeutical approach to treat “type 3 diabetes”.

HYPOTHESIS AND OBJECTIVES

Hypothesis and global aim

The concept “type 3 diabetes” suggests that Alzheimer’s disease (AD) is associated with chronic deficits in insulin signaling, and therefore this neurodegenerative disease can be considered a neuroendocrine disorder with common features with diabetes mellitus (DM). In this context, we hypothesize that:

- AD- and DM-related conditions can lead to changes in IDE expression and trafficking in microglial cells.
- IDE plays an important role in microglial cell polarization.
- IDE might be a pathophysiological link between AD and DM, possibly involved in the brain insulin resistance process.
- Marine natural compounds from the furanocembranolide family are good therapeutical approaches to target neuroinflammation concomitant with metabolic impairment.

The main aim of this study is to characterize the physiological roles of IDE in microglial cells *in vitro* and *in vivo*, in order to get a better understanding about the underlying causes of type 3 diabetes, and to provide a therapeutic approach feasible to treat type 3 diabetes.

Specific objectives

This general aim can be subdivided into the following specific objectives:

1. To explore the effects of DM and AD stimuli on microglial functions and the regulation of IDE expression in a cell-line paradigm.
2. To characterize IDE subcellular localization and trafficking, as well as the evolution of molecular features determining IDE location.
3. To evaluate the role of IDE *in vivo* in a constitutive knock-out mouse paradigm, analyzing metabolic, behavioral, and molecular biological parameters in the brain.
4. To assess the physiological roles of IDE specifically in primary microglial cells, analyzing proliferation, microglial polarization, phagocytosis and A β managing.
5. To test furanocembranolides as a possible treatment for “type 3 diabetes”, feasible to simultaneously improve insulin resistance and neuroinflammation.

MATERIALS AND METHODS

1. Experimental animals

1.1. Animal facilities

Experimental procedures were approved by University of Valladolid Research Animal Ethical Committee and Junta de Castilla y León (JcyL) authorities in accordance with the European Guidelines for Care and Use of Mammals in Research (European Commission Directive 86/609/CEE and Spanish Royal Decree ECC/566/2015). Mice were housed in positive pressure-ventilated racks at $25\pm 1^\circ\text{C}$ with 12 h light/dark cycle (light on from 09:00 to 21:00) at the animal facility of the University of Valladolid (Uva, Spain). Cage enrichment included cotton bedding and opaque tubes. Filtered and UV-irradiated water and standard rodent pellet diet (Global Diet 2014; Harlan Inc., Indianapolis, IN, USA) were available *ad libitum*.

1.2. Constitutive IDE-knockout (IDE-KO) mouse

The *Ide* gene is located in chromosome 19 in mice (NCBI Reference Sequence: NC_000085.6). IDE-knockout mouse ($Ide^{\text{tm}1a(\text{EUCCOMM})\text{Wtsi}}$, hereinafter referred to as IDE-KO) on a C57/BL6J background was kindly provided by Dr. Malcolm Leissring from University of California (Irvine, USA). This mouse has *LoxP* sites flanking exon 3 of the *Ide* gene (Abdul-Hay et al., 2011). *Exon 3* contains the catalytic site sequence, critical for the proteolytic activity of the enzyme. Cre-*LoxP* recombination results in the deletion of exon 3 of the *Ide* gene, causing a frameshift with two stop codons in exon 4 and therefore, an early termination of translation. The main genomic characteristics of these mice are described at the Mouse Genome Informatics (MGI:4431946) and NCBI (GenBank JN963136.1). To get a better understanding about the genetics of these mice, we constructed a genetic map using the information mentioned above (**Figure 13**).

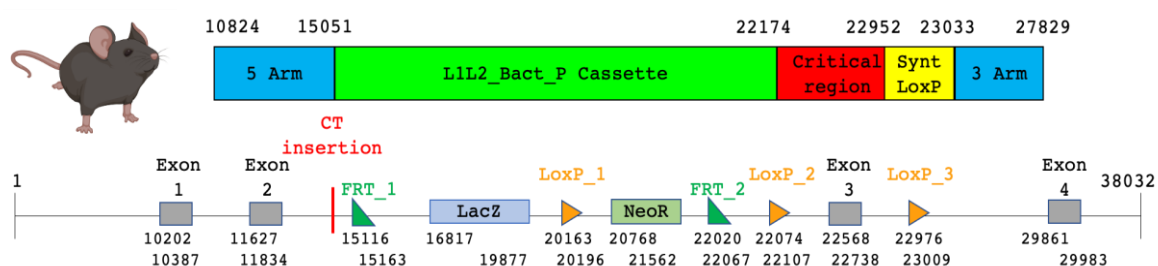


Figure 13. Genetic map of mutant IDE-KO allele. The *L1L2_Bact_P* cassette is inserted between exons 2 and 3, and contains the *LacZ* (β -galactosidase, reporter gene) and *NeoR* (Neomycin Resistance) genes flanked by two *FRTs* (Flippase Recognition Targets) and two *LoxP* (floxed sites, recognized by *Cre* recombinase) sites. The critical region, which comprises exon 3 flanked by two *LoxP* sites, is removed in the IDE-KO allele.

1.2.1. Mouse genotyping

Genomic DNA was extracted from mouse tail samples of 2-5 mm by proteinase K digestion in the presence of detergents. Each tail sample was incubated in 200 μ l of lysis buffer [50 mM KCl, 10 mM Tris pH 8.5, 10 μ g/ml gelatin, 0.045% NP-40, 0.045% Tween-20, 0.5 mg/ml proteinase K] overnight at 55°C. Once the tissue was dissolved, samples were boiled for 10 minutes and then cooled on ice and centrifuged for 5 minutes at 16400 g. Then, DNA templates were prepared by making a 1:30 dilution of each sample. Two pairs of primers were designed to unambiguously genotype IDE-KO mice (**Table 1**), selecting target regions that are present in the wild-type, non-transgenic mouse.

Table 1. Primer sequences used for IDE-KO mice genotyping. Abbreviations: *Fwd* = forward, *Rev* = reverse, *Tm* = melting temperature.

Name	Sequence (5'-3')	Tm (°C)	Target
Ide Exon 3 Fwd	TTCCTGTGCCCTTGTTGA	59.7	Exon 3
Ide Exon 3 Rev	GTACGTTTGAAGCCCCGGTA	60.0	
Ide Intron Fwd	AACTGCCACCTGTCCAATCC	60.2	Introns 2-3
Ide Intron Rev	GGAAACCACTATGCCTACCTCT	59.2	

The first pair of primers (Ide Exon) is targeted to the exon 3 of *Ide*, which is removed in the IDE-KO mice; therefore, the WT allele produces an amplicon of 332 bp, while IDE-KO allele presents no amplicon. The second pair of primers (Ide Intron) is designed to amplify the intronic regions flanking exon 3; in this case, the WT allele produces an amplicon bigger in size than the IDE-KO allele (1427 vs 741 bp, respectively) due to the removal of exon 3 in IDE-KO (**Figure 14A**).

To detect *Ide* alleles, two parallel amplification reactions (initial denaturalization 2 min at 94°C, followed by 35 cycles [2 min 94°C; 30 s 62°C; 45 s 72°C] plus final extension 10 min at 72°C) were carried out with the primers described above (**Table 1**). PCR reactions [1X DreamTaq PCR Master Mix, 1 μ M primer Forward, 1 μ M primer Reverse, 1 μ l DNA template in Nuclease free water] were performed in a volume of 10 μ l. The resultant PCR products were mixed with loading buffer for nucleic acids [40% sucrose, 0.25% orange G, 1 mM EDTA], loaded into 1.5% agarose gels and electrophoresed in Tris-acetate buffer [0.04 M Tris-acetate, 1 mM EDTA]. Gels were stained with RedSafe, and the amplicons were visualized by an ultraviolet transilluminator. An example of genotyping results is shown in **Figure 14B**.

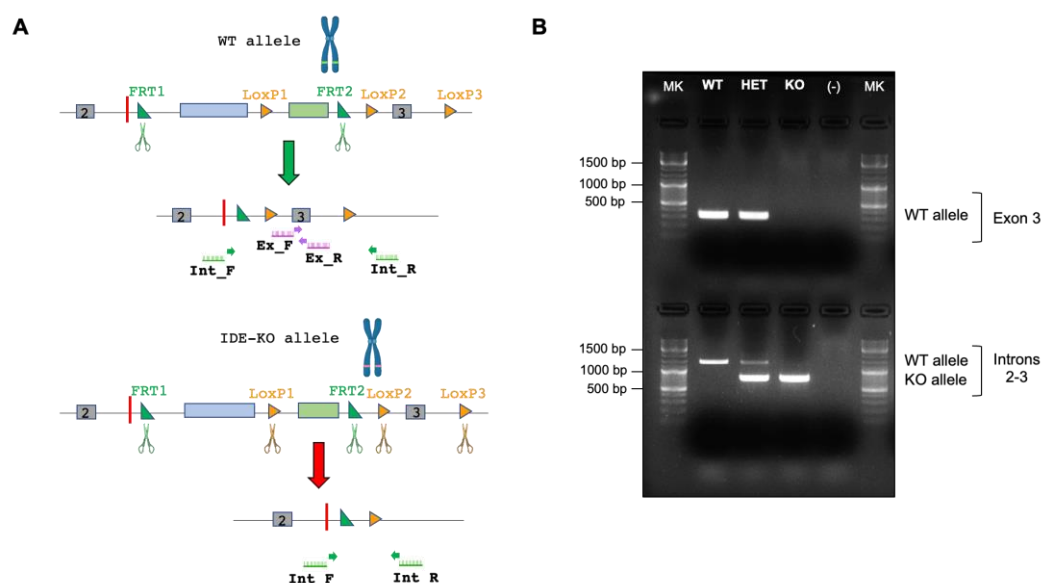


Figure 14. Genotyping of mice from the *Ide*-Null cohort. A) Genetic structure of WT and IDE-KO alleles after cutting with flippases (green scissors) and Cre recombinases (orange scissors). The WT allele produces both the exonic and intronic amplicons, while the IDE-KO allele only generates the intronic amplicon, and this is shorter than the WT one because of the removal of exon 3. **B)** Representative image of PCR results for mice genotyping. Expected bands: WT (wild type): 332 bp in IDE exon 3 and 1427 bp in IDE introns 2-3; HET (heterozygous): 332 bp in IDE exon 3 and 1427 and 741 bp in IDE introns 2-3; IDE-KO (*Ide* knockout): no band in exon 3 and 741 bp in introns 2-3. Abbreviations: MK = marker.

1.2.2. Experimental procedures

To characterize the global role of IDE, we studied 12-month-old mice from the three possible genotypes for the *Ide* gene: wild-type (WT), heterozygous (IDE-HET) and knockout (IDE-KO). We analyzed a cohort of 60 mice, consisting in 10 mice per sex and genotype. This cohort was used to perform behavioral tests, metabolic measurements after a six-hour fasting and molecular biology studies. The experimental paradigm for this study is summarized at **Figure 15**.

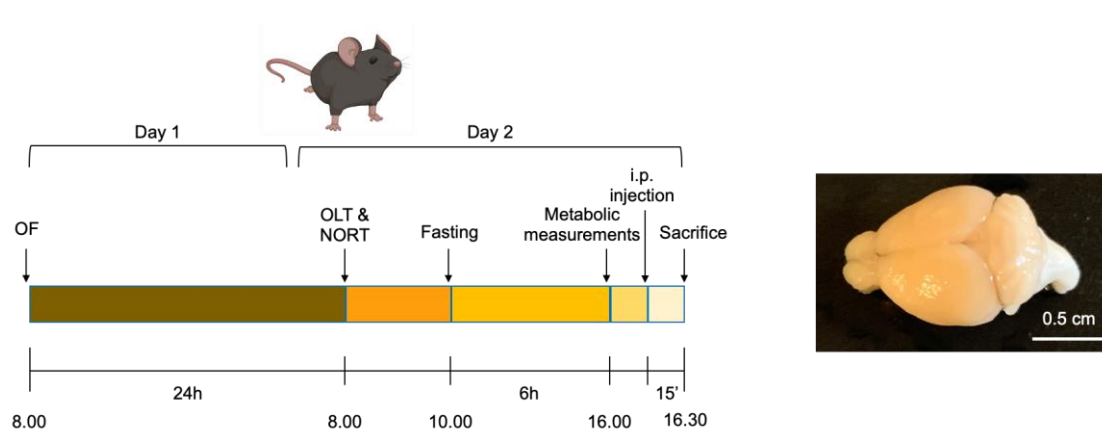


Figure 15. Experimental paradigm for metabolic, behavioral and molecular biology studies. Schematic figure representing the timing of experiments performed with these mice. The picture on the right shows one of the brains collected for the molecular biology studies. Abbreviations: OF = open field, OLT = object location test, NORT = novel object recognition test, i.p. = intraperitoneal.

1.2.2.1. Behavioral experiments

To evaluate the effects of genetic deletion of IDE in the brain of middle-aged mice, we performed behavioral studies with a MIR-100 infrared digital camera and the Activity Monitor acquisition and analysis program (Med Associates). All procedures were in accordance with institutional guidelines for animal care and administration. Behavioral tests were modified from previously described methods (Ennaceur and Delacour, 1988; Denninger et al., 2018). An open field squared box constructed from wood, 45 cm by 45 cm with 30 cm high walls, was used. The floor of the box was blue, while the walls were white, and two of these walls in opposite positions had two different figures, a circle and a star, to allow spatial orientation.

The procedure included 4 phases, performed in two days: open field test and habituation (first day), and object familiarization trial, object location test and novel object recognition test (second day). All the experimental sessions for behavioral tests were performed between 8 a.m. and 10 a.m. (see **Figure 16A** for more details).

Open field test and habituation

Each mouse was brought in an individual cage to the testing room 14 hours before the experiment to familiarize with the environment. For the open field test (OF), mice were allowed to freely explore the arena in the absence of objects for 5 minutes. Locomotor behavior, ambulatory distance, stereotypic counts and ratio center/periphery were automatically analyzed for each mouse. This open field session was followed by a 20 minute-resting period and two new training sessions in which mice were habituated to the empty arena for 6 minutes per session.

Object recognition tests

The object location test (OLT) and the novel object recognition test (NORT) are two behavioral tasks commonly used to evaluate the function and relative health of specific brain regions involved in memory. These tests are based on the inherent preference of mice for the novelty to reveal memory for previously encountered objects. All objects used in this study were made from the same material (plastic Lego® parts) but differed in terms of shape, height and color (**Figure 16B**). We had two identical sets of objects, which were fixed on the floor of the arena to ensure that the mice could not displace them. To prevent the existence of olfactory cues between mice, the entire box and objects were thoroughly cleaned with 70% ethanol solution and water after each session.

Each mouse took a familiarization trial followed by two testing trials.

Object familiarization trial (OFT)

During the object familiarization session, two identical objects were placed at parallel positions within the box at same distance from the nearest corner (6 cm). Mice were allowed to explore the identical objects for 10 minutes, and then returned to their home cages for 40 minutes (inter-trial interval).

Object location test (OLT)

The first testing trial was carried out 40 minutes after the end of the OFT. In this session, one of the objects was moved to an opposite position with respect to the other object, being both objects placed in diagonal positions within the box at same distance from the nearest corner. This session also lasted 10 minutes and was followed by a 40 minute-resting period.

Novel Object Recognition Test (NORT)

For the second testing trial, performed 40 minutes after the previous one, the familiar object that had not been moved during the OLT was replaced by a new object. In this final exploratory task, mice were placed back to the same arena to carry out a 10 minute-testing session.

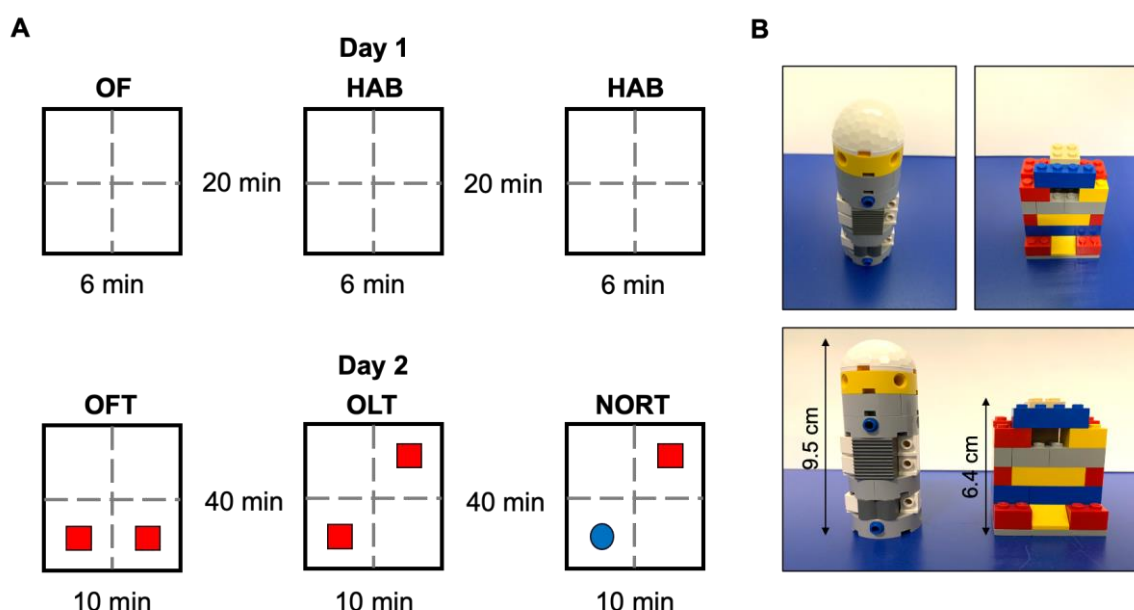


Figure 16. Behavioral tests protocol. **A)** Scheme of test protocols, performed in two consecutive days. **B)** Objects used in the behavioral tests. Abbreviations: OF = Open Field, HAB = habituation, OFT = Object Familiarization Trial, OLT = Object Location Test, NORT = Novel Object Recognition Test.

Behavioral tests analyses

The behavioral tests used in this study examine different types of memory: OLT evaluates spatial learning, which relies primarily on hippocampal activity, while NORT, in contrast, assesses non-spatial learning of object identity, which relies on multiple brain regions (Denninger et al., 2018).

For the OLT test, healthy mice are expected to remember the location of the objects during the initial exposure, therefore they will spend more time in investigating the moved object due to their novelty preference. In contrast, mice with impaired spatial contextual learning will demonstrate no preference for objects in the novel location. Similarly, mice with good memory will spontaneously prefer investigating the novel object during the NORT test.

Since the seminal paper from Ennaceur and Delacour (Ennaceur and Delacour, 1988), different methods have been developed to assess the performance of mice on memory tests (Hammond, 2004;

Gaskin et al., 2010; Antunes and Biala, 2012). After reviewing many analysis methods, we followed the protocol described by Denninger and coworkers (Denninger et al., 2018) with minor modifications. At this point, it is necessary to clarify the concept of “exploration”, which is fundamental in the behavioral tests analyses. It is considered “exploration of an object” when the animals direct their nose at a distance of 2 cm to the object and/or touch the object with the nose, while turning around or sitting near the object without looking at it was not considered as an exploration (Ennaceur and Delacour, 1988). To accomplish this exhaustive analysis an independent, blinded researcher analyzed the videos by drawing a transparent square that provides a border of 2 cm around each object over the screen to help to distinguish active exploration of the objects. The researcher annotated every time that the mouse explored any of the two objects, and to analyze the results obtained by the mice in the behavioral tests, the Discrimination Index was calculated with the following formula:

$$\text{Discrimination Index} = \frac{\text{Novel location or object explorations} - \text{Familiar location or object explorations}}{\text{Total explorations}}$$

A positive value for the discrimination index indicates more times investigating the novel location or object, while a discrimination index of zero or lower indicates no preference for the novelty.

1.2.2.2. Metabolic characterization

Male and female mice were studied in terms of body weight, glucose levels and plasma insulin.

Body weight

Body weight was monitored by using a digital weight scale (Ohaus, Switzerland). Two body weight measures were obtained: one the first day, just after the habituation phase, in no-fasting conditions, and the other one the second day, after a six-hour fasting.

Blood glucose measurement and plasma collection

Blood sampling after six hour-fasting was performed by cutting 5 mm of tissue from the tail tip with a scalpel and gently massaging the tail. The first blood drop collected from the tail vein was directly loaded in a glucometer.

Blood was collected from the tail vein into Microvette®, capillary tubes pre-coated with potassium-EDTA for the preparation of plasma. Then, blood samples were centrifuged (3300 g for 10 minutes at 4°C) to obtain plasma fraction. Plasma samples were stored at -80°C.

Determination of plasma insulin concentration

The ELISA (enzyme-linked immunosorbent assay) technique is a plate-based assay designed for detecting and quantifying soluble substances. To determine insulin levels in experimental mice, we used Mouse Ultrasensitive Insulin ELISA (CrystalChem) assays following the manufacturer's instructions. Briefly, plasma samples were added to microplate wells pre-coated with a first anti-insulin antibody (guinea pig anti-insulin), known as the capture antibody, and incubated for 2 hours at 4°C. Insulin was immobilized on the plate by its binding to the capture antibody, while the unbound

proteins were washed away. Horseradish peroxidase (HRP)-conjugated anti-insulin antibody was then added and bound to the mouse insulin/guinea pig anti-insulin complex immobilized on the microplate. After washing away the excess of antibody, the 3,3',5,5'-tetramethylbenzidine (TMB) substrate solution was added. Detection was accomplished by measuring the activity of the reporter enzyme (HRP) oxidizing the TMB to produce a colorimetric, measurable product.

1.2.2.3. Molecular biology studies

After behavioral and metabolic studies, each group of 10 mice was randomly divided into two subgroups, which were treated “acutely” with an intraperitoneal injection of Humulin® (5U/kg of body weight) or vehicle (PBS). Mice were euthanized by CO₂ inhalation 15 minutes after injection.

Brain dissection and tissue harvesting

Mouse brains were quickly removed following decapitation after CO₂ anesthesia and subsequent cervical dislocation and cut into several coronal blocks; all of them were further divided into two following a mid-sagittal section. The pieces obtained correspond to olfactory bulbs, cortex regions, cerebellum and hippocampus, the latter was collected after brain dissection under a stereoscope. Tissues were immediately frozen by immersion in isopentane and stored at -80°C.

Insulin signaling studies by immunoblotting

The olfactory bulb has the highest concentration of insulin and the fastest transport rate, which is about 2.3-7.6 times faster than the remaining areas, and this region also possesses the highest concentration of insulin receptors (Banks et al., 2012; Gray and Barrett, 2018). Therefore, studies on insulin signaling were performed at the olfactory bulb. Olfactory bulb tissues, which had an average weight of 30 mg, were mechanically homogenized with a pestle in 5 volumes (150 µl) of homogenization buffer [0.5% sodium deoxycholate, 10 mM HEPES pH 7.6, 100 mM KCl, 1 mM EDTA pH 8.0, 1% NP-40, 0.1% SDS, 10% glycerol, 1 mM DTT, 1X Protease inhibitor cocktail, 1 mM PMSF, 1X Phosphatase inhibitor cocktail 2, 1X Phosphatase inhibitor cocktail 3] and incubated on ice for 30 minutes. Then, samples were centrifuged at 16400 g for 10 minutes at 4°C to pellet undigested tissue, and supernatants were used in subsequent steps. Protein concentration from each sample was estimated by using the Micro BCA™ Protein Assay Kit. Protein extracts (50 µg) were mixed with protein sample buffer [63 mM Tris-HCl pH 6.8, 10% (v/v) glycerol, 2% (w/v) SDS, 100 mM DTT, 0.05% (w/v) bromophenol blue], heated at 70 °C for 5 minutes and then analyzed by immunoblotting.

1.3. Leptolide treatment in mice fed with high-fat diet

C57/Bl6J male mice were purchased from Charles River Laboratory (Écullly, France). Male mice were chosen for metabolic phenotyping to avoid the potential variability related to estrous cycle. Mice were maintained in positive pressure-ventilated racks at 25°C with 12 h light/dark cycle, fed *ad libitum* with standard rodent chow diet and allowed free access to filtered and UV-irradiated water.

At 6 weeks of age, mice were randomly divided into two groups: one of them was fed with standard diet (SD) (33% protein; 58% carbohydrate; 9% fat) (#V1535, Ssniff, Soest, Germany) while the other was fed with a 60% kcal high-fat diet (HFD) (20% protein; 20% carbohydrate; 60% fat) (#D12492, Research Diets, New Brunswick, NJ, USA) for 6 weeks. After this time, each experimental group was randomly divided into two subgroups, which were treated with one-daily intraperitoneal injection of leptolide (0.1 mg/kg of body weight) or vehicle (DMSO, 0.001% with respect to the mouse plasma volume) in saline for another 4 weeks. All mice were maintained on their corresponding diet during the 4-week treatment, and finally they were euthanized at 16 weeks of age. After 4 weeks of treatment, leptolide-treated mice showed improved glucose tolerance by intraperitoneal glucose tolerance test (area under the curve: leptolide 36.6 ± 0.8 versus vehicle 39.6 ± 0.8 ; $p < 0.05$) and improved insulin sensitivity measured by the HOMA index [fasting insulin ($\mu\text{UI/mL}$) x fasting glucose (mM)/22.5] (leptolide 0.7 ± 0.1 versus vehicle 1.2 ± 0.2 ; $p < 0.05$).

2. Cell cultures

2.1. Cell lines

The cell lines used in this work were obtained from American Type Culture Collection (ATCC). Cells were grown at 37°C in humidity-saturated atmosphere containing 5% CO₂.

2.1.1. BV-2

BV-2 murine microglial cell line was generated by Blasi *et al.* by infecting primary female microglial cultures with a *v-raf/v-myc* oncogene carrying retrovirus J2 (Blasi *et al.*, 1990). BV-2 cells were grown in 25 cm² cell-culture flasks covered with 5 ml of RPMI 1640 supplemented with 5% heat-inactivated FBS, 1% L-glutamine (final concentration 2 nM) and 1% P/S (final concentration: 100 U/ml penicillin, 100 U/ml streptomycin). To detach cells, GHCKS solution (2 g/l D-glucose, 4.77 g/l HEPES, 6.37 g/l NaCl, 0.3 g/l KCl, 3 g/l Na₃Citrate·2H₂O, pH 7.5) was used. For maintenance, cells were harvested and reseeded at 1:10 three times a week. BV-2 cells present the peculiarity that when growing in complete medium with FBS they have a rounded morphology, and to differentiate them into a “microglial-like” morphological phenotype, BV-2 cells must be grown in low-serum medium, which decreases their replication rate.

2.1.1.1. Estimation of the duplication time for the BV-2 cell line

To characterize the proliferation kinetics of BV-2 cell line, we performed an experiment to calculate the duplication time of these cells when growing in complete medium. Three identical flasks of 25 cm² were seeded at a density of 500000 cells/flask (20000 cells/cm²), and every 24 hours one of these flasks was harvested with GHCKS solution as described above (**Figure 17A**). Cells were counted with a Neubauer chamber, and after collecting all data we estimated the number of cell divisions (n) and the duplication time for each temporal point, using the equation $N_f = N_0 \cdot 2^n$, where N_0 and N_f are the initial and final number of cells, respectively (**Figures 17B** and **17C**). With

the data about number of duplications within time, we performed a linear regression fit to construct an equation to estimate the number of cell divisions, obtaining $y = 0.0418x + 0.094$, being “x” the time in hours and “y” the number of cell divisions, with an R^2 of 0.96 (**Figure 17D**). With these data, we estimated that the average duplication time for the BV-2 cell line growing in complete medium is ~22 hours. A representative image of the BV-2 cell line is shown in **Figure 17E**.

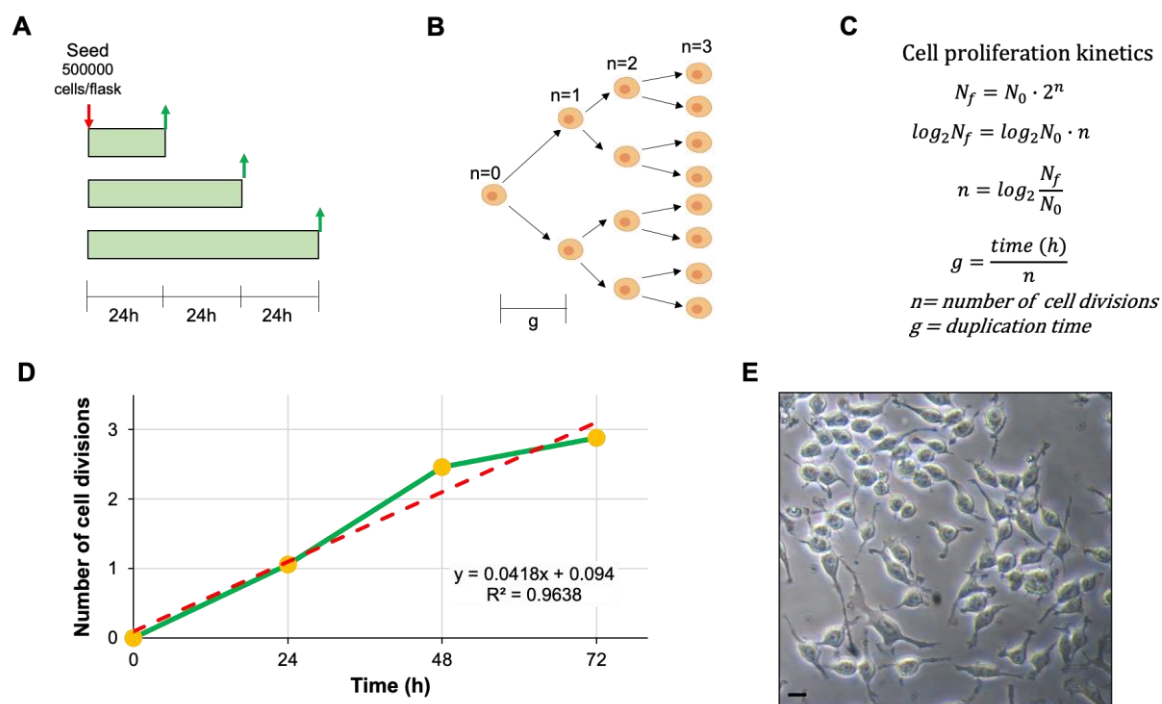


Figure 17. Proliferation kinetics in BV-2 cell line. **A)** Experimental design. **B)** Graphical explanation of number of cell divisions (n) and duplication time (g). **C)** Equations used to determine BV-2 proliferation kinetics. **D)** Graphical representation of the number of cell divisions versus time. **E)** Representative image from the BV-2 microglial cell line (scale bar: 20 μm).

2.1.2. Raw264.7

Raw264.7 cells are monocyte/macrophage like cell lineage, originated from *Abelson leukemia* virus transformed cell lineage derived from adult male BALB/c mice (Raschke et al., 1978). Raw264.7 cells were grown in 25 cm^2 cell culture flasks covered with 5 ml of RPMI 1640 supplemented with 5% FBS, 1% L-glutamine and 1% P/S. Cells were detached in GHCKS solution, using a cell scraper. For maintenance, cells were harvested and reseeded at 1:10 three times a week.

2.1.3. Mycoplasma testing

To discard *Mycoplasma* contamination, our cell lines were periodically tested by using the “Mycoplasma gel detection kit” (Biotools, Spain), following manufacturer’s instructions.

2.2. Primary microglial cultures

To avoid potential maternal effects of IDE, and to generate WT and IDE-KO mice of homogeneous genetic background, the experimental cohorts used to produce primary cultures were the F1 generation of homozygous crosses of IDE-KO and IDE-WT littermates born from heterozygous crosses of an IDE-KO line at C57BL/6J background.

Neonatal (0-1 days old) mice were used to produce primary cultures. First, we collected newborn pups from breeding cages. To analyze possible differences between male and female glia, we performed a gender assessment according to the method described by Wolterink-Donselaar and colleagues (Wolterink-Donselaar et al., 2009). Basically, it involved the exploration of the anogenital region of newborn mice for the identification of a pigment spot on the scrotum in male mice, visible to the naked eye from the first day of life, whereas female pups lack pigmentation in this region.

After sexing newborn mice, primary microglial cultures were prepared following the method described by Saura *et al.* (Saura et al., 2003). Each pup was used to raise an individual culture. Solutions were prepared in Earle's Balanced Salt Solution (EBSS), as summarized in **Table 2**.

Table 2. Composition of dissection and digestion media used in primary glial cultures.

Reagent	Dissection media	Digestion media
BSA	3.2 µg/ml	3.0 µg/ml
DNase I	27.5 µg/ml	60 µg/ml
P/S/A	100 U/ml penicillin 100 U/ml streptomycin 0.25 µg/ml amphoterycin B	100 U/ml penicillin 100 U/ml streptomycin 0.25 µg/ml amphoterycin B
Trypsin	-	0.25 mg/ml

We sacrificed the pup by cutting off its head, anchored the head by the snout using a bent needle and cut open the scalp along the midline from the posterior end to the snout to get the skull exposed. To get rid of the skull, three cuts using microdissection scissors were needed: one cross section in the middle of the cerebellum, the second one longitudinal from the sagittal suture to the middle point between the eyes, and the final one transversal at the olfactory bulb. Finally, we removed the skull putting one end of the microsurgical forceps beneath the skull but above the brain tissue and pulling toward the snout along the midline. Cerebral cortices were scooped out using a microspatula, with a movement from mid back to front outside. Brain meninges were removed by rolling the cortices on a sterile filter paper, and the tissue was immersed in 2 ml of dissection media in a Petri dish (**Figure 18A**).

The tissue was minced with a surgical blade for 1 minute, and then centrifuged (200 g 2 minutes, brake low, room temperature (RT)) to remove medium and red blood cells. Pelleted tissue was resuspended in 1 ml of digestion media and incubated for 15 min at 37°C under agitation (750 rpm). Trypsinization reaction was stopped by adding 100 µl FBS / 1 ml of digestion media (**Figure 18B**).

Digested tissue was then centrifuged (200 g 5 minutes) to pellet cells and discard trypsin solution. Cells were resuspended in 1 ml of dissection media and mechanically dissociated with a Pasteur pipette. The sample was incubated for 5 minutes at RT to pellet by gravity cell clumps, while individual cells remained in suspension, to seed both fractions separately. Cells were plated onto different surfaces (from 2.24 to 78.5 cm²) at a density of 62500 cells/cm² and incubated at 37°C in 5% CO₂ with 95% humidity (**Figure 18C**).

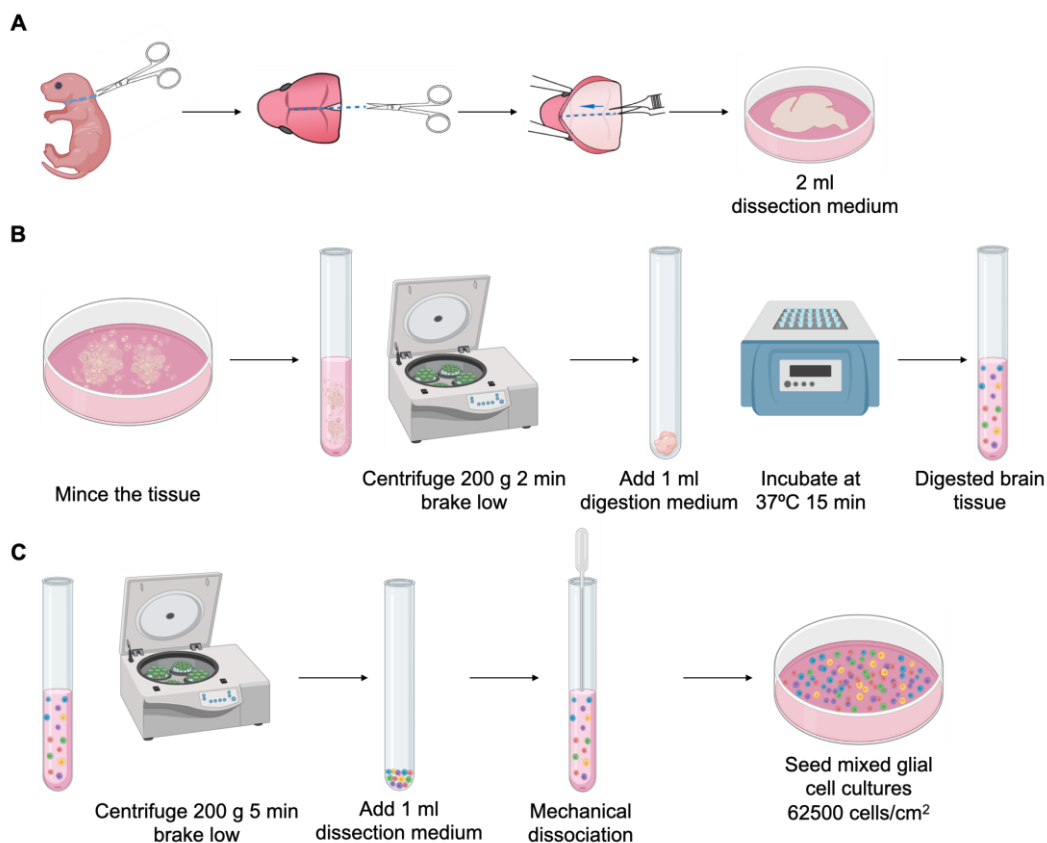


Figure 18. Protocol to prepare primary microglial cultures. A) Newborn pup brain dissection. B) Tissue processing and digestion. C) Brain cells seed.

Culture media were replaced one day after cell seeding, and then every 5-7 days. At 14 days *in vitro* (DIV), cell cultures had reached almost 90% of confluence, but they were maintained one additional week to boost microglial proliferation. At 20 DIV, culture media were refreshed and, 24 hours later, at 21 DIV, microglia were isolated by mild trypsinization, as previously described (Saura et al., 2003). Culture media were collected to be used as “conditioned media”, containing astrocytic factors essential for microglial proliferation. Meanwhile, cell cultures were washed twice with PBS and incubated in a solution of mild trypsin (0.8 mg/ml Trypsin-EDTA in DMEM-F12 without FBS) for 1 hour at 37°C in 5% CO₂. During the incubation time, conditioned media were centrifuged at 300 g for 5 minutes to pellet floating cells to be avoided, while supernatants were transferred to new tubes and supplemented with macrophage colony stimulator factor (M-CSF, 25 ng/ml). After 1 hour in mild trypsin, the astrocytic layer of the cultures had completely been detached, while the microglial cells remained attached to the culture surface. Trypsin was inactivated by adding 10% FBS, the media

were removed, the remaining microglial cells were washed twice with PBS, and conditioned media supplemented with M-CSF were added to microglial cultures. Isolated microglia remained 48-120 hours in conditioned media supplemented with M-CSF, in order to get “resting” microglia (Witting and Möller, 2011) before being used in any experiment.

2.3. Cell treatments

The presence or absence of serum, the most variable component in a cell culture medium, might be at the root of the large body of divergent data on microglia responses to a given stimulus. Since microglia reside in the brain, the only time these cells are exposed to serum components is during breakage of the BBB and, indeed, several serum components have been identified as microglia-activating signals (Witting and Möller, 2011). Therefore, we decided to perform our experiments under low- or no-serum conditions. Treatments were carried out in RPMI 1640 11.1 mM D-glucose (except from specific glucose treatments, which were carried out in RPMI 1640 without D-glucose, supplemented with the corresponding amounts of D-glucose). The following treatments were used:

- D-glucose: 2-22 mM in RPMI 1640 without D-glucose, 0.2% FBS-CHST, 24-72 h.
- L-glucose: 5.5-16.5 mM in RPMI 1640 without D-glucose, 0.2% FBS-CHST, 24-72 h.
- Mannitol: 5.5-16.5 mM in RPMI 1640 without D-glucose, 0.2% FBS-CHST, 24-72 h.
- LPS: 100-1000 ng/ml in RPMI 1640 without FBS, 8-24 h.
- Paraquat (PQ): 25-500 μ M in RPMI 1640 without FBS, 8-24 h.
- IL4+IL-13: IL-4 (20 ng/ml) + IL-13 (50 ng/ml) in RPMI 1640 without FBS, 18-48 h.
- Human insulin: 500 nM in RPMI 1640 without FBS, 5-60 minutes.
- A β oligomers: 0.1-10 μ M in RPMI 1640 without FBS, 8-24 h.
- FAM-A β oligomers: 1 μ M in RPMI 1640 without FBS, 0.5-24 h.
- Myelin-DiI: 20 μ g/ml in RPMI 1640 without FBS, 3-24 h.

2.3.1. Furanocembranolides experiments

The compounds were dissolved in DMSO to make concentrated stock solutions (ranging from 25 to 100 mM, depending on the amount of product available) within their solubility range. The final concentration of furanocembranolides added to BV-2 cells was 0.1 μ M in serum-free culture media.

Identical dilutions from the carrier, DMSO, were prepared as controls to rule out the possibility that the effects observed in experimental conditions could be due to the presence of DMSO. The maximal final concentration of DMSO added to the cells was 0.0004%, well below the cytotoxicity threshold.

For the *in vitro* screening, LPS was added to the cell cultures at a final concentration of 1 μ g/mL for 24 hours.

2.4. Extracellular media processing

To detect secreted proteins in microglial conditioned media, culture media were collected after cell treatments and centrifuged (300 g, 5 minutes, RT) to pellet detached cells and discard them. The supernatants were collected and centrifuged again (16000 g, 30 minutes, 4°C) to pellet debris. Cell- and debris-free conditioned media were then concentrated using Amicon Ultra Centrifugal Filter Units following the manufacturer's instructions. The concentration factor achieved was 20-40x, depending on the molecular weight cutoff of the filters. Protein concentrations were BCA-quantified, and 80 µg of sample were analyzed by immunoblot.

2.5. Proliferation assays

Primary microglial cells from both WT and IDE-KO mice were seeded on 12 mm diameter coverslips and allowed to attach to the culture surface for 24 h. Then, Click-iT Plus EdU assays were performed in complete medium (DMEM-F12 + 10% FBS + 1% L-glutamine + 1% P/S). Cells were treated with 10 µM EdU (5-ethynyl-2'-deoxyuridine) solution for 24-30 h, either in control (complete medium) or proliferative (complete medium supplemented with 50 µg/ml M-CSF) conditions. Afterwards, cells were washed with PBS and fixed with freshly prepared 4% paraformaldehyde in PBS for 15 minutes at RT under agitation. After washing three times with PBS, cells were permeabilized with 0.1% Triton X-100 in PBS for 10 minutes at RT under agitation. Then, the permeabilization buffer was removed and cells were washed twice with PBS. To detect EdU, Click-iT Plus reaction cocktail was prepared following manufacturer's instructions. Next, 250 µl of reaction cocktail were added to each coverslip. The plate was rocked briefly to ensure a good distribution of the reaction cocktail over the sample, and cells were incubated for 30 minutes at RT under agitation protected from light. EdU detection is based on a click reaction, a copper catalyzed covalent reaction between an alkyne, contained by the EdU, and a picolyl azide, contained by the Alexa Fluor dye (**Figure 19**).

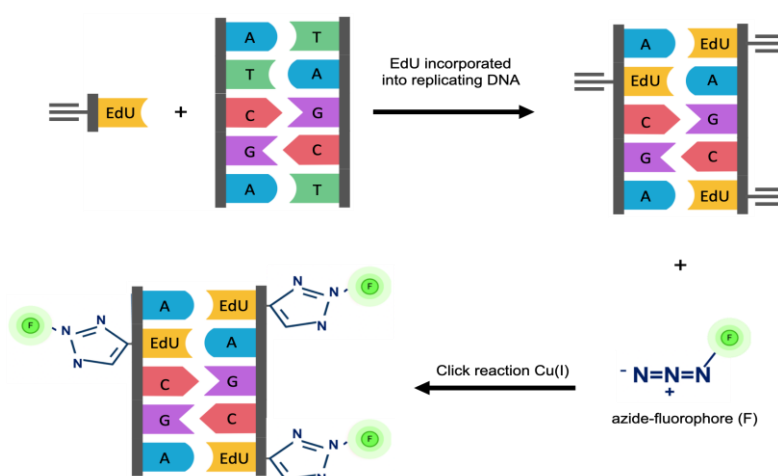


Figure 19. Principle of the EdU 'click' reaction. EdU, a nucleoside analog of thymidine, incorporates into replicating DNA and forms a covalent bond with a picolyl azide fluorophore in the presence of Cu(I), consequently resulting in a fluorescently tagged replicating DNA.

The reaction cocktail was removed, and samples were washed three times with PBS. Cell nuclei were stained by incubating samples with Hoechst 33342 solution (5 µg/ml) for 30 minutes at RT under agitation, and then samples were washed three times to remove excess of dye. Finally, coverslips were mounted with Vectashield, and samples were visualized with an Eclipse 90i fluorescence microscope (Nikon) equipped with a DS-Ri1 digital camera. Images were acquired using a 20X objective under the same conditions of illumination, diaphragm and condenser adjustments, exposure time, background correction and color levels. Images were analyzed using FIJI software, and results were expressed as percentage of proliferating cells ([EdU(+) cells/total nuclei] x 100).

3. MTT assays

The MTT (3-(4,5-dimethylthiazol-2-yl)-2,5-diphenyl-2H-tetrazolium bromide) is one of the most popular techniques for the quantitative assessment of cell viability and cytotoxicity (Mosmann, 1983). The MTT assay relies in tetrazolium salt as an indicator of the intracellular reducing potential, assumed to come mainly by cytosolic dehydrogenases. Tetrazolium reduction results in the formation of violet-blue, water insoluble formazan product, whose absorption in the visible region in theory correlates with the number of metabolic intact and alive cells in the sample. We developed different MTT-based protocols depending on the biological question (Pascua-Maestro et al., 2018).

3.1. Standard MTT colorimetric assay

Cells were seeded in different plate formats, ranging from 6 to 96-well plates, with a cell density of 50000 cells/cm². After receiving their respective treatments, cells were washed with PBS and treated with MTT (62.5µg/ml) for 3 hours in phenol red-free DMEM without FBS. After MTT exposure, cells were incubated in an isopropanol - 10% Triton-X100 solution to solubilize formazan. Formazan production was measured by spectrophotometry using the SOFTmax Pro microplate reader (Molecular Devices). Absorbance was collected at $\lambda = 570$ nm, subtracting the background measured at $\lambda = 690$ nm.

3.2. Normalized multi-well plate formazan detection method

One of the main concerns about the MTT assay for long-time treatments is the fact that the number of cells present in each sample at the end of the assay might be affected by the treatment received. To overcome this, we developed a method to estimate the number of cells present in each well to be able to normalize formazan signal to the total number of cells. To assess the ability of Hoechst to estimate the number of cells per well, we seeded different amounts of cells (0-40000) in a 96 well-plate with black walls in triplicates. Once the cells were attached to the plate, cell nuclei were stained with Hoechst 33342 (0.2 µg/ml) for 15 minutes at 37°C. After incubation, cells were washed with PBS and Hoechst fluorescence was measured ($\lambda_{\text{excitation}}=340\text{nm}$, $\lambda_{\text{emission}}=535\text{nm}$) in a GENios Pro Fluorimeter. We performed a regression fit between the number of cells and the fluorescence

collected, and obtained a formula with an R^2 of 0.88, which postulates Hoechst staining as a suitable method to easily count cells in a sample.

For normalized multi-well plate MTTs, cells were seeded to a final density of 30000 cells/cm² in a 96 well-plate with black walls. After receiving their correspondent treatment, culture medium was removed, and Hoechst staining was performed as described above to estimate the number of cells for each sample. Then, a standard MTT colorimetric assay was performed. By this way, combining quantitative formazan detection with nuclear labeling, we were able to measure the reducing power or metabolic activity per cell.

4. RNA isolation, cDNA synthesis and RT-qPCR

4.1. RNA isolation

Cells were washed with PBS twice and then collected and lysed with QIAzol Lysis Reagent. Cellular mRNA was extracted following manufacturer's protocol. Briefly, QIAzol solution containing lysed cells was mixed with 1:5 volume of chloroform and mixed vigorously. Then, samples were centrifuged (16400 g, 15 minutes, 4°C) and two phases of different density were formed, separated by a DNA interphase: an organic phenolic phase, containing denatured proteins, and the upper aqueous phase containing RNA. The aqueous phase was collected, transferred into a new tube, and mixed 1:1 with isopropanol to precipitate RNA. After 10 minutes of incubation at RT, samples were centrifuged at 10000 g for 10 minutes to pellet RNA. The isopropanol was discarded, and RNA pellets were washed with 70% ethanol overnight at -80°C, allowed to dry for 15 minutes at RT and resuspended in nuclease free water. RNA concentration and purity was measured with a NanoDrop spectrophotometer (**Figure 20A**).

To assess the quality of the RNA extracted and to check the absence of genomic DNA, samples were loaded into a 2% agarose gel for electrophoresis and run at 80V for 30 minutes. To visualize the nucleic acids, the gel was stained with RedSafe and illuminated with ultraviolet ray (GelDoc XR, BioRad) (**Figure 20B**).

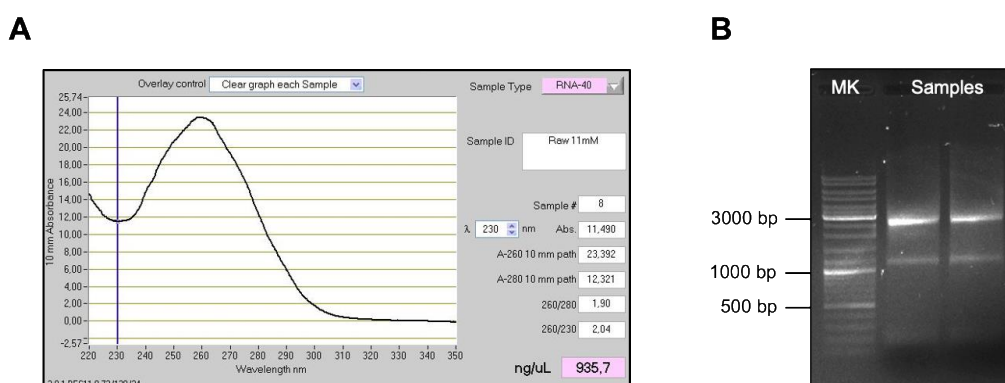


Figure 20. RNA quantification and quality assessment. A) RNA quantification by NanoDrop. B) RNA visualization by agarose gel electrophoresis. Abbreviations: MK = marker.

4.2. DNase I treatment and cDNA synthesis

After quantification, 500 ng of total RNA were treated with DNase I (0.1 U/ μ l) to eliminate any genomic DNA remain, in a reaction volume of 5 μ l. The process had two steps: 30 minutes at 37°C (optimal temperature for DNase I) and 5 minutes at 85°C (to inactivate the enzyme). Following DNase treatment, 500 ng of total RNA were reverse-transcribed (RT-PCR) with Prime-Script using Oligo-dT primers and random hexamers (**Table 3**). The reaction had two steps: 60 minutes at 42°C (RT-reaction) and 5 minutes at 90°C (to inactivate the retrotranscriptase).

Table 3. Reaction mix for RT-PCR.

Reagent	Volume	Final concentration
5X Prime Script RT Buffer	2.0 μ l	1X
Oligo dT Primer 50 μ M	0.5 μ l	5 μ M
Random 6-mers 100 μ M	0.5 μ l	10 μ M
Prime Script RT Enzyme Mix I	0.5 μ l	-
RNase-free dH ₂ O	1.5 μ l	-
Sample (RNA treated with DNase)	5.0 μ l	50 ng/ μ l

4.3. RT-qPCR

The resulting cDNA was used as a template for quantitative real-time polymerase chain reaction (RT-qPCR) using TB-Green and a Rotor-Gene 3000 thermocycler. The PCR program is summarized in **Table 4**.

Table 4. RT-qPCR program.

Step	Conditions	
Initial denaturalization	95°C 30 s	
Cycles (x45)	Denaturalization	95°C 5 s
	Annealing	60°C 15 s
	Extension	72°C 15 s
Melting	Ramp from 65°C to 95°C, rising 0.5°C each step of 5 s	

The genes analyzed by RT-qPCR are shown in **Table 5**. RpL18 was used as the reference housekeeping gene.

Table 5. Genes analyzed by RT-qPCR. Abbreviations: *Fwd* = forward, *Rev* = reverse.

Gene	Gene ID	Amplicon size (bp)	Sequence 5'-3'
IL-1 β	NM_008361.4	180	Fwd: TGTAATGAAAGACGGCACACCCAC Rev: GGCTTGTGCTCTGCTTGTGAGG
IDE	NM_031156.3	194	Fwd: CTTCCAAGTCAGCTAGTCCG Rev: AGGGTATTGAAGCAAGGCTC
TGF- β	NM_011577.2	186	Fwd: CGCAACAACGCCATCTATGA Rev: ACCAAGGTAACGCCAGGAAT
TNF- α	NM_013693.3	193	Fwd: TCTTCTCATTCTGCTTGTGGCAG Rev: TGGTTTGCTACGACGTGGGCT
RpL18	NM_009077.2	204	Fwd: TTCCGTCTTTCCGGACCT Rev: TCGGCTCATGAACAACCTCT

To validate the specificity of the amplification products, melting curves were analyzed and qPCR products were loaded into a 2% agarose gel and run at 100 V for 30 minutes.

Data analysis was performed using the $2^{-\Delta\Delta Ct}$ method (Livak and Schmittgen, 2001), a relative quantification method of gene expression based on the comparison of the Ct (threshold cycle) values of different target genes normalized to those of the endogenous control (housekeeping gene), in this case rRNA 18S (RpL18). Briefly, fold regulation is calculated as follows:

- ΔCt is the difference in Ct values between the gene of interest (GOI) and the housekeeping gene (HKG): $\Delta Ct = Ct(GOI) - Ct(HKG)$.
- $\Delta\Delta Ct$ is the difference between the ΔCt of the experimental condition and the ΔCt of control condition: $\Delta\Delta Ct = \Delta Ct (experimental) - \Delta Ct (control)$.
- The relative expression of the GOI is calculated as $2^{-\Delta\Delta Ct}$.

To perform this normalization, the efficiency of the amplification of both, the experimental gene and the endogenous control must be close to 1 and differ less than 10%. An efficiency of 1 means that the amount of DNA template doubles in each cycle. To determine the efficiency of the reaction, we performed a PCR with serial dilutions of one sample and obtained the Ct value for each dilution. Representing Ct against the number of copies of each dilution, we can fit a line to these data and calculate its slope, from which efficiency can be obtained.

Statistically significant differences of gene transcriptional changes were evaluated with a U-Mann Whitney test using ΔCt of each replica (calculated by subtracting the average CT of the reference gene for each sample). The statistical level of significance was set at $p < 0.05$. Three different mRNA preparations from three independent cell cultures were assessed for each condition.

5. Polyacrylamide gel electrophoresis and immunoblotting

5.1. Sample preparation

Cells were collected in lysis buffer [0.5% sodium deoxycholate, 10 mM HEPES pH 7.6, 100 mM KCl, 1 mM EDTA pH 8.0, 1% NP-40, 0.1% SDS, 10% glycerol, 1 mM DTT, 1X Protease Inhibitors] and incubated on ice for 30 minutes. Then, protein content was quantified using the Micro BCA™ Protein Assay Kit, following manufacturer's instructions. Protein extracts were mixed with protein sample buffer [63 mM Tris-HCl pH 6.8, 10% glycerol, 2% SDS, 100 mM DTT, 0.05% bromophenol blue] and heated at 70°C for 5 minutes. Depending on the experiment, 15-80 µg of protein samples were loaded per lane.

5.2. Gel electrophoresis and transference

Polyacrylamide gel electrophoresis (PAGE) is a technique used to separate macromolecules according to their electrophoretic mobility, which is a function of the length, conformation and charge of the molecule. When sodium dodecyl sulfate (SDS), a chemical denaturant, is added, molecules charge negatively and lose their native state; in this situation, their mobility depends only on their length. In summary, SDS-PAGE is a method of separating molecules based on the difference of their molecular weight.

Depending on the molecular weight of the target protein, samples were run in gels with different percentage of acrylamide (5-15%) under denaturing conditions. Gel electrophoresis was carried out at constant voltage (100 V) in electrophoresis buffer [25 mM Tris, 190 mM glycine, 1% SDS, pH 8.3], using the BioRad electrophoresis system. Proteins were then transferred into PDVF Immobilon-P membranes at constant current (400 mA) for 90-180 minutes (0.75- and 1.5-mm gels, respectively) in transfer buffer [25 mM Tris, 190 mM glycine, 20% MeOH, pH 8.5], using the BioRad Gel Transfer device.

5.3. Immunoblot

Transferred membranes were incubated for 1 hour at RT with blocking solution, that is TBS [0.5 M Tris-base, 1.5M NaCl, pH 7.5] plus 0.05% Tween-20 supplemented with either 5% non-fat dry milk or 3% BSA. Blots were subsequently incubated overnight at 4°C or, alternatively, for 2 hours at RT with the corresponding antibody in blocking solution. Primary antibodies used are summarized in **Table 6**.

Table 6. Primary antibodies for immunoblotting.

Antibody	Reference	Blocking	Dilution (concentration*)	Species	Size (kDa)
AKT	Cell Signaling	5% milk	1:1000	Rabbit	60
ApoD	Santa Cruz	5% milk	1:1000 (0.2 µg/ml)	Goat	30
Arginase-1	Santa Cruz	5% milk	1:500 (0.2 µg/ml)	Mouse	35-38
CD81	GeneTex	5% milk	1:1000 (1.08 µg/ml)	Rabbit	26
COX-2	Cayman	5% milk	1:20000 (0.05 µg/ml)	Rabbit	72
Flotillin-1	BD Laboratories	5% milk	1:1000 (0.25 µg/ml)	Mouse	48
GFAP	Santa Cruz	5% milk	1:2000 (0.1 µg/ml)	Mouse	50
Iba1	Santa Cruz	5% milk	1:200 (1 µg/ml)	Mouse	17
IDE	Merck	3% BSA	1:80000 (0.013 µg/ml)	Rabbit	110
Insulin Receptor	Cell Signaling	5% milk	1:1000	Rabbit	95
Integrin α M (CD11b)	Santa Cruz	5% milk	1:200 (1 µg/ml)	Goat	170
Phospho-Insulin Receptor	Cell Signaling	5% milk	1:500	Rabbit	95
Phospho-AKT (Ser473)	Cell Signaling	5% milk	1:1000	Rabbit	60
PMCA	Santa Cruz	5% milk	1:1000 (0.2 µg/ml)	Mouse	140
β -actin-HRP	Sigma	5% milk	1:200000 (0.015 µg/ml)	Mouse	42
β -amyloid (B-4)	Santa Cruz	5% milk	1:1000 (0.2 µg/ml)	Mouse	4-46

(*) Concentrations of antibodies are specified when available.

Afterwards, membranes were washed 3 times for 10 minutes with TBS-Tween20 0.05%, incubated with corresponding secondary antibodies conjugated with peroxidase in blocking solution for 1 hour at RT, and washed again 3 times. Secondary antibodies used are schematized in **Table 7**.

Table 7. Secondary antibodies for immunoblotting.

Antibody	Reference	Blocking	Dilution (concentration)	Species
Anti mouse-HRP	Dako Cytomation	5% milk	1:10000	Goat
Anti rabbit-HRP	Jackson ImmunoResearch	5% milk	1:10000 (0.08 µg/ml)	Goat
Anti goat-HRP	Jackson ImmunoResearch	5% milk	1:10000 (0.04 µg/ml)	Donkey

Bound peroxidase activity was visualized with Enhanced Chemoluminescence (ECL) reagents (Millipore), and the signal was visualized with a BioRad GS-800 Densitometer, coupled with a high sensitivity CCD camera. The integrated optical density of the immunoreactive protein bands was measured in images taken within the linear range of the camera, avoiding signal saturation.

5.4. Membrane stripping and reprobing

To detect more than one protein on the same membrane, a mild stripping protocol was performed in order to remove primary and secondary antibodies from the blot. The membrane was incubated for 10 minutes at RT with stripping buffer [3.5 mM SDS, 1% Tween-20, 0.2 M glycine, 0.1 N HCl], then the buffer was discarded, and fresh stripping buffer was added for another 10 minutes. Subsequently, the stripping buffer was removed, and the membrane was washed for 5 times with washing buffer (TBS-Tween 20 0.05%), 10 minutes each wash. Once stripped, membranes were either reprobed with other antibodies or dried and stored between cellulose acetate sheets at RT.

6. Luminex and ELISA assays from primary microglial culture supernatants

Primary microglial cultures were isolated as described in Section 2.2 and incubated for 5 days in astrocyte-produced conditioned media supplemented with 20 ng/ml M-CSF. Then, cells were serum-starved for 3 hours and exposed to different stimuli, prepared in RPMI 1640 medium (11.1 mM D-glucose, 1% L-glutamine, 1% P/S) without FBS for 18 hours.

The experimental conditions assessed were: 100 ng/ml LPS; 20 ng/ml IL-4 + 50 ng/ml IL-13; 25 μ M PQ and 1 μ M A β oligomers. Each condition was performed in sextuplicate (samples from male and female microglial cells, triplicates of each sex). After the incubation period, culture media were collected, centrifuged (1000 g, 10 min, 4°C) to pellet cell debris and stored at -20°C.

6.1. Luminex assay

Luminex multiplex assays from R&D Systems are bead-based multianalyte profiling kits for detecting protein analytes in biological samples. The kits utilize color-coded superparamagnetic microparticles (beads) coated with analyte-specific antibodies. Beads recognizing different target analytes are mixed together and incubated with the sample. Captured analytes are subsequently detected using a cocktail of biotinylated detection antibodies and a streptavidin-phycoerythrin conjugate. The Luminex assay principle is summarized in **Figure 21**. First, samples were added to a mixture of color-coded beads, pre-coated with analyte-specific capture antibodies. The antibodies bound to the analytes of interest. Secondly, biotinylated detection antibodies specific to the analytes of interest were added and formed an antibody-antigen sandwich. Phycoerythrin-conjugated streptavidin was added and bound to the biotinylated detection antibodies. Finally, beads were read using a Luminex 100[®] Analyzer. The excitation system in this analyzer involves two solid-state lasers: a classification laser (red) excites fluorochromes embedded in the beads as they flow single-file through the cuvette and identifies each type of bead, while a reporter laser (green) excites the phycoerythrin-derived signal on the bead surface and quantifies the analyte present in the sample. Photodiodes and a photomultiplier tube receive both fluorescent signals, which are further digitalized and sent to a digital signal processor.

We performed a 5-plex assay, in which we measured IL-1 β , IL-6, TNF- α , IL-4 and IL-10. The Luminex assay kit provided a cocktail of standards of known concentration. A standard curve was created for each analyte by reducing the data to generate a five-parameter logistic curve-fit, and cytokine concentrations were calculated from the standard curve.

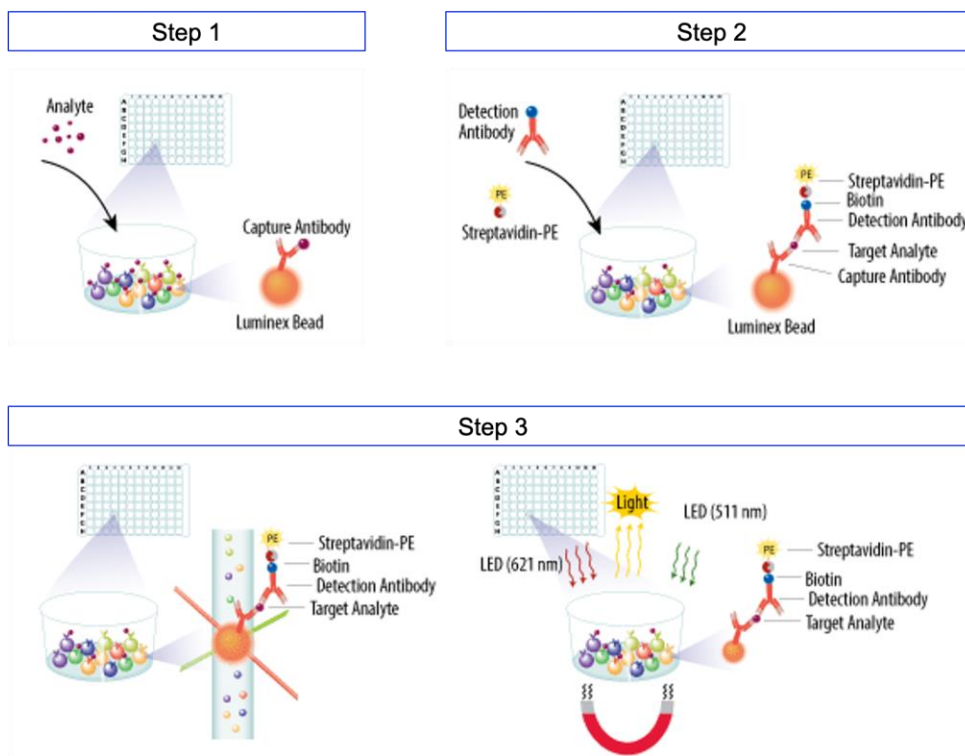


Figure 21. Luminex assay principle. Step 1, capture antibodies, bound to color-coded beads, bind to their specific target analytes. Step 2, biotinylated detection antibodies are added and bind to target analytes, forming an antibody-antigen sandwich. Then, phycoerythrin (PE)-conjugated streptavidin is added and binds to the biotinylated detection antibody. Step 3, beads are read using a Luminex 100[®] Analyzer with two lasers: a classification laser, which identifies the beads, and a reporter laser, which quantifies the analytes. Adapted from R&D Systems website.

6.2. Enzyme-linked immunosorbent assay (ELISA) to detect TGF- β

TGF- β is first synthesized as a precursor protein consisting of a large N-terminal portion called the latency-associated peptide and a short C-terminal fragment, which is the mature cytokine (Travis and Sheppard, 2014). For accurate quantification, latent TGF- β must be activated to the immunoreactive form in a two-step activation procedure: first, incubation with acid (0.17N HCl) for 10 minutes at RT, followed by neutralization with base (0.17 N NaOH/0.71 M HEPES). Because of the sample pretreatment, TGF- β cannot be multiplexed with other cytokines. TGF- β active form was quantified in cell culture supernatants using the assay DuoSet ELISA Mouse TGF- β 1 (R&D Systems), following manufacturer's instructions. Briefly, a microplate was pre-coated with capture antibody overnight at RT and subsequently blocked with 5% Tween20 in PBS for 1 hour at RT. Samples and standards were then added and incubated for 2 hours at RT: any analyte present was bound by the immobilized antibody, while unbound materials were washed away. A second

biotinylated antibody was added and incubated for 2 hours at RT: this detection antibody bound to a different epitope of the captured analyte (unbound antibody was washed away). Streptavidin-HRP was used to bind to the detection antibody (unbound streptavidin-HRP was washed away). TMB substrate solution was added to the wells and a blue color developed proportionally to the amount of analyte present in the sample. Color development was stopped by adding 2 N H₂SO₄, turning the color in the wells to yellow. Finally, the absorbance of the sample at 450 nm was measured.

7. Amyloid β_{1-42} (A β_{1-42}) oligomers preparation

During recent years, it is becoming increasingly clear that amyloid β_{1-42} oligomers, rather than monomers, fibrils or amyloid plaques, are the most relevant neurotoxin in Alzheimer's disease. However, preparation of A β oligomers constitutes a complex method, and the difficulty to obtain reproducible oligomer preparations between different batches is the main reason for the existence of different protocols (Caballero et al., 2016). Based on the methods described by Núñez and coworkers (Núñez et al., 2018), we designed a new protocol to prepare A β oligomers, which is summarized in **Figure 22**.

First, 1 mg of amyloid β_{1-42} peptide (4514.10 g/mol) was equilibrated at RT for 30 minutes and then solved in 222 μ l of ice-cold 1,1,1,3,3,3-hexafluoro-2-propanol (HFIP) to reach a concentration of 1 mM. The peptide was incubated at RT for 1 hour to allow monomerization and randomization of structure. Then, the monomerized A β peptide/HFIP solution was placed back on ice for 1 hour, to reduce HFIP evaporation during aliquoting. The A β peptide/HFIP solution was quickly aliquoted in three non-siliconized vials (74 μ l/vial) and allowed to evaporate with caps opened for 2 hours at RT. The tubes were spun in a SpeedVac centrifuge (800g, 10 minutes at RT, less than 25°C to avoid peptide denaturalization) to remove the HFIP and to get the A β peptide as a film. The peptide film was then resuspended in 14.6 μ l of DMSO to get A β 5 mM. To completely dissolve the film, samples were under orbital agitation (70 rpm) for 30 minutes. Then, the A β peptide solution was sonicated in an ultrasonic bath for 10 minutes and finally spared in 1.6 μ l aliquots and frozen at -20°C until use (**Figure 22A**).

For A β oligomerization, aliquots of monomerized A β were left at RT until thawed, and then were added 98.4 μ l of oligomerization medium (DMEM without additives to avoid interferences with the oligomerization process). In parallel, 1.6 μ l of DMSO were mixed with 98.4 μ l of oligomerization medium to obtain a carrier control. Samples were then sonicated in bath for 10 minutes. To optimize the oligomerization, we assessed two temperatures (4°C and 37°C) and two times (24h and 48h) and determined that the best oligomerization protocol in our hands was to incubate A β at 4°C for 24 hours (**Figure 22B**).

To check the reproducibility of A β oligomers preparations, after each experiment we characterized an aliquot of A β oligomers by protein electrophoresis followed by either Coomassie

staining or immunoblotting (**Figure 22C**). For Coomassie staining, the gel containing the A β samples was stained with Coomassie solution [0.2% Coomassie brilliant blue in methanol] overnight at 4°C and destained with destaining solution [7.5% acetic acid, 25% EtOH] for 30 minutes at RT, both processes under agitation. For immunoblotting, proteins were transferred from the gel into a PVDF membrane, as described in Section 5.

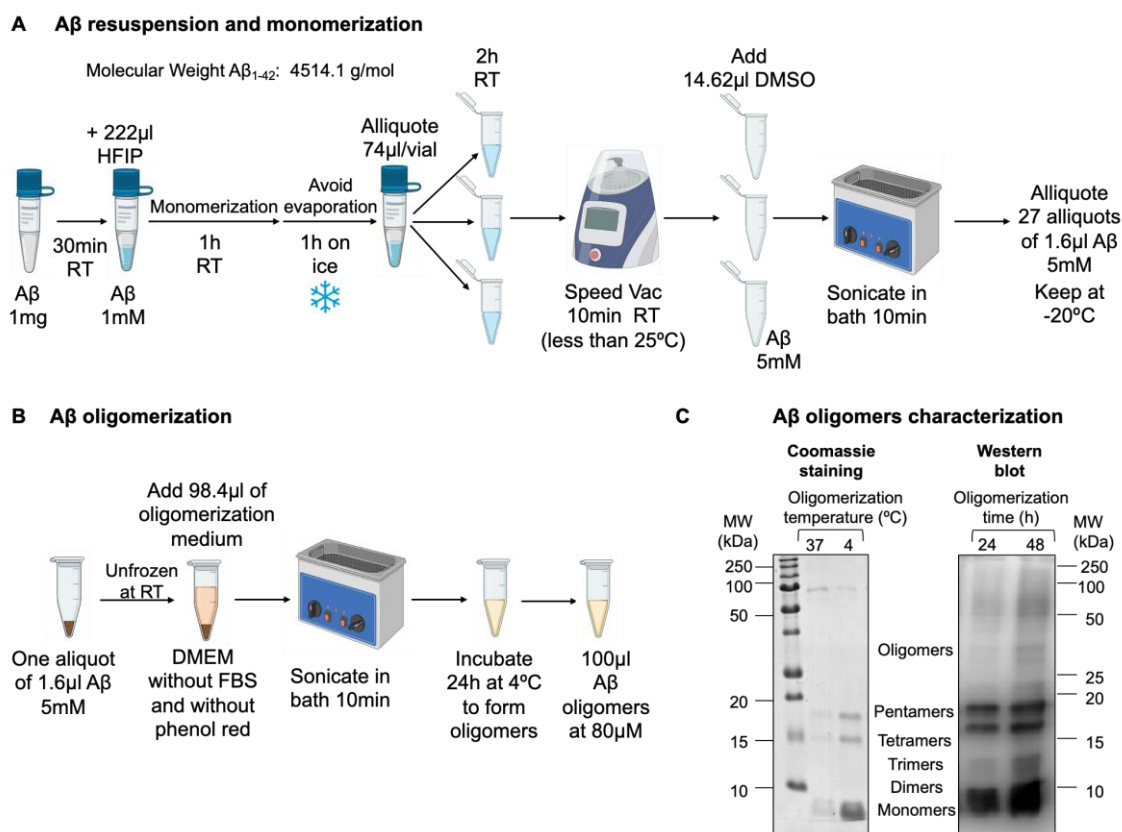


Figure 22. Protocol to prepare A β oligomers. **A)** A β_{1-42} resuspension and monomerization. **B)** A β oligomerization. **C)** A β oligomers characterization: the A β oligomers were visualized either by Coomassie staining or by Western blot.

7.1. Fluorescent amyloid- β_{1-42} (FAM-A β) oligomers preparation

The protocol to prepare fluorescently labeled A β oligomers was slightly different from the standard one. First, 0.5 mg of 5-FAM-amyloid β_{1-42} peptide (4872.41 g/mol) was allowed to equilibrate at RT for 30 minutes and then solved in 102.6 μ l of ice-cold HFIP to reach a concentration of 1 mM. The peptide was incubated at RT for 1 hour and on ice for 1 hour. The FAM-A β peptide/HFIP solution was quickly aliquoted in two non-siliconized vials (50 μ l/vial) and allowed to evaporate with caps opened for 2 hours at RT. The tubes were spun in a SpeedVac centrifuge (800g, 10 minutes at RT, less than 25°C to avoid peptide denaturalization) to remove the HFIP and to get the A β peptide as a film. The peptide film was then resuspended in 10.26 μ l of DMSO to get FAM-A β 5mM. Samples were under orbital agitation (70 rpm) for 30 minutes. Then, the FAM-A β peptide solution was sonicated in an ultrasonic bath for 10 minutes and finally spared in 1.6 μ l aliquots and frozen at -20°C until use. For A β oligomerization, aliquots of monomerized FAM-A β were left at RT

protected from light until unfrozen, and then were added 98.4 μ l of oligomerization medium (DMEM without additives to avoid interferences with the oligomerization process). In parallel, 1.6 μ l of DMSO were mixed with 98.4 μ l of oligomerization medium to obtain a carrier control. Samples were then sonicated in bath for 10 minutes, and then incubated at 4°C for 24 hours to form oligomers.

8. Immunocytochemistry

The immunocytochemistry (ICC) technique is used to visualize the localization of a specific protein or to detect a protein expression pattern in cells by using specific primary antibodies that recognize target's epitopes and fluorescence-coupled secondary antibodies recognizing the first ones. In addition, nuclear staining allows to identify individual cells.

8.1. Seeding procedures

BV-2 cells were counted using a Neubauer chamber, and 75000 cells were plated on 12 mm diameter coverslips (\sim 66500 cells/cm²) in complete medium (RPMI 1640 + 5% FBS + 1% L-glutamine + 1% P/S). After receiving their correspondent treatments, cells were washed twice with PBS and processed as described in the following sections.

8.2. *In vivo* labeling

To detect cell-surface proteins, live cells attached to 12 mm diameter glass coverslips were incubated at 4°C for 5 minutes to stop the endocytosis machinery. Then, cells were exposed to an antibody cocktail in RPMI medium with 1% FBS for 20 minutes at RT. After washes with PBS, cells were fixed with 4% formaldehyde in PBS for 10 min at RT. Then, cells were permeabilized with 1% non-immune goat serum in 0.1% Tween-20 in PBS. Alexa Fluor 488 or 594-conjugated IgGs (Jackson Labs) were used as secondary antibodies. After washes in PBS, samples were mounted with Vectashield with DAPI.

8.3. Post-fixation labeling

To ensure free access of the antibodies to their target intracellular antigens, cells must be fixed and permeabilized. Fixation methods fall generally into two classes: cross-linking reagents and organic solvents. Both methods were tested in this work.

8.3.1 Paraformaldehyde fixation

Paraformaldehyde is a cross-linker reagent that forms intermolecular bridges, normally through free amino groups, thus creating a network of linked antigens. The classical protocol for cell fixation involved incubating the cells with freshly prepared 4% paraformaldehyde (methanol-free) in PBS for 15 minutes at RT under agitation, followed by three washes with PBS. However, it was necessary to overcome some problems such as cell detachment and excessive permeabilization. Therefore,

fixation conditions were changed to incubation with 2% paraformaldehyde in PBS during 10 minutes at RT, a mild fixation protocol that in our hands produced better results.

8.3.2. Methanol fixation

Methanol is an organic solvent commonly used as a fixative agent. Methanol removes lipids and dehydrates the cells, while precipitating the proteins on the cellular architecture. Cells were incubated in ice-cold methanol for 5 minutes at -20°C , and then three washes with PBS were performed.

8.3.3. Immunolabeling

After being fixed either with paraformaldehyde or methanol, samples were blocked with 1% non-immune goat serum either in PBS (non-permeabilizing conditions) or in 0.1% Tween-20 in PBS (permeabilizing conditions) for 30 minutes at RT. Cells were then incubated with primary antibodies in blocking solution overnight at 4°C . After washes in PBS, samples were incubated with fluorophore-bound secondary antibodies in PBS-Tween 0.1% for 1 hour protected from light. Following washes in PBS, samples were mounted with Vectashield Vibrance.

8.4. Antibodies used for ICC

Antibodies used for ICC experiments are summarized in **Tables 8** and **9**.

Table 8. Primary antibodies used in immunocytochemistry.

Antibody	Reference	Species	Fixation	Permeabilization and blocking	Dilution (Concentration)
IDE	Merck Millipore	Rabbit polyclonal	MetOH or PFA	PBS-Tween 0.1% 1% Goat Serum	1:10000 (0.1 $\mu\text{g}/\text{ml}$)
CD11b	DSHB	Rat monoclonal	PFA	PBS-Tween 0.1% 1% Goat Serum	1:500 (0.04 $\mu\text{g}/\text{ml}$)
Maackia – biotin	EY Lab.	-	PFA	PBS with 1% Goat Serum	1:500

Table 9. Secondary antibodies used in immunocytochemistry.

Antibody	Reference	Species	Dilution (Concentration)
Anti rabbit–Alexa Fluor 488	Jackson ImmunoResearch	Goat	1:2000 (0.75 $\mu\text{g}/\text{ml}$)
Anti rat–Alexa Fluor 594	Jackson ImmunoResearch	Goat	1:2000 (0.75 $\mu\text{g}/\text{ml}$)
Alexa Fluor 594–Streptavidin	Jackson ImmunoResearch	-	1:1000

8.5. Image acquisition

Labeled cells were visualized with an Eclipse 90i fluorescence microscope (Nikon) equipped with a DS-Ri1 (Nikon) digital CCD camera. Confocal images were obtained with a 63X oil immersion objective (HCX PL Apo CS NA = 1.4; Leica) attached to a confocal DMI 6000B microscope with a TCS SP8 confocal system (Leica) equipped with AOBs and AOTF systems. Fluorophores were excited with WLL laser (Leica) and a 405 line (Leica) controlled by LAS AF software (Leica).

Images were acquired under the same conditions of illumination, diaphragm and condenser adjustments, exposure time, background correction and color levels. Images were analyzed using FIJI (ImageJ) software.

9. Electron microscopy

BV-2 cells were plated on 12 mm diameter plastic coverslips at a density of 175000 cells/cm². To obtain a high density at the center of the coverslip, cells were seeded using a 100 µl drop and allowed to attach to the surface. One day after plating, cells were cultured in a low-serum medium (1% FBS-Charcoal stripped) for 24 hours. Then, cells were fixed in 4% paraformaldehyde plus 0.3% glutaraldehyde in PBS for 10 minutes at RT under agitation. After three washes in PBS, cells were blocked with 1% non-immune goat serum in PBS-Tween20 0.1% for 30 minutes at RT under agitation. Microglial cells were then incubated with rabbit serum anti-IDE primary antibody (1:20000) in blocking solution overnight at 4°C and washed three times with PBS. Samples were later incubated with ultra-small gold-conjugated goat anti-rabbit secondary antibodies (EMS) in PBS for 48 h at 4°C. After several washes with PBS, samples were post-fixed in 2% glutaraldehyde in PBS for 20 min, washed and the ultra-small gold particles were silver enhanced for 20 min at RT with AURION R-Gent Silver Enhancement for Electron Microscopy (EMS) following the manufacturer's indications. Later, samples were post-fixed with 0.5% OsO₄ in PBS for 20 min at 4°C and washed with PBS, dehydrated through a graded series of ethanol, and embedded in Epoxy EMBED-812 resin (EMS). Ultrathin sections were obtained with an Ultracut E ultramicrotome (Reichert/Leica), contrasted with uranyl acetate and lead citrate, and analyzed using a Tecnai Spirit Twin 120 kv electron microscope with a CCD Gatan Orius SC200D camera with DigitalMicrograph software. Electron microscopy was performed in collaboration with Dr. Concepción Lillo, from the Electron Microscopy Service-NUCLEUS (University of Salamanca).

10. Immunohistochemistry

Mouse brains were quickly removed after sacrifice and divided into two pieces following a mid-sagittal section. Brains were fixed by immersion in 4% paraformaldehyde overnight at 4°C and embedded in paraffin following standard procedures. Coronal slices (5 µm) were performed with a rotary microtome (Microm, Wayzata, MN, USA), serially mounted on Polysine™ slides (Menzel-Gläser), and dried. Sample processing was performed by CNB Histology Facility (UAM-CSIC, Madrid, Spain). Tissue slices were dewaxed in xylene and rehydrated through an ethanol series into PBS. Antigen retrieval was carried out using a sodium citrate buffer [10 mM sodium citrate, 0.05% Tween 20, pH 6.0]. The slices were then blocked and permeabilized with Triton X-100 (0.25% in PBS) and 1% non-immune goat serum. The following primary antibodies were used: mouse anti-GFAP (1 µg/ml, Santa Cruz Biotechnology) and rabbit anti-Iba1 (0.5 µg/ml, Wako). As secondary

antibodies, Alexa488-conjugated goat anti-mouse IgG and Alexa594-conjugated goat anti-rabbit IgG (1.5 µg/ml, Jackson ImmunoResearch) were used.

10.1. Image acquisition

Immunostained sections were visualized with an Eclipse 90i fluorescence microscope (Nikon) equipped with a DS-Ri1 (Nikon, Minato, Tokyo, Japan) digital camera. Images were acquired under the same conditions of illumination, diaphragm and condenser adjustments, exposure time, background correction and color levels. For each region, two different series 20 µm apart from each other were examined.

10.2. Image quantification

Astroglial and microglial fluorescence levels were quantified with FIJI (ImageJ) software. Astrogliosis was measured as a GFAP fluorescence intensity per unit area. For microgliosis measurements, Iba1-positive areas were calculated in each photograph, and the microglial reactivity was measured in terms of percentage of area Iba1-positive per section.

11. Biochemical membrane preparations

Cells were grown in 75 cm² flasks up to 80% confluence, and then harvested with GHCKS solution (BV-2 cell line) or mild trypsin (primary glial cultures). Samples were centrifuged (300 g, 5 minutes) and cell pellets were completely dried and stored at -80°C until use.

11.1. Crude membrane preparations

Cell pellets were mechanically homogenized in TNE-PI solution [50 mM Tris-HCl pH 7.4, 150 mM NaCl, 5 mM EDTA, 1X Protease Inhibitors] in a Dounce homogenizer by doing 20 strokes at 400 rpm on ice. Then samples were centrifuged (2840 g, 10 minutes, 4°C) and two phases were obtained: a pellet composed of dense cellular elements (nuclei, endoplasmic reticulum, mitochondria, etc.) and a soluble supernatant. The pellet was resuspended in lysis buffer [10 mM HEPES pH 7.6, 100 mM KCl, 1 mM EDTA pH 8.0, 0.5% sodium deoxycholate, 1% NP-40, 0.1% SDS, 10% glycerol, 1 mM DTT, 1X Protease Inhibitors], while the supernatant was transferred into a Quick-Seal tube and ultracentrifuged (100 Ti rotor, 100000 g, 75 minutes, 4°C) in a Beckman Coulter Optimal-100XP Ultracentrifuge. After centrifugation, two phases were obtained: supernatant, composed by cytosolic materials, and pellet, constituted by cell membranes. The membrane pellet was resuspended in lysis buffer, while the supernatant was concentrated using Amicon Ultra-4 Centrifugal Filter Devices, following manufacturer's instructions (centrifugation 2840 g, 40 minutes, 4°C; initial and final sample volumes were recorded to calculate a concentration factor). Protein concentrations were quantified using the Micro BCA™ protein assay kit. All fractions resulting from subcellular fractionation were analyzed by immunoblotting, as described in Section 5.

11.2. Lipid rafts isolation

Membrane preparations were performed as described above, but the membrane pellets were resuspended in TNE-PI solution, instead of lysis buffer, to maintain the integrity of cell membranes.

11.2.1. Membrane preparations quantification by Coomassie gel staining

To estimate the amount of starting material, membrane samples were run together with a standard curve (5-50 μg of a brain protein extract) on a 10% polyacrylamide gel. Proteins were stained by incubation in Coomassie solution [0.2% Coomassie brilliant blue in methanol] overnight at 4°C, followed by incubation in destaining solution [7.5% acetic acid, 25% ethanol] for 30 minutes at RT, both processes under agitation. Then, the gel was scanned using a GS-800 Calibrated Densitometer (**Figure 23A**) and the optical density (O.D.) for each lane was quantified using the Quantity One 1-D analysis software. A linear regression fit was performed to adjust the O.D. value for each standard curve point to the correspondent protein quantity, obtaining the formula $y = 1.59x + 63.92$, with an $R^2 = 0.98$ (**Figure 23B**). From this equation, the amount of protein present in each membrane preparation was estimated.

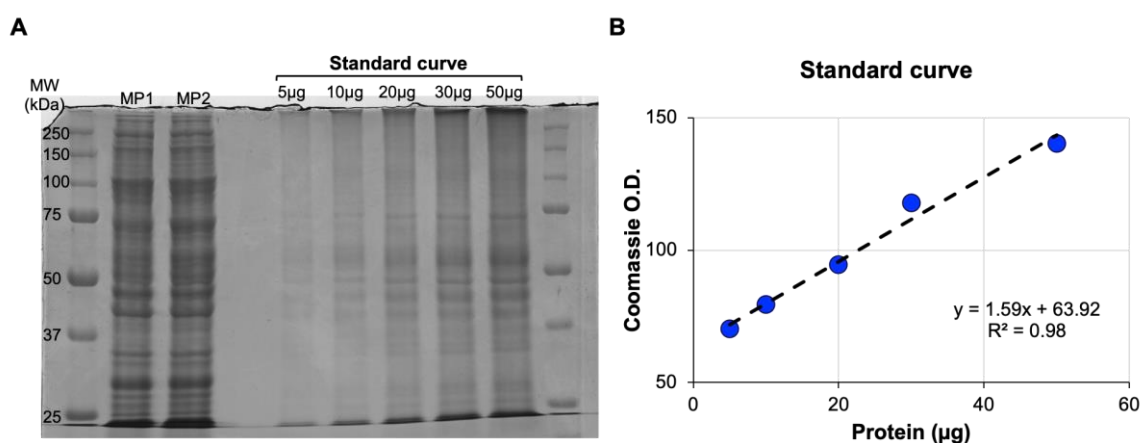


Figure 23. Protein quantification in membrane preparation samples. **A)** Polyacrylamide gel stained with Coomassie, with two membrane preparation samples (MP1 and MP2) and five samples constituting the standard curve. **B)** Linear regression fit between known protein quantities from the standard curve and optical densities.

11.2.2. Methods for lipid rafts isolation

After the publication, in 1992, of the seminal paper about membrane microdomains (Brown and Rose, 1992), “lipid rafts” and “detergent-resistant membranes” (DRM) became almost synonymous, describing the separation of a low-density, Triton-X100-insoluble fraction from epithelial cells. However, alternative biochemical methods for the isolation of lipid rafts were developed in order to address the possible artifactual nature of cellular fractions prepared using differential detergent solubilization.

11.2.2.1. Chemical methods

Chemical methods for lipid rafts isolation are based on the detergent-insolubility of these membrane domains. Since the use of different detergents have been described to allow separation of biochemically distinct DRMs, lipid rafts isolated with two different detergents (Triton-X100 and Triton-X114) were compared.

Triton-X100

Triton-X100-resistant membrane domains were isolated following the method described by Grassi and coworkers (Grassi et al., 2021), with minor modifications. The protein/detergent ratio turned out to be a critical parameter for the correct Triton-X100-resistant membranes isolation since an excess of detergent solubilizes even membrane domains with a high lateral order. This parameter was empirically determined for the BV-2 cell line as 400 µg proteins/µl Triton-X100. A total of 2 mg of membrane proteins were incubated with 1 ml of 0.5% Triton-X100 for 30 minutes at 4°C in orbital agitation.

Triton-X114

Triton-X114-resistant membranes were isolated as described by del Caño-Espinel (Caño Espinel, 2014). In brief, 400 µg of membrane proteins were incubated with 1% Triton-X114 in a volume of 1 ml for 40 minutes at 4°C in orbital agitation. In this case, the protein/detergent ratio was 40 µg proteins/µl Triton-X114.

11.2.2.2. Mechanical methods

To obtain a more comprehensive result of lipid rafts, and also to rule out the possibility of chemical artifacts when incubating the biological membranes with detergents, an alternative biochemical method was explored. In this protocol, 750 µg of membrane proteins were subjected to 5 sonication pulses. Each pulse (20 seconds, 30% amplitude) was followed by 1 minute cool-down incubation on ice. Immediately after the last pulse, sample was placed onto the sucrose gradient.

11.2.3. Sucrose density gradient

After the corresponding lipid rafts isolation protocol, samples were immediately transferred to Ultra-Clear centrifuge tubes containing 2.25 ml of 80% sucrose solution in TNE-PI, to have the samples in a final concentration of 55% sucrose (lowest part of gradient). Discontinuous sucrose gradients were created by adding, very gently, 6 ml of 35% sucrose in TNE-PI and then 3 ml of 5% sucrose in TNE-PI. The gradients were ultracentrifuged (SW40 rotor, 100000 g, 21 hours, 4°C), and a total of 12 fractions, 1 ml each, were collected top to bottom.

11.2.4. Protein precipitation and analysis

To precipitate proteins, each gradient fraction was incubated in 20% trichloro-acetic acid solution for 20 minutes. Protein precipitates were washed twice with cold ethanol, centrifuged (16000 g, 30 minutes, 4°C) and lyophilized in a SpeedVac centrifuge (800g, 15 minutes, at 35°C). Dried protein samples were resuspended in protein sample buffer for subsequent immunoblotting.

12. Extracellular vesicles isolation

Primary microglia, grown in 78.5 cm² Petri dishes, were detached from astrocytes as described in Section 2.2 and incubated in astrocyte-produced conditioned media supplemented with M-CSF (20 ng/ml) for 48 hours. After one wash with PBS at 37°C, cells (4 independent cultures with same cell density per experimental condition) were incubated with different treatments, prepared in RPMI medium without FBS, for 24 hours. Stimuli used were: 100 ng/ml LPS; 20 ng/ml IL-4 + 50 ng/ml IL-13; 25 μM PQ and 1 μM Aβ oligomers. Then, culture media were collected, pooled into 2 samples (each one coming from 2 independent cultures) and centrifuged (450 g, 10 minutes, 4°C) to pellet cells. The supernatants were subsequently filtered through a 0.2 μm PES filter to remove debris. Equal volumes of cell- and debris-free conditioned media were ultracentrifuged (100 Ti rotor, 120000 g, 75 minutes at 4°C) to pellet extracellular vesicles (EVs), and the resulting pellets were resuspended in protein sample buffer and analyzed by immunoblot.

13. Myelin preparations

Myelin isolation and labeling was performed as previously described, following a method based on discontinuous gradient centrifugation of sucrose (García-Mateo et al., 2018). Two-month-old mice were anesthetized with CO₂ and subsequently euthanized by cervical dislocation. The brain was quickly extracted and homogenized in 5 ml of 0.3 M sucrose in TED [20 mM Tris-HCl (pH 7.4), 2 mM EDTA (pH 8.0) and 1 mM DTT] buffer in a Dounce homogenizer, performing 10 strokes at 400 rpm. The homogenized tissue suspension, in 0.3 M sucrose solution, was placed on 0.83 M sucrose (1:1 ratio) and ultracentrifuged (30 minutes, 75000 g, 4°C) (SW40 rotor, Ultra-Clear 12.5 ml tubes). The myelin band, formed at the interphase between sucrose solutions (0.3 M / 0.83 M), was picked up and subsequently purified by sequential osmotic-shock wash steps. Initially, the myelin was mechanically homogenized in hypotonic solution (TED buffer) in a Dounce homogenizer, performing 10 strokes at 400 rpm. Then, samples were ultracentrifuged (15 minutes, 75000 g, 4°C) to pellet the myelin, while the cytosolic and microsomal contaminants were discarded away in the supernatant. This step was repeated twice. The resulting myelin was finally resuspended in 200 μl of sterile PBS. The yield of purified myelin, measured by the total amount of proteins in the sample, was determined by using the Micro BCA Protein Assay kit with minor modifications to the manufacturer's protocol: due to the high amount of lipids that compose myelin, samples needed to be solubilized in PBS with 2% SDS and, consequently, the standard curve for this assay was also prepared in the same buffer (PBS supplemented with 2% SDS).

DiI was used for myelin labeling. Myelin proteins (1 mg/ml) were incubated for 30 minutes at 37°C with 12.5 μg/ml of DiI in DMSO. Excess DiI was washed with sterile PBS and removed by ultracentrifugation (20 minutes, 24000 g, 4°C).

14. Flow cytometry

Flow cytometry is a biophysics laser-based technology for analyzing the characteristics of cells or particles. It is used to measure fluorescence intensity produced by fluorescently labeled antibodies detecting proteins, ligands that bind to specific cell-associated molecules, or fluorescent molecules exogenously added and endocytosed by cells. Experiments were performed in a Gallios flow cytometer, and data were processed and analyzed with Kaluza analysis software.

14.1. LIVE/DEAD viability assay

To determine the viability of primary microglial populations, we used the “LIVE/DEAD™ Fixable Near-IR Dead Cell Stain Kit” from Thermo Fisher Scientific. This assay is based on the reaction of a fluorescent reactive dye with cellular amines. The dye can permeate the compromised membranes of dying cells and react with free amines both in the interior and on the cell surface, resulting in intense fluorescent staining; while viable cells only have available cell-surface amines to react with the dye, resulting in a relatively dim staining. A staining control was routinely prepared by dividing one untreated primary microglial sample into two aliquots, one of which was heated at 99°C for 5 minutes to kill the cells, and after cooling both aliquots were rejoined; in this way, this sample should have 50% death and 50% alive cells (**Figure 24**).

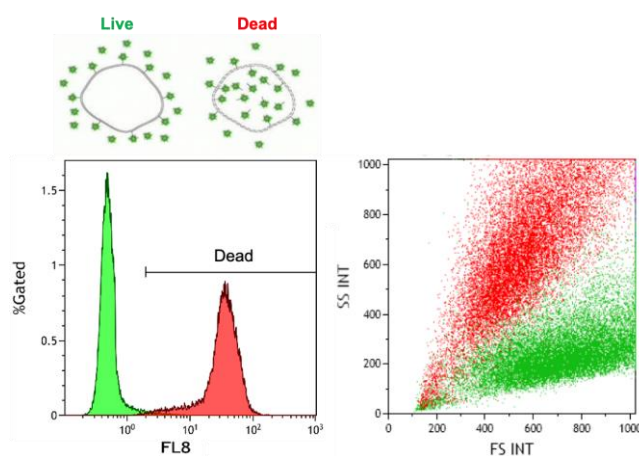


Figure 24. Principle of the LIVE/DEAD™ Fixable Dead Cell Stain Kits. *Live cells react with the dye only on their surface to yield weakly fluorescent cells, while cells with compromised membranes react with the dye throughout their volume, yielding brightly stained cells. This method clearly distinguishes the two populations, live (green) and dead (red) cells.*

Primary microglial cells plated on diverse formats (from 6-well plates to 9.5 cm² Petri dishes) were exposed to different treatments for 8 hours. After treatments, cells were washed with PBS, exposed to 1 ml of trypsin/EDTA 0.25% (2.5 mg/ml) for 15 minutes at 37°C, and added 2 ml of DMEM-F12 medium + 10% FBS for trypsin inactivation. Cells were harvested by resuspension with a micropipette and centrifuged (400 g, 5 minutes, 4°C, brake low), the supernatant was removed, and cell pellets were resuspended in 1 ml of FACS buffer (2% FBS, 3 mM NaN₃, 1 mM EDTA in PBS).

Samples were added 0.5 μ l of Live/Dead dye, mixed by vortex, incubated for 1 minute at RT and centrifuged (400 g, 5 minutes, 4°C, brake low) to wash away the excess of dye. Cell pellets were resuspended in 500 μ l of FACS buffer and immediately analyzed in a Gallios flow cytometer, exciting the cells with a red laser (633 nm), and collecting the fluorescence intensity in the 755 LP channel (>755 nm). At least 10000 cells of each condition were analyzed.

14.2. Myelin phagocytosis and degradation assays

Confluent primary microglial cultures, grown in 6-well plates (9.61cm²/well), were obtained as described in Section 2.2. Treatments with DiI-labeled myelin were prepared as follows: an aliquot of 10 μ g myelin-DiI was thawed from -20°C, sonicated in bath for 5 minutes and then added to microglial cultures in RPMI 1640 medium (final myelin concentration: 20 μ g/ml). Different time courses of treatments were explored: 3-18 hours for phagocytosis and 3-24 hours for degradation.

After the incubation period, non-phagocytosed and unbound myelin was removed by washing three times with PBS. Cells were collected as described above, by combining trypsin/EDTA incubation (2.5 mg/ml, 15 minutes, 37°C) and micropipette resuspension. After centrifugation (400 g, 5 minutes, 4°C), cells were resuspended in 500 μ l of FACS buffer and immediately analyzed in a Gallios flow cytometer. The amount of myelin phagocytosed and/or degraded was determined by measuring cellular fluorescence intensity recorded in the 575 BP30 channel (560-590 nm) after excitation with a blue laser (488 nm). At least 20000 cells of each condition were analyzed. The histograms of untreated microglia, not exposed to myelin-DiI, were used to define the fluorescence threshold value to consider events as DiI-positive microglia.

14.3 FAM-A β oligomers internalization and degradation assays

Treatments with FAM-A β oligomers (final concentration 1 μ M), prepared in RPMI 1640 medium without FBS, were added to primary microglial cultures grown at 6-well plates. Different time courses of treatments were explored: 30-180 minutes for internalization and 1-24 hours for degradation.

After the incubation period, cells were washed three times with PBS to remove non-internalized FAM-A β . Cells were collected as described above: trypsin/EDTA treatment (2.5 mg/ml, 15 minutes, 37°C) followed by resuspension with micropipette and centrifugation (400 g, 5 minutes, 4°C). To discard the signal from FAM-A β externally bound to cell membranes, cells were incubated with 0.05% trypan blue in PBS (pH 7.4) for 1 minute at RT to quench only extracellular signal, as previously described (Bjerknes and Bassoe, 1984), and illustrated in **Figure 25**. Then, samples were centrifuged (400 g, 5 minutes, 4°C) to wash out excess of trypan blue, cell pellets were resuspended in 500 μ l of FACS buffer and immediately analyzed in a Gallios flow cytometer. The amount of FAM-A β oligomers was determined by measuring cellular fluorescence intensity recorded in the 525 BP40 channel (505-545 nm) after illumination with a blue laser (488 nm).

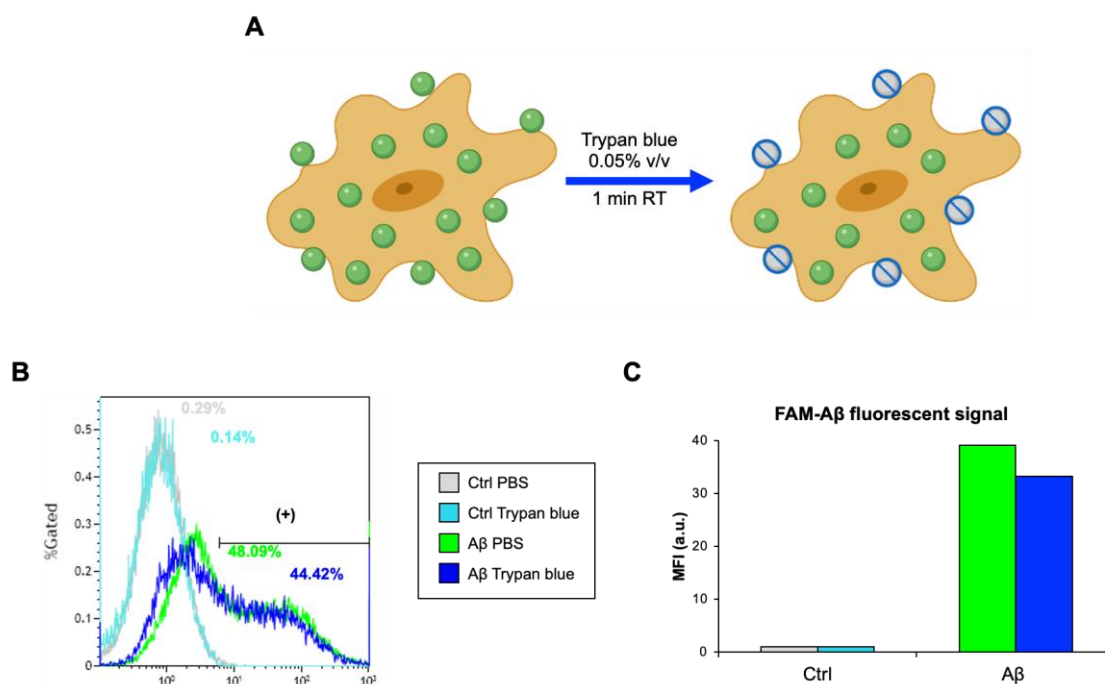


Figure 25. Technique to quench the fluorescence of extracellular, microglial-attached, FAM-A β oligomers. **A)** Trypan blue incubation for 1 minute at RT specifically quenches the fluorescence of extracellular, membrane bound, FAM-A β oligomers (represented as green circles). Since trypan blue is a vital dye, it is excluded by viable cells with intact membranes, thus not affecting the fluorescence of internalized FAM-A β particles, while it traverses the membrane of dead cells, being also a good live/dead marker that allows to discard dead cells from further analyses. **B)** Flow cytometry analysis of primary microglial cells either untreated or exposed to FAM-A β oligomers for 1 hour, and then incubated with PBS or trypan blue to quench extracellular FAM signal. The histogram depicts the percentage of cells gated at each experimental condition. **C)** Bar plot depicting the FAM-A β mean fluorescence intensity from the cells analyzed in B, with a clear decrease in FAM fluorescent signal in cells incubated with trypan blue.

15. Bioinformatic analyses

Bioinformatics is a multidisciplinary science field that develops methods and software tools for collecting, analyzing and understanding complex biological data. Otherwise, phylogenetics is the field of systematics that focus on evolutionary relationships between organisms, groups of organisms or even the genes and proteins found within organisms (Baxevanis et al., 2020). This *in silico* work was aimed to infer phylogenetic relationships between IDE and its homologous proteins, that is, how these proteins shared a common ancestor at some point in the past, with the final objective of elucidating the mechanism of exportation of IDE protein during evolution and its predicted subcellular localization.

15.1. Phylogeny based on protein sequence

Molecular phylogenetics is the study of evolutionary relationships performed by comparing biological sequences (nucleotides or amino acids). For sequence data analysis, each column of an alignment is considered to be a character or trait, with each amino acid residue or nucleotide in the column representing the particular state of that character (Baxevanis et al., 2020).

15.1.1. Sequence searches

Our initial biological question was aimed to find protein sequences that are homologous to IDE in any kingdom. The PSI-BLAST algorithm (Position-Specific Iterated BLAST) (Altschul, 1997), implemented in the NCBI online interface, was used to perform a sequence search to find homologous proteins to human IDE. The search was restricted to the non-redundant protein sequences global database, with a low-complexity region filter, and was set with the following parameters: to use a BLOSUM62 matrix, to exclude models and environmental samples, and to show only the sequences with an E-value lower than $1e-15$. General selection criteria for protein sequences were identity $\geq 25\%$ and coverage greater than 50%. After this initial search, 205 protein sequences were selected to construct an IDE's PSSM (Position-Specific Scoring Matrix), a scoring matrix in which amino acid substitution scores are given separately for each position in a protein multiple sequence alignment. Subsequent BLAST searches were performed individually in all taxonomic groups, maintaining the same criteria described above but using IDE's PSSM. With this strategy, we potentiated the retrieval of more distant homologues that in a general search would have been missed due to the high degree of conservation in IDE's primary sequence.

The recovered sequences were used to construct an IDE's database. To avoid overloading the database with redundant sequences (for example, truncated proteins identical to their longer form), two or more sequences belonging to the same organism and having $\geq 99\%$ identity were excluded, selecting only one representative per organism.

15.1.2. Multiple sequence alignments (MSAs)

Selected sequences were aligned using the MAFFT online server (Katoh et al., 2019), according to the following workflow: (1) To compare primary sequences from clan ME proteins, we used the MAFFT-Lins-i algorithm. (2) To study the global phylogeny of all IDE's homologous proteins, we first built a MSA from *Chordata* using the iterative algorithm L-ins-i. Then, we used the MAFFT-Add algorithm to include the remaining sequences with a progressive L-ins-i method keeping alignment length (parameters: BLOSUM62; Gap 1.53; Offset 0.0). (3) To study the evolution of IDE across species, sequences from 14 representative organisms were selected and aligned using the MAFFT E-ins-i algorithm, including a structural alignment between human IDE (PDB Id: 3CWW) and bacterial pitrilysin (PDB Id: 1Q2L). MSAs were visualized with Alignment Viewer (<http://alignmentviewer.org>).

15.1.3. Phylogenetic reconstruction

Phylogenetic trees based on MSAs were inferred using the IQ-TREE online server (<http://iqtree.cibiv.univie.ac.at>). First, a best-fit substitution model was selected by running the ModelFinder algorithm (Kalyaanamoorthy et al., 2017). Then, a maximum likelihood (ML) tree was created by using the algorithm implemented on the IQ-TREE server (Nguyen et al., 2015). Finally, branch support analysis was performed by using an Ultrafast Bootstrap approximation with 1000 replicas (Hoang et al., 2018). The resultant phylogenetic tree was visualized using FigTree v1.4.4 (<http://tree.bio.ed.ac.uk/software/figtree/>).

15.2. Bioinformatic prediction software

The presence of signal peptides was predicted using the SignalP5.0 server, based on a deep convolutional and recurrent neural network architecture (Almagro Armenteros et al., 2019). The subcellular localization of eukaryotic IDE's homologs was predicted using the DeepLoc-1.0 server, which uses deep neuronal networks to predict protein subcellular localization relying only on sequence information (Almagro Armenteros et al., 2017).

16. RNA sequencing (RNA-Seq)

RNA-Seq is a sequencing technique that uses next-generation sequencing (NGS) to reveal the presence and quantity of RNA in a biological sample by analyzing the transcriptome.

16.1. RNA isolation and quality control

WT and IDE-KO primary microglial cultures were prepared as described in Section 2.2. Each sample came from a 10 cm-diameter Petri dish (78.5 cm²). RNAs were extracted using the RNeasy kit (Qiagen), following manufacturer's instructions. The purity and yield of total RNA was assessed in a NanoDrop ND-1000 spectrophotometer, and then samples were processed by the Genomics Unit from the Instituto Gulbenkian de Ciencia (Lisbon, Portugal).

RNA quality was evaluated by microcapillary electrophoresis in a TapeStation System (Agilent Technologies, Waldbronn, Germany), and the integrity of RNA samples was calculated using the RNA integrity number (RIN) algorithm, which generates RIN values ranging from 10 (intact) to 1 (totally degraded) (Schroeder et al., 2006). All samples had RIN values between 9.9 and 10.

16.2. Library construction and sequencing

Libraries were prepared using the QuantSeq 3' mRNA-Seq Library Prep Kit for Illumina, according to the protocols recommended by the manufacturer. Sequencing was performed using NextSeq500 High Output kit (75 cycles), single-ended, 20 million reads per sample, in a HiSeq2000 platform.

16.3. Bioinformatic pipeline for RNA-Seq data analysis

Raw sequence data were subjected to a quality control check by using FastQC (Andrews, 2010). Then, accurate mapping of millions of short-sequence reads to the mouse reference genome (mm10 GRCm38) was performed using the STAR aligner (Dobin et al., 2013). The quality of the alignments was assessed with Qualimap2 (Okonechnikov et al., 2015), and then the aligned reads were visualized with the Integrative Genomics Viewer software (Robinson, 2011). Next, gene expression was quantified by featureCounts (Liao et al., 2014), and analysis of differential gene expression between WT and IDE-KO microglial cells was performed by using DESeq2 (Love et al., 2014). Finally, functional enrichment analyses were carried out with gprofiler2 (Kolberg et al., 2020) (see **Figure 26**). Five independent RNA samples of each genotype (WT and IDE-KO) were obtained, but we started sequencing triplicates. The principal component analysis of the sequenced samples suggested to discard one sample of each genotype, so the transcriptomic analysis was performed, for the moment, comparing 2 samples per genotype.

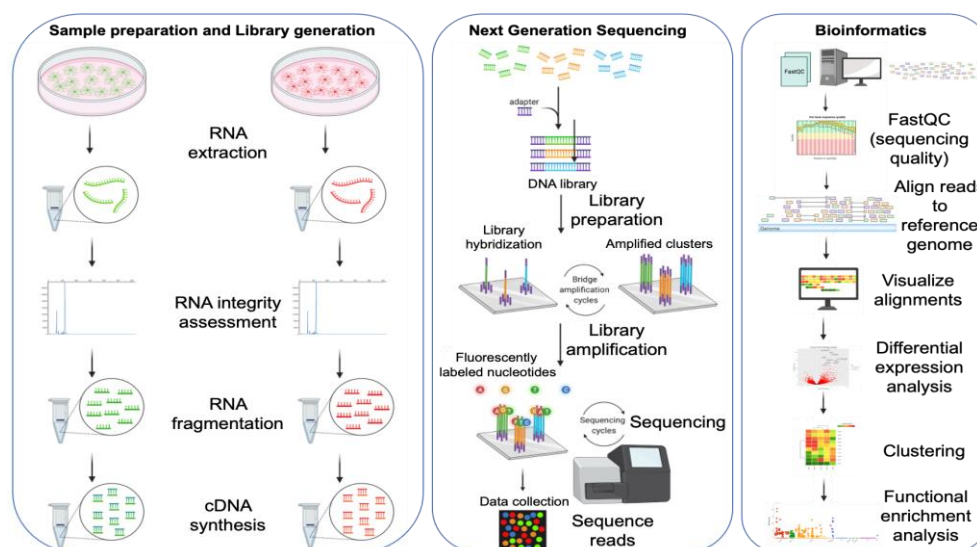


Figure 26. Transcriptome analysis pipeline. Steps for RNA-seq experiments: sample preparation and library generation, NGS and bioinformatic analyses based on Linux command lines and R.

17. Statistical analyses

Data are represented either as mean \pm standard error of the mean (SEM) or median \pm interquartile range. Statistical analyses were performed with SigmaPlot and RStudio. To check the normality of distributions, Kolmogorov-Smirnov test was used. To analyze statistically significant differences between two sets of data, we applied Student's t-test (parametric data) or Mann-Whitney U test (non-parametric data). Comparisons between more than two groups of data were performed using ANOVAs of as many ways as factors (for parametric data) and Kruskal-Wallis test (for non-parametric data). Post-hoc analyses were carried out using Bonferroni tests (parametric data) or Holm-Sidak tests (non-parametric data). A P value <0.05 was used as a threshold for significant changes. The tests used for each experiment are stated in figure legends.

18. Reagents and resources

Table 10. Reagents and resources used during this thesis (continued)

REAGENT OR RESOURCE	SOURCE	IDENTIFIER
Antibodies		
Alexa Fluor 594-conjugated Streptavidin	Jackson Immuno Research	Cat#016-580-084
Donkey anti goat IgG - HRP	Jackson Immuno Research	Cat#705-035-003
Goat anti ApoD	Santa Cruz Biotechnology	Cat#sc34760
Goat anti integrin α M (M-19) (CD11b)	Santa Cruz Biotechnology	Cat#sc-6614
Goat anti mouse IgG - HRP	Dako Cytomation	Cat#P0448
Goat anti Mouse IgG-Alexa 488	Jackson Immuno Research	Cat#115-545-003
Goat anti Mouse IgG-Alexa 594	Jackson Immuno Research	Cat#115-585-166
Goat anti rabbit IgG - HRP	Jackson Immuno Research	Cat#111-035-003
Goat anti Rabbit IgG-Alexa 488	Jackson Immuno Research	Cat#111-545-003
Goat anti rabbit-gold conjugated	Electron Microscopy Sciences	Cat#25105
Goat anti-Rat IgG Alexa 594	Jackson Immuno Research	Cat#111-585-144
Insulin receptor β (4B8)	Cell Signaling Technology	Cat#3025
Maackia amurensis lectin, biotin conjugated	EY Laboratories	Cat#BA-7801-5
Mouse anti arginase-1	Santa Cruz Biotechnology	Cat#sc-271430
Mouse anti Flotillin-1	BD Laboratories	Cat#610820
Mouse anti GFAP (2E1)	Santa Cruz Biotechnology	Cat#sc-33673
Mouse anti Iba1	Santa Cruz Biotechnology	Cat#sc-32725
Mouse anti IDE (F-9)	Santa Cruz Biotechnology	Cat#sc-393887
Mouse anti PMCA1/4 (5F10)	Santa Cruz Biotechnology	Cat#sc-20028
Mouse anti β -actin-HRP conjugated	Sigma Aldrich	Cat#A3854
Mouse anti β -amyloid (B-4)	Santa Cruz Biotechnology	Cat#sc28365
Rabbit anti Akt	Cell Signaling Technology	Cat#9272
Rabbit anti COX-2	Cayman	Cat#160126
Rabbit anti Iba1	Wako	Cat#019-19741
Rabbit anti IDE	Merck Millipore	Cat#AB9210
Rabbit anti insulin receptor β (Tyr1150/1151) (19H7)	Cell Signaling Technology	Cat#3024
Rabbit anti Phospho-Akt (Ser473)	Cell Signaling Technology	Cat#9271
Rat anti CD11b (Mac-1)	DSHB	Cat#M1/70.15.11.5.2
Chemical, peptides and recombinant proteins		
1,1,1,3,3,3-hexafluoro-2-propanol (HFIP)	Sigma-Aldrich	Cat#105228
1,1'-Dioctadecyl-3,3,3',3'-tetramethylindocarbocyanine perchlorate (DiI)	Sigma-Aldrich	Cat#42364
2-(p-Nonylphenoxy)ethanol (NP-40)	Sigma-Aldrich	Cat#N-6507
2-methylbutane (isopentane)	Merck	Cat#M32631
2-Propanol (isopropanol)	Merck	Cat#109634
5-FAM-amyloid β protein (1-42)	Bachem AG	Cat#4090151
Acetic acid (glacial 100%)	Merck	Cat#100063
Acrylamide-bis ready-to-use solution 30% (37.5:1)	Merck	Cat#100639
Agarose	Thermo Fisher Scientific	Cat#10583355
Amyloid β protein (1-42)	Bachem AG	Cat#4014447
AURION R-Gent Silver Enhancement	Electron Microscopy Sciences	Cat#500.033
Bovine serum albumin (BSA)	Sigma-Aldrich	Cat#A7906
Chlorhidric acid (HCl) 37%	PanReac AppliChem	Cat#131020
Chloroform	Merck	Cat#102442
Coomassie brilliant blue	BioRad	Cat#161-0400
D-glucose solution	Gibco	Cat#A24940
D-Mannitol	Sigma-Aldrich	Cat#M4125
Deoxyribonuclease I, bovine pancreas	Sigma-Aldrich	Cat#9003-98-9
DEPC-Treated Nuclease free water	Ambion	Cat#AM9915G
Dimethyl sulphoxide (DMSO)	Sigma-Aldrich	Cat#D2650
Dithiothreitol (DTT)	BioRad	Cat#1610610

Table 10. Reagents and resources used during this thesis (continued)

REAGENT OR RESOURCE	SOURCE	IDENTIFIER
Dnase I, Rnase-free	Fermentas	Cat#EN0521
Dodecyl sulfate sodium salt, 99%, for biochemistry	Acros Organics	Cat#230425000
Dream Taq Hot Start PCR Master Mix	Thermo Fisher Scientific	Cat#15669374
Dulbecco's Modified Eagle Medium w/o phenol red	Lonza	Cat#BE12917F
Dulbecco's Modified Eagle Medium:Nutrient Mixture F-12 (DMEM/F-12)	Gibco	Cat#21331020
Earle's Balanced Salt Solution (EBSS)	Lonza	Cat#BE10-502F
EDTA, tetrasodium tetrahydrate salt	Calbiochem	Cat#34103
Epoxy Embed-812 resin	Electron Microscopy Sciences	Cat#14120
Ethanol for Molecular Biology	Merck	Cat#108543
Foetal bovine serum (FBS)	Gibco	Cat#11573397
Foetal bovine serum Charcoal stripped (FBS-CHST)	Gibco	Cat#12676011
Formaldehyde, 10%, methanol free, ultra pure	Polysciences	Cat#04018
Gelatin	Sigma-Aldrich	Cat#G2500
Glutaraldehyde	Merck	Cat#G5882
Glycerol	Sigma-Aldrich	Cat#G7893
Glycine	Thermo Fisher Scientific	Cat#10070150
HEPES	Sigma-Aldrich	Cat#H4034
Hoechst 33342	Invitrogen	Cat#H3570
Humulin R	Eli Lilly and Company	Cat#HI-0210
Immobilon ECL Ultra Western HRP substrate	Millipore	Cat#WBULS0100
Insulin solution human, sterile-filtered, BioXtra	Sigma-Aldrich	Cat#I9278
L-glucose	Sigma-Aldrich	Cat#G5500
Lipopolysaccharides (LPS) from Escherichia coli O111:B4	Sigma-Aldrich	Cat#L2630
LIVE/DEAD™ Fixable Near-IR Dead Cell Stain Kit	Invitrogen	Cat#L10119
Methanol (Reag.Ph.Eur) for UHPLC	PanReac AppliChem	Cat#221091
Methyl viologen dichloride hydrate (paraquat)	Sigma-Aldrich	Cat#856177
Normal goat serum (NGS)	Thermo Fisher Scientific	Cat#1077043
Osmium tetroxyde (OsO4)	Sigma-Aldrich	Cat#201030
Penicillin Streptomycin	Gibco	Cat#15140122
Penicillin Streptomycin Amphotericin B	Lonza	Cat#17-745E
Phosphatase inhibitor cocktail 2	Sigma-Aldrich	Cat#P5726
Phosphatase inhibitor cocktail 3	Sigma-Aldrich	Cat#P0044
Phosphate-buffered saline (PBS), pH 7.2	Gibco	Cat#11530546
PMSF	Sigma-Aldrich	Cat#P7626
Poly-L-lisine solution 0.01%	Merck	Cat#P4707
Potassium chloride (KCl)	Merck	Cat#K34333136
PrimeScript RT-PCR kit	Takara Bio, Japan	Cat#RR064A
Protease inhibitor cocktail	Sigma-Aldrich	Cat#P8340
Proteinase K from Tritirachium album	Sigma-Aldrich	Cat#P8044
QIAzol lysis reagent	Qiagen	Cat#79306
Recombinant murine IL-13	PeptoTech	Cat#210-13
Recombinant murine IL-4	PeptoTech	Cat#214-14
Recombinant murine M-CSF	PeptoTech	Cat#315-02
RedSafe nucleic acid staining solution	iNtRON Biotechnology	Cat#21141
Roswell Park Memorial Institute (RPMI) 1640 Medium	Gibco	Cat#11530586
Roswell Park Memorial Institute (RPMI) 1640 Medium, no glucose	Gibco	Cat#11560406
Sodium chloride (NaCl)	Acros Organics	Cat#10478283
Sodium citrate dihydrate	Merck	Cat#106448
Sodium deoxycholate	Sigma-Aldrich	Cat#D6750
Sucrose	Sigma-Aldrich	Cat#S0389
TB Green Premix Ex Taq II (Tli Rnase H Plus)	Takara Bio, Japan	Cat#RR820A
Thiazolyl Blue Tetrazolium Bromide (MTT)	Sigma-Aldrich	Cat#M5655

Table 10. Reagents and resources used during this thesis (continued)

REAGENT OR RESOURCE	SOURCE	IDENTIFIER
Trichloroacetic acid (TCA)	Carlo Erba Reagents	Cat#307557
Tris(hydroxymethyl)aminomethane hydrochloride	VWR Life Science	Cat#441514A
Tris(hydroxymethyl)aminomethane, for biochemistry	Acros Organics	Cat#140500025
Triton-X100	Acros Organics	Cat#10671652
Triton-X114	Sigma-Aldrich	Cat#93422
Trypan blue stain	Lonza	Cat#17-942E
Trypsin-EDTA 0.25%	Gibco	Cat#11570626
Tween-20	BioRad	Cat#1706531
Vectashield Vibrance antidode mounting medium	Vector Laboratories	Cat#30304
Commercial assays		
Click-iT EdU imaging kit	Invitrogen	Cat#C10086
DuoSet ELISA mouse TGF- β 1	R&D systems	Cat#DY1679
Luminex assay	R&D systems	N/A
Micro BCA protein assay kit	ThermoFisher Scientific	Cat#23235
Sample activation kit 1	R&D systems	Cat#DY010
Ultra-sensitive mouse insulin ELISA kit	Crystal Chem	Cat#90080
Mycoplasma get detection kit	Biotoools	Cat#90021
NextSeq 500/550 High Output kit v2.5 (75 cycles)	Illumina	Cat#20024906
QuantSeq 3' mRNA-Seq Library Prep Kit for Illumina	Lexogen	Cat#015
RNeasy Plus Mini Kit	Qiagen	Cat#74104
Equipment		
Bioblock scientific ultrasonic processor	VibraCell	
BioRad electrophoresis system	BioRad Laboratories	
BioRad Gel Transfer Device	BioRad Laboratories	
Centrifuge 5415R	Eppendorf	
Confocal DMI 6000B microscope TCS SP8 confocal system	Leica Microsystems	
Digital weight scale	Ohaus	
Dounce homogenizer	Sartorius	
Eclipse 90i fluorescence microscope	Nikon	
Gallios Flow Cytometer	Beckman Coulter	
Gel Doc XR	BioRad Laboratories	
Gel XL Ultra V-2 Horizontal Electrophoresis System	LabNet International	
GENios Pro Fluorimeter	MTX Lab Systems	
Glucometer	Contour X	
GS-800 Calibrated Densitometer	BioRad Laboratories	
JEOL JEM-1011 HR transmission electron microscope	JEOL USA	
Leica VT1200S Vibratome	Leica Microsystems	
Luminex 100 Analyzer	Luminex	
MIR-100 infrared digital camera	Med Associates	
MJ Mini Personal Thermal Cycler	BioRad Laboratories	
NanoDrop N-D1000	ThermoScientific	
Optimal-100XP Ultracentrifuge	Beckman Coulter	
Rotanta 460R Hettich centrifuge	Hettich	
Experimental models (cell lines)		
BV-2 cell line	ATCC	N/A
Raw264.7 cell line	ATCC	N/A
Experimental models (organisms)		
Mouse Ide ^{mla} (EUCOMM)Wtsi	Provided by Dr. Leissring	MGI:4431946
Materials		
0.2 μ m Fisherbrand Sterile PES syringe filter	Thermo Scientific	Cat#15206869
10 cm diameter Nunclon Delta Petri dishes	Thermo Scientific	Cat#172958
12 ml conical tubes with screw caps	Sanicompras	Cat#3114051VE
15 ml SuperClear centrifuge tubes with screw caps	Labcon	Cat#3141335018
24-well x 1ml multidish cell culture (Nunc)	Thermo Scientific	Cat#142475

Table 10. Reagents and resources used during this thesis.

REAGENT OR RESOURCE	SOURCE	IDENTIFIER
35 mm diameter Nunclon Delta Petri dishes	Thermo Scientific	Cat#153066
4-well x 1ml multidish cell culture dish (Nunc)	Thermo Scientific	Cat#176740
50 ml conical centrifugal tubes	Thermo Scientific	Cat#362696
6-well x 3ml multidish cell culture (Nunc)	Thermo Scientific	Cat#140675
96-microwell, Nunclon D-Treated microplate	Thermo Scientific	Cat#167008
96-well black/clear flat bottom TC-treated imaging microplate	Falcon	Cat#353219
Amicon Ultra-0.5 ml centrifugal filters 10K	Merck Millipore	Cat#UFC501024
Amicon Ultra-4 Centrifugal filters 10K	Merck Millipore	Cat#UFC801024
Cell scraper	Falcon	Cat#353085
Eppendorf tubes	Eppendorf	N/A
Microscope slides Menzel-Gläser	Thermo Scientific	Cat#15998086
Microvette capillary tubes	Sarstedt	Cat#16444
PVDF Immobilon-P membranes, 0.45 µm	Merck Millipore	Cat#WBKL50100
Quick-Seal tubes (13x64 mm)	Beckman Coulter	Cat#344619
Round coverslips for cell culture	Thermo Scientific	Cat#174942
T25 EasYFlask, TC surface, filter cap, Nunc (flask 25 cm ²)	Thermo Scientific	Cat#156340
T75 EasYFlask, TC surface, filter cap, Nunc (flask 75 cm ²)	Thermo Scientific	Cat#156499
Ultra-Clear centrifuge tubes (14x95 mm)	Beckman Coulter	Cat#344060
Software and algorithms		
Activity monitor (v.5.0)	Med Associates	
DeepLoc-1.0	Almagro-Armenteros <i>et al.</i> (2017)	http://www.cbs.dtu.dk/services/DeepLoc/
Deseq2	Love <i>et al.</i> (2014)	https://bioconductor.org/packages/release/bioc/html/DESeq2.html
Excel	Microsoft Office	
FastQC	Babraham Bioinformatics	https://www.bioinformatics.babraham.ac.uk/projects/fastqc/
FeatureCounts	Liao <i>et al.</i> (2014)	http://bioinf.wehi.edu.au/featureCounts/
FigTree		http://tree.bio.ed.ac.uk/software/figtree/
Fiji	Schindelin <i>et al.</i> (2012)	https://imagej.net/Fiji
Gprofiler2	Kolberg <i>et al.</i> (2020)	https://biit.cs.ut.ee/gprofiler/gost
Integrative Genomics Viewer (IGV)	Robinson <i>et al.</i> (2011)	http://software.broadinstitute.org/software/igv/home
Kaluza analysis software (v.1.3)	Beckman Coulter	
Prism 6.0	GraphPad	https://www.graphpad.com/
Qualimap 2	Okonechnikov <i>et al.</i> (2015)	http://qualimap.conesalab.org
Quantity One 1D Analysis software	BioRad Laboratories	
R	R Development Core Team, 2020	https://www.R-project.org/
SigmaPlot (v.11.0)	Systat Software	
SignalP-5.0	Almagro-Armenteros <i>et al.</i> (2019)	http://www.cbs.dtu.dk/services/SignalP/
SOFTmax Pro software package (v.4.7)	Molecular Devices	
STAR	Dobin <i>et al.</i> (2014)	https://github.com/alexdobin/STAR
XFluor4 GENiosPro software	TECAN	

RESULTS

CHAPTER 1. EFFECTS OF DM- AND AD-RELATED STIMULI ON MICROGLIAL FUNCTIONS AND REGULATION OF IDE EXPRESSION IN A CELL-LINE PARADIGM

“Type 3 diabetes”, despite being a controversial term sometimes used to refer to Alzheimer’s disease (AD), highlights the possibility that dementia might be triggered by a type of insulin resistance happening specifically in the brain. Peripheral insulin resistance is linked with high blood glucose levels, which can cause bouts of inflammation, and is also connected with higher levels of A β in the brain. In this scenario, it becomes especially relevant to understand the effects that chronic exposure to high D-glucose induces on microglia, the primary immune cells in the brain and the main cell type involved in amyloid clearance.

We used an *in vitro* paradigm in which the murine cell lines BV-2 (microglia) and Raw264.7 (macrophages) were exposed to different AD- and DM-related conditions such as chronic high D-glucose, LPS as a pro-inflammatory stimulus, paraquat as an oxidative stressor and IL-4+IL-13 as an anti-inflammatory stimulus. In many ways, microglia and macrophages are similar: they are immune cells that guard their environment and phagocytose offenders, and both produce an array of cytokines and growth factors depending on the exact stimulus that led to their activation. However, they differ in many aspects such as their lineage, location on the body, activation triggers and expressed biomarkers. Therefore, the comparison of both cell types was relevant.

Finally, a combination of high D-glucose and A β oligomers was studied in microglial cells as the experimental paradigm of type 3 diabetes.

1.1. Chronic high D-glucose stimulates metabolic activity specifically on microglial cells

To analyze how chronic exposure to high D-glucose affects metabolic activity, we performed multi-well plate MTT assays, normalized to the number of cells by Hoechst staining. Cells were plated on a 96-well plate and, after an overnight serum fasting, cells were exposed to different concentrations of D-glucose (2-22 mM) and L-glucose or mannitol as osmotic controls for 72 hours. Culture media were replaced at 36 hours so that the D-glucose concentration did not change due to consumption by the cells. Moreover, this media refreshment also avoided osmotic differences between treatments since, unlike D-glucose, L-glucose and mannitol cannot be metabolized by the cells (**Figure 27A**). Microglial cells showed a significant increase in their metabolic activity when they were chronically exposed to high (11 mM) or very high (22 mM) D-glucose, in comparison to the control condition (5.5 mM D-glucose), while low D-glucose (2 mM) showed no effects on metabolic activity. Osmotic controls showed also increased metabolic activity, but significantly lower than D-glucose alone, which indicates a partial effect of osmolarity, but the highest increase of metabolic activity can be attributed to high D-glucose chronic exposure (**Figure 27B**).

Macrophages showed no differences in their metabolic activity with respect to the control condition in none of the experimental conditions studied (**Figure 27C**). These results indicate that chronic high D-glucose exposure stimulates metabolic activity specifically on microglial cells, while macrophages remain unchanged.

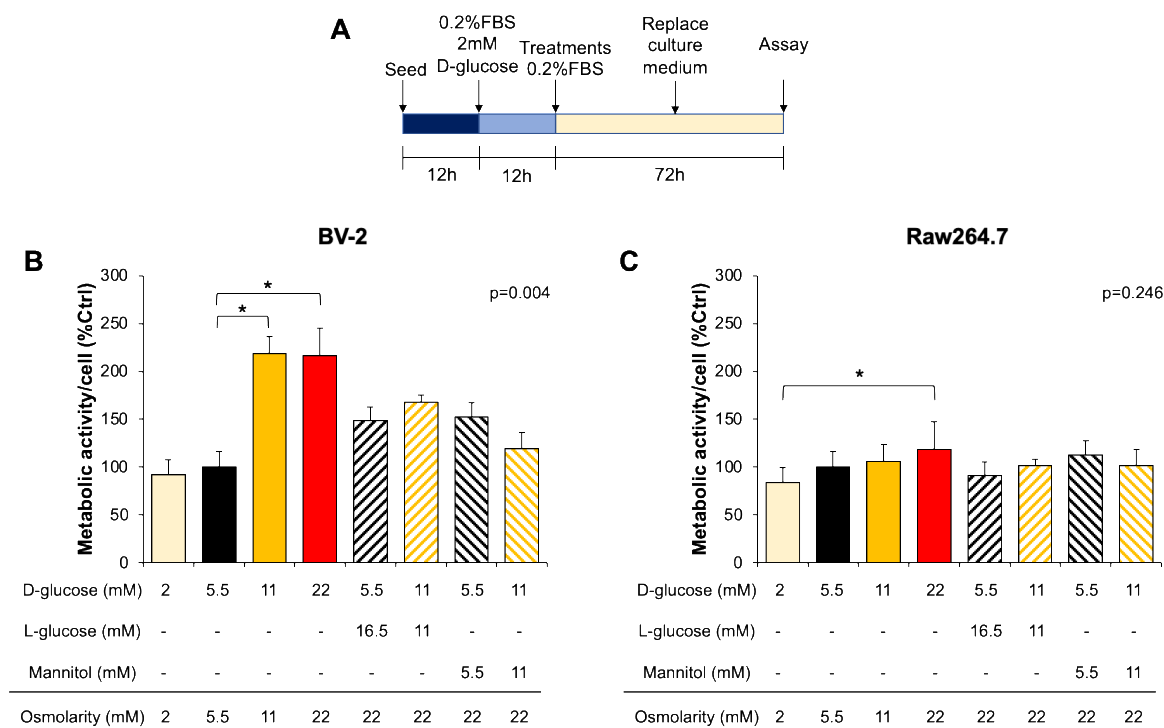


Figure 27. Metabolic activity per cell in microglial and macrophages cell lines exposed to different D-glucose concentrations for 72 hours. **A)** Treatment protocols used to analyze metabolic activity per cell after chronic D-glucose exposure. **B)** Metabolic activity per cell in BV-2 microglial cells. **C)** Metabolic activity per cell in Raw264.7 macrophages. Solid bars represent D-glucose treatments, while striped bars depict osmotic controls. $N=4$ wells per condition. Error bars show SEM. Statistical differences were assessed by ANOVA on ranks followed by post-hoc pairwise comparisons using Bonferroni t -tests (*, $p < 0.05$). Only biologically relevant differences are shown.

1.2. Chronic high D-glucose and osmolarity polarize microglial cells towards a mild pro-inflammatory phenotype

Elevations in D-glucose levels are common in both DM and AD. We explored the effect of chronic exposure to high D-glucose (and osmolarity) on cell polarization. Cells were plated on 6-well plates and 12 hours post-seed they were serum starved overnight. Then, cells were exposed to a curve of concentrations of D-glucose (2-22 mM), using L-glucose as osmotic control, for 72 hours, with a culture media replacement at 36 hours to minimize osmotic differences between treatments (**Figure 27A**). Cell polarization was characterized by quantifying mRNA expression levels of two well-characterized pro-inflammatory cytokines, IL-1 β and TNF- α . IL-1 β was significantly upregulated in both cell types, with a combined effect of D-glucose and osmolarity in microglia, and an osmotic-specific increase in macrophages (**Figures 28A** and **28B**). However, TNF- α response was

specific to D-glucose rather than osmolarity: TNF- α was specifically upregulated by high D-glucose (11 and 22 mM) in microglia, and significantly downregulated by any D-glucose different to the control concentration (5.5 mM) in macrophages (**Figures 28A** and **28B**).

These results suggest that the transcription of IL-1 β and TNF- α is regulated by different mechanisms: IL-1 β is sensitive to osmolarity, while TNF- α only responds to D-glucose variations in the culture media. Moreover, the importance of taking osmolarity into account is highlighted by these experiments, since it can be a confounding factor when it comes to the *in vitro* experiments, where cells are devoid of the buffering systems they usually possess in the body.

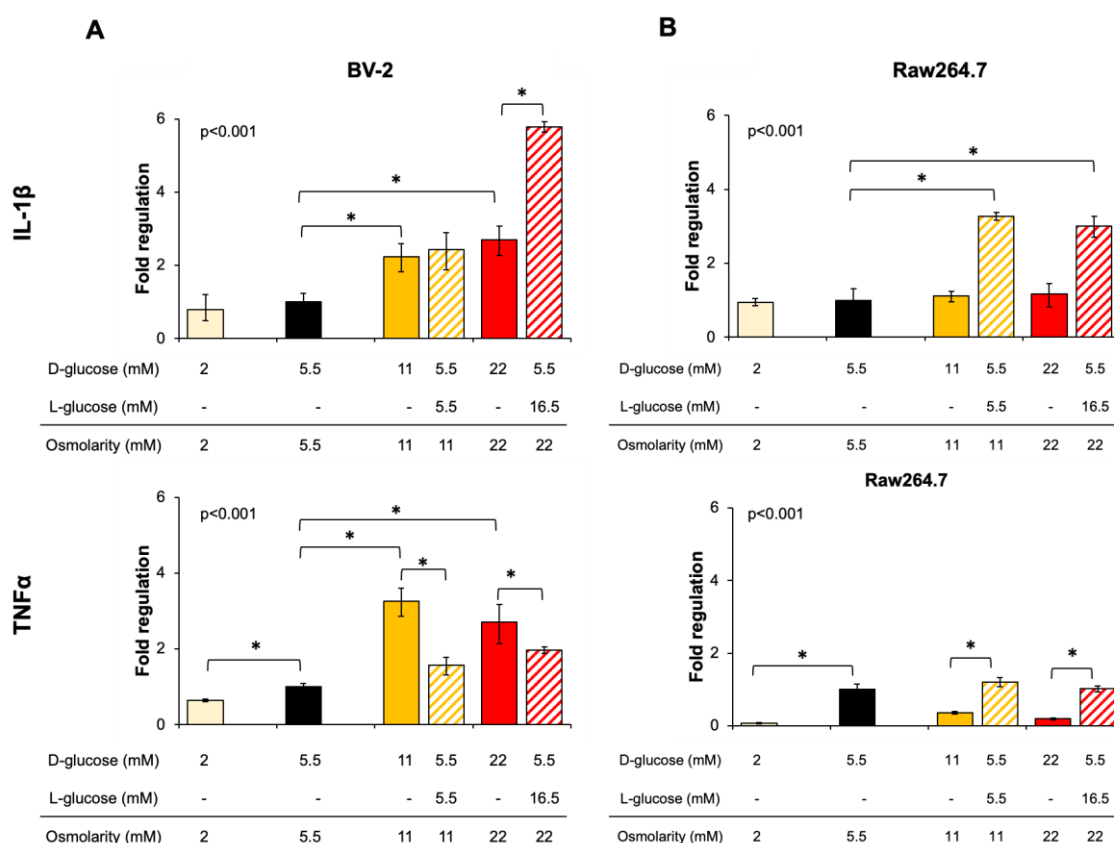


Figure 28. Pro-inflammatory response in microglia and macrophages exposed to different D-glucose concentrations for 72 hours. Total fold change of IL-1 β and TNF- α mRNA expression normalized to the 5.5 mM D-glucose (control condition) in microglia (**A**) and macrophages (**B**). Each bar represents the mean value between three independent experiments ($N=3$), and error bars show SEM. Solid bars represent D-glucose treatments, while striped bars depict osmotic controls. Statistical differences were assessed by one-way ANOVA, followed by Holm-Sidak post-hoc tests (*, $p < 0.05$).

1.3. Chronic high D-glucose induces changes in microglial glycolyx

The glycolyx, literally meaning “sugar coat”, consists of cell-derived proteoglycans, glycoproteins and glycolipids that cover the external surface of plasma membranes. The glycolyx of brain cells displays a high amount of sialic acids, the most abundant terminal sugars in mammalian glycans. This sialic acid functions as a biological mask, shielding recognition sites of cell membranes from the immune system to prevent immune reactions (Linnartz-Gerlach et al., 2014). To explore the

effect that chronic high D-glucose has on microglial glycocalyx, we treated the cells for 72 hours with different concentrations of D-glucose (and L-glucose as osmotic control) and then quantified sialic acid content by biotin-conjugated *Maackia* lectin labeling in absence of detergents, coupled to fluorescence detection with Alexa 594-conjugated streptavidin (**Figure 29A**). Sustained exposure to high D-glucose concentrations produced an increase in sialic acid exposed on the microglial surface, while L-glucose did not induce any change on microglial glycocalyx (**Figure 29B**).

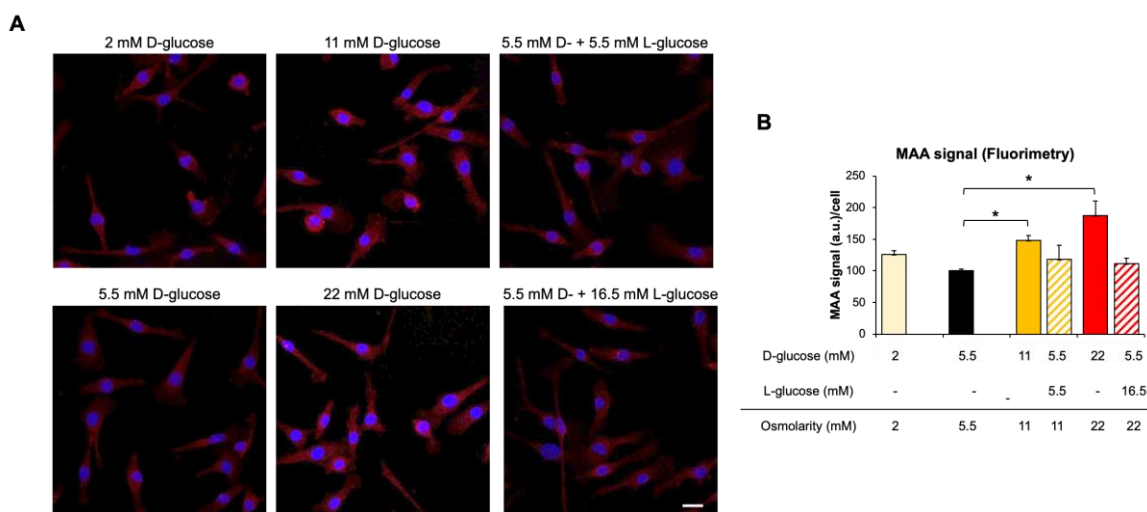


Figure 29. Hypersialylation of microglial cells chronically exposed to high D-glucose concentrations. Sialic acid content in BV-2 microglial membranes monitored by *Maackia amurensis* (MAA) lectin labeling. **A**) Representative fluorescence images (scale bar: 20 μ m). **B**) Fluorescence signal quantification ($n = 150$ cells/treatment from 2 independent experiments). Statistical differences were assessed by ANOVA on ranks ($p < 0.001$), followed by multiple comparisons versus 5.5mM D-glucose group by Dunn's method. (*, $p < 0.05$).

Functionally, this hypersialylated phenotype in microglial cells exposed to high D-glucose might be relevant in various cell functions such as microenvironment interaction, membrane organization or downregulation/control of immune reactivity.

1.4. IDE expression is not regulated by chronic high D-glucose

The effects of D-glucose on microglia and macrophages led us to study whether this hyperglycemia, characteristic of DM, would be able to regulate IDE expression. Intracellular IDE protein production upon different chronic D-glucose treatments was quantified by immunoblot, and no significant changes were observed in IDE protein levels in any of the treatments explored (**Figure 30**), which indicates that chronic exposure to high D-glucose does not regulate IDE intracellular protein levels neither in microglia nor in macrophages.

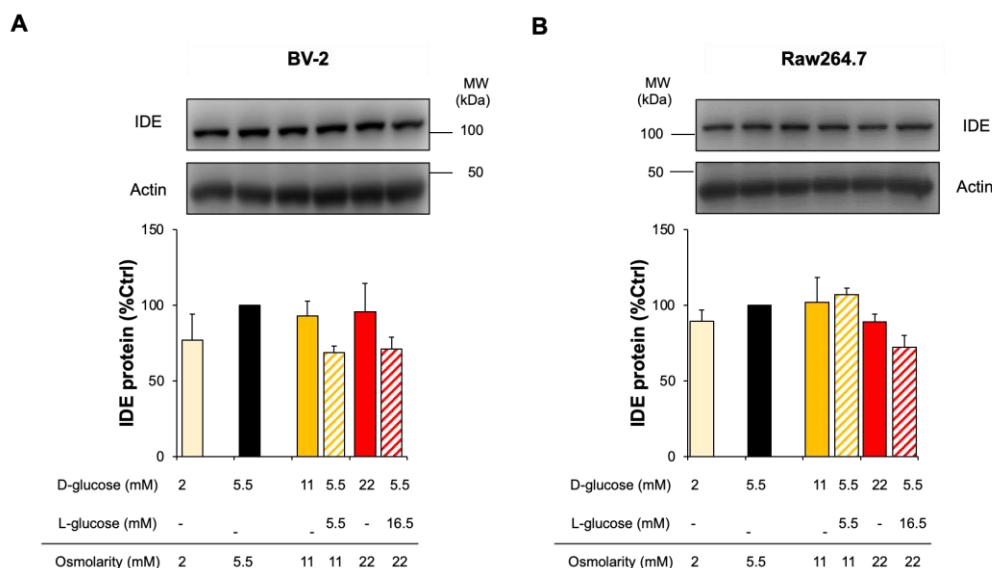


Figure 30. IDE protein expression in BV-2 and Raw264.7 cells exposed to different D-glucose concentrations for 72 hours. Representative immunoblots of BV-2 (A) and Raw264.7 (B) cells, and their respective protein quantifications. Experimental protein bands were normalized with actin. $N=3$ independent experiments. Statistical differences were analyzed by using one-way ANOVA.

1.5. IDE expression is differentially regulated in microglia and macrophages, and changes along with the polarization state

The absence of effect of high D-glucose on IDE expression led us to explore other more extreme paradigms, such as pro-inflammatory “polarization” with LPS and anti-inflammatory “activation” with IL-4 + IL-13, oxidative stress with Paraquat (PQ) and amyloid stress with A β oligomers. Initially, we assessed the effects of the harmful insults (LPS, PQ and A β) on cell viability by performing conventional MTT assays with the BV-2 cell line, following the experimental protocol shown in **Figure 31A**. The survival results showed good correlations between dose of the stimulus and decrease of survival (**Figure 31B**). The dose for each stimulus was chosen with a maximum cell death of 50%.

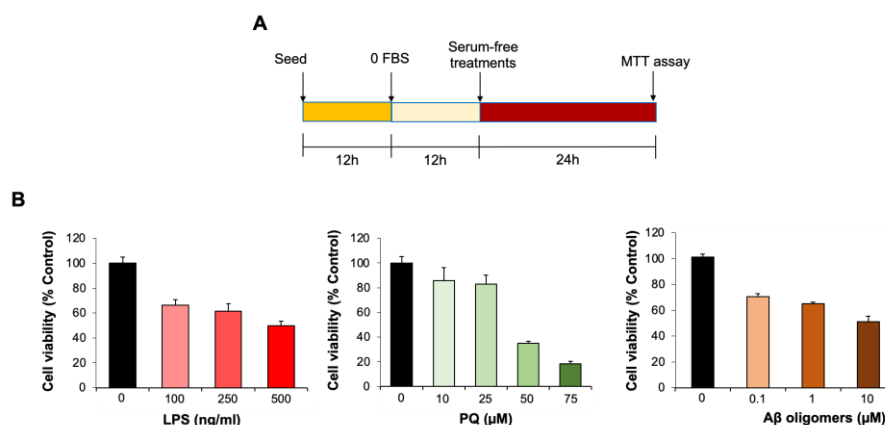


Figure 31. Cell viability assays in BV-2 to select the dose for each stimulus. A) Experimental protocol. B) MTT results, expressed as the mean \pm SEM of 3 independent wells per condition. Statistical differences were assessed by one-way ANOVA, which was significant ($p < 0.01$) in the three stimuli analyzed.

Microglia and macrophages were challenged with LPS (500 ng/ml) for 24 hours, as depicted in **Figure 32A**. At the mRNA level, “pro-inflammatory” polarization was checked by monitoring IL-1 β , a cytokine whose production has been described to be highly upregulated by LPS. Both cell types responded to LPS producing high amounts of IL-1 β mRNA, but macrophages showed a stronger response (**Figure 32B**, upper panels). IDE mRNA synthesis was significantly increased by LPS challenge in macrophages, while it remained unchanged in microglia (**Figure 32B**, lower panels). At the protein level (**Figure 32C**), COX-2 was used to monitor the LPS-induced response and, again, macrophages showed a higher response than microglia (**Figure 32D**, upper panels). IDE intracellular protein was significantly decreased (by 50%) in microglia upon LPS treatment, while it remained unchanged in macrophages (**Figure 32D**, lower panels).

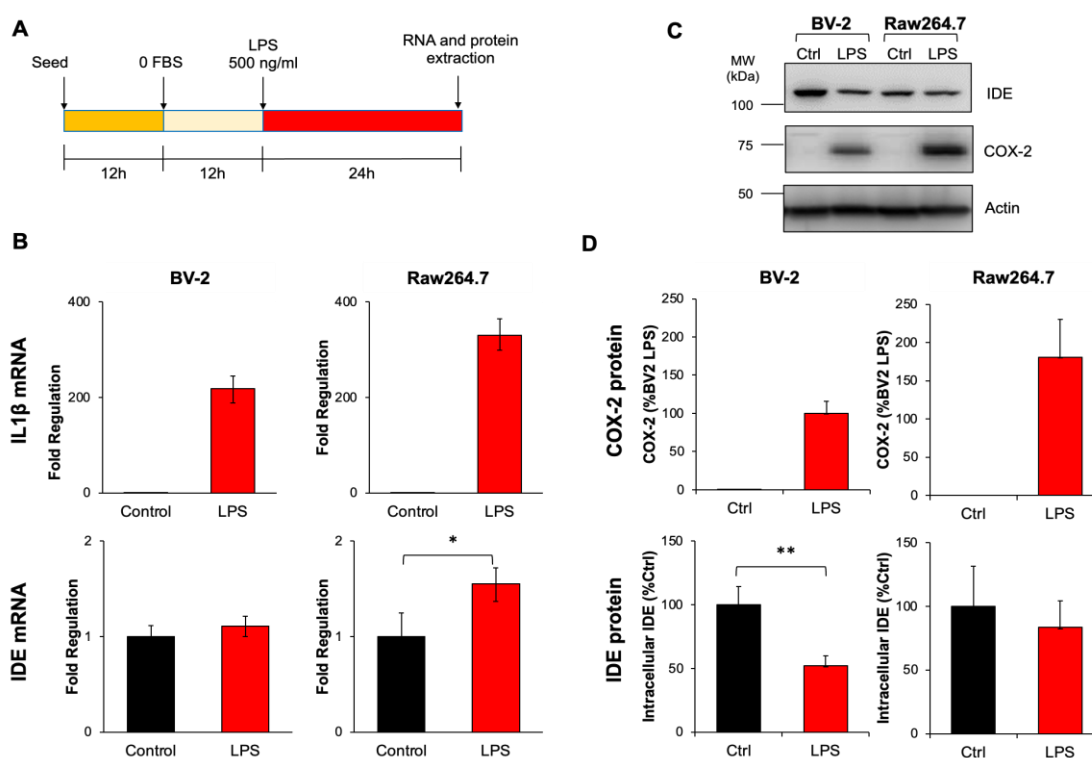


Figure 32. LPS-induced pro-inflammatory polarization of microglia and macrophages and effects on IDE mRNA and protein expression. **A)** Treatment protocol used to induce pro-inflammatory polarization. **B)** Transcriptional effects of LPS treatment on IL-1 β (upper panel) and IDE (lower panel) mRNA. **C)** Representative immunoblot of LPS-stimulated BV-2 and Raw264.7 cells. **D)** Quantification of the immunoblots (experimental protein bands were normalized with actin). $N=3$ independent experiments. Statistical differences were analyzed separately in each cell type by *t*-test. (*, $p < 0.05$; **, $p < 0.01$).

In summary, LPS-treated BV-2 microglia showed no changes in IDE mRNA but a decrease in IDE intracellular protein, while LPS-stimulated Raw264.7 macrophages had an increase in IDE mRNA with no changes in IDE intracellular protein. Two different hypotheses could explain these results: (a) an LPS-induced post-transcriptional regulatory control of IDE mRNA, preventing translation, or (b) differences in IDE secretion, which would be stimulated by LPS exposure. The second hypothesis will be further addressed in Chapter 2.

We then polarized the cells by treating them with IL-4 and IL-13 (20 ng/ml and 50 ng/ml, respectively) for 24 and 48 hours (**Figure 33A**). At the mRNA level, TGF- β was used as a marker of “anti-inflammatory” response: microglia showed their peak at 24 hours, while macrophages exhibited a time-dependent polarization (**Figure 33B**, upper panels). IDE mRNA production remained unchanged in microglia, while it was significantly upregulated, in a time-dependent manner, in macrophages, mimicking the increase in TGF- β production (**Figure 33B**, lower panels). At the protein level, we intended to monitor Arg-1 production. Surprisingly, this protein was not induced in macrophages (macrophages do express Arg-1, but the absence might be attributable to this specific cell line), while it was significantly expressed in microglia, in a time-dependent manner (**Figures 33C** and **33D**, upper panel). IDE intracellular protein tended to be increased by 25% in microglia and decreased a 15% in macrophages (**Figures 33C** and **33D**, lower panels).

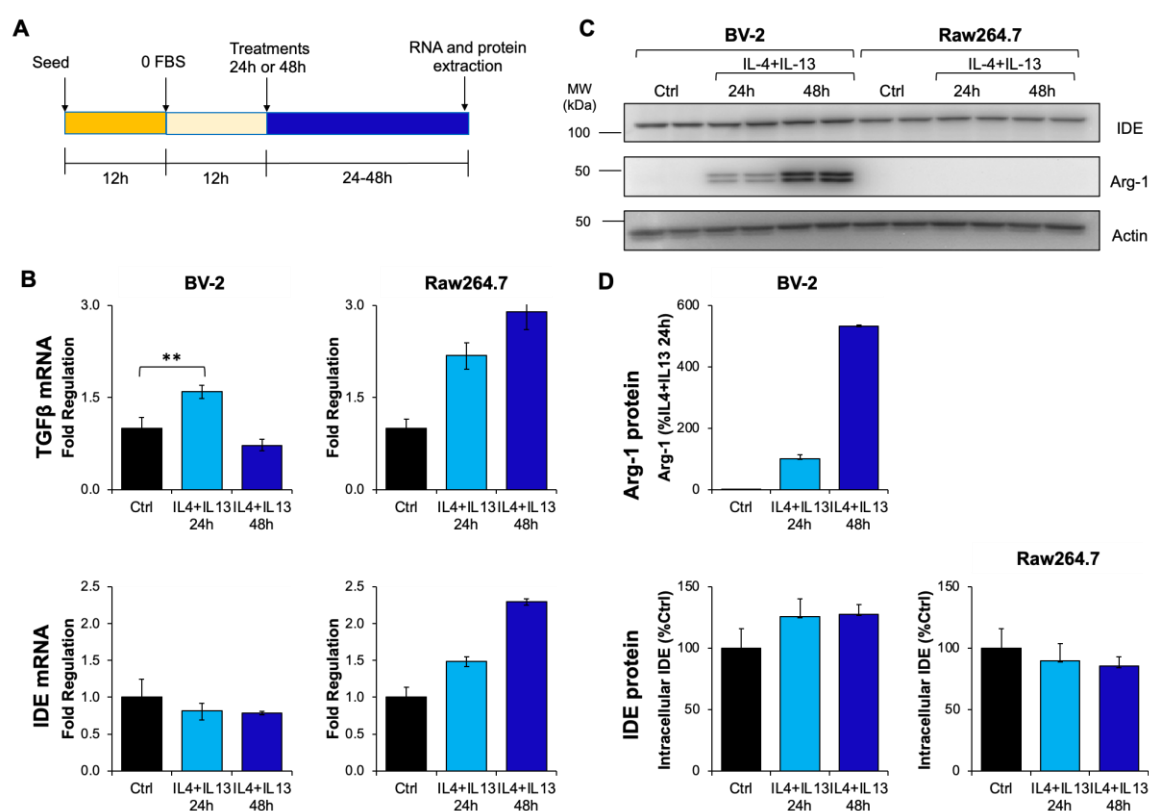


Figure 33. IL-4+IL-13-induced anti-inflammatory polarization of microglia and macrophages and effects on IDE mRNA and protein expression. **A)** Treatment protocol used to induce anti-inflammatory polarization. **B)** Transcriptional effects of IL-4+IL-13 treatment on TGF- β (upper panel) and IDE (lower panel) mRNA. **C)** Representative immunoblot of IL-4+IL-13 stimulated BV-2 and Raw264.7 cells. **D)** Quantification of the immunoblots (experimental protein bands were normalized with actin). $N=2$ independent experiments. Statistical differences were analyzed by using one-way ANOVA (**, $p<0.01$).

These results can be explained again by either a post-transcriptional regulatory control of IDE mRNA or by differential IDE secretion. In any case, IDE seems to be differentially regulated in microglia and macrophages.

Another common stress factor within neurodegenerative disorders is oxidative stress. Exposure to paraquat (PQ) for 24 hours was used to generate oxidative stress in the immune cell lines (**Figure 34A**). We tested different PQ concentrations in both cell lines and, while macrophages resisted up to 75 μM PQ, microglial viability was dramatically decreased at 50 μM PQ, indicating higher sensibility for microglial cells to this kind of damage. Oxidative stress significantly increased IDE intracellular protein (around 75%) in BV-2, while did not have any significant effect in Raw264.7 (**Figure 34B**).

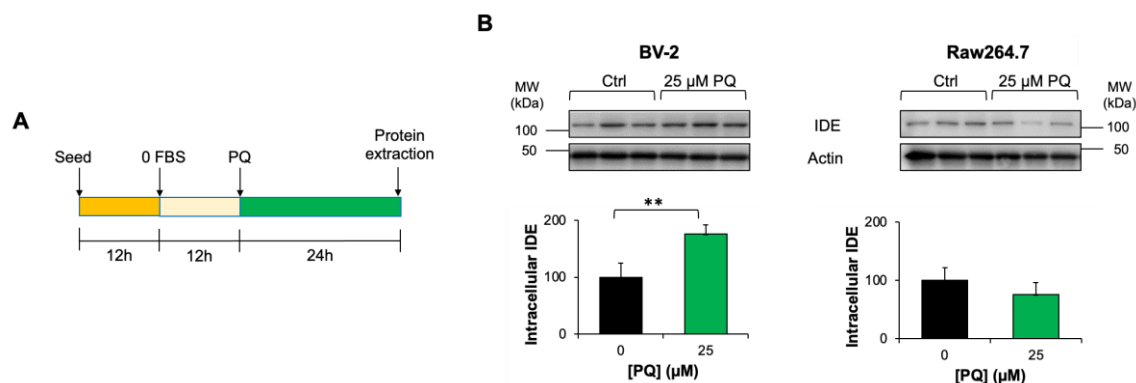


Figure 34. IDE protein expression in microglia and macrophages upon PQ-induced oxidative stress.

A) Treatment protocol to experimentally induce oxidative stress. **B)** Representative immunoblots of the intracellular IDE protein in microglial and macrophagic primary cell lines after challenge with PQ, and their respective quantifications (experimental proteins were normalized with actin). $N=3$ independent experiments per condition. Statistical differences were assessed by *t*-test. (**, $p<0.01$).

1.6. D-glucose combined with A β oligomers regulates IDE intracellular and extracellular distribution

Since IDE has been described to degrade A β , a relevant question is whether amyloid peptides can modulate IDE expression. We performed time-course experiments in BV-2 microglial cells combining normal (5.5 mM) or high (22 mM) D-glucose exposure for 24 hours with A β oligomers treatment (1 μM , for 3-24 hours) as a simplified experimental paradigm for type 3 diabetes (**Figure 35A**). Intracellular IDE protein showed a tendency to be diminished in an A β exposure time-dependent, glucose independent manner. In other words, A β oligomers decreased intracellular IDE indistinctly in both normal and high D-glucose, with a correlation of A β exposure time and IDE decrease (**Figure 35B**). Conversely, extracellular IDE showed the opposite tendency, with a significant effect of A β on the exportation of IDE to the extracellular media in a time-dependent manner. In this case, high D-glucose had a tendency to decrease IDE exportation at longer times (12-24h) of A β exposure (**Figure 35C**).

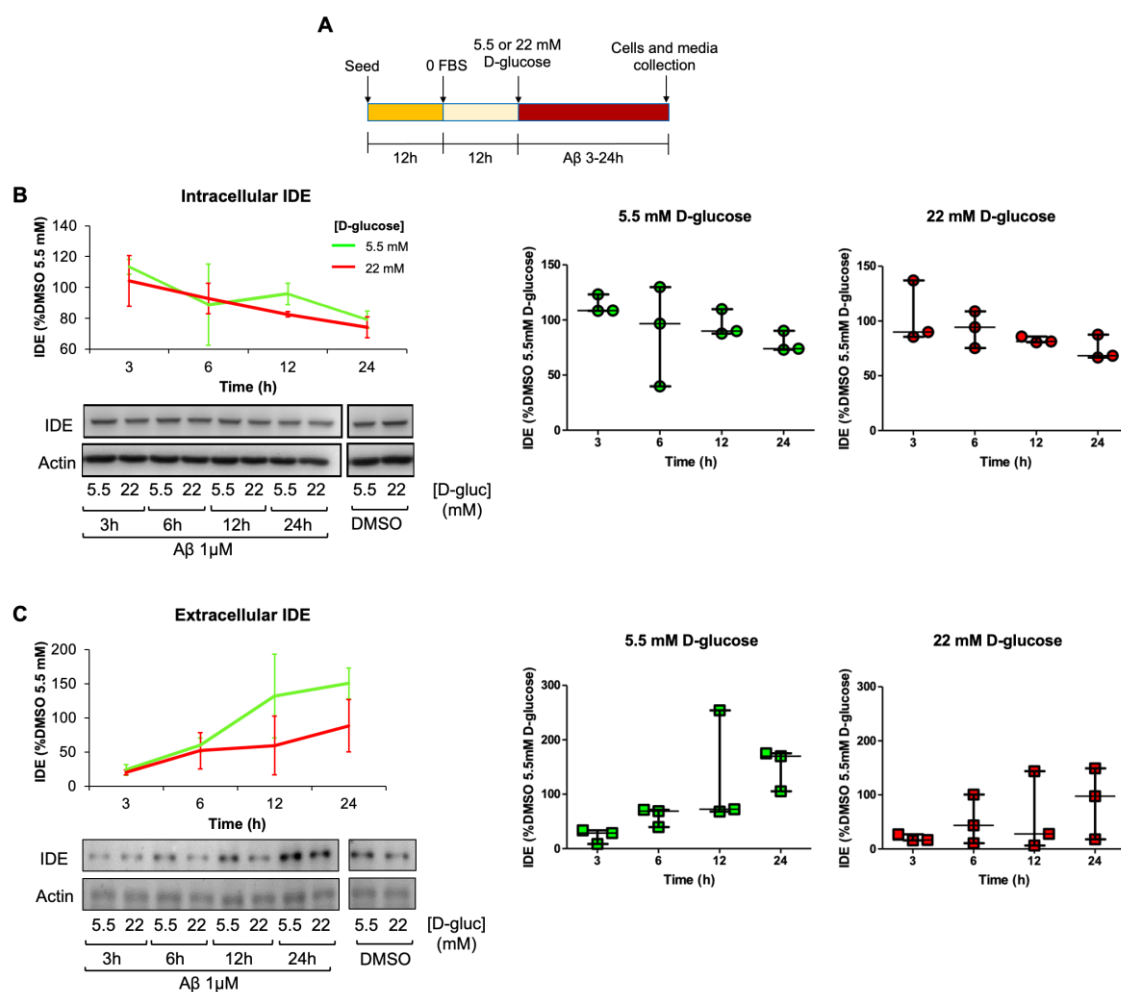


Figure 35. Time-course of IDE distribution after amyloid- β oligomers treatment. **A)** Graphical representation of treatment protocol. **B)** Intracellular IDE protein. **C)** Extracellular IDE protein. Representative immunoblots are shown (actin was used to normalize the Western blot data). The graphs on the left represent the mean \pm SEM ($N=3$ independent experiments), while the graphs on the right depict the three individual values of each sample with the median and interquartile range. Statistical differences were assessed by two-way ANOVA considering the factors D-glucose and A β (p -values: intracellular A $\beta=0.08$, intracellular D-glucose 0.56, extracellular A $\beta=0.028$, extracellular D-glucose=0.164), followed by post-hoc Holm-Sidak comparisons.

Due to the high variation observed between triplicates, none of the individual time points was statistically significantly different from the other time points, although the trends were coherent and similar in the presence of both glucose levels. These results suggest modulation of IDE traffic, rather than a mere regulation of its expression, when microglial cells are exposed to A β oligomers.

CHAPTER 2. IDE MOLECULAR EVOLUTION AND SUBCELLULAR LOCALIZATION AND TRAFFIC IN MICROGLIAL CELLS

IDE is an ancient protein evolutionarily conserved from bacteria to humans. The subcellular localization of IDE is crucial for understanding how this enzyme can perform its proposed proteolytic functions. However, there is great controversy about the *real* location of IDE within the cell, since it has been described to be in many different organelles. To shed some light on this question, we performed a bioinformatic analysis to find IDE's homologous proteins in all kingdoms. From IDE's phylogenetic tree, we explored the evolution of the signal peptide in its homologs and their predicted subcellular localization. After our *in silico* studies, we investigated IDE's subcellular localization in microglial cells by combining diverse biochemical and immunocytochemical techniques. We used native protein in order to avoid transfections that could generate artifacts altering its physiological trafficking and/or distribution.

2.1. Molecular phylogeny on clan ME metallopeptidases

IDE belongs to the clan ME of metalloproteases. Enzymes of this clan are ubiquitously present throughout the tree of life and include proteases with highly divergent primary sequences, but a strikingly high 3D structure conservation (Rawlings and Salvesen, 2013). To get an insight about IDE origin, we started performing a global phylogeny of the clan ME metalloendopeptidases. The main characteristics of the proteins selected for this analysis are shown in **Table 11**.

Table 11. Clan ME metallopeptidases. Information obtained from (Rawlings and Salvesen, 2013)

Protein name	Family	Organism	Localization
Pitrilysin	M16A	<i>Escherichia coli</i>	Periplasm
Nardilysin	M16A	<i>Homo sapiens</i>	Cytosol and mitochondria
IDE	M16A	<i>Homo sapiens</i>	Ubiquitous
Ste23	M16A	<i>Saccharomyces cerevisiae</i>	Cytosol and membrane
Ax11p	M16A	<i>Saccharomyces cerevisiae</i>	Mitochondria
Plinsulysin	M16A	<i>Solanum lycopersicum</i>	Ubiquitous
Stromal processing peptidase (SPP)	M16B	<i>Arabidopsis thaliana</i>	Chloroplasts
MPPA	M16B	<i>Homo sapiens</i>	Mitochondria
MPPB	M16B	<i>Homo sapiens</i>	Mitochondria
YmxG	M16B	<i>Rickettsia prowazekii</i>	Cytosol
Presequence protease 1 (PreP1)	M16C	<i>Arabidopsis thaliana</i>	Mitochondria and chloroplasts
Eupitrilysin	M16C	<i>Homo sapiens</i>	Mitochondria
Falcilysin	M16C	<i>Plasmodium falciparum</i>	Cytosol, apicoplast and vacuoles
G1L	M44	<i>Vaccinia virus</i>	Virion

Primary structure analysis of clan ME metallopeptidases clearly grouped the proteins into their corresponding families (**Figure 36A**), revealing a good correlation between their functional classification (Rawlings and Salvesen, 2013) and the sequence-based relationships. The comparison of domains of each protein shows a conserved pattern between families: M16B proteins have only an insulinase and a M16 inactive domain, except for SPP, which might have undergone a duplication

event. The M16C subfamily includes also an M16C-associated domain, while the M16A subfamily possess a third domain in the middle (**Figure 36B**). The mitochondrial processing peptidase (MPP) is a heterodimeric M16B metalloprotease composed of a catalytic β -subunit (MPPB) and a non-catalytic α -subunit (MPPA) (Kutejová et al., 2013), which resemble to the IDE-N (domains 1-2, containing the catalytic site) and IDE-C (domains 3-4, inactive) domains, respectively. Therefore, IDE might have evolved from a heterodimer that consists of individual IDE-N and IDE-C subunits.

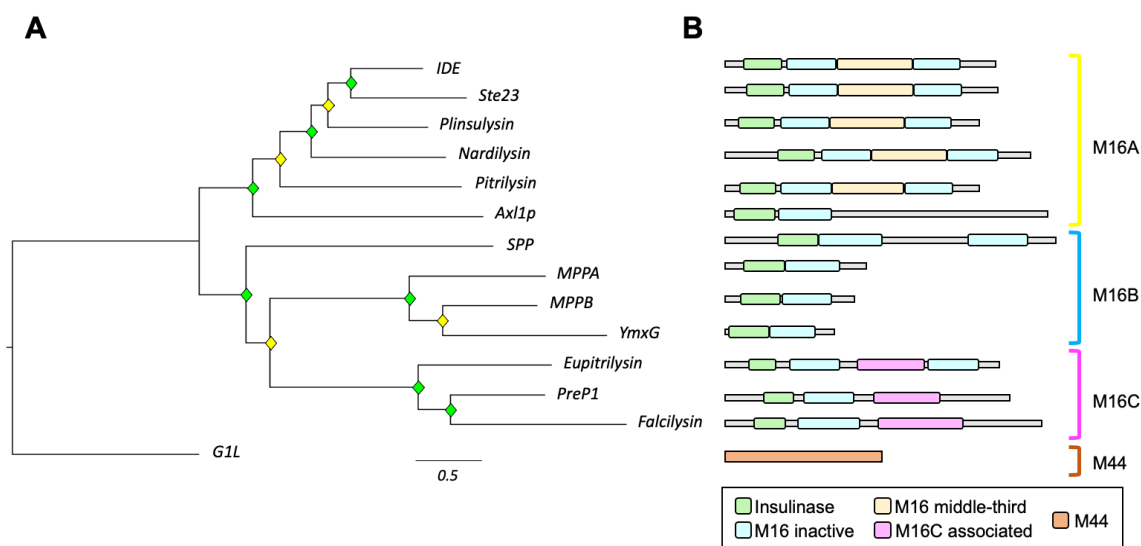


Figure 36. Phylogenetic analysis of clan ME metalloproteases. **A)** *Phylogenetic relationships of clan ME metalloproteases based on protein sequence. A ML phylogenetic tree was constructed from a sequence-based MSA of 14 ME proteins, using a substitution model LG+F+I+G4 according to BIC. Diamonds label nodes with a bootstrap value >60% (yellow) and >80% (green). Scale branch length represents number of amino acid substitutions per site.* **B)** *Domain arrangement for each protein, retrieved from Pfam and HMMER databases.*

2.2. IDE evolution and molecular phylogeny: from *Archaea* to *Eukarya*

Since IDE is a multidomain protein (see **Figure 36B**), our preliminary searches for homologs produced many hits that had to be manually curated: many candidates were metalloproteinases but had only one or two out of the four domains that form IDE. To standardize the selection process, the following inclusion criteria were considered: sequence identity $\geq 25\%$; query cover > 50% (more than 500 amino acids, half the length of human IDE protein); and presence of the insulinase domain and at least three out of four IDE's domains, to discard M16B- and M16C-like enzymes.

Attending to these selection criteria, a multiple sequence alignment (MSA) with the candidate proteins and human IDE was performed to visually analyze each sequence and determine whether it could be considered IDE-like. A database of IDE homologs, containing 2165 sequences, was constructed (see **Table 12**). The presence of IDE in all kingdoms is remarkable, with an unique IDE homolog in *Archaea* and many IDE-like proteins in *Proteobacteria*, while other prokaryotic *phyla* do not present any similar proteins. Surprisingly, IDE was also found in various *Mimiviruses*. In *Eukarya*, IDE is widely represented and presents a high degree of conservation.

Table 12. Summary of the database of IDE homologs.

Prokarya			
Phylum	Sequences	Average Length	Average Identity (%)
Archaea	1	939.0	32.2
Chlamydiae	11	877.3	31.1
Lentisphaerae	1	953.0	33.1
Planctomycetes	5	893.6	33.1
Verrucomicrobia	5	952.6	31.9
Proteobacteria	325	942.0	34.5
Total	348	926.2	32.7
Viruses			
Clade	Sequences	Average Length	Average Identity (%)
Viruses	14	896.2	29.4
Protists			
Phylum	Sequences	Average Length	Average Identity (%)
Haptista	7	1070.7	35.3
Rhodophyta	4	1013.3	36.6
Apicomplexa	30	1172.8	32.2
Ciliophora	16	1079.1	32.9
Alveolata	22	1341.8	32.4
Discosea	1	942.0	39.1
Evosea	3	884.0	33.7
Euglenozoa	38	1076.8	32.8
Opisthokonta	4	1113.8	33.8
Bacillariophyta	10	1057.9	33.0
Oomycota	48	1045.3	35.4
Stramenopiles	13	1020.7	32.6
Total	196	1068.2	34.2
Fungi			
Phylum	Sequences	Average Length	Average Identity (%)
Ascomycota	498	1167.6	38.1
Basidiomycota	164	1141.7	35.9
Chytridiomycota	12	957.5	36.8
Microsporidia	2	694.5	31.0
Mucoromycota	54	1002.6	45.3
Zoopagomycota	9	937.4	36.9
Total	739	983.5	37.3
Viridiplantae			
Phylum	Sequences	Average Length	Average Identity (%)
Chlorophyta	18	1141.7	37.7
Streptophyta	290	926.1	36.7
Total	308	1033.9	37.2
Metazoa			
Phylum	Sequences	Average Length	Average Identity (%)
Annelida	4	1030.0	39.6
Arthropoda	129	1033.4	43.2
Bryozoa	4	845.5	38.5
Cnidaria	4	977.3	45.7
Echinodermata	1	818.0	57.0
Mollusca	9	964.2	46.4
Nematoda	76	1181.5	43.9
Platyhelminthes	20	954.3	37.5
Rotifera	1	1078.0	44.3
Tardigrada	4	1068.3	45.8
Chordata	308	988.2	64.6
Total	560	994.4	46.0

From our database, we selected 216 sequences (for more details, see **Table A1** in Annex section) to infer a global tree (**Figure 37**). All prokaryotic sequences are clustered together, with the *Archaea* sequence separated from bacterial proteins. These taxa present long branches, suggesting that IDE might have undergone functional explorations leading to sequence divergence in these organisms. The viral sequences are clustered within protists, which makes perfect sense since *Mimiviruses* are protist viruses that have large genomes with many horizontally acquired genes. The protist sequences are split into various groups, which is reasonable since protists are a diverse collection of unicellular organisms with puzzling affinities. The *Viridiplantae* (plants and green algae) sequences appear in two different groups, and a notable shortening of some of these branches (green brackets) suggests that the function of the protein is being fixed by selection constraints. The fungal sequences are grouped all together and separated by *phyla*. Interestingly, in *Metazoans* IDE and its homologous protein nardilysin (NRD) are clearly separated into two clusters very distant in the tree, with IDE in the vicinity of the fungal branches, whereas NRD is grouped with the protists.

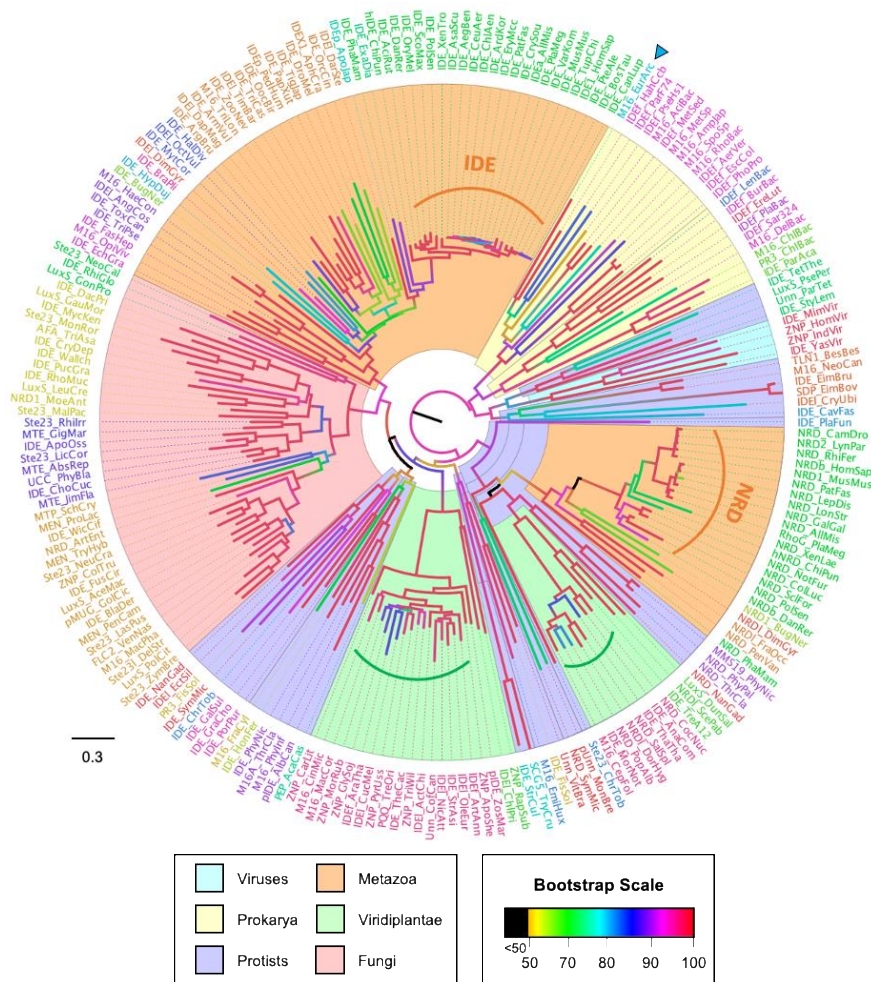


Figure 37. Global phylogeny of IDE-like proteins. A phylogenetic tree was reconstructed from a sequence-based MSA of 216 IDE homologs. The substitution model LG+I+G4 was chosen according to BIC, and the tree was inferred using a ML method. Major species groups are highlighted by different colors as indicated. Arrowhead points to the only Archaea representative. Brackets highlight clades with short branches (low divergence). Scale branch length represents number of amino acid substitutions per site.

To deepen into IDE evolution, 14 representative organisms were selected. The phylogenetic relationship and evolutionary timescale of the selected organisms were estimated with TimeTree (Kumar et al., 2017) (**Figure 38A**), and the sequence-based phylogeny for IDE proteins is shown in **Figure 38B**. High conservation in vertebrate species, compared with nonvertebrate chordates and other *phyla*, is indicative of selective constrains acting on IDE function early in vertebrate evolution.

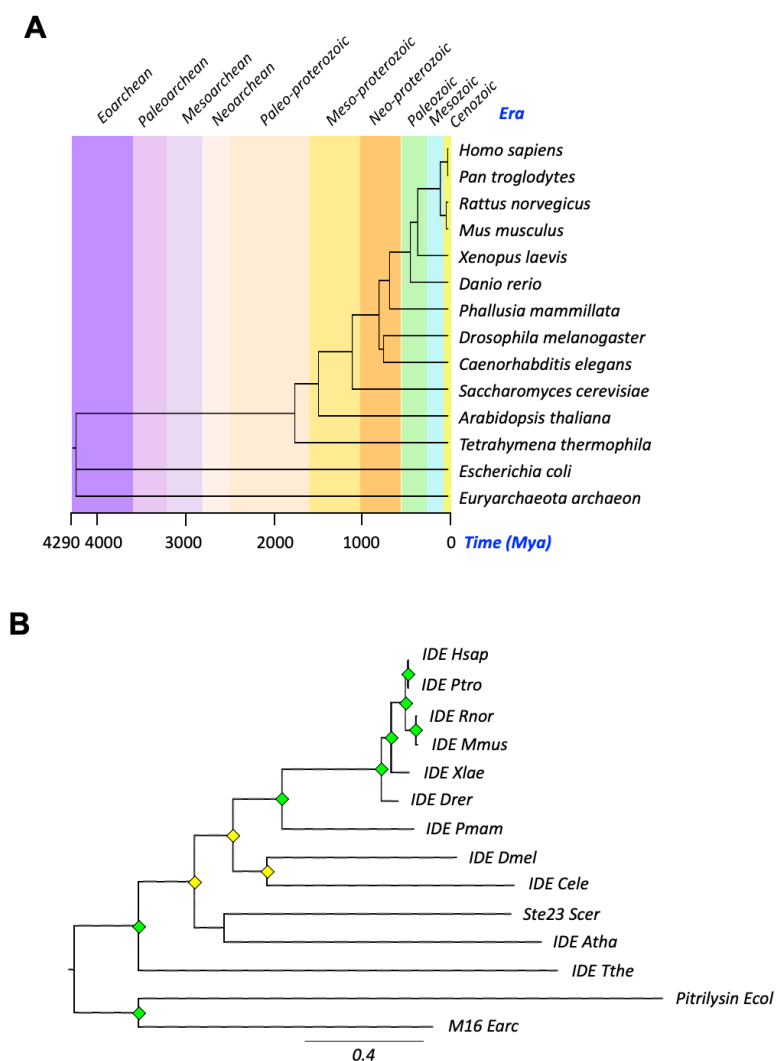


Figure 38. Evolution timescale and IDE phylogeny. **A)** Phylogeny and evolution timescale of the 14 organisms selected for IDE phylogeny. **B)** Phylogenetic tree of 14 IDE-like proteins reconstructed from a protein sequence-based MSA and a ML method (substitution model LG+I+G4, chosen according to BIC). Diamonds label nodes with a bootstrap value >60% (yellow) and >80% (green). Scale branch length represents number of amino acid substitutions per site.

2.3. Bioinformatic predictions of signal peptide on IDE's homologous proteins reveal a shift in exportation between prokaryotes and eukaryotes

Signal peptides are a kingpin mechanism for subcellular protein sorting and localization, common to all cellular life. These signal sequences are short amino acid sequences in the N-terminal region of many nascent polypeptides that target proteins into or across membranes in *Archaea*, *Bacteria* and *Eukarya*. There are two secretory pathways: the general secretory pathway (Sec), universal for all

organisms, and the twin-arginine translocation (Tat) pathway, that operates only in prokaryotes, chloroplasts, and some mitochondria. During or after membrane translocation, a signal peptidase removes the signal peptide. Most signal peptides are cleaved by signal peptidase I (SPI), but bacterial lipoproteins are split by a second signal peptidase (SPII), which cuts signal peptides that contain a conserved C-terminal ‘lipobox’.

The analysis of the database containing IDE’s homologous proteins using SignalP5.0 revealed that a high percentage (61.5%) of IDE-like proteins have an N-terminal signal peptide in *Prokarya*. It is worth noting the great variability found inside *Gammaproteobacteria*, where in some orders the signal peptide is totally absent (*Aeromonadales*), while in others it predominates (*Alteromonadales*). Within *Eukarya*, very few sequences were predicted to have a signal peptide. In comparison with prokaryotes, the number of IDE-like eukaryotic proteins that have a signal peptide is surprisingly low (1.7%) (**Figure 39**), and none of the 308 IDE-like sequences from *Chordata* was predicted to have signal peptide. Remarkably, the Sec/SPI pathway was clearly majoritarian.

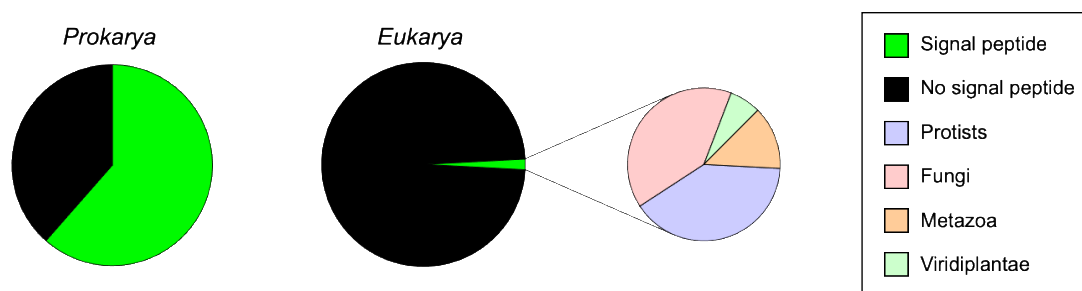


Figure 39. Signal peptide predictions in prokaryotic and eukaryotic sequences. 61.5% of IDE-like sequences have signal peptide in prokaryotes, while only 1.7% of eukaryotic sequences possess this trait.

Taken together, these results indicate a shift during evolution in the mechanism exporting IDE to the extracellular space, with a great percentage of prokaryotic sequences presenting the N-terminal signal peptide required for canonical secretion, while the trend is inverted in eukaryotes. Among the few eukaryotic sequences that possess signal peptide, 80% of them belong to protists and fungi, with very few sequences with signal peptide in plants and metazoans. The most parsimonious explanation for this pattern is that the simpler, less evolved, prokaryotes and unicellular eukaryotes have signal peptides, which facilitate IDE transport to the extracellular space, while multicellular organisms seem to have lost this universal secretory mechanism.

2.4. Bioinformatic subcellular localization prediction indicates that IDE is primarily cytosolic in all kingdoms

The function of a protein depends on the organelle where it is located, since it constitutes the physiological context for its functions. IDE’s subcellular localization has been extensively studied by many groups and has been reported in many different compartments; however, there is no clear consensus about IDE’s actual localization. To address this question from another perspective, the subcellular localization of eukaryotic IDE-like proteins from our database was predicted using

DeepLoc1.0. From the total of 1815 eukaryotic proteins analyzed, the majority (65%) were predicted to be cytosolic. Other subcellular locations found were mitochondrion (17.6%), nucleus (9.1%), plastid (3.5%), endoplasmic reticulum (1.9%), cell membrane (0.8%), Golgi apparatus (0.8%), extracellular (0.8%), lysosome/vacuole (0.4%) and peroxisome (0.1%) (**Figure 40**). Analyzing the predicted subcellular localizations individually for each kingdom, the cytoplasm is again the preferred location; however, interesting differences between groups can be observed. Protists exhibit the greatest diversity of localizations, which agrees with the proposed exploration of functions in this group appreciated in the global phylogeny (**Figure 37**). In this group, the cytoplasm is followed by nucleus and mitochondrion, but the most striking results are the extracellular and cell membrane locations, hardly seen in other groups, which might be indicative of a *bona fide* exportation pathway. Fungi have a dramatic decrease in the number of predicted subcellular localizations, with the cytoplasm clearly predominant, followed by mitochondrion and plastids. The *Viridiplantae* kingdom presents different results, with many of the proteins predicted to be cytosolic or nuclear. Finally, metazoan proteins are preferentially located in the cytoplasm, followed by mitochondrion and nucleus as alternative locations (**Figure 40**).

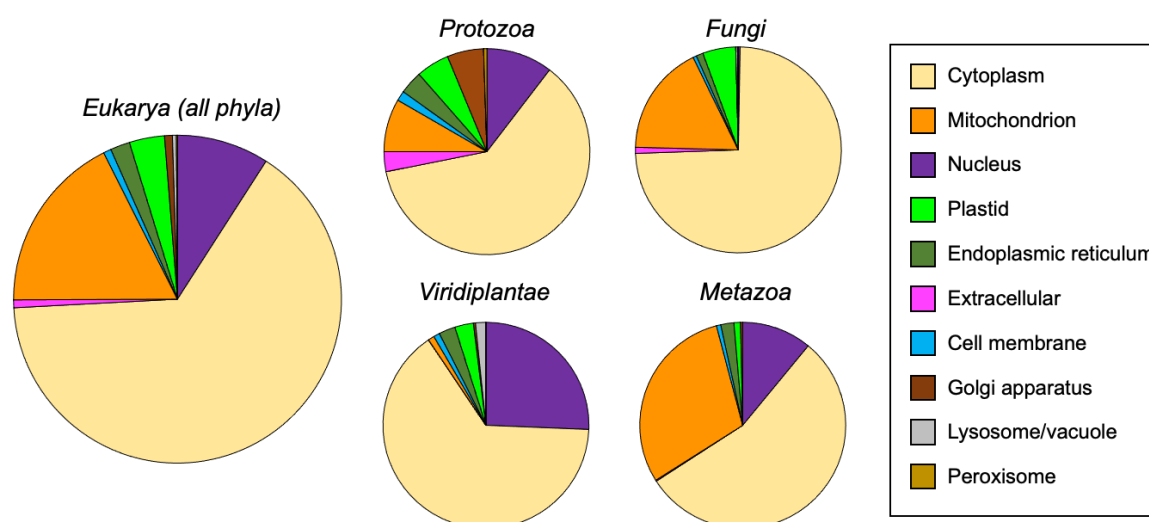


Figure 40. Subcellular localization predictions for IDE-like eukaryotic proteins. Results are depicted collectively in all phyla (left graph) or individually in each phylum (right graphs).

These results strongly support the hypothesis that IDE is mainly cytosolic. In regard to other predicted localizations, the high percentage of mitochondrial IDE in metazoans can be explained by a mitochondrial isoform of IDE, described by Leissring and colleagues, originated from an alternative translation initiation codon 123 nucleotides upstream of the canonical translation start site, which results in the addition of a 41-amino acid N-terminal mitochondrial targeting sequence (Leissring et al., 2004). However, the expression of this mitochondrial isoform is limited by the fact that the upstream initiation codon does not contain a strong Kozak consensus sequence (Leissring et al., 2004). The nuclear localization, especially abundant in plants, had never been described for IDE, which does not have a nuclear localization signal (NLS). A thorough analysis of nuclear predicted

IDE-like sequences revealed that, unlike IDE, they have a N-terminal disordered region with numerous polar and basic residues. Such region could be detected as a NLS, since the characteristic motifs of NLSs are usually composed by 4-8 basic amino acids, which generally contain 4 or more positively charged residues (Lu et al., 2021). The other locations, although quite residual, reveal the diversity of functions that this protein might be performing in different organisms.

2.5. IDE is mainly cytosolic, but it also associates to membranes in glial cells

After our initial *in silico* studies, we analyzed IDE subcellular localization and trafficking in microglial cells.

We performed biochemical cell fractionation of primary glial cultures enriched in microglia and astrocytes, respectively, and analyzed the resultant fractions by immunoblot. In both microglia and astrocytes IDE was mostly cytosolic, as our bioinformatics analysis predicted, but small fractions were associated with membranes and dense organelles (including nuclei, endoplasmic reticulum and mitochondria) (**Figure 41A**). These results indicate that IDE association with plasma membrane is independent on the glial cell type, although the amounts of membrane-bound IDE can slightly vary between cell types.

With the antecedents stated above, a relevant question is whether IDE association to membranes is stable upon exposure of cells to inflammatory (LPS) or oxidative (PQ) stress conditions. In microglial BV-2 cells, IDE was also mostly cytosolic, but a significant fraction appeared associated with membranes and, to a lesser extent, with dense organelles. This IDE partition between soluble and membrane fractions was independent of the stimulus (**Figure 41B**) and confirms the ubiquitous subcellular distribution of IDE in microglial cells and its stable association with membranes.

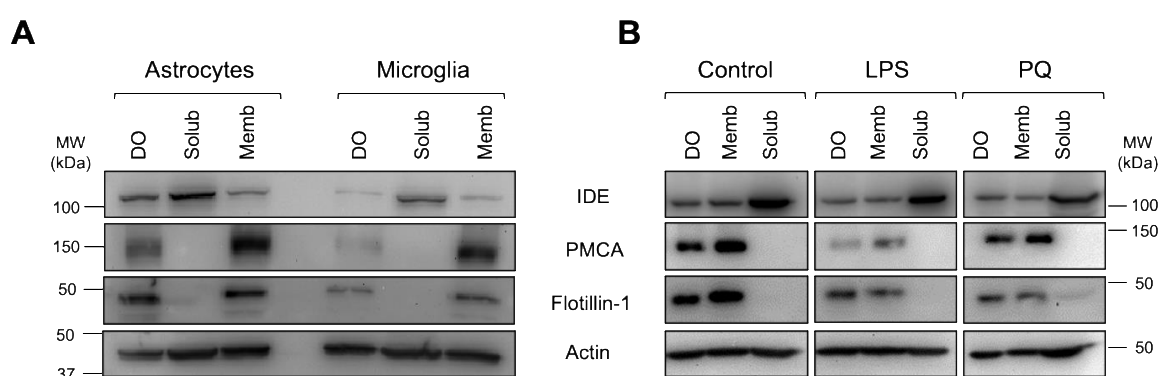


Figure 41. IDE is stably associated to membranes of glial cells. **A**) Immunoblot analysis of primary glial cells upon centrifugal fractionation in dense organelles (DO), membrane (Memb), and soluble (Solub) fractions. **B**) Immunoblot analysis of BV-2 microglial cells treated for 24 hours with different stimuli (100 ng/ml LPS; 25 μ M PQ) and fractionated in dense organelles (DO), membrane (Memb), and soluble (Solub) fractions.

2.6. IDE interacts with particular lipid rafts in microglial cells

Lipid rafts are specific microdomains in cellular membranes, enriched in cholesterol and sphingolipids, and involved in many cell signaling processes. Such microdomains have been described to promote the amyloidogenic processing of APP (Hicks et al., 2012), and they are also involved in insulin signaling by interaction with the insulin receptor (Bickel, 2002). Therefore, the search of IDE at microglial lipid rafts was mandatory. There is only one antecedent that described the presence of IDE in such microdomains in the neuronal cell line N2a, using Triton-X100 as detergent (Bulloj et al., 2008). To test whether IDE-membrane association occurs in particular membrane microdomains, we isolated lipid rafts from BV-2 membrane preparations with different chemical (Triton-X100 and Triton-X114) and mechanical (sonication) methods, using flotillin-1 as lipid raft marker. IDE was detected in both Triton-X100- and sonication-resistant membrane domains (**Figures 42A** and **42B**, respectively), while it was absent in Triton-X114-resistant membrane domains (**Figure 42C**). In all cases, IDE protein was also detected in non-raft fractions. Taken together, our findings support the interaction of IDE with membranes and reveal the association of IDE with lipid rafts with specific physicochemical properties.

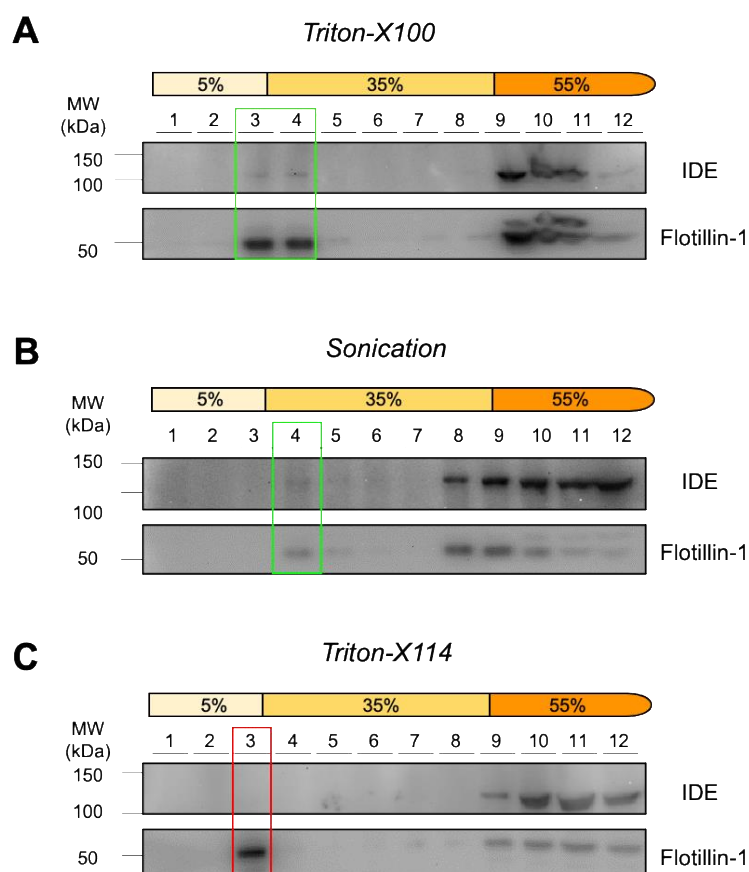


Figure 42. IDE is associated to membrane microdomains with specific properties in the microglial cell line BV-2. Immunoblot analyses of membrane fractionation on discontinuous sucrose gradients of BV-2 membrane preparations after using different lipid rafts isolation methods: **A)** Triton-X100, **B)** sonication and **C)** Triton-X114. Rectangles highlight either the presence (green) or the absence (red) of IDE in lipid rafts. $N = 2$ independent experiments.

2.7. IDE associates to microglial membranes by their cytosolic side

Having demonstrated that IDE associates with the plasma membrane, the obvious next step, crucial to understand its functions, is to establish on which side of the membrane this interaction occurs. To address this point, we performed immunocytochemistry and electron microscopy experiments using the polyclonal anti-IDE antibody (AB9210, Merck), previously validated for immunostaining (Fernández Díaz et al., 2018). Furthermore, we checked the specificity of this antibody on WT and IDE-KO primary microglial cultures. First, we explored different settings on immunocytochemistry experiments to try to decipher IDE subcellular localization in BV-2 microglial cells. Non-permeabilized conditions did not present IDE labeling (**Figure 43A**), suggesting that IDE is not present at the extracellular side of the plasma membrane. On the other hand, under permeabilizing conditions IDE signal was present inside the cells in a punctate pattern (**Figure 43B**), suggesting that IDE is cytosolic and might be associated with vesicular organelles. To further confirm the absence of IDE on the cell surface, we performed *in vivo* immunolabeling experiments using CD11b, a surface integrin, as a positive control. Confocal images showed no IDE signal, while CD11b yielded a robust labeling throughout the cell surface (**Figure 43C-C'**). However, after fixation and permeabilization, abundant IDE signal was evident inside the cells in a clear punctate pattern (**Figure 43D-D'**).

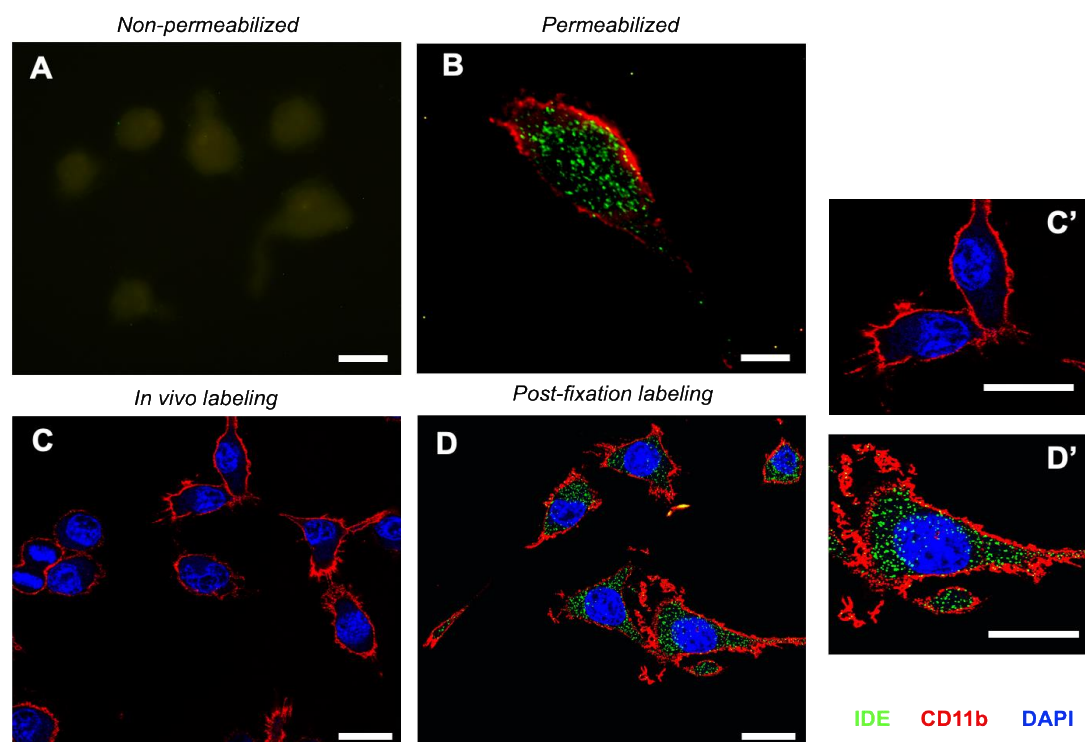


Figure 43. IDE associates to membranes only at the cytoplasmatic side. A-B) Representative fluorescence microscopy images of IDE signal in non-permeabilized (A) and permeabilized (B) BV-2 cells. Only background autofluorescence can be detected in A. Image B shows a deconvolved Z-stack. C-D) Representative confocal sections of IDE signal after 20-minute *in vivo* labeling (C) and in post-fixation permeabilized cells (D). Close-up views shown in C' and D'. Calibration bars in A and B: 10 μm ; C, C', D and D': 20 μm .

These results indicate that microglial IDE is associated with membranes exclusively at the cytoplasmatic side, with no detectable IDE exposed on the cell surface, at least by the antibody used (whose epitope is at the N-terminal portion of IDE). However, it would be highly desirable to corroborate these results with other antibodies targeting different regions of the IDE protein.

2.8. IDE is found in multivesicular bodies and their microvesicles in secretory state microglia

The subcellular localization of IDE in BV-2 microglia was further confirmed by morphological criteria derived from immunoelectron microscopy. Two different physiological states were clearly observed in BV-2 cultured cells: some of them presented very few vesicles and were probably in their “resting” or “surveillance” state, and, on the other hand, other cells had numerous vesicles in the vicinity of the plasma membrane, which could be in the “activated” secretory state (**Figure 44A**). IDE labeling was only found in cells with multiple vesicles, suggesting a role for IDE when microglial cells acquire a phenotype within the spectrum of active-secretory responses. IDE was mostly cytosolic and found in large vesicles clustered in close proximity to the plasma membrane (**Figure 44B**). After exhaustive exploration, IDE was not found inside any organelle, except for an occasional signal in mitochondria (inset in **Figure 44F**). However, IDE was found in multivesicular bodies (MVBs), morphologically distinctive by a mean diameter of 200-500 nm and characterized by an electron lucent matrix and the presence of microvesicles formed by invagination on their surface. IDE was found on the external side of MVBs or in their intraluminal vesicles (**Figures 44C-E**). Larger MVBs with IDE positive microvesicles were found close to the cell surface, probably in their way to the secretion of their content (**Figures 44F and 44G**). These results reinforce our *in silico* predictions about IDE subcellular localization, being mostly cytosolic in microglial cells. The mitochondrial location of IDE might be explained by the expression of the longer IDE isoform (IDE-Met¹), which contains a mitochondrial targeting sequence (Leissring et al., 2004), being a minority in microglia. Furthermore, a striking feature is the preferential location of IDE in MVB and their microvesicles, a location suggesting a non-canonical extracellular vesicle-mediated secretion of IDE to the extracellular space. These results led us to analyze IDE exportation under different stimuli.

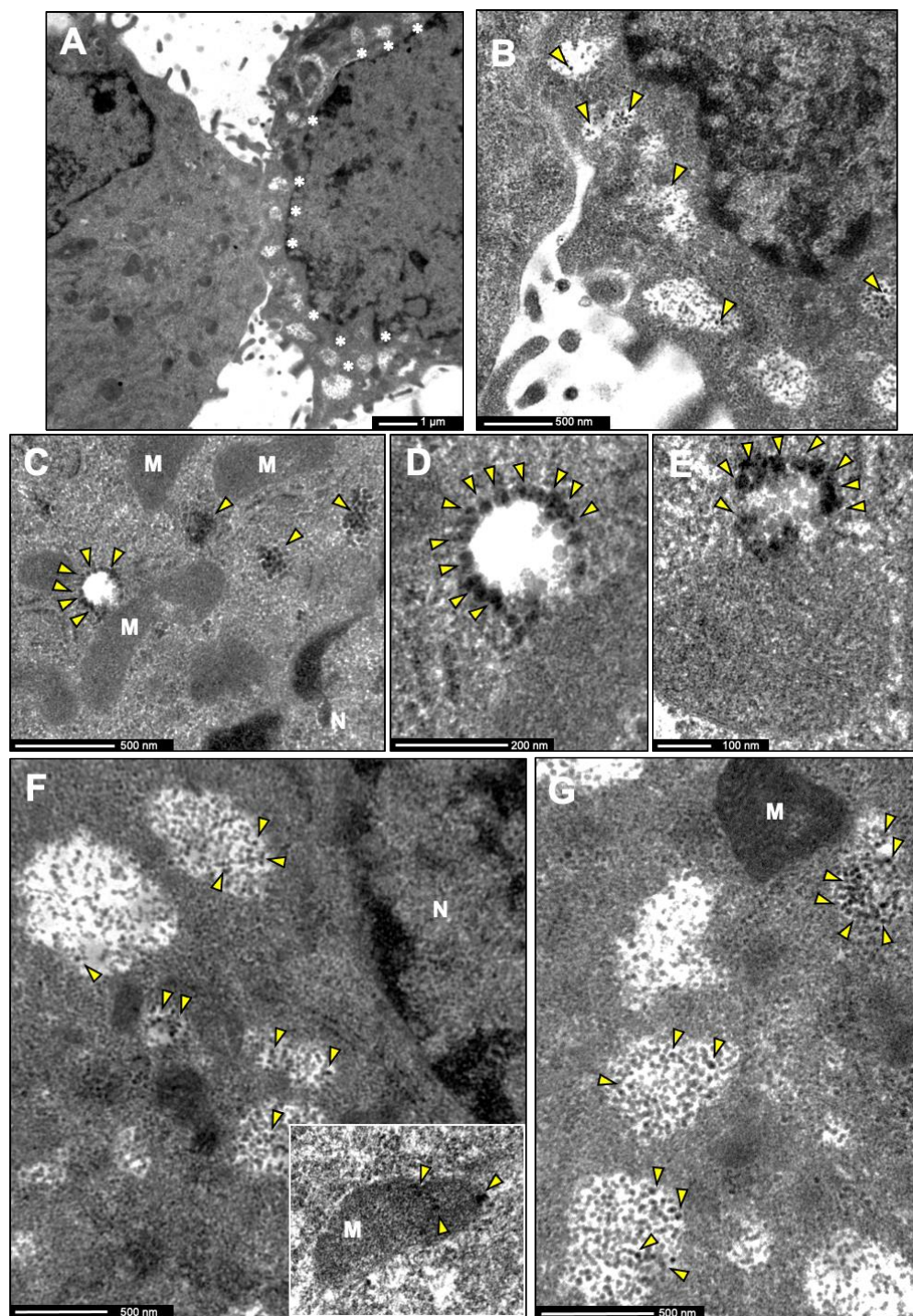


Figure 44. Immunoelectron microscopy micrographs of the subcellular localization of IDE in BV-2 microglial cells. IDE labeling is shown by means of silver-enhanced gold particles. **A-B)** Representative images of the two types of BV-2 cells found in electron microscopy sections, some with scarce vesicles (left) and others with numerous vesicles (right, pointed out by white asterisks). IDE labeling was only detected in cells with multiple vesicles. **B)** Inset from A, showing a closer view of the vesicles and the IDE signal (yellow arrowheads). **C-E)** Representative images of immunogold labeling of IDE in small multivesicular bodies (MVBs) and their nascent and internal microvesicles (yellow arrowheads). **F-G)** Images showing larger MVBs, generally found closer to the cell surface (as in B), with IDE labeling in microvesicles inside them (yellow arrowheads). The inset in (F) shows a unique mitochondrion with IDE signal found in our samples. Abbreviations: M = Mitochondria, N = Nucleus.

2.9. IDE exportation in extracellular vesicles is regulated by the activation state of microglial cells

We wondered if any relevant stimulus for microglial cells, able to regulate their polarization state, could be implicated in regulating the export of IDE to the extracellular space. Based on the antecedents that described IDE in exosomes (Bulloj et al., 2010; Tamboli et al., 2010; Glebov et al., 2015), we initially explored the presence of IDE in the extracellular media of primary microglial cultures exposed to different stimuli for 24 hours. The treatments assayed produced remarkable morphological changes in microglia (**Figure 45A**). We found that exportation of IDE from microglia was regulated by the activation state of the cells, being increased under inflammatory (LPS) and oxidative (PQ) stimuli (**Figures 45B and 45C**). Since actin has been described to be in extracellular vesicles (EVs) (Meldolesi, 2018), we quantified extracellular actin (**Figures 45B and 45C**) to estimate the “secretory activity” of microglia, which resulted higher in pro-inflammatory and oxidative conditions. Furthermore, IDE and actin showed a strong positive correlation, related with the microglial polarization state (**Figure 45D**).

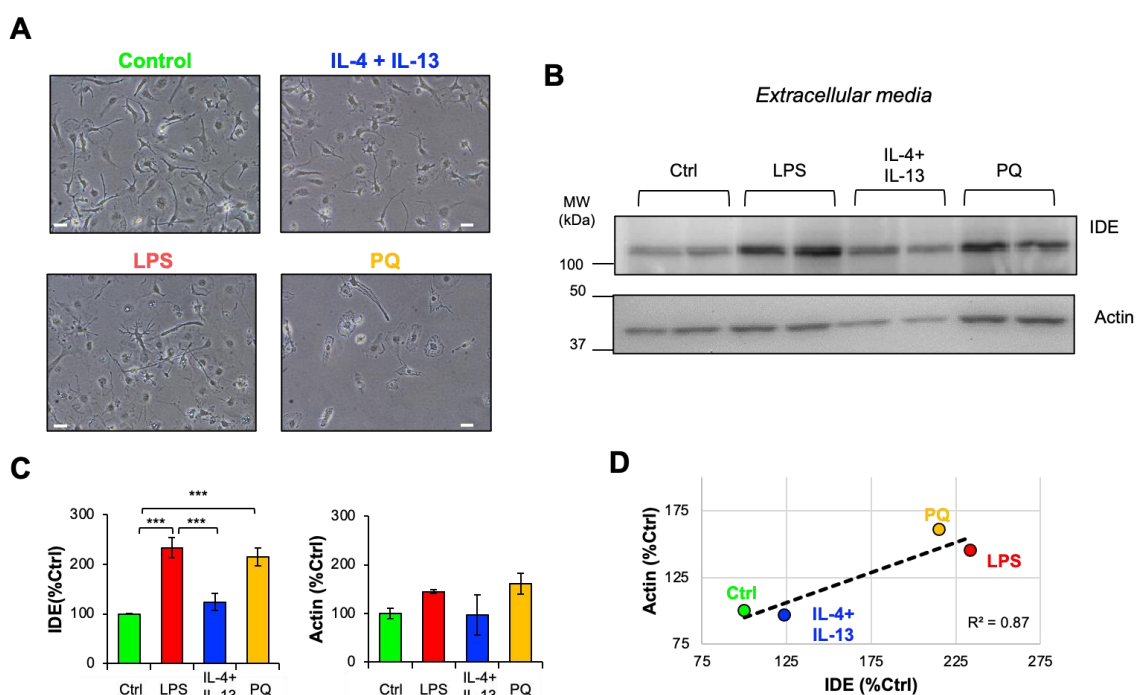


Figure 45. Extracellular IDE protein from primary microglial cultures exposed to different stimuli.

A) Representative images of microglial cells subjected to different stimuli for 24 hours. Morphological changes can be observed with different treatments. **B)** Immunoblot analysis of extracellular IDE and actin secreted to the culture media under different stimuli. Identical volumes of extracellular media, coming from cultures with identical density, were processed and analyzed. Indeed, actin was not used to normalize IDE, but it was analyzed as a target protein instead. **C)** Immunoblot quantifications, normalized to control condition. Statistical differences were assessed by one-way ANOVA (IDE: $p = 0.15$, Actin: $p = 0.25$) followed by pairwise comparisons by t -tests (***, $p < 0.001$). $N = 3$ independent experiments. **D)** Scatterplot representing the amount of extracellular IDE and actin. Both proteins show a positive linear correlation (linear regression fit, $R^2 = 0.87$).

These results suggest that microglial IDE is exported in EVs, and the amount of IDE present in these EVs is regulated by the activation state of the microglia. To further investigate this hypothesis, we purified EVs from conditioned media produced by primary microglia treated with different pro-/anti-inflammatory stimuli, this time including oligomeric A β , and analyzed them by immunoblot. We confirmed the presence of IDE in EVs and found that, besides the expected 110-kDa IDE band, there was another band around 60 kDa, whose specificity was validated by the IDE-KO sample (**Figure 46**). The antibody used in these experiments is a polyclonal antibody whose epitope is located at amino acids 150-300 of a rat IDE sequence, therefore the putative “half-IDE” isoform corresponds to the N-terminal portion of IDE. The origin of this “half-IDE” isoform might be explained by the breakdown of the protein by its hinge region. Interestingly, full-length IDE only seemed to be present after stimulation, while the shorter isoform was present in all conditions. In accordance with our previous experiments (**Figure 45**), IDE exportation was dependent on the stimulus: lower in control conditions and after IL-4+IL-13 stimulation, and higher upon LPS and A β treatments. EV-associated IDE secretion under PQ treatment was lower than expected, which could be explained by EVs breakdown due to oxidative stress (Sharifi-Rad et al., 2020). To further characterize our EVs preparations, CD81 and actin were analyzed. In contrast to actin, which showed a homogeneous expression between conditions, CD81 exhibited great differences between samples (**Figure 46**), which indicates the production of different types of exosomes upon differential microglial stimulation. Intriguingly, IDE-KO derived EVs showed a strong expression of both CD81 and actin when compared to WT EVs in control conditions, suggesting a higher production of EVs by IDE-KO microglia (**Figure 46**).

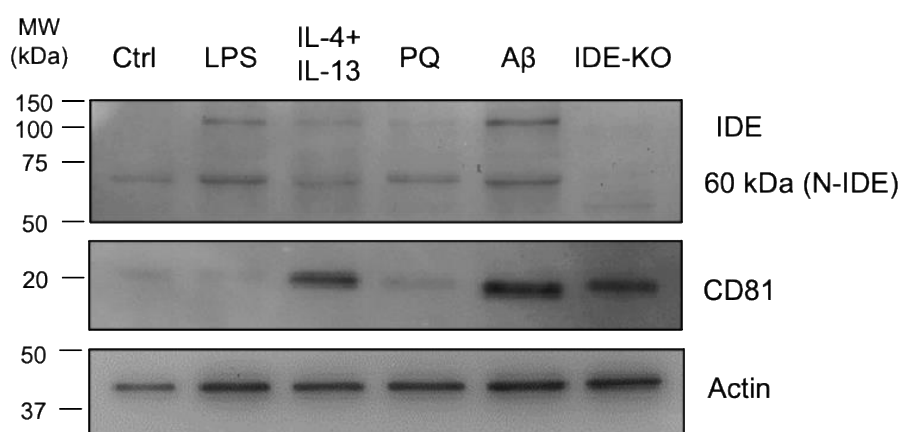


Figure 46. Immunoblot analyses of IDE, CD81 and actin in extracellular vesicles preparations. *Two pools of conditioned media originated from 4 independent cultures were analyzed. EVs from IDE-KO microglia were included as negative controls for the IDE antibody. A putative “half-IDE” 60-kDa form was detected. CD81 and actin were analyzed as EVs markers.*

These results reinforce that IDE is secreted in MVB-derived EVs, but also demonstrate, for the first time, that this mechanism of IDE exportation is modulated by the polarization of microglial cells, which is particularly relevant to neurodegenerative states in the brain.

CHAPTER 3. ROLE OF IDE *IN VIVO* IN A CONSTITUTIVE KNOCK-OUT MOUSE PARADIGM

IDE was initially described as an insulin-degrading enzyme, therefore the majority of studies performed *in vivo* with genetically modified mice (overexpressing or downregulating *Ide*) focused on metabolism. However, since IDE has also been described as an A β -degrading protease, the constitutive *Ide*-knockout mouse is also a relevant model to analyze the role of IDE in brain function. Studies on *Ide*-deficient mice described that relevant metabolites of APP processing, such as A β ₄₀ and A β ₄₂ (Miller et al., 2003; Farris et al., 2003), CTF γ (Miller et al., 2003) and AICD (Farris et al., 2003), as well as brain insulin (Farris et al., 2003), are elevated at 7-12 weeks of age when insulin activity is diminished. In line with this, APP transgenic mice overexpressing human IDE showed reduced brain A β levels and retarded amyloid plaque formation (Leissring et al., 2003). In order to get a global insight on the role of IDE *in vivo*, we performed a comprehensive analysis of metabolic, behavioral and molecular parameters on a cohort of 12-month-old wild-type (WT), heterozygous (IDE-HET) and knockout (IDE-KO) mice for the *Ide* gene. With all the variables collected, we performed a multivariate analysis to understand the correlations between different parameters, followed by a principal component analysis (PCA) to reduce dimensions, and a multinomial logistic regression model to explain the genotypes and determine which variables are more significant.

3.1. Progeny produced by *Ide* heterozygous breeding does not follow Mendelian inheritance

The experimental cohort (WT, constitutive IDE-HET and constitutive IDE-KO mice) was generated from heterozygous breeding. Remarkably, the progeny obtained from such crosses did not follow Mendelian inheritance ($\chi^2 = 12.6$; degrees of freedom = 2; $p = 0.002$; $N = 179$ mice from 29 litters). Intriguingly, the major deviation from expected proportions was caused by the increase of IDE-HET mice in detriment of IDE-KO mice (**Figure 47**). These results suggest that total absence of IDE causes embryonic lethality, posing an important role for IDE during development.

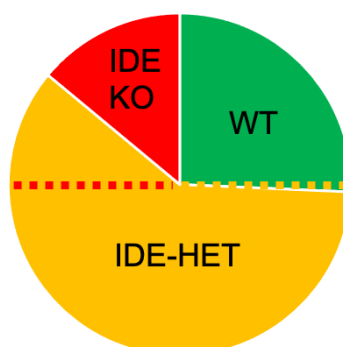


Figure 47. Progeny resultant from IDE heterozygous breeding. Proportions of WT (26%), IDE-HET (60%) and IDE-KO (14%) mice born from IDE heterozygous crosses. The dotted lines depict the expected proportions for each genotype. Statistical differences were assessed by chi-squared test ($p=0.002$).

3.2. *Ide* gene dose generates subtle effects in metabolic parameters of 12-month-old mice

Previous studies on constitutive IDE-KO mice showed that deletion of *Ide* causes constitutive hyperinsulinemia (from 2 months of age) and age-dependent effects on glucose and insulin tolerance, with a significant intolerance to both substances at 6 months of age (Abdul-Hay et al., 2011). However, since there are no data about older animals, we performed a small metabolic characterization of our experimental cohort of mice at 12 months of age.

First, we checked if total or partial loss of IDE altered body weight. We observed that this parameter remained unchanged in female mice, while IDE genotype had a significant effect on body weight in males. Interestingly, haploinsufficiency of *Ide* produced a tendency toward decreased body weight, while total *Ide* ablation significantly decreased the weight of these mice (**Figure 48**). These results indicate that IDE's effect on body weight is sex-specific (only in males) and dose-dependent (slight effect in IDE-HET but significant effect in IDE-KO mice).

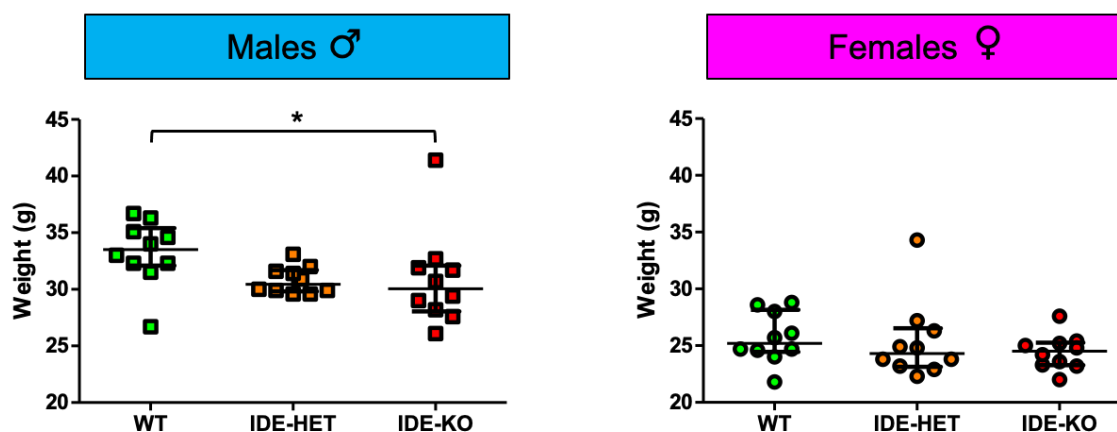


Figure 48. Body weight of WT, IDE-HET and IDE-KO mice at 12 months. Body weight of male and female mice under non-fasting conditions. $N=10$ mice per sex and genotype. Each symbol represents a mouse, and horizontal lines stand for the median \pm interquartile range. Statistical differences were assessed by ANOVA on ranks followed by pairwise comparisons by Tukey test. Males: $p=0.026$, WT males vs IDE-KO males: $p<0.05$. Females: $p=0.458$. (*, $p<0.05$).

Next, we measured blood glucose and plasma insulin levels under 6 hour-fasting conditions. We chose a short morning fast (6 hours) since it has been shown that overnight fasting provokes a catabolic state in mice, while shorter fasting is sufficient to assess insulin action within a more physiological context (Ayala et al., 2010). Glucose levels were significantly decreased in IDE-HET males, in comparison to WT males, while females showed the same tendency, but not significant. Intriguingly, IDE-KO mice exhibited a bimodal distribution in both sexes, with half of the individuals above and below the median of WTs (**Figure 49A**). Plasma insulin concentration remained unchanged, with no significant differences neither between genotypes nor sexes (**Figure 49B**).

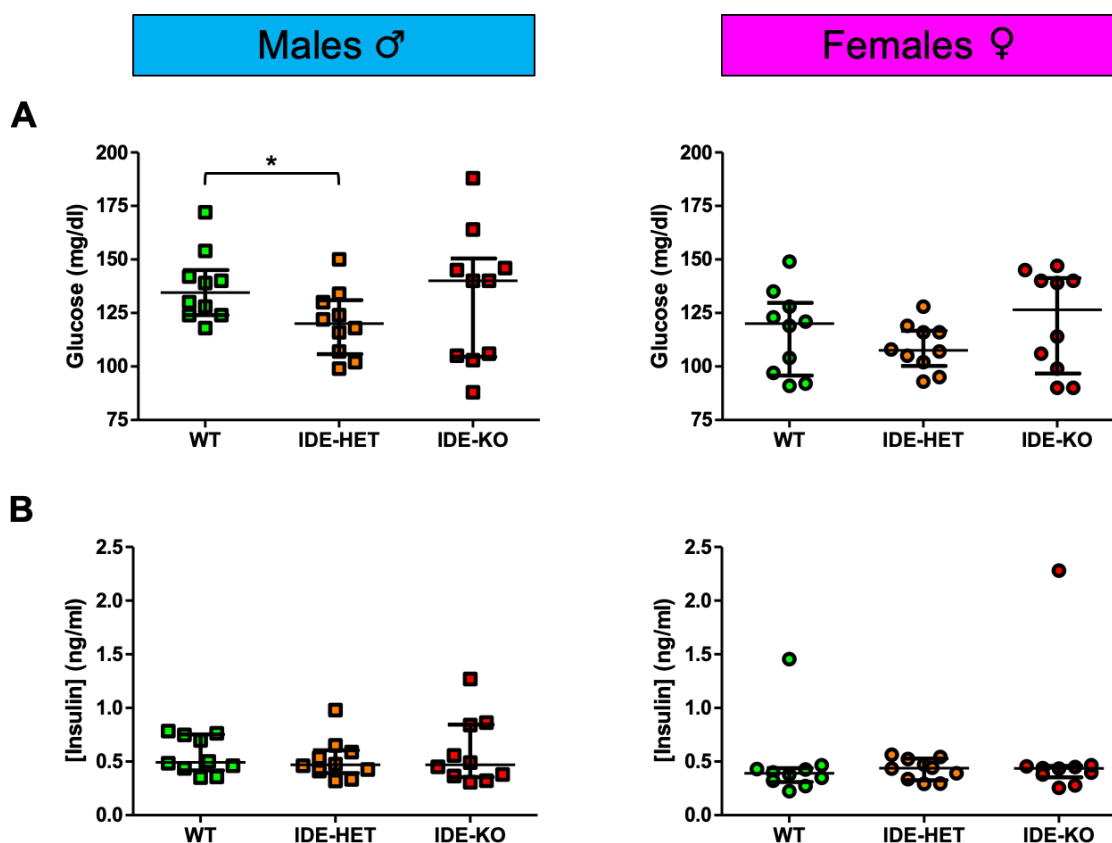


Figure 49. Blood glucose and plasma insulin levels after six hours fasting. **A)** Blood glucose of male and female mice after 6 hours fasting. **B)** Plasma insulin concentration of male and female mice after 6 hours fasting. $N=10$ mice per sex and genotype. Each symbol represents a mouse, and horizontal lines stand for the median \pm interquartile range. Statistical differences were assessed by one-way ANOVA. Males: glucose (one-way ANOVA $p=0.233$; post-hoc t -test: WT vs IDE-HET $p=0.029$), insulin (ANOVA on ranks, $p=0.852$). Females: glucose (ANOVA on ranks $p=0.567$), insulin (ANOVA on ranks, $p=0.471$). (*, $p<0.05$).

In summary, IDE deficiency produced subtle effects on metabolic parameters in 12-month-old mice. These effects were sex-dependent (only evident in male mice) and, in the case of body weight, correlated with the gene dosage of IDE. On the other hand, blood glucose concentration after moderate fasting was significantly decreased in male IDE-HET mice, while IDE-KO mice showed two different subgroups, with lower and higher blood glucose, respectively, which could indicate two stages of metabolic impairment.

3.3. Behavioral analyses reveal sex- and genotype-dependent effects of IDE deficiency on behavioral and memory tasks

To better characterize the role of IDE in brain function, the behavioral performance of mice and mnemonic function was studied at 12 months of age. Two different behavioral tests were carried out to evaluate spontaneous locomotor activity and object exploration tasks.

3.3.1. Open field

During the open field test, many locomotor and behavioral variables were analyzed for each mouse. The distance traveled by the mice showed a significant difference between sexes (globally, females traveled more distance), and a tendency to be reduced in IDE-KO females compared to WT females (**Figure 50A**). Stereotypic behavior showed no differences between genotypes or sexes (**Figure 50B**), indicating that experimental groups had a certain level of normal behavioral functioning. The relative time spent in center *versus* periphery (relative time (C/P)), indicative of lack of anxiety in mice, did not show significant differences among genotypes or sexes (**Figure 50C**). Taken together, these results indicate that partial or total IDE deletion does not produce significant abnormalities in the locomotor behavior of mice.

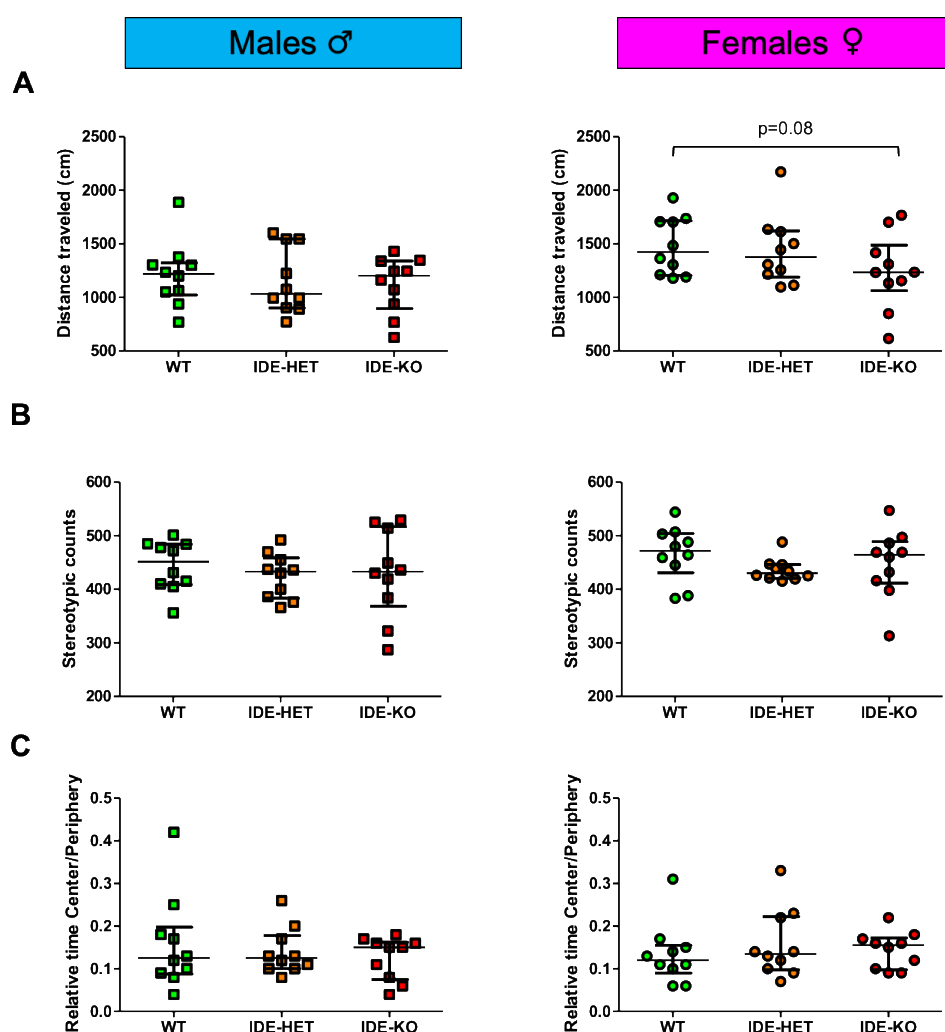


Figure 50. Open field results. A) *Distance traveled*, B) *Stereotypic counts* and C) *relative time center/periphery* during the open field. Each symbol represents a mouse, and horizontal lines stand for the median \pm interquartile range. Global statistical differences were analyzed by two-way ANOVAs considering the factors sex and genotype: the sex exhibited a significant effect on distance traveled ($p = 0.006$), with a tendency to be decreased distance in IDE-KO females ($p = 0.008$). Stereotypic counts and relative time center/periphery did not show any significant difference.

3.3.2. Memory tests

Memory tests analyze spontaneous exploratory behavior conditioned by the formation of various types of memory (spatial and non-spatial) during the testing process. These tasks were evaluated in 12-month-old mice by combining different versions of the novelty preference paradigm.

During the object familiarization trial (OFT) mice were allowed to explore two identical objects in relation to spatial environmental cues. In a typical training trial, groups of mice are not expected to show a significant preference on average for either a particular object or a location in the arena, as it was the case for our experimental groups (**Figure 51A**). Furthermore, the total explorations of all mice were compared to ensure that there was no baseline difference in exploration that may affect subsequent memory tests.

After the OFT, mice were removed from the arena, and during a break of 40 minutes (inter-trial interval), one of the familiar objects was moved to a novel location, which is the protocol for the object location test (OLT). After the inter-trial interval, mice were reintroduced to the arena and allowed to freely explore. In general, since mice prefer novelty, if they remember the location of the objects from their initial exposure, they will spend more time investigating the moved object. Thus, a positive discrimination index suggests that the mouse remembers where the object was located during training. Interestingly, significant genotype- and sex-dependent differences were observed in the performance of mice on the OLT. Surprisingly, IDE-KO males were significantly better than WT males at recognizing the object moved, while IDE-HET males remained unchanged. In contrast, WT females were significantly better than IDE-HET and showed a tendency to also perform better than IDE-KO females on the OLT (**Figure 51B**). These differences indicate a differential effect of IDE deletion on hippocampal-based, spatial memory, with an improvement in KO males and a worsening in KO females in comparison with WT mice. Curiously, haploinsufficiency of IDE resulted in a tendency to worse object recognition in both sexes.

After another 40-minute break, we carried out the novel object recognition test (NORT), wherein the familiar object that had not been moved before was substituted by a novel, different object. As expected in OLT, mice with good memory of the objects will spontaneously prefer investigating the novel object. Thus, a positive discrimination index in NORT suggests that the mouse remembers the familiar object. Performance on the NORT did not show interactions between genotype and sex. Male IDE-HET showed a tendency to better recognize the novel object, while female IDE-HET showed a significant improvement in detecting the novel object, in comparison to WT mice. Remarkably, IDE-KO males showed a tendency to perform worse than WT males, while IDE-KO females showed the opposite tendency (**Figure 51C**).

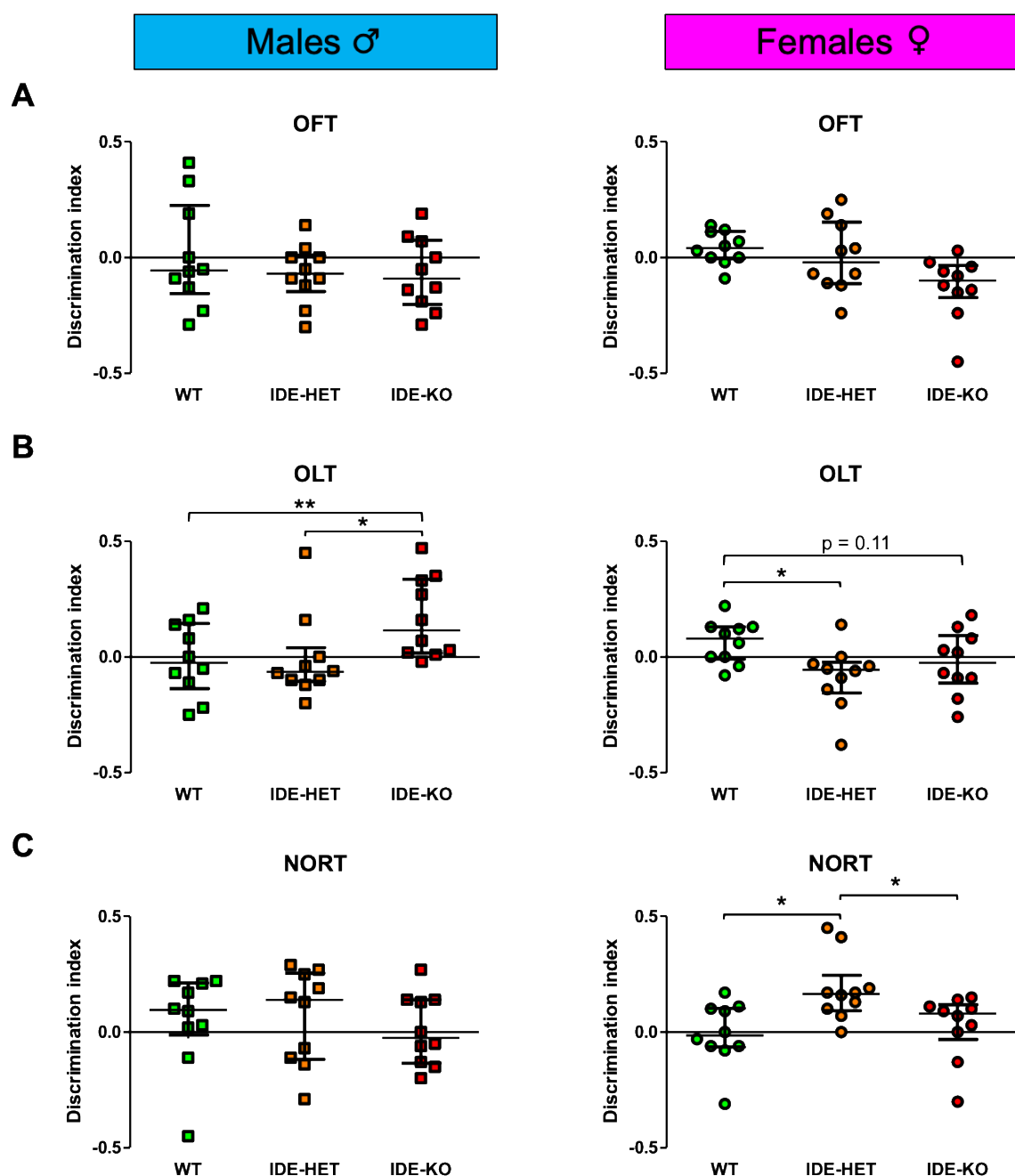


Figure 51. Object recognition tests results. **A)** Object familiarization trials (OFTs) scores. **B)** Object location test (OLT) results. **C)** Novel Object Recognition Test (NORT) results. Each symbol represents a mouse, and horizontal lines stand for the median \pm interquartile range. Global statistical differences were analyzed by two-way ANOVAs considering the factors sex and genotype, followed by Holm-Sidak all pairwise multiple comparisons. OFT did not present significant differences. OLT: there was a significant interaction between genotype and sex ($p = 0.024$). NORT: there were significant differences only among females. (*, $p < 0.05$, **, $p < 0.01$).

To better understand the recognition tests results, the scores obtained by each individual mouse were transformed into a categorical variable whose possible values were “passed” (positive discrimination index), “null” (null discrimination index) or “failed” (negative discrimination index). Conceptually, this transformation considers how many mice of each genotype succeeded or failed in

the object recognition tasks (**Table 13**). In general terms, mice performed better in the NORT than in the OLT (63% vs 45% mice passed, respectively).

Table 13. OLT and NORT results analyzed by categorical variables.

Genotype	Sex	OLT				NORT			
		Passed	Null	Failed	%Passed	Passed	Null	Failed	%Passed
WT	Males	4	1	5	40.0	8	0	2	80.0
	Females	6	2	2	60.0	4	1	5	40.0
	Total	10	3	7	50.0	12	1	7	60.0
IDE-HET	Males	2	1	7	20.0	6	0	4	60.0
	Females	1	1	8	10.0	9	1	0	90.0
	Total	3	2	15	15.0	15	1	4	75.0
IDE-KO	Males	9	0	1	90.0	4	1	5	40.0
	Females	5	0	5	50.0	7	1	2	70.0
	Total	14	0	6	70.0	11	2	7	55.0
TOTAL		27	5	28	45.0	38	4	18	63.3

Focusing on the OLT, the most surprising results were the outstanding performance of IDE-KO males (90% of the individuals passed this test) and the poor performance of IDE-HET mice, independently of sex (85% individuals from this group failed this test) (**Table 13**). The NORT task showed a higher success rate. In this case, WT males obtained much better scores than WT females (80% vs 40% mice passed, respectively), and IDE partial or total loss of function showed a negative effect, IDE dose-dependent, in the performance of males (80% WT, 60% IDE-HET and 40% IDE-KO males passed this test). Conversely, the opposite tendency was observed in females, with 90% of IDE-HET and 70% of IDE-KO females succeeding in the NORT, compared with only 40% of WT females (**Table 13**). Collectively, these results suggest an interaction between IDE dosage, the sex of the mice and their performance on each specific test (OLT or NORT).

3.4. Expression of IDE, insulin receptor, and AKT1 are sex-dependent in the olfactory bulb, an insulin signaling high-expression site in the brain

The olfactory bulb was chosen to study insulin signaling because, in mice, it is the brain region which contains the highest number of insulin receptors. We initially checked that the insulin dose we were administering to the mice was reaching the brain and having an effect on cerebral insulin receptors. A pilot experiment performed on WT mice (3 months old) showed that the insulin dose selected (5 U/kg) was able to induce the phosphorylation of insulin receptors (**Figure 52A**). Strikingly, insulin signaling at the olfactory bulb of the 12-month-old mice cohort was constitutively and highly activated, which diminished the effects of the injected insulin (**Figure 52B**).

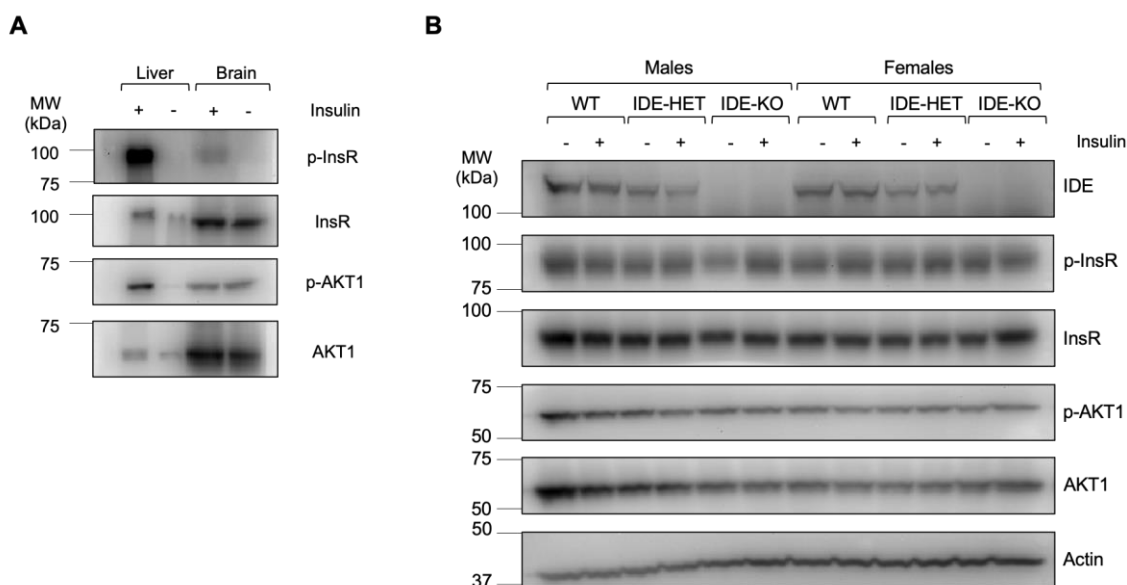


Figure 52. Immunoblots of insulin signaling in the brain. A) Pilot experiment to check that the insulin dose selected (5 U/kg) was able to reach the brain and activate the phosphorylation of insulin receptors. Liver samples were included as positive controls. **B)** Representative immunoblot of olfactory bulb insulin signaling in 12-month-old mice.

Because we were not able to detect differences between WT and IDE-KO in insulin signaling activation, we decided to focus on non-phosphorylated proteins (InsR and AKT1) to continue with the study. First, we checked the effect of *Ide* gene ablation on the IDE protein and found a differential effect on males, where IDE-HET mice did not show a significant decrease on the IDE protein, and females, where the IDE-HET group showed a reduction of around 50% of the protein, being a good model of knockdown (**Figure 53A**).

The most remarkable effects on the insulin signaling proteins analyzed were observed not between genotypes but between sexes: female mice expressed significantly lower insulin receptor (**Figure 53B**) and AKT1 (**Figure 53C**) in comparison with males. Comparing genotypes, IDE-HET and IDE-KO males showed a tendency to have more insulin receptor protein than WT, although not statistically significant due to the higher dispersion of mutant mice in comparison with WT. Less dispersed values were observed in females, but no clear differences were found between genotypes. AKT1 showed also great variability in males, with a tendency to be increased in IDE-HETs, while females exhibited again less dispersed values.

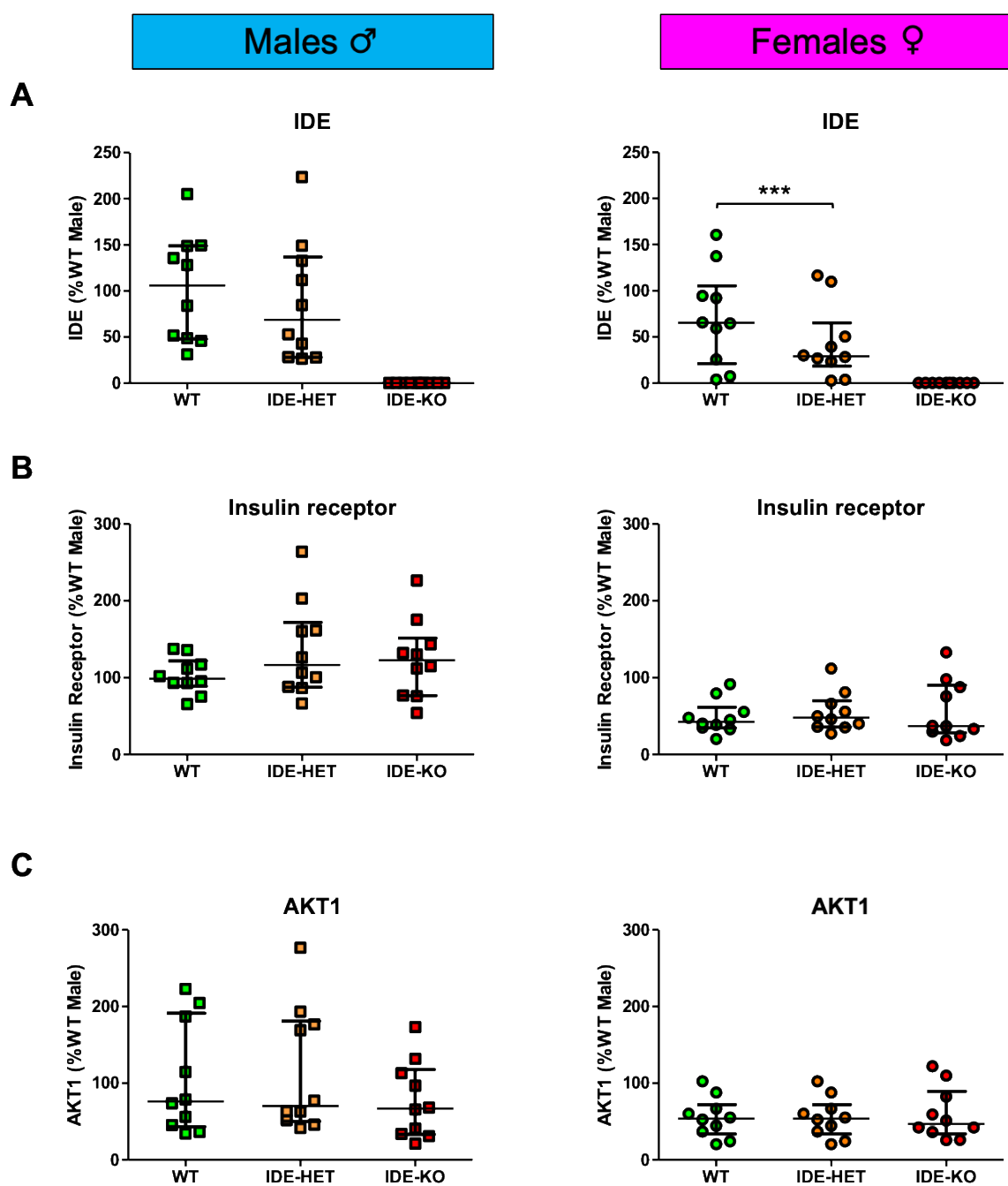


Figure 53. Results from immunoblots of insulin signaling-related proteins. A) IDE. B) Insulin receptor. C) AKT1. Each symbol represents a mouse, and horizontal lines stand for the median \pm interquartile range. Global statistical differences were analyzed by two-way ANOVAs considering the factors sex and genotype. IDE (genotype $p < 0.001$, sex $p = 0.03$). Insulin receptor (genotype $p = 0.265$, sex $p < 0.001$). AKT1 (genotype $p = 0.5$, sex $p = 0.004$). (***, $p < 0.001$).

3.5. Gliosis markers CD11b and GFAP, glial-derived neuroprotector ApoD, and A β oligomers, also show sex-dependent changes

The term “inflammaging” denotes the increase of inflammatory markers in the blood, cells and tissues associated with aging. This aging-dependent, low-grade chronic inflammation is of particular relevance in the brain, since it is one of the underlying factors for the development of many neurodegenerative processes (Komleva et al., 2021). Since our experimental cohort was middle-aged, formed by one-year-old mice, we analyzed the inflammatory state of their brains by targeting different proteins relevant for neurodegenerative processes: Iba1 and CD11b (markers of microgliosis), GFAP (marker of astrogliosis), ApoD (one of the most consistently upregulated proteins in the mammalian aging brain) and A β oligomers (whose accumulation in the brain is one of the most important causes of AD).

The microgliosis marker Iba1 showed no differences either between genotypes or sexes (**Figure 54A**), while CD11b was significantly upregulated in female mice, independently of their genotype (**Figure 54B**). In accordance with this, the astrogliosis marker GFAP was overexpressed in females (**Figure 54C**), indicating a global overactivation of gliosis in female mice. On the other hand, the neuroprotective protein ApoD showed higher expression in males than in females and, among males, the IDE-KO group showed a tendency to have less ApoD (**Figure 54D**). Finally, A β oligomers were significantly higher in males than in females (**Figure 54E**). Collectively, these results indicate that the main effects on inflammaging markers are due to sex rather than genotype.

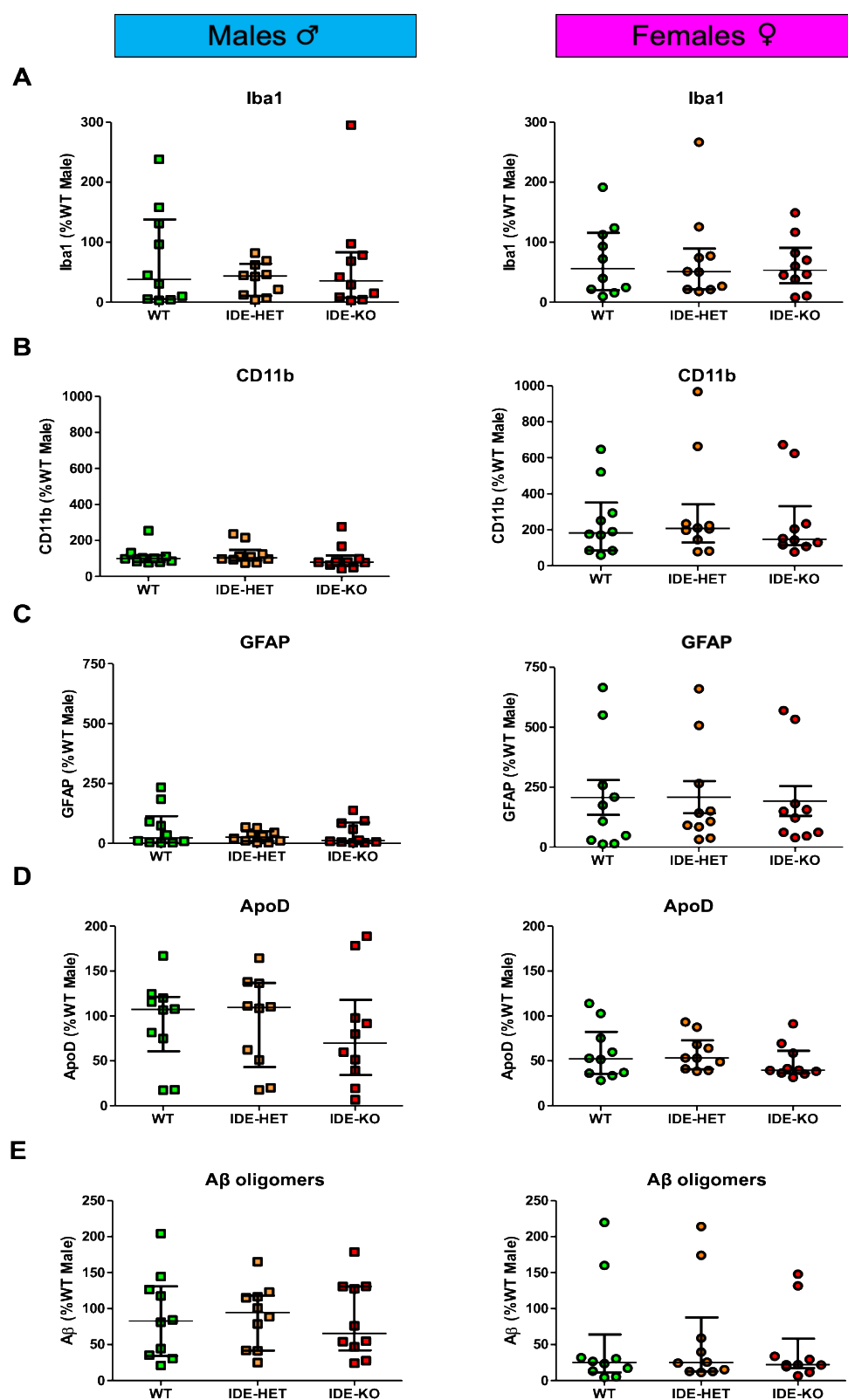


Figure 54. Results from immunoblots of “inflammaging” markers. A) *Iba1*. B) *CD11b*. C) *GFAP*. D) *ApoD*. E) *Aβ oligomers*. Each symbol represents a mouse, and horizontal lines stand for the median \pm interquartile range. Global statistical differences were analyzed by two-way ANOVAs considering the factors sex and genotype. *Iba1* (genotype $p=0.77$, sex $p=0.55$); *CD11b* (genotype $p=0.75$, sex $p=0.001$); *GFAP* (genotype $p=0.91$, sex $p<0.001$); *ApoD* (genotype $p=0.62$, sex $p=0.003$); *Aβ* (genotype $p=0.88$, sex $p=0.025$).

3.6. Multivariate analysis helps to visualize IDE-dependent effects on brain-related variables

In some variables, such a high dispersion is observed that they can even become bimodal. This suggests that there might be coordinately changing patterns of variables in each individual mouse, and this “individual mouse barcode” could condition the particular response of the brain to the total or partial lack of IDE. Taking this into account, a multivariate analysis was conducted to try to reveal relevant relationships.

Initially, to get an overview between all the variables analyzed, a correlation analysis was performed. Since our input variables had different scales, data were first standardized and then correlations were calculated between each pair of variables (**Figure 55**). Positive correlations were appreciated between genotype (represented by the number of functional copies of *Ide* gene present, being WT = 2, IDE-HET = 1, and IDE-KO = 0) and locomotor parameters such as distance traveled, ambulatory events or center entries, while a negative correlation is found between the IDE dose and OLT performance. The most striking correlations found in the “sex” variable were the higher mobility of female mice in the OF, and the reduced expression of insulin receptor and ApoD in females. The OLT test was inversely correlated with CD11b and GFAP, indicating that gliosis produces impairments in hippocampal memory, while the NORT, that relies on multiple brain regions, showed weak positive correlations between test performance and “inflammaging” markers. Curiously, the social factor “number of cage mates” showed negative correlations with weight, blood glucose and NORT performance. All metabolic parameters analyzed showed negative correlations with OF parameters, indicating an important effect of metabolism on locomotor behavior. Weight showed a positive correlation with blood glucose and also with the proteins involved in metabolism (insulin receptor, AKT1 and IDE) and, surprisingly, with ApoD expression. On the other hand, a negative correlation was found between blood glucose and gliosis markers, while the “inflammaging” markers showed positive correlations between them. Finally, A β oligomers showed negative correlations with locomotor parameters, while they were directly correlated with gliosis markers, especially with Iba1, related with microgliosis.

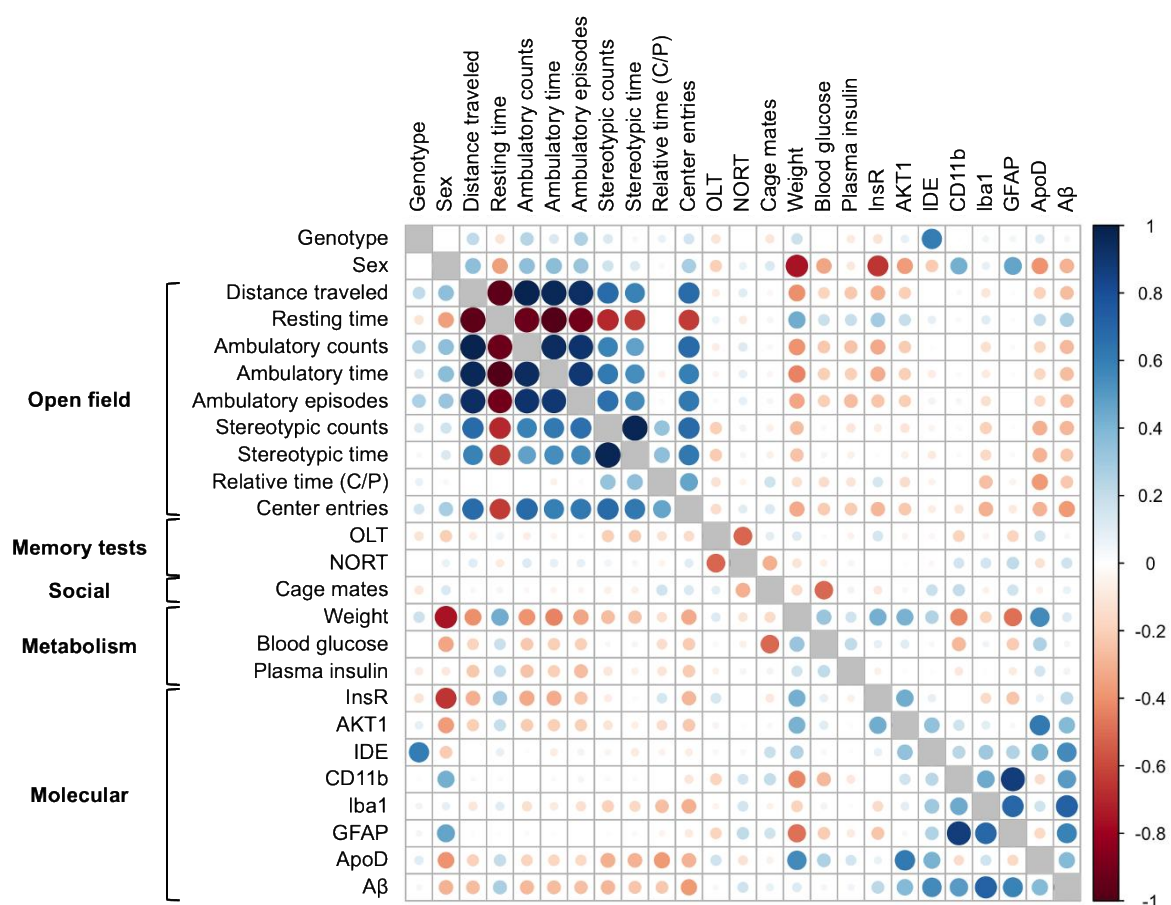


Figure 55. Correlation plot with all the variables analyzed in the 12-month-old mice cohort. Correlation coefficients were calculated using the Pearson correlation method. The plot shows relationships between behavioral, social, metabolic and molecular variables with genotype and sex. Circles represent the correlation value, with the size of the circle indicating the magnitude of the correlation, and the color standing for the sign (blue for positive, red for negative correlations). Categorical variables are coded as follows: genotype is WT = 2, IDE-HET = 1 and IDE-KO = 0. Sex is coded as 0 = male and 1 = female.

The correlation analysis allowed us to detect variables with high collinearity (for example distance travelled and ambulatory events), which were discarded from the PCA since their redundancy introduces noise in the analysis. Therefore, the PCA was performed with 18 variables. The PCA reduced these variables to 2 new dimensions which are able to explain 41.5% of total variance (**Figure 56A**). These dimensions clearly separated and clustered OF variables (lower left quadrant), metabolism-related parameters (right quadrants) and “inflammaging” markers (upper quadrants). Remarkably, the two behavioral tests were opposite to each other and orthogonal to the genotype variable. Regarding IDE, it apports to Dimension 1 the same direction as the metabolic parameters, while in component 2 IDE clusters with inflammaging markers (see **Figure 56A**). When representing the 60 individuals in a graph whose axes are the 2 new dimensions, the clearest difference was observed across Dimension 1 between males and females, indicating that the variable “sex” has a strong weight in the final outcome of the analysis (**Figure 56B**).

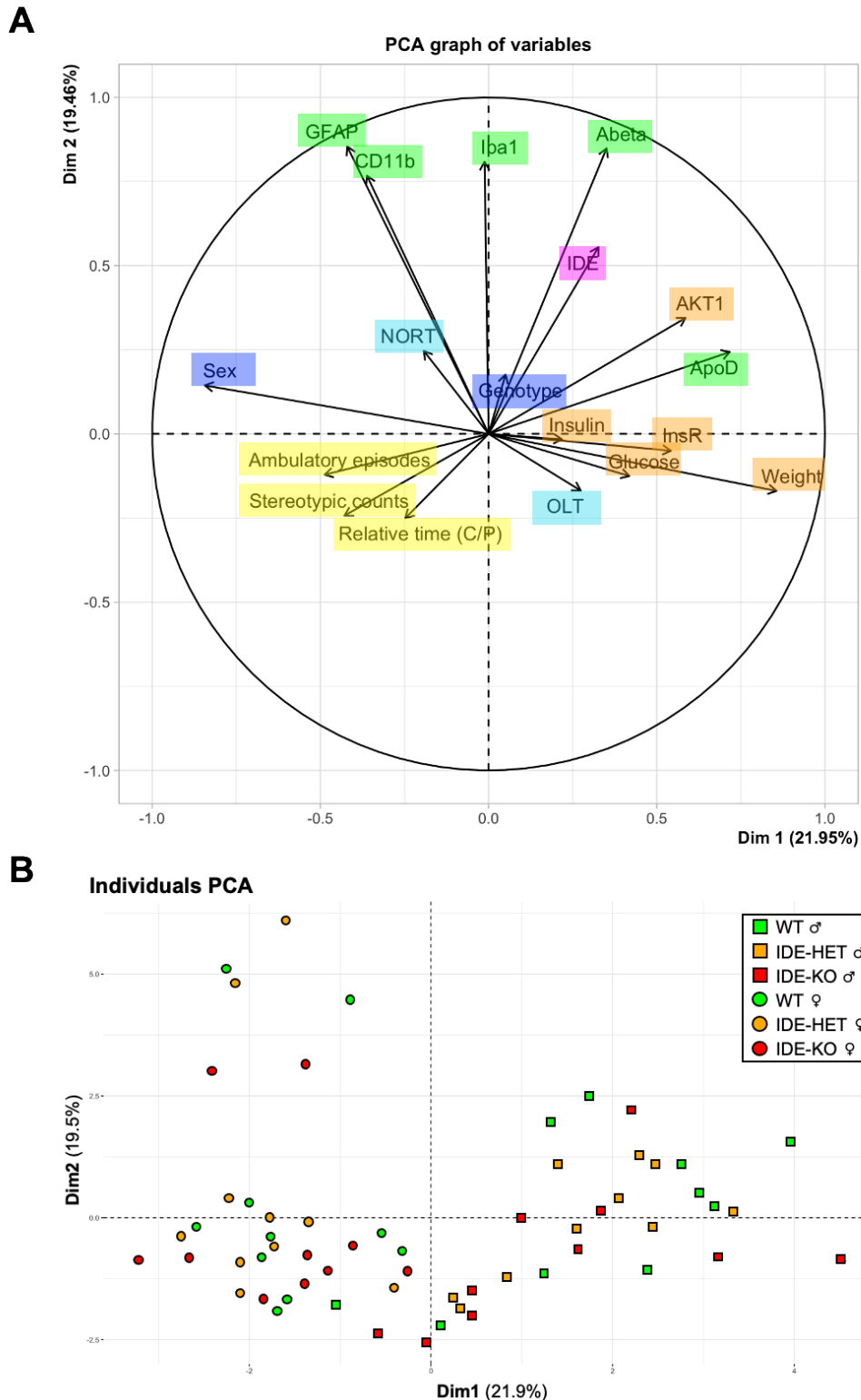


Figure 56. Principal Component Analysis on the IDE-Null cohort. A) Graphical representation of the PCA showing the direction of the variables in a 2D graph whose axis are the new dimensions generated by the analysis. Percentage of total variance explained by new dimensions: 41.5% (21.95% dimension 1 and 19.46% dimension 2). Variables are highlighted as follows: OF-related in yellow, behavioral tests in pale blue, metabolic parameters in orange, inflammaging-related markers in green, categorical variables in dark blue, and IDE in pink. **B)** Representation of the individuals across the new dimensions, 1 and 2, generated by PCA. Note the separation between females and males (only left and mostly right quadrants, respectively).

Considering our previous results, we decided to perform PCAs separately in males and females to try to find other effects that could be “masked” by the sex differences. PCA showed better performance in females than in males (44.27% vs 38.52% of total variance explained, respectively) (**Figures 57A** and **57B**). In terms of cognitive tests, OLT and NORT variables were opposite to each other in both sexes, as expected since they involve different cognitive mechanisms, and orthogonal to genotype and IDE protein amount. “Inflammaging” markers were strongly associated with positive values in Dimension 1, with higher weight in females than in males. With respect to metabolism, proteins related with insulin signaling such as the insulin receptor and AKT were inversely related with metabolic parameters, indicating synergistic antagonism between them. Remarkably, the weight of IDE protein apports to Dimension 1, the most explicative one, in the same direction as Iba1, GFAP and A β in both sexes. Finally, the eigenvalue for IDE was of greater magnitude in females than in males, which is in concert with the higher expression of IDE in males (**Figure 53A**). In view of these results, it is relevant to study the role of IDE in glial responses and A β managing, which will be addressed in Chapter 4.

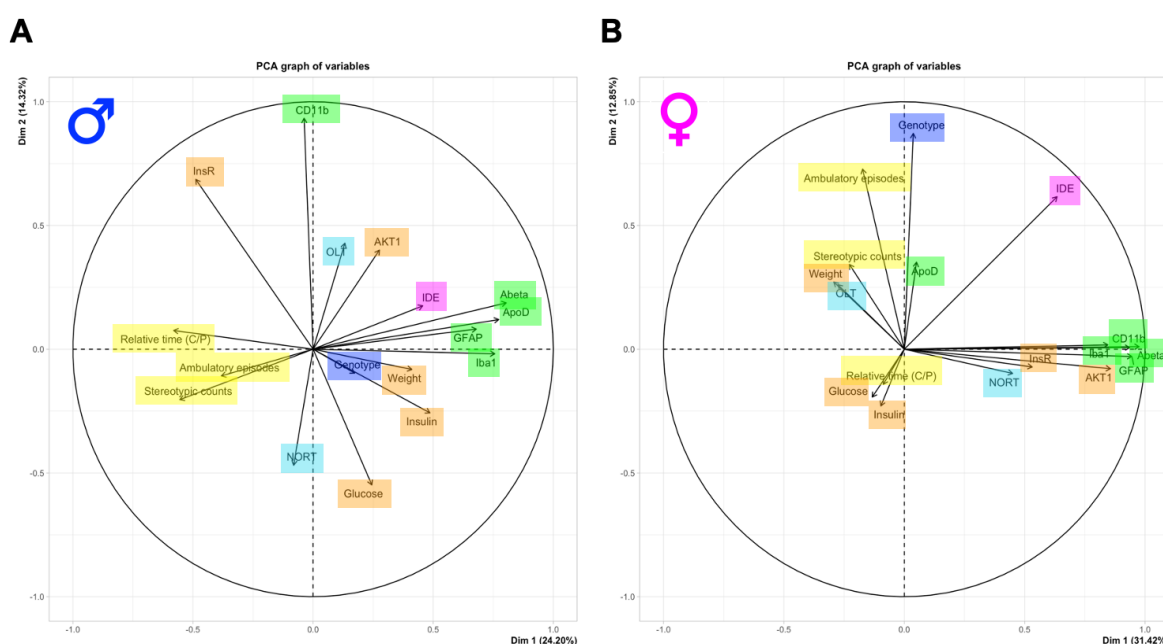


Figure 57. Principal Component Analyses of the IDE-Null cohort, separated by sex. A) PCA analysis in males: 38.52% of total variance explained (24.20% by Dimension 1 and 14.32% by Dimension 2). **B)** PCA analysis in females: 44.27% of total variance explained (31.42% by Dimension 1 and 12.85% by Dimension 2). Variables are highlighted as follows: OF in yellow, behavioral tests in pale blue, metabolic parameters in orange, inflammaging-related markers in green, categorical variables in dark blue, and IDE in pink.

We further assessed whether the PCA-selected variables were able to significantly differentiate mice by their genotype. For that purpose, a multinomial logistic regression was used. The WT category was selected as the “reference group”. After screening of the variables, no problems (multicollinearity, missing data) appeared to be present. The goodness of fit was checked by the Hosmer-Lemeshow test ($X^2 = 3.7$, degrees of freedom = 14, p-value = 0.997). **Table 14** contains the

parameter estimates for both IDE-HET and IDE-KO equations. When classifying the difference between WT and IDE-HET, relative time center/periphery, OLT performance, weight, blood glucose and GFAP levels were significant. When predicting the IDE-KO genotype, sex, relative time center/periphery, OLT and NORT, weight, plasma insulin and IDE levels turned out to be significant.

Table 14. Multinomial logistic regression model. WT genotype was set as the reference category. Predictors for the classification of genotype are shown with their coefficients and statistical significance. Residual deviance: 28.52. AIC: 100.52 (*, $p < 0.05$; **, $p < 0.01$; ***, $p < 0.001$)

	Variable	Coefficient	P-value	Significance
IDE-HET	(Intercept)	53.60	0.000	***
	Sex (F)	0.53	0.813	
	Ambulatory episodes	-0.08	0.265	
	Stereotypic counts	-0.02	0.223	
	Relative time (C/P)	-17.01	0.000	***
	OLT	-15.32	0.000	***
	NORT	-1.56	0.690	
	Weight	-0.77	0.000	***
	Blood glucose	-0.07	0.047	*
	Plasma insulin	-6.94	0.115	
	InsR	0.02	0.386	
	AKT	-0.01	0.761	
	IDE	0.00	0.849	
	CD11b	0.00	0.744	
	Iba1	0.02	0.348	
	GFAP	-0.04	0.049	*
ApoD	-0.03	0.290		
A β	0.05	0.192		
IDE-KO	(Intercept)	-6.43	0.000	***
	Sex (F)	-8.72	0.000	***
	Ambulatory episodes	-0.71	0.186	
	Stereotypic counts	0.14	0.890	
	Relative time (C/P)	-17.73	0.000	***
	OLT	12.15	0.000	***
	NORT	-27.91	0.000	***
	Weight	-1.21	0.045	*
	Blood glucose	0.28	0.873	
	Plasma insulin	-8.65	0.000	***
	InsR	0.20	0.926	
	AKT	-0.72	0.438	
	IDE	-1.50	0.046	*
	CD11b	0.11	0.967	
	Iba1	-0.04	0.971	
	GFAP	0.12	0.959	
ApoD	0.47	0.766		
A β	0.26	0.868		

Overall, the model was predictive of the group classification: the model correctly classified 86.7% of mice, with 100% of IDE-KO mice being classified correctly, while the success rate for both WT and IDE-HET groups was 80%, with a global misclassification error of 13.3% (**Figure 58**).

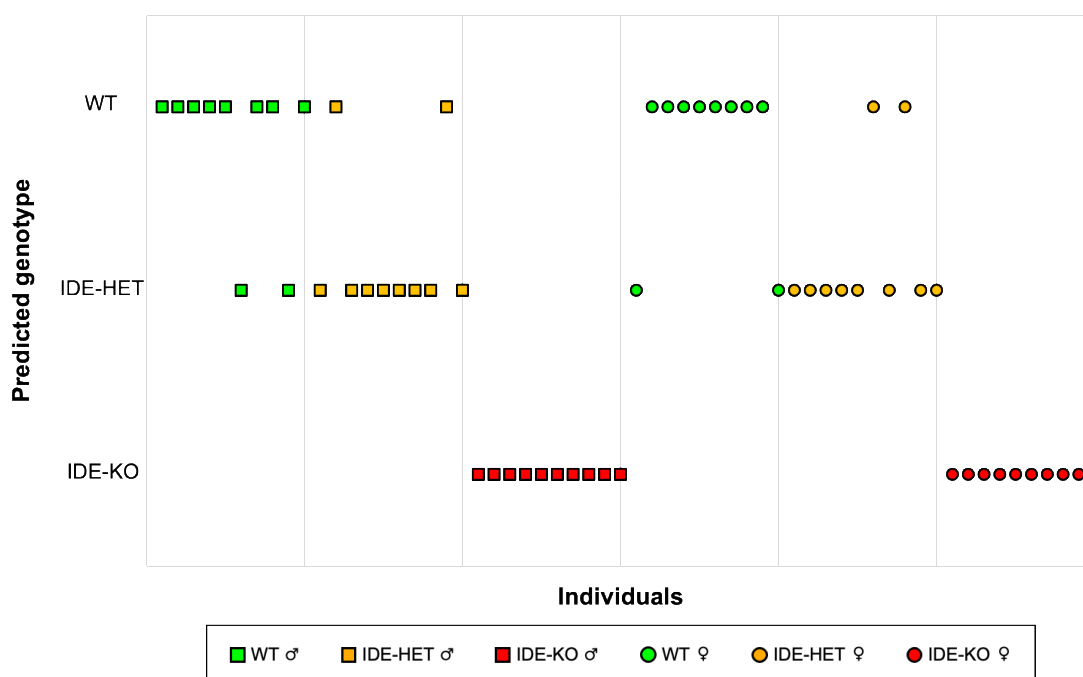


Figure 58. Multinomial logistic regression model results. Predicted genotype for each individual mouse by applying the regression model generated. The success rate for the model was 86.7%. Note that 100% of IDE-KO mice are classified correctly.

In summary, individual analyses of behavioral, metabolic, and molecular parameters revealed that the main differences between mice were not genotype-dependent, but sex-related instead. Insulin signaling proteins were significantly downregulated in the olfactory bulb of female mice, while gliosis markers were found to be upregulated in females. Due to the small sample size ($N = 10$ mice per group), the analysis of individual variables has a relatively low statistical power, that is, it must be emphasized that some significant differences might have emerged simply from random variation within the small samples. Interestingly, the multivariate analysis, where the meaning and relationships between variables are blind to the workflow, produced an unambiguous “barcode” for the IDE-knockout mice, able to correctly classify the individuals in the sample, and disclosing IDE relationship with brain-relevant variables such as “inflammaging” markers, including gliosis markers and A β oligomers.

CHAPTER 4. ROLE OF IDE SPECIFICALLY IN PRIMARY MICROGLIAL CELLS

The previous Chapter revealed some interesting relationships between IDE and brain-related variables *in vivo*, which prompted us to study *in vitro* the role of IDE specifically in microglial cells. *In vitro* research has many advantages over *in vivo* experimentation, such as tight control of the environment and elimination of potential confounding factors. We decided to carry out our experiments in primary microglial cultures from WT and IDE-KO newborn mice to avoid artifacts coming from cell transfections or differential IDE downregulation between experiments.

Since there are no publications in the literature about IDE-KO microglia, we characterized these cells by performing a screening of biological properties starting from cell viability and proliferation, followed by insulin signaling, cell polarization upon different stimuli, myelin phagocytosis and degradation and finally A β managing (endocytosis and degradation). In addition, an RNA-seq characterization was conducted to reveal the main cellular processes affected by the lack of IDE in microglial cells.

4.1. IDE absence slightly affects microglial cell viability

Our first experiments were devoted to evaluate if genetic IDE ablation from microglial cells affects microglial viability. Daily observations of primary WT and IDE-KO microglial cultures indicated that the cell viability was not compromised in IDE-KO microglia; however, we went one step further and assessed microglial viability with and without IDE when cells were exposed to harmful stimuli relevant for microglial function. To that end, we treated primary microglial WT and IDE-KO cultures for 8 hours with 1 μ g/ml LPS, 500 μ M PQ or 4 μ M A β oligomers, and then analyzed cell viability by flow cytometry, using the Live/Dead viability assay (**Figure 59A**). LPS treatment showed similar effects on both cell types, with a slightly higher percentage of cell death in IDE-KO microglia (7.3% vs 4.3% in WT cells, **Figure 59B**). PQ exposure had the greatest effect on reducing survival (**Figure 59C**), with a 13.1% of WT cells dead, while IDE-KO microglia exposed to oxidative stress had a slightly higher mortality (20.9%). Challenge with A β oligomers presented the smallest effect on survival and showed no difference between genotypes (death rates of 5% in WT and 5.1% in IDE-KO microglia, **Figure 59D**).

Collectively, these results indicate no relevant effects of *Ide* gene function on microglial cell viability, although the most toxic stimuli tested (pro-inflammatory and oxidative) showed slightly higher mortality in microglial cells lacking IDE.

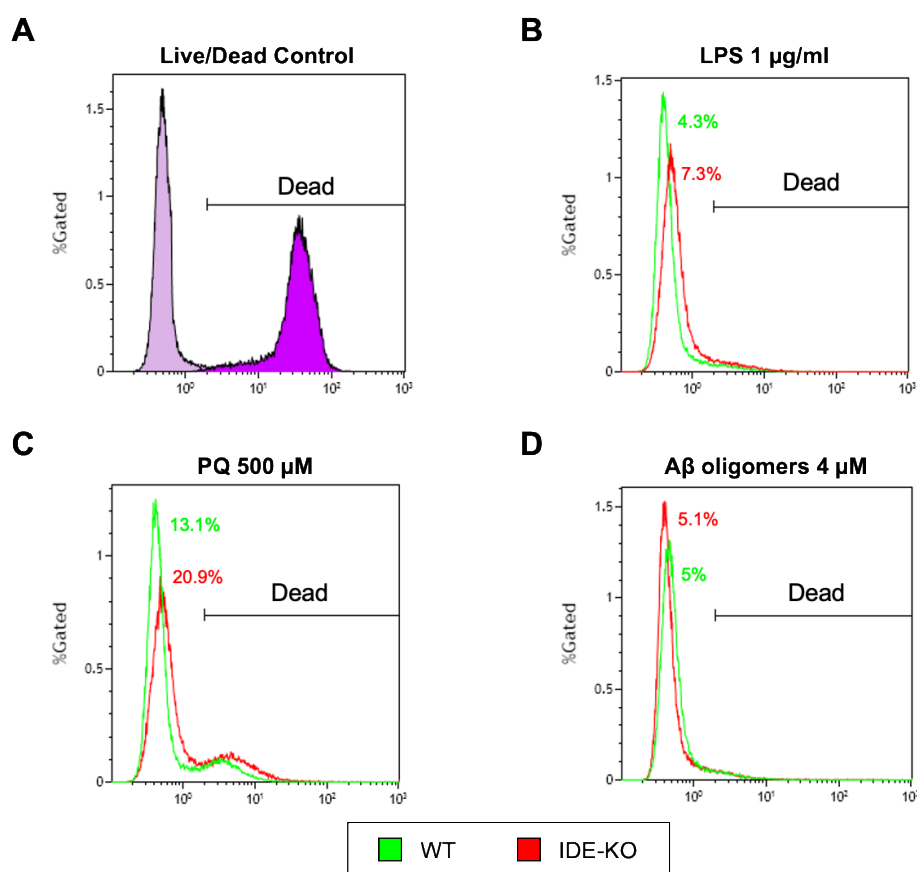


Figure 59. Comparison of cell viability in WT and IDE-KO primary microglia upon different stressful stimuli. Cells were treated for 8 hours with the stimuli and then analyzed by flow cytometry using the Live/Dead cell viability assay kit. **A)** Live/Dead control to select the gate for dead cells. **B)** Microglial cells exposed to 1 $\mu\text{g/ml}$ LPS. **C)** Microglial cells treated with 500 μM PQ. **D)** Microglial cells exposed to 4 μM A β oligomers. At least 50000 cells/condition were analyzed from 2 independent experiments. A representative experiment is shown.

4.2. IDE-KO microglial cells proliferate less and present a delayed response to the cytokine M-CSF

In many neurodegenerative conditions, including AD, microgliosis has been described to be accompanied by a significant increase in the number of microglia present within the brain parenchyma (Gomez-Nicola and Perry, 2015; Olmos-Alonso et al., 2016). Since we found that IDE expression changes along with microglial polarization state (Chapter 1), we hypothesized that IDE absence could result in altered polarization phenotypes and putative impaired microglial proliferation. To address this question, we performed EdU Click-iT assays. Primary microglial cultures were exposed to EdU for 24 and 30 hours in complete medium in the presence or absence of M-CSF, a well-known stimulator of microglial proliferation via CSF1R pathway (Askew and Gomez-Nicola, 2018). At 24 hours, IDE-KO microglia proliferated significantly less than WT cells and, while WT microglia showed an increase in their proliferation when incubated with M-CSF (50 ng/ml), IDE-KO cells were not responsive to this cytokine (**Figure 60A**). At 30 hours WT microglia presented higher proliferation than IDE-KO in control conditions, but interestingly at this time point

IDE-KO microglia showed a significant increase in proliferation in response to M-CSF, almost equalizing the proliferation rates observed in WT cells incubated with this cytokine (**Figure 60B**). Collectively, these results indicate that microglial proliferation is decreased in the absence of IDE, and the putative mechanism for this impairment is a delayed response to M-CSF, a growth factor constitutively expressed by astrocytes and, to a lesser extent, by microglial cells, that selectively promotes microglial division (Lee et al., 1993).

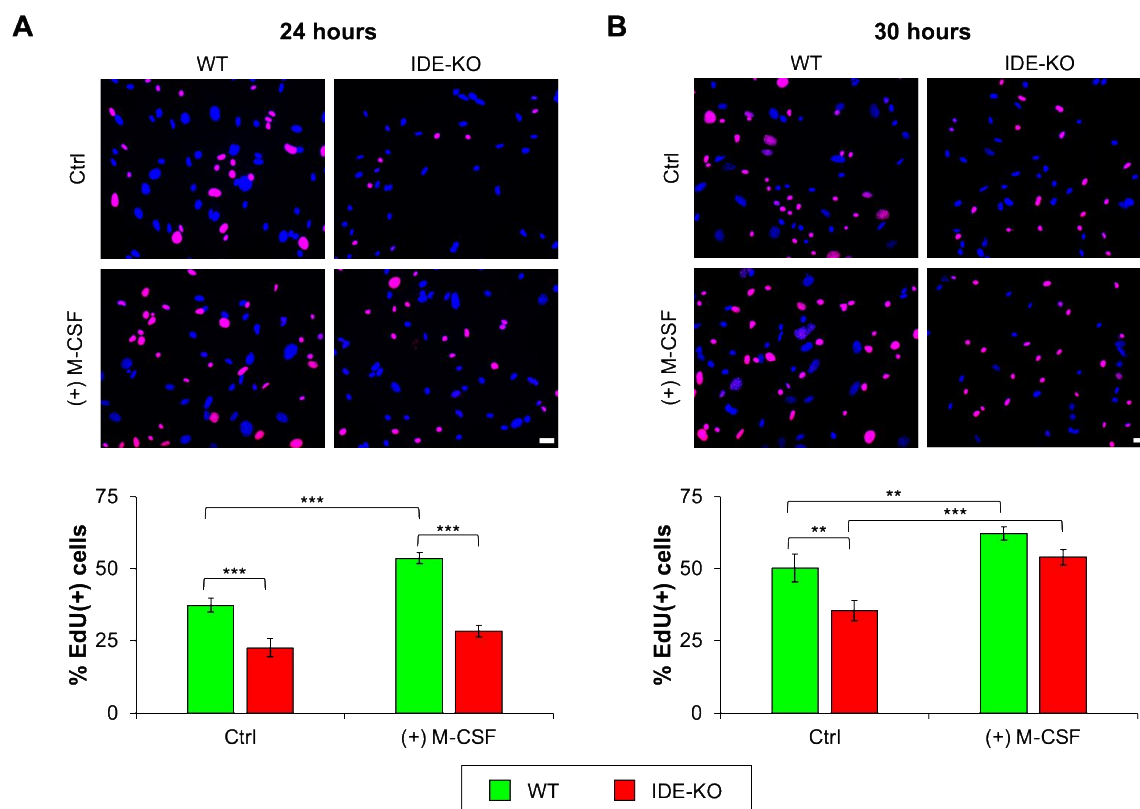


Figure 60. Quantification of cell proliferation in WT and IDE-KO primary microglia by EdU assay. **A)** Proliferation assay at 24 hours. **B)** Proliferation assay at 30 hours. Scale bars: 20 μ m. Statistical differences were evaluated by 2-way ANOVA considering the factors genotype and treatment. Green = WT, Red = IDE-KO. In both temporal points, both factors were statistically significant ($p < 0.001$). Pairwise multiple comparisons were performed using the Holm-Sidak post-hoc test. (** $P < 0.01$, *** $P < 0.001$). $N = 600-1800$ cells/condition.

4.3. IDE does not regulate insulin signaling in microglial cells

In the previous Chapter we described a high expression of insulin receptors in the olfactory bulb, but no effects of IDE partial or total absence were found. However, in those experiments we analyzed all brain cell types, which can have opposite responses that cancel out in the biological homogenate. Thus, we decided to address this question specifically in microglial cells. Although a prominent role of IDE in brain function is universally assumed, very little is known about the effects of insulin and its signaling pathways in microglial cells. To tackle this question, WT and IDE-KO microglial cells were serum starved for 12 hours and then treated with human insulin (500 nM) for different times (5-60 minutes) (**Figure 61A**). Insulin stimulation induced the phosphorylation of both the insulin

receptor and AKT1 in microglial cells in a time-dependent manner, but no significant differences were found between WT and IDE-KO microglia (**Figure 61B**, upper graphs). Moreover, IDE absence did not alter the expression of proteins involved in the insulin signaling, InsR and AKT1 (**Figure 61B**, lower graphs). In addition, IDE protein expression in microglial cells was not regulated by insulin treatment, at least at the dose assayed (**Figure 61C**, left panel). Similarly, the expression of the integrin CD11b, a marker of microglial activation, did not exhibit differences neither between genotypes nor upon insulin treatment (**Figure 61C**, right panel). These results indicate that microglia respond to insulin by activating the insulin signaling pathway, but this activation is independent of IDE, whose expression is not regulated by insulin treatment in microglia.

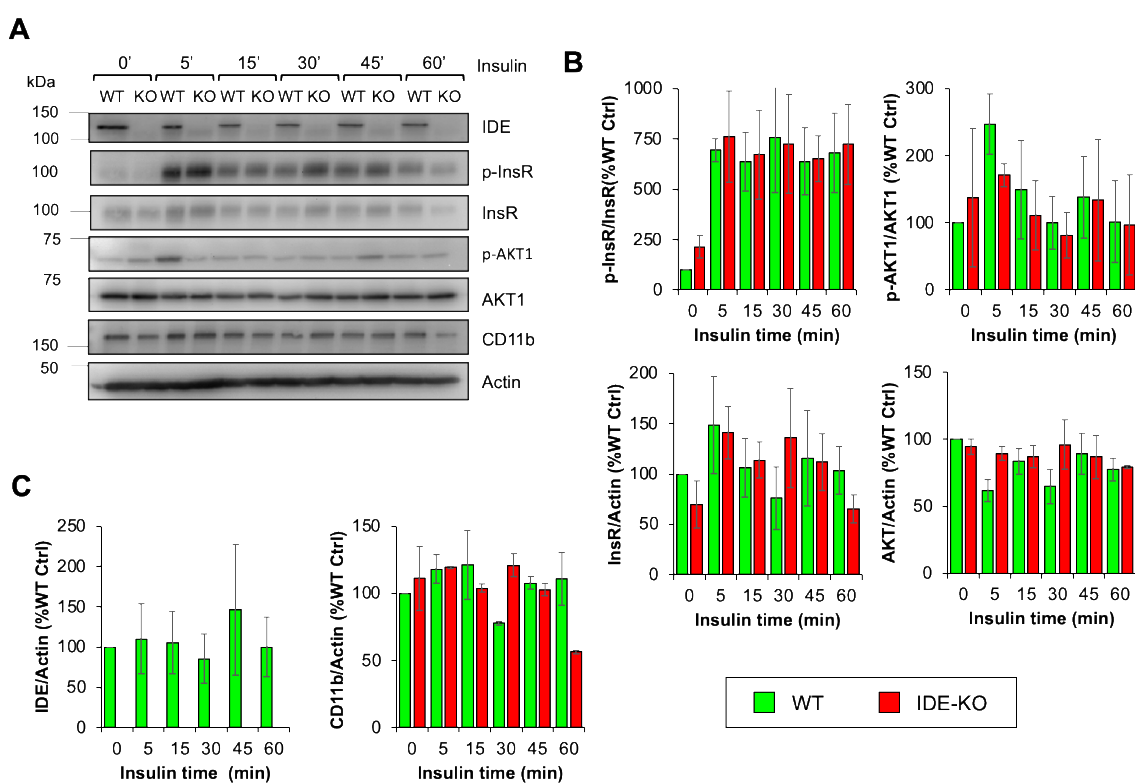


Figure 61. Comparison of insulin signaling in WT vs IDE-KO microglia. **A)** Representative immunoblot of intracellular proteins. **B)** Quantification of proteins involved in the insulin signaling pathway: InsR, AKT and their phosphorylated forms. **C)** Quantification of IDE and CD11b. $N = 3$ independent experiments. Data are presented as mean \pm SEM. Statistical differences were globally assessed by 2-way ANOVA considering the factors genotype and insulin time, followed by post-hoc pairwise comparisons by Holm-Sidak methods. The factor genotype was only significant in IDE ($p < 0.001$).

4.4. Microglial polarization is altered in the absence of IDE

One of our initial hypotheses, supported by the results obtained in Chapter 1 (intracellular IDE protein decreases with LPS and increases with IL-4+IL-13 treatment) and Chapter 2 (IDE exportation is differentially regulated by the polarization state of microglia), was that IDE plays a prominent role in the polarization of microglial cells. We characterized the cytokine production profiles of primary microglia subjected to different stimuli across the microglial polarization axis. To this end, we

analyzed the cytokines released to the extracellular milieu by WT and IDE-KO microglial cells treated with LPS (pro-inflammatory stimuli), IL-4 + IL-13 (anti-inflammatory stimuli), PQ (oxidative stress) and A β oligomers (amyloid stress) for 18 hours. Since sex has been described to play an important role in microglial responses, and we found interesting sex-dependent effects on gliosis (Chapter 3), this study was performed in both male and female microglial cells. The data obtained from the cytokine profiling (Luminex and ELISA assays) are summarized in **Table 15**.

Table 15. Cytokine profiling in WT and IDE-KO primary microglia subjected to different stimuli.

Males ♂										
[pg/ml]	Control		LPS		IL-4+IL-13		PQ		A β	
	WT	IDE-KO	WT	IDE-KO	WT	IDE-KO	WT	IDE-KO	WT	IDE-KO
TNF- α	<0.24	<0.24	308.89±52.01	246.15±14.59	0.70±0.69	4.55±0.79	0.19±0.02	0.94±0.04	<0.24	7.39±1.03
IL-1 β	<23.02	<23.02	207.70±13.65	226.40±36.12	<23.02	<23.02	<23.02	<23.02	<23.02	<23.02
IL-6	<2.52	<2.52	530.04±85.75	595.24±75.64	0.28±0.12	1.82±0.69	<2.522	<2.522	<2.522	4.15±1.30
IL-4	<6.13	<6.13	<6.13	<6.13	299.44±37.90	202.25±21.52	<6.13	<6.13	<6.13	<6.13
IL-10	<1.38	<1.38	8.23±0.98	7.37±1.73	0.30±0.06	0.28±0.07	<1.38	<1.38	<1.38	<1.38
TGF- β	54.72±9.32	60.13±11.08	75.51±4.29	77.01±2.58	76.96±12.16	78.27±6.67	29.03±3.48	13.81±1.05	75.51±4.29	80.99±4.58

Females ♀										
[pg/ml]	Control		LPS		IL-4+IL-13		PQ		A β	
	WT	IDE-KO	WT	IDE-KO	WT	IDE-KO	WT	IDE-KO	WT	IDE-KO
TNF- α	<0.24	<0.24	269.46±19.10	235.18±27.44	<0.24	2.38±1.04	0.17±0.10	0.53±0.13	<0.24	0.53±0.10
IL-1 β	<23.02	<23.02	165.10±18.78	198.61±84.58	<23.02	<23.02	<23.02	<23.02	<23.02	<23.02
IL-6	<2.52	<2.52	609.54±66.94	640.37±96.98	0.10±0.04	0.50±0.18	<2.52	<2.52	<2.52	<2.52
IL-4	<6.13	<6.13	<6.13	<6.13	353.96±14.17	252.44±27.61	<6.13	3.52±1.17	<6.13	<6.13
IL-10	<1.38	<1.38	5.72±0.46	6.76±0.09	0.13±0.04	0.13±0.04	<1.38	2.73±0.91	<1.38	<1.38
TGF- β	45.35±9.12	55.04±2.83	87.89±2.54	82.87±5.34	39.39±22.74	78.29±4.31	32.99±7.57	7.54±4.35	89.88±5.04	96.60±4.84

Data expressed as mean \pm SEM between three biological samples. Statistical differences were globally analyzed by 3-way ANOVA (factors: genotype, sex and treatment) and then individually for each sex by 2-way ANOVA. Pairwise comparisons were performed using a Holm-Sidak test. Significant genotype-dependent differences are highlighted with bold letters.

To obtain an overview about the responses of each genotype and sex to each treatment, a heatmap was constructed (**Figure 62**). The uppermost differences are observed in microglia treated with pro-/anti-inflammatory stimuli, which produced strong responses. Oxidative and amyloid treatments triggered responses with a significantly lower cytokine production, that cannot be appreciated in the global heatmap. However, unsupervised hierarchical clustering of the experimental groups produced very consistent results. Anti-inflammatory cytokines IL-4 and TGF- β are grouped together in a separated cluster from the pro-inflammatory cytokines IL-1 β , IL-6 and TNF- α , whereas IL-10 is the only ungrouped cytokine, probably because of its mild induction upon LPS treatment and its unexpected absence under IL-4+IL-13 exposure. Attending to experimental groups, the clustering algorithm correctly grouped all samples by treatment (**Figure 62**).

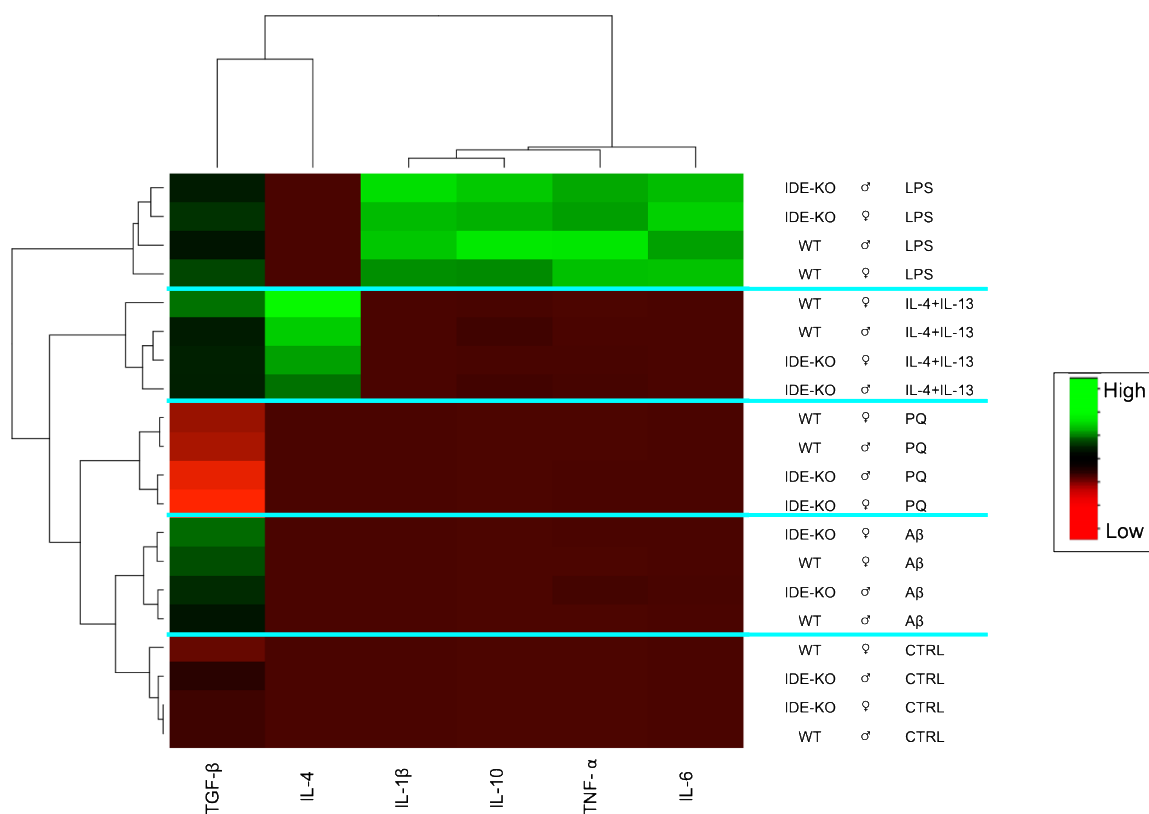


Figure 62. Heatmap showing the results of the cytokine profiling. Each row represents a group, composed by three independent biological samples. Blind classifications of samples and cytokines by unsupervised hierarchical clustering, represented by dendrograms, determine the order of rows and columns shown.

To facilitate interpretation, cytokine profiling results are divided into pro-/anti-inflammatory treatments (**Figure 63A**) and oxidative and amyloid stresses (**Figure 63B**). IL-6 was overexpressed upon LPS treatment, with no significant changes between genotype or sex. IL-4 was highly expressed after IL-4+IL-13 treatment and was higher in WT than in IDE-KO, and greater in females than in males. IL-10 was only expressed upon LPS treatment (mild expression in comparison with other cytokines, as shown in **Table 15**), and surprisingly absent when cells were exposed to IL-4+IL-13. TGF- β was overexpressed in both LPS and IL-4+IL-13 treatments in comparison to control conditions, and was higher in females than in males (see **Table 15**). IL-1 β and TNF- α were both significantly expressed after LPS treatment, and were higher in males than in females (**Figure 63A**).

PQ-induced oxidative stress significantly diminished TGF- β in both sexes, being this decrease greater in IDE-KO than in WT microglia, and associated with a mild production of TNF- α by IDE-KO cells (**Table 15** and **Figure 63B**). Finally, A β oligomer treatment produced an overexpression of TNF- α and IL-6 specifically in IDE-KO male microglia, while TGF- β was upregulated in both genotypes, and was slightly higher in females than in males (**Table 15** and **Figure 63B**).

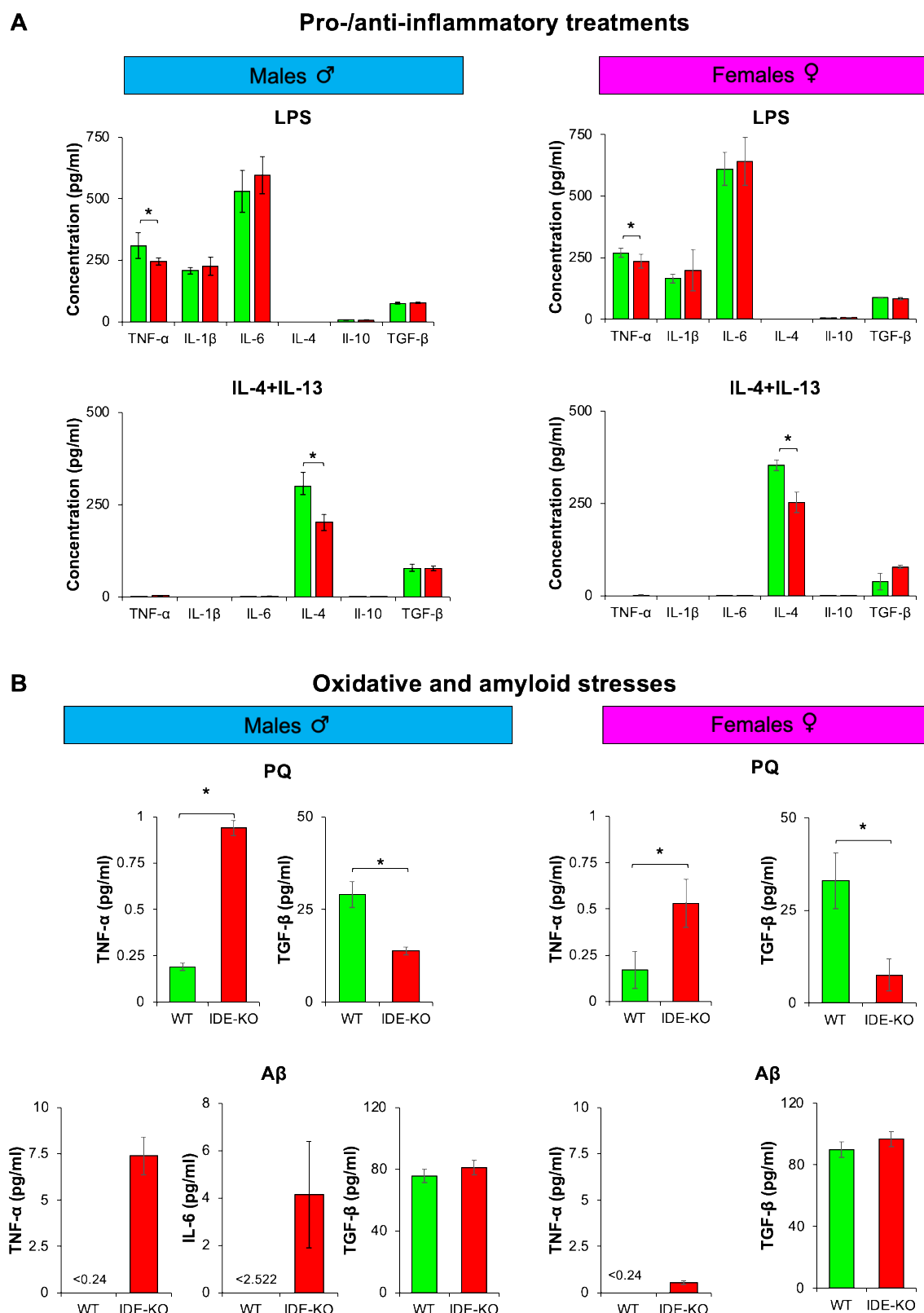


Figure 63. Cytokine profiles separated into pro-/anti-inflammatory treatments and oxidative and amyloid stresses. A) Pro-/anti-inflammatory treatments. B) Oxidative and amyloid stresses (only cytokines above detection levels are shown). Statistical differences were globally analyzed by 3-way ANOVA (factors: genotype, sex and treatment) and then individually for each sex by 2-way ANOVA. Pairwise comparisons were performed using a Holm-Sidak test. (*, $p < 0.05$).

In summary, WT microglia responded to LPS by producing significantly higher amounts of TNF- α than IDE-KO microglia. On the contrary, IDE-KO microglia produced significantly lower IL-4 than WT microglia when stimulated with IL-4+IL-13 (**Table 15**). Collectively, these results suggest that IDE-KO microglial cells exhibit impaired polarization under inflammatory stimuli, producing an attenuated response to both pro- and anti-inflammatory stimulation. Regarding oxidative and amyloid treatments, only TNF- α and TGF- β were detected, while the remaining cytokines were below detection levels. PQ-induced oxidative stress led to significantly higher levels of TNF- α and reduced amount of TGF- β in IDE-KO microglia in both sexes. Remarkably, A β oligomer treatment triggered the production of TNF- α and IL-6 specifically in IDE-KO male microglia, while TGF- β remained unchanged (**Table 15**). These results indicate a more pro-inflammatory response to oxidative stress in IDE-KO microglia, which might be more sensitive to this type of stress, and a sex-specific pro-inflammatory response to A β oligomers.

4.5. Myelin phagocytosis by microglial cells shows sex- and IDE-dependent effects, while myelin degradation remains unaltered

Microglia are brain professional phagocytes that play several critical roles in the CNS, such as the engulfment of dying cells and the removal of myelin debris generated upon injury or degenerating conditions, to prevent inflammation. Myelin phagocytosis and clearance were studied in WT and IDE-KO male and female microglia by flow cytometry, using murine myelin labeled with the fluorophore DiI.

We first performed a time-course quantitative assessment of the process of phagocytosis, exposing microglial cells to myelin-DiI for a range of times between 3 and 24 hours, and analyzing the mean fluorescence intensity (MFI) for each sample. Myelin phagocytosis showed sex-dependent effects: male IDE-KO microglia showed lower myelin phagocytosis than WT microglia at any time explored, while in female microglia the phagocytosis was higher in IDE-KO than in WT cells at 3 hours, though this difference disappeared at longer times of myelin exposure (**Figure 64A**). Myelin degradation (after a 3 hour-phagocytosis period), however, was exactly the same in male microglia, while IDE-KO females showed higher myelin levels at 3 hours of degradation, probably attributable to their increased phagocytosis. However, myelin degradation did not show differences between genotypes in subsequent times (**Figure 64B**).

Collectively, these data indicate that IDE affects in a sex-dependent way the time-course of myelin phagocytosis, without changes in the myelin degradation process.

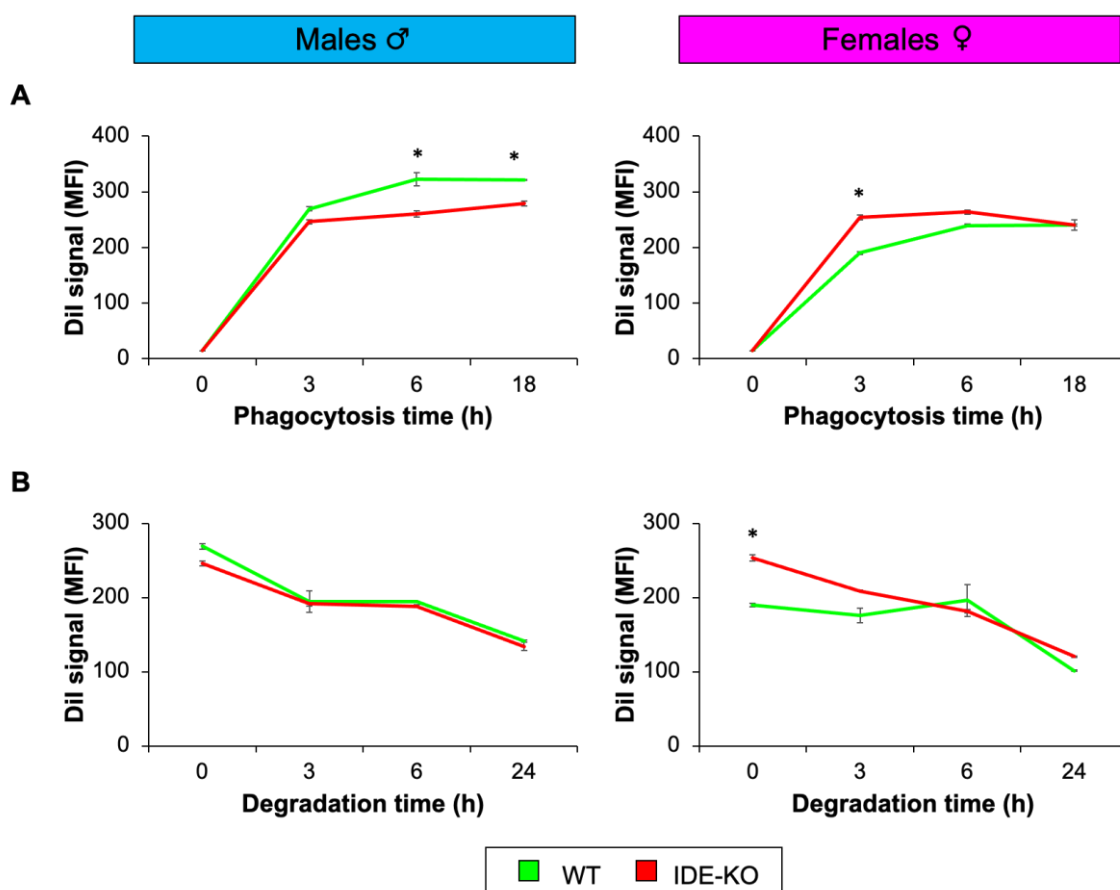


Figure 64. Myelin-DiI phagocytosis and degradation in WT and IDE-KO microglia. **A)** Myelin phagocytosis. **B)** Myelin degradation. Data are presented as mean \pm SEM between two biological samples. Significant differences were analyzed by three-way ANOVA considering the factors genotype, sex and time, followed by post-hoc Holm-Sidak comparisons. Phagocytosis: genotype $p=0.31$, sex $p<0.001$, time $p=0.002$; interaction genotype-sex $p<0.001$. Degradation: genotype $p=0.32$, sex $p=0.04$, time $p<0.001$; interaction genotype-sex $p=0.032$. (*, $p<0.05$).

4.6. Lack of IDE alters A β oligomer internalization dynamics and impairs A β oligomer degradation in male microglia

One of the uppermost functions for microglial cells is the clearance of pathological protein aggregates such as the A β peptides. Controlling brain proteostasis is a two-step process that starts with the internalization of soluble A β oligomers and finishes with the subsequent degradation of such species (Ries and Sastre, 2016). However, there should be a delicate balance between A β internalization by microglial cells, the pro-/anti-inflammatory responses triggered by this process, and the efficient removal of A β to achieve amyloid clearance without producing undesired neurotoxic effects. Due to the sex-differential responses observed in the cytokine profile, these experiments were done in male microglia.

A β internalization experiments were performed by exposing primary WT and IDE-KO microglial cultures to FAM-A β oligomers (1 μ M) for a range of times between 0.5-3 hours, and then analyzing the cells by flow cytometry. Remarkably, IDE-KO microglia showed a transitory accelerated

FAM-A β internalization in comparison to WT microglia, reflected by a higher percentage of FAM-A β positive cells (**Figure 65A**). However, the MFI remained unchanged between genotypes across all the experiment (**Figure 65B**). Some representative plots of this experiment are shown at **Figure 65C**. These results suggest that IDE absence in microglia results in an alteration of A β oligomers internalization dynamics, with a transitory accelerated A β internalization, without affecting the net amount of A β internalized in comparison with WT cells.

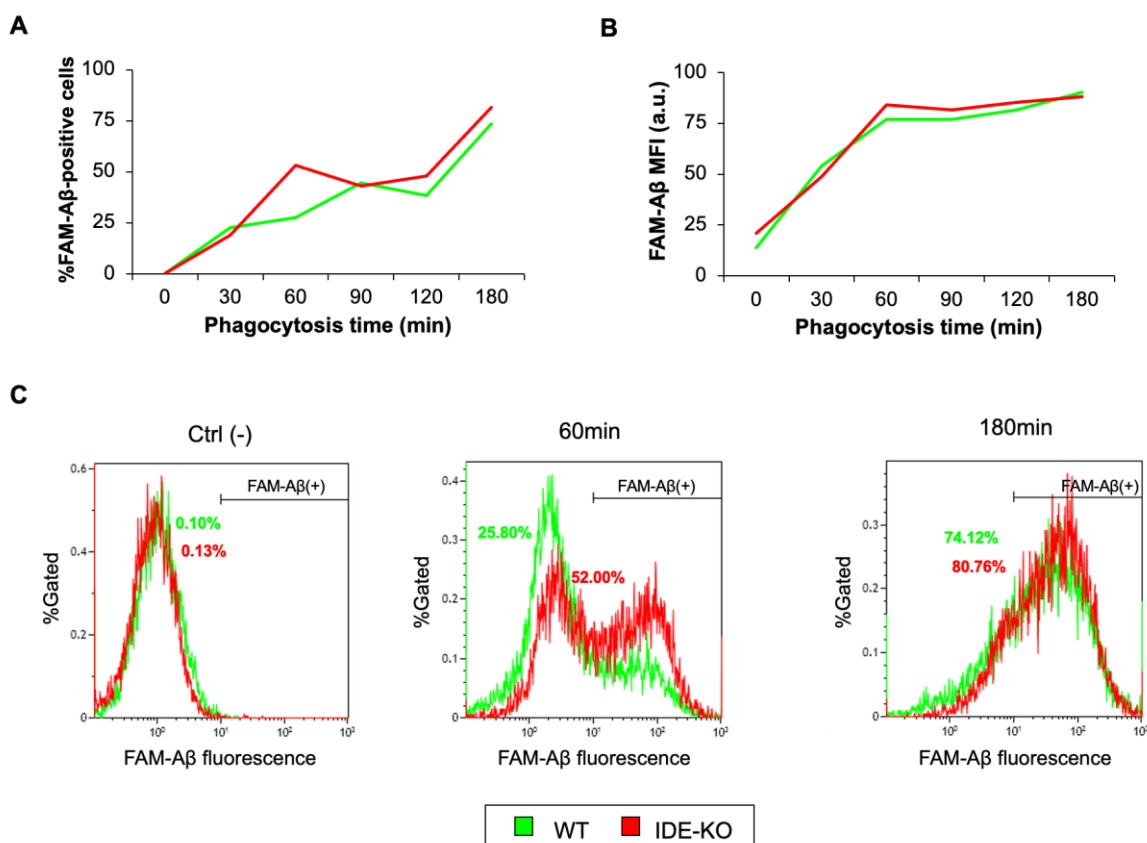


Figure 65. FAM-A β oligomers internalization in WT and IDE-KO microglia. **A)** Percentage of FAM-A β positive cells during different time points (0-180 minutes). **B)** Mean Fluorescence Intensity of the cells analyzed in (A). **C)** Representative plots showing different time points of the experiment: the negative control to select the gate, 60 minutes (where the percentage of FAM-A β positive cells is significantly higher in IDE-KO than in WT microglia), and 180 minutes, the final point of this experiment. $N = 2$ independent experiments; a representative one is shown.

The A β degradation experiments were performed after a 3-hour exposure to FAM-A β oligomers. Many temporal points, ranging from 1 to 24 hours, were explored. After 3 hours, the majority of cells were positive for FAM-A β (90.4% WT and 95.9% IDE-KO). During the first 8 hours of A β degradation, the percentage of positive cells kept quite high and showed oscillations from one temporal point to another, while at 16 and 24 hours there was a significant decrease (**Figure 66A**). Attending to the MFI for each sample, there was an increase in the A β signal during the first hour of degradation, which could be attributable to remaining FAM-A β traces or to the internalization of FAM-A β -overloaded dying cells by other alive cells. Except this temporal point, which represented

the peak of FAM-A β fluorescence, during the following degradation hours a decreased in FAM-A β fluorescence was observed, as expected. In all the time points analyzed, IDE-KO microglial cells showed higher FAM-A β content than WT cells, indicating an impairment in A β oligomers degradation in IDE-KO microglia (**Figure 66B**). Some representative plots are shown in **Figure 66C**.

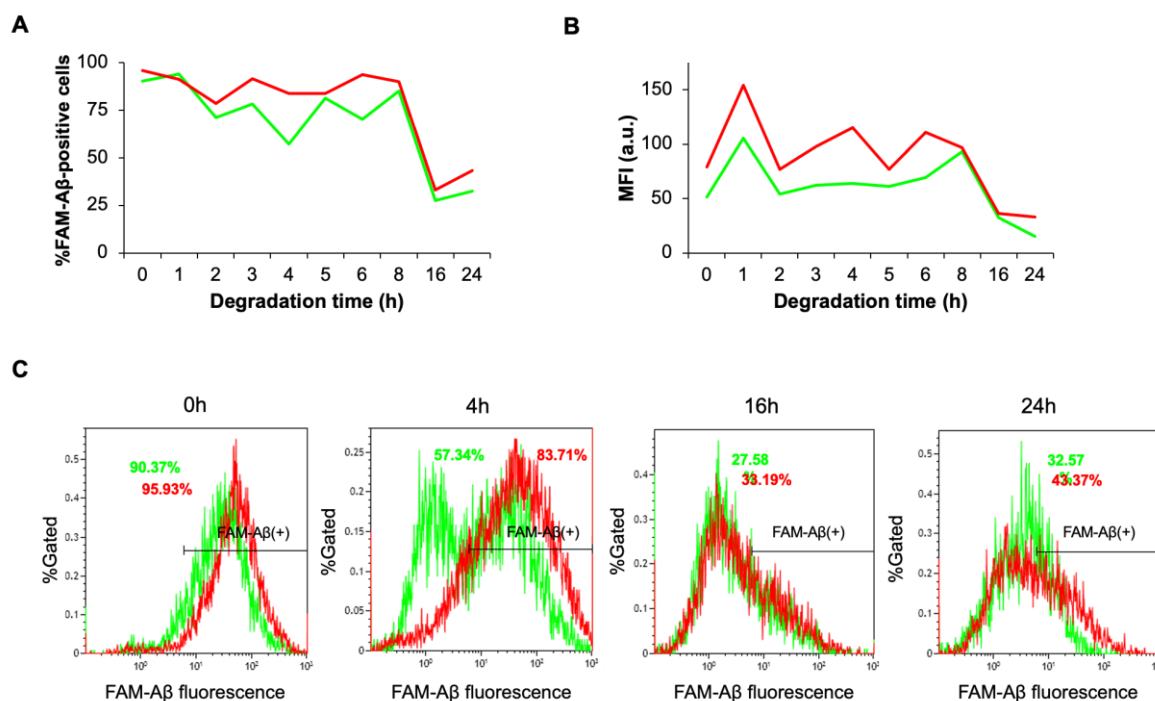


Figure 66. FAM-A β oligomers degradation in WT and IDE-KO microglia. **A)** Percentage of FAM-A β positive cells during different time points. **B)** Mean Fluorescence Intensity of the cells analyzed in (A). **C)** Representative plots showing different time points of the experiment. $N = 2$ independent experiments; a representative one is shown.

4.7. Transcriptomic analyses reveal that absence of *Ide* alters pathways such as response to cytokines, immune system processes and regulation of response to stress

To understand the impact of *Ide* absence on microglial phenotype, we compared the transcriptomic profile of WT and IDE-KO microglia by RNA-seq (**Figure 67A**). We identified a total of 430 differentially expressed genes (DEGs): 249 genes were upregulated, and 181 genes were downregulated in IDE-KO microglia in comparison with WT microglia ($FDR < 0.05$). A complete list of DEGs can be found in the Annex section (**Tables A2** and **A3**). For all subsequent comparisons, we considered as DEGs those with an absolute \log_2 fold change (FC) equal to or greater than 1 ($\log_2 FC \geq 1$; two-fold change), with resulted in 103 DEGs (59 upregulated and 44 downregulated genes in IDE-KO vs WT microglia, as shown in **Figure 67B**). From the upregulated genes with an assigned function on “MouseMine” database (MGI), the largest differences were observed for *Slfn1* (negative regulator of G1/S transition of mitotic cell cycle) and the chemokines *Ccl7* (involved in several responses to cytokine stimulus and chemotaxis) and *Ccl5* (involved in negative regulation of apoptotic processes, positive regulation of chemotaxis and response to TNF). Regarding to

downregulated genes, the largest differences were observed for *Rps19* (involved in the Notch signaling pathway), *Atp6v1d* (part of the proton-transporting V-type ATPase complex, involved in cilium assembly) and *Chchd2* (involved in cellular response to oxidative stress).

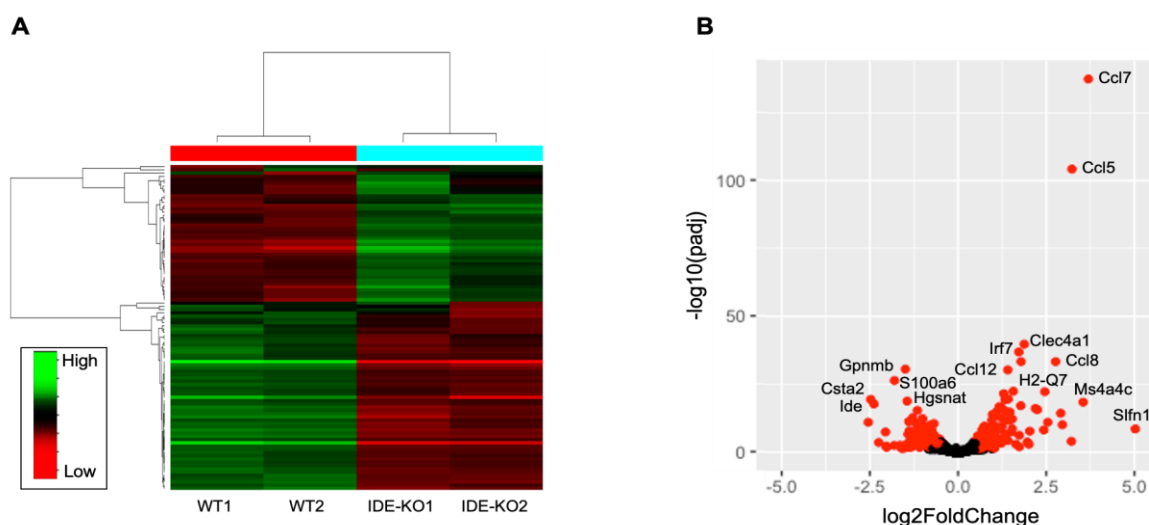


Figure 67. Transcriptomic profiling of WT and IDE-KO microglia. **A)** Heatmap representation of the top 100 differentially expressed genes in IDE-KO vs WT microglia. Clustering of genes by expression profile is shown on the left. **B)** Volcano plot showing in red the genes that are differentially expressed ($FDR < 0.05$) with an absolute \log_2 fold-change equal to or greater than 1 (2-fold change).

To delve into the biological meaning of the set of DEGs between genotypes, a gene set enrichment analysis was performed (**Figure 68A**). The main biological processes affected were related to: defense response (GO:0006952) and regulation of defense response (GO:0031347); response to cytokines (GO:0034097 and GO:0071345) and regulation of cytokine production (GO:0001817); immune response (GO:0006955), innate immune response (GO:0045087) and immune system processes (GO:0002376); response to external (GO:0009605) and biotic stimulus (GO:0009607) and response to stress (GO:0006950); and inflammatory responses (GO:0006954) and regulation to inflammatory responses (GO:0050727), among others. These results are in concert with our previous data that link IDE with microglial polarization and their response to external stimuli. Then, we analyzed separately upregulated and downregulated genes. The set of upregulated genes in IDE-KO microglia are involved in defense and immune responses, involving chemokine, TNF and TLR signaling pathways (**Figure 68B**). On the other hand, downregulated genes in the IDE-KO microglia are mainly involved in regulation of cell adhesion, apoptotic clearance and regulation of inflammatory response and response to stress (**Figure 68C**).

Overall, transcriptomic profiling strongly supports the data presented in this Chapter, and suggests relevant roles for IDE in microglial physiology, such as regulation of immune response, response to stimuli and stress and, ultimately, microglial activation phenotypes.

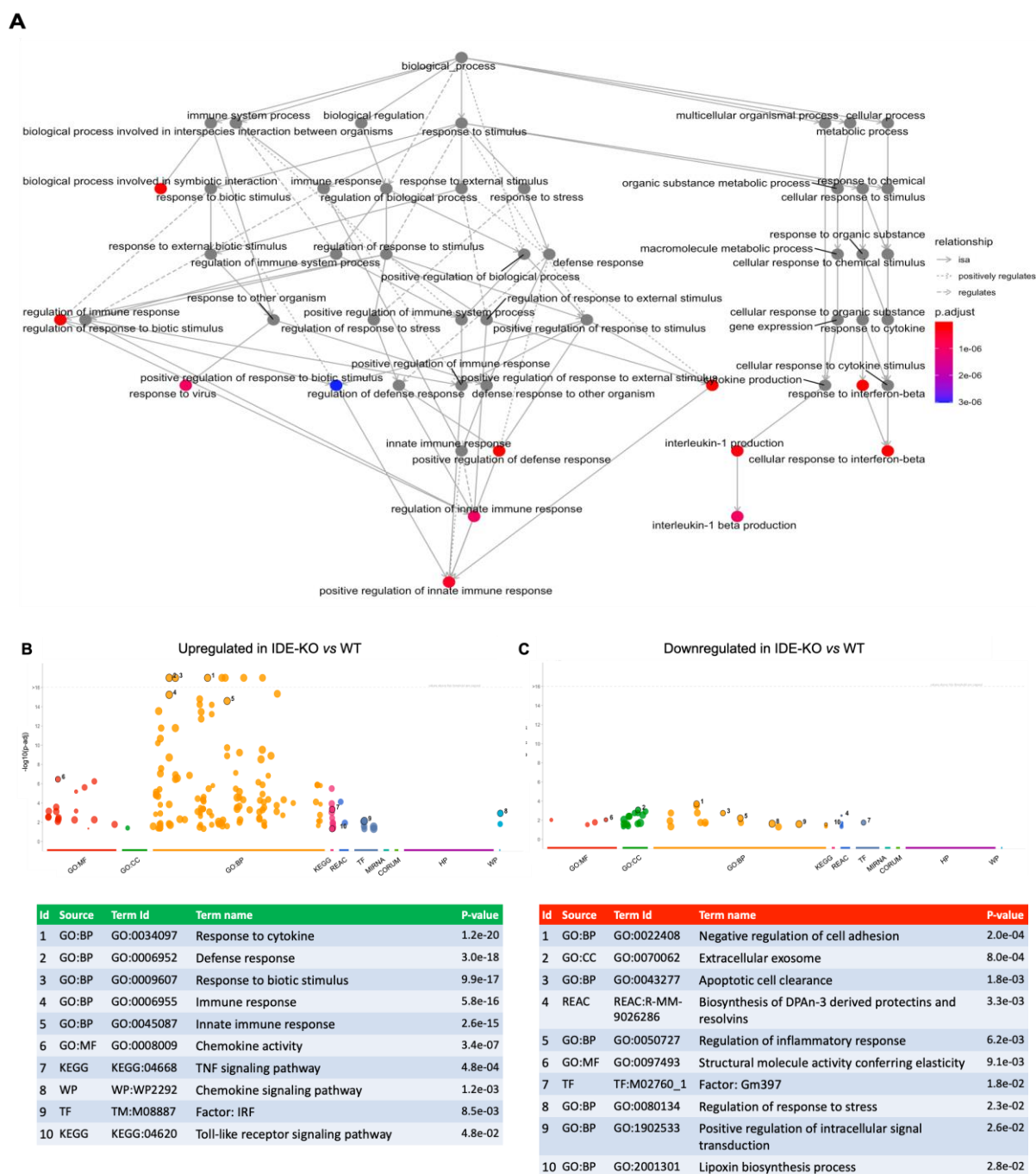


Figure 68. Gene enrichment analysis on differentially expressed genes between WT and IDE-KO microglia. A) GO acyclic graph showing the relationships between the most significant GO terms. B-C) Manhattan plots illustrating the enrichment analyses results separated by fold-change. The x-axis represents functional terms that are grouped by data sources, while the y-axis shows the adjusted enrichment p-values in negative log10 scale. The circle sizes are in accordance with the corresponding term size. Data sources: GO = Gene Ontology, it has three major categories: MF = Molecular Functions, BP = Biological Process, and CC = Cell Component, describes in which part of the cell the particular gene product is physically located; biological pathway databases: includes Reactome, KEGG and WikiPathways; regulatory motifs in DNA: TF = Transcription Factors; micro-RNAs (MIRNA), and protein databases: CORUM and HP = Human Protein Atlas.

CHAPTER 5. NOVEL THERAPEUTICS FOR NEURODEGENERATIVE PROCESSES: MODULATION OF GLIAL RESPONSES BY FURANOCEMBRANOLIDES

The “neurocentric” approach to treat neurodegenerative diseases has dominated the research focus for many years, with great efforts to develop drugs to avoid neuronal death. Nevertheless, with the increasing knowledge about glial cells, it is becoming evident that controlling inflammation within the brain requires the study of glia, and the functional state of glial cells must always be considered when developing immunomodulatory therapies for CNS diseases. Microglia, which play a prominent role in brain inflammation, are crucial mediators for the neurodegenerative process. Inspired by the need of developing new “gliocentric” therapies against neuroinflammation, we explored the potential effects of furanocembranolides as modulators of microglial responses *in vitro*, and then assessed the anti-glioinflammatory effects of one of these products *in vivo*, in a mouse model of high-fat diet-induced obesity and insulin resistance.

Our results reveal a promising direct biological effect of furanocembranolides on microglial cells as bioactive anti-inflammatory molecules. Among them, leptolide provides us a feasible therapeutic approach to treat neuroinflammation concomitant with metabolic impairment.

5.1. *In vitro* screening of furanocembranolides with anti-inflammatory properties on microglial cells

Seven furanocembranolides recently characterized by Dr. Mercedes Cueto’s group (**Figure 12**) were screened *in vitro* by measuring their ability to modulate interleukin-1 β (IL-1 β) production by microglial BV-2 cells after LPS stimulation.

Microglial cells were treated with the carrier (DMSO), the furanocembranolide alone, or with LPS simultaneously with either the carrier or the furanocembranolide (**Figure 69A**). First, we assessed the effects of these treatments on microglial viability by using the MTT assay. Among all the furanocembranolides tested in this study, only leptolide increased microglial viability (around 28%), while the other compounds did not have significant effects on cell viability. LPS treatments significantly decreased BV-2 viability, as expected, with no differences among compounds or carrier alone (**Figure 69B**).

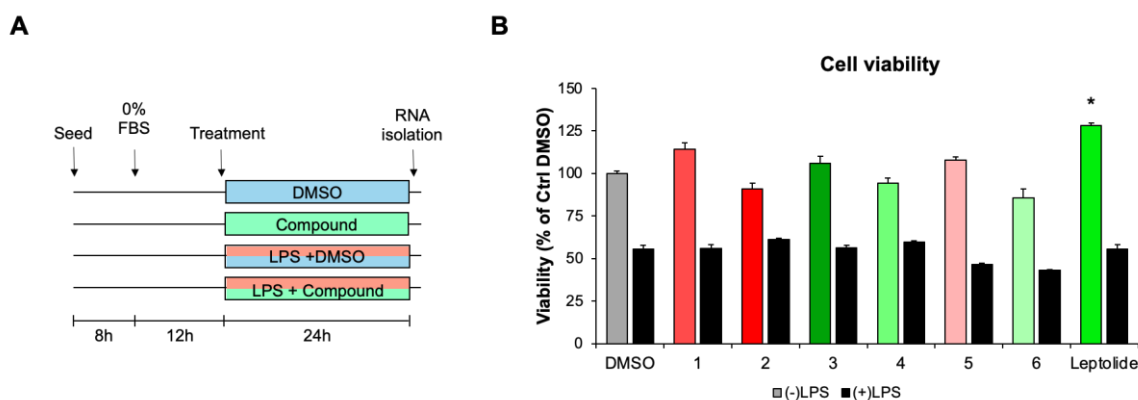


Figure 69. Furanocembranolide treatments and effects on BV-2 viability. **A)** Schematic representation of treatments with furanocembranolides performed on BV-2 microglial cells. **B)** MTT colorimetric assay to assess cell viability in BV-2 cells treated with the furanocembranolide alone (colored bars) and simultaneously with LPS and the furanocembranolide (black bars). Statistical differences were assessed by two-way ANOVA considering the factors compound and treatment, followed by Holm-Sidak pairwise comparisons. (*, $p < 0.05$).

Then, we examined whether treatment with furanocembranolides could reduce LPS-stimulated IL-1 β mRNA expression in BV-2 cells. We monitored IL-1 β since this cytokine is an “alarmin” or sentinel that detects cellular damage and acts as an amplifier of immune reactions. LPS stimulation produced a marked increase in IL-1 β expression, as expected (**Figure 70**). In contrast, simultaneous treatment with compound 3 (**Figure 70C**), 4 (**Figure 70D**) and leptolide (**Figure 70G**) caused a marked decrease in IL-1 β mRNA synthesis, while compound 6 (**Figure 70F**) showed a tendency ($p = 0.051$) to diminish inflammation. Compounds 1 (**Figure 70A**) and 5 (**Figure 70E**) had no significant effects, whereas compound 2 had a potent pro-inflammatory effect that exacerbated the LPS-induced inflammatory response (**Figure 70B**). Therefore, it seems that small changes in the functional groups of the furanocembranolide skeleton may have a dramatic effect on the pro- or anti-inflammatory activity, as extensively discussed at (Corraliza-Gómez et al., 2020). Curiously, three of the compounds induced slight but statistically significant changes in IL-1 β mRNA fold regulation in control conditions: compound 2 increased and compound 6 and leptolide decreased IL-1 β expression (**Figure 70H**).

Taken together, our results reveal a promising direct biological effect of furanocembranolides as bioactive modulators of microglial responses.

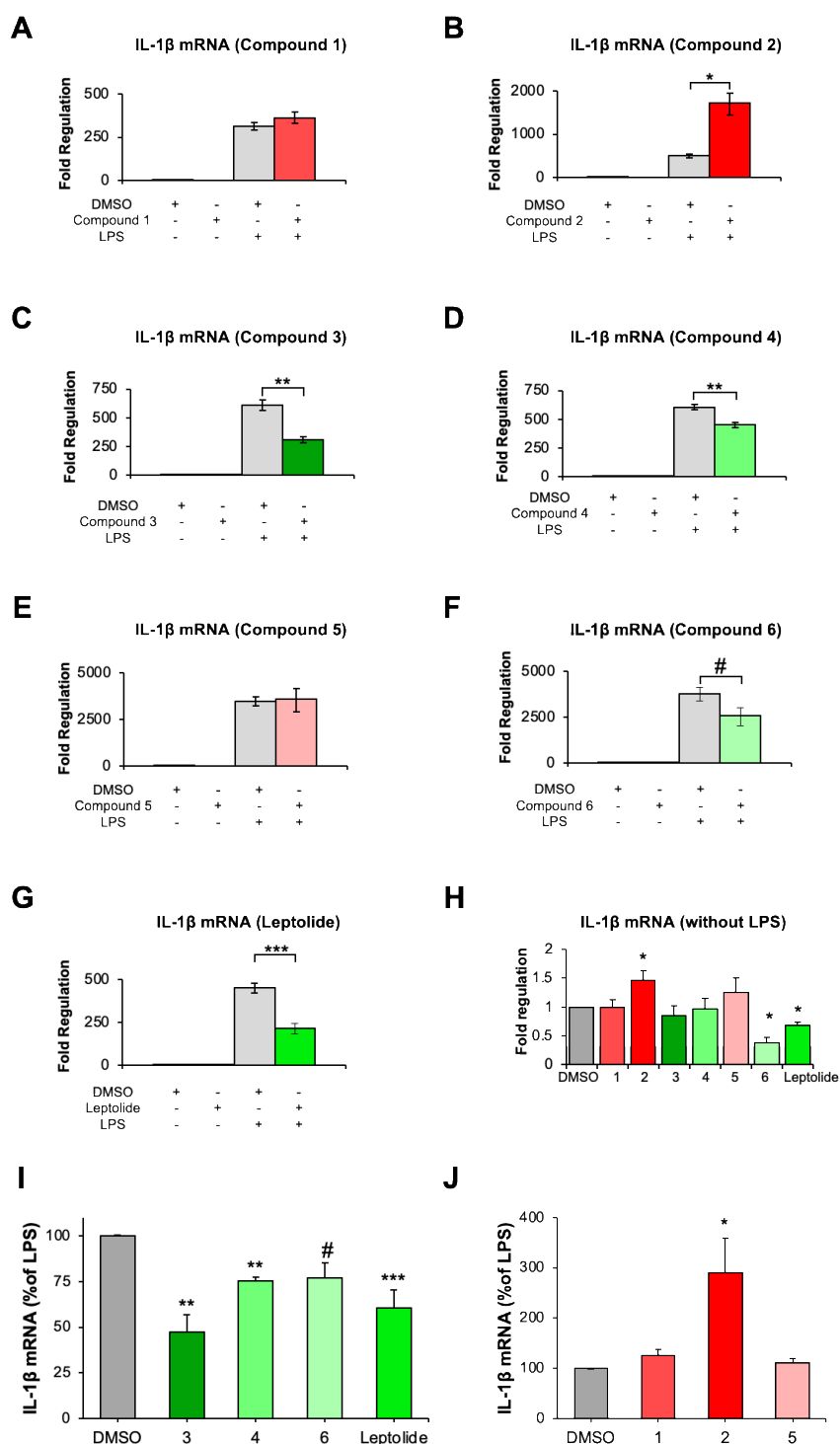


Figure 70. Expression of IL-1 β mRNA in vitro after LPS stimulation and/or furanocembranolide treatment. A-G) Representative experiments showing total fold change of IL-1 β mRNA expression in comparison with basal conditions (vehicle alone). Each bar depicts the mean value between quintuplicate qPCR runs, and error bars represent standard deviation. H) Fold change of IL-1 β mRNA expression BV-2 cells treated with furanocembranolides without LPS. I-J) IL-1 β mRNA fold regulation normalized to the LPS+DMSO response (considered 100%), separated into furanocembranolides that increase (I) or decrease (J) the response. Each bar represents the mean between three independent experiments, and error bars show SEM. Statistical differences were assessed by two-way ANOVA, followed by Holm-Sidak post-hoc tests (* $p < 0.05$, ** $p < 0.01$, *** $p < 0.001$) and by pairwise comparison of raw data by t-test (# $p = 0.051$).

The *in vitro* results prompted us to assess anti-glioinflammatory effects of leptolide *in vivo* in a high-fat diet-induced obese mouse model. Interestingly, leptolide treatment ameliorated both microgliosis and astrogliosis in this animal model.

5.2. Leptolide treatment *in vivo* ameliorates microgliosis in a mouse model of obesity and insulin resistance

High-fat diet (HFD) yielded an increase in Iba1 expression, and leptolide treatment significantly reduced Iba1 in both dentate gyrus and cortex (**Figure 71A**). Moreover, from a qualitative point of view, it was observed that microglial cells from standard diet (SD)-fed mice are smaller and have a branched appearance. This morphology was similar to that attributed to the “resting or surveillant state” of microglia, in comparison with those of control HFD-fed mice. These cells are larger and show a more amoeboid form associated with an activated, more pro-inflammatory state. Interestingly, in HFD-mice treated with leptolide, microglial cells tend to shift morphologically towards a “resting state” (**Figure 71A**), indicating a reversion to healthier conditions.

For statistical analyses, we performed three-way ANOVA considering diet, treatment and brain region as factors. All factors proved to be statistically significant, but neither drug nor diet showed dependence on region. There was a significant interaction between diet and drug ($p=0.005$). Within the SD group, leptolide treatment significantly reduced Iba1 staining below basal levels (SD-vehicle). Interestingly, leptolide treatment of HFD-fed mice resulted in a significant decrease in microgliosis, showing very similar behavior in both brain regions analyzed (**Figure 71B**).

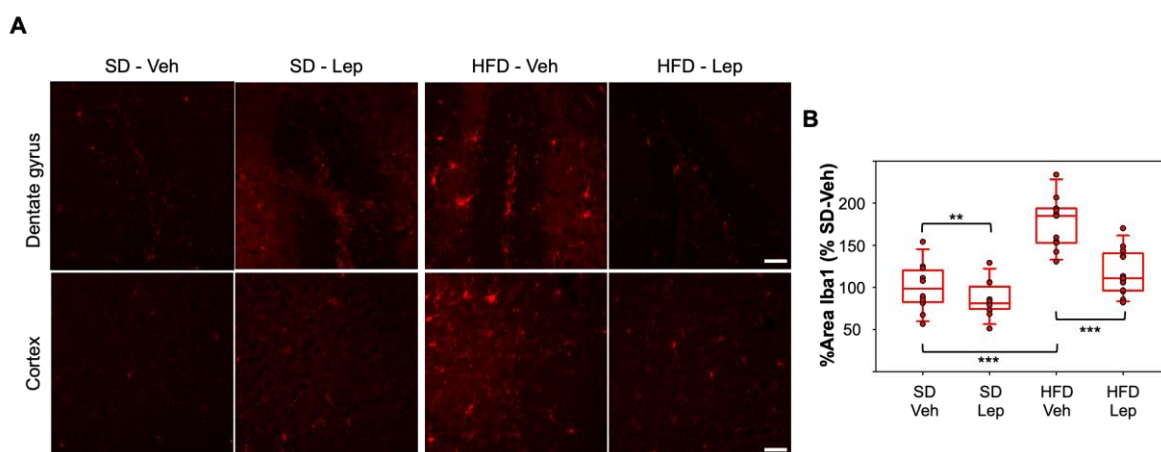


Figure 71. Leptolide treatment ameliorates microgliosis triggered by HFD. **A)** Representative immunofluorescence images from paraffin sections of mouse brains stained with Iba1. Calibration bars: 50 μ m. **B)** Immunohistochemical quantification of Iba1 protein expression, measured as percentage of Iba1-positive area per section, normalized to SD-Veh, considered 100% ($N = 11-13$ mice per group). Each dot represents the mean value of Iba1-positive area (between dentate gyrus and cortex) for an individual mouse. Statistical differences were assessed by three-way ANOVA followed by Holm-Sidak post-hoc tests. (**, $p < 0.01$; ***, $p < 0.001$). Only biologically relevant differences are shown. Abbreviations: SD = Standard Diet; HFD = High Fat Diet; Veh = Vehicle; Lep = Leptolide.

5.3 Leptolide treatment *in vivo* also reduces astrogliosis

HFD resulted in an increase in GFAP expression, and this phenotype was partially reverted by treatment with leptolide in both regions studied, with a significant decrease in astrogliosis. Within SD-fed mice, leptolide had no significant effects (**Figure 72A**). For statistical analyses, we performed three-way ANOVA, as stated before. Diet, drug and region proved to be statistically significant factors. There was a tendency towards interaction between diet and drug ($p = 0.08$). Leptolide treatment of HFD-fed mice resulted in a significant decrease in astrogliosis (**Figure 72B**).

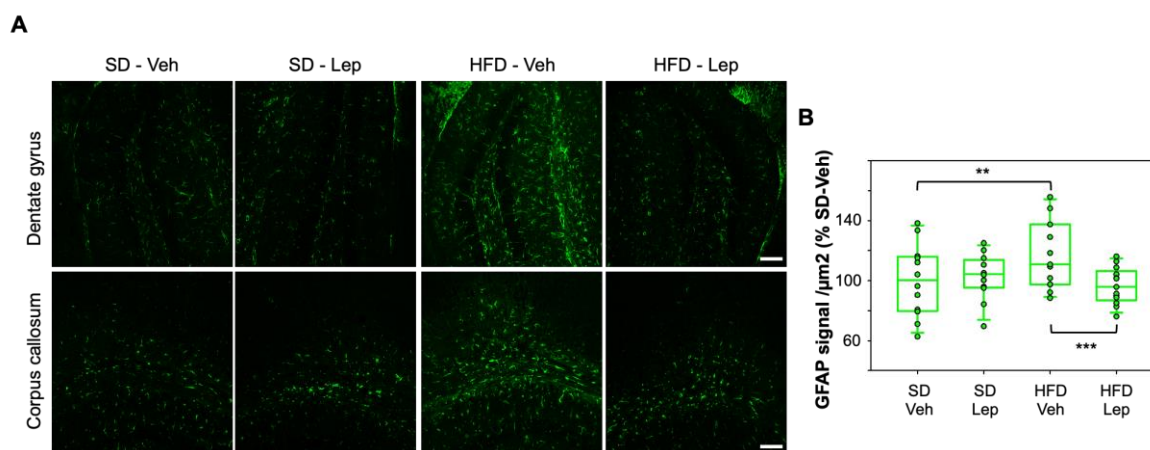


Figure 72. Leptolide treatment ameliorates astrogliosis triggered by HFD. A) Representative immunofluorescence images from paraffin sections of mouse brains stained with GFAP. Calibration bars: $50\mu\text{m}$. B) Immunohistochemical quantification of GFAP expression measured as intensity of fluorescence per area, normalized to SD-Vehicle, considered as 100% ($n=11-13$ mice per group). Each dot represents the mean value of GFAP intensity per area (between dentate gyrus and corpus callosum) for an individual mouse. Statistical differences were assessed by three-way ANOVA followed by Holm-Sidak post-hoc tests. (**, $p < 0.01$; ***, $p < 0.001$). Only biologically relevant differences are shown. Abbreviations: SD = Standard Diet; HFD = High Fat Diet; Veh = Vehicle; Lep = Leptolide.

In summary, we demonstrated that leptolide, which had already shown protective effects on systemic insulin resistance (Villa-Pérez et al., 2017), has also a potent anti-glioinflammatory activity *in vivo*, targeting both microglia and astrocytes. Remarkably, the results regarding gliosis in the dentate gyrus for both glial cell types were also validated in the corpus callosum, the largest white matter structure in the brain, and in the cerebral cortex, which plays an essential role in memory and cognition. Our results on leptolide provide a hopeful therapeutic approach to treat neuroinflammation concomitant with metabolic impairment. However, further research is necessary to address the mechanism by which furanocembranolides exert their therapeutic outcomes on glial cells.

DISCUSSION

Alzheimer's disease (AD) and diabetes mellitus (DM) are two of the most prevalent diseases in the elderly population. After decades of research and clinical trials, there is still no cure for any of these disorders. Multiple lines of evidence suggest a connection between AD and DM, although the underlying links are not fully understood. During the recent years, the term "type 3 diabetes" has been proposed to describe the hypothesis that AD is triggered by a type of insulin resistance that occurs specifically in the brain (De la Monte, 2019). In this context the insulin degrading enzyme (IDE), which has been described to be able to degrade both insulin and amyloid β , emerges as a candidate pathophysiological link between both diseases.

Differential chronic high D-glucose effects on microglia and macrophages

Hyperglycemia is a key risk factor for the development of metabolic syndrome and is also associated with cognitive decline (Moreno-Navarrete et al., 2017). In fact, increased glucose levels in the brain are considered to induce neuronal apoptosis via oxidative stress, leading to cognitive impairment (Sadeghi et al., 2016). Recent studies have demonstrated that a high glucose milieu can aggravate AD pathogenesis by disturbing APP processing in neurons, resulting in A β accumulation and plaque formation (Macauley et al., 2015; Yang et al., 2013). Glucose is the main energy source in the brain, and it is an essential fuel for microglial cells, whose survival essentially relies on the presence of sufficient glucose (Liu et al., 2018). Increasing evidence suggests a role of metabolic reprogramming in the regulation of the innate inflammatory response in both microglia and macrophages. Interestingly, the metabolic pathways involved in immune cell activity have been described to adapt and contribute to their phenotypes (Orihuela et al., 2016). As detailed in Chapter 1, we found that high D-glucose, with a partial effect of osmolarity, significantly increased metabolic activity specifically in microglial cells, while macrophages remained unchanged. These results indicate that microglial cells are more sensitive than macrophages to changes in their nutritional environment. This affirmation makes sense when considering the localization of each cell type in the body, with macrophages being more exposed to postprandial fluctuations in glucose levels than microglia, isolated in the brain and not used to suffer such glucose changes, at least under physiological conditions.

In the recent years, the concept of immunometabolism has emerged from evidence indicating that metabolic processes regulate immune cell activation (Devanney et al., 2020). In line with this, we assessed the effects that chronic high D-glucose stimulation has on the production of the pro-inflammatory cytokines IL-1 β and TNF- α . Since osmoregulatory conditions *in vitro* are quite distinct from the physiological body environment, we included L-glucose as an osmotic balancer to discern the effects resulting from osmolarity. IL-1 β was upregulated by osmolarity in both microglia and macrophages, but TNF- α was significantly upregulated by D-glucose specifically in microglial cells. In the literature, some studies support that high glucose treatments increase the expression of pro-inflammatory cytokines in both microglia (Quan et al., 2011) and macrophages (Iwata et al., 2007; Li et al., 2016; Shanmugam et al., 2003), while others propose that high glucose contributes to

the polarization of macrophages to an anti-inflammatory phenotype characterized by the expression of CD14 and CD206 and the increased secretion of TGF- β (Lin et al., 2020). These contradictory results could be explained by variations in the experimental settings (time of glucose exposure, glucose concentrations, medium renewal...) as well as by the absence of good osmotic controls. In our study, we tested mannitol and L-glucose as osmotic balancers, and this was a critical point to discriminate between D-glucose and osmotic effects. The pro-inflammatory effects of osmolarity on glial cells had previously been described *in vivo* (Iwama et al., 2011), but in this work we demonstrate for the first time the pro-inflammatory effects of osmolarity *in vitro*. Although these osmotic changes do not usually occur under physiological conditions, they are relevant under some pathological situations such as BBB disruption or osmotic demyelination syndrome, diseases in which osmolarity-induced pro-inflammatory microglial polarization might play a relevant role.

Interestingly, diabetic patients have endothelial glycocalyx alterations, which are associated with vascular damage (Zhu et al., 2017). As presented in Chapter 1, chronic D-glucose exposure increased sialic acid on microglial surface in a dose-dependent manner, with no effect of L-glucose. The overexposure of sialic acids during hyperglycemic conditions suggests that, upon chronic high D-glucose conditions, microglial surface interactions might be impaired, which is relevant for different microglial functions such as the recognition and internalization of A β peptides.

IDE intracellular protein levels are regulated by microglial activation states

The omnipresence of IDE in different cells, blood and cerebrospinal fluid suggests that this ubiquitous protein performs crucial biological functions in many different tissues and organs.

Since the discovery that IDE, highly expressed in the brain, can degrade A β and thereby could contribute to A β clearance in the cerebral tissue, IDE became an interesting enzyme to be targeted in AD research. In the present work we studied IDE regulation of expression in both microglia and macrophages. Chronic exposure to different D-glucose concentrations did not change IDE protein levels neither in microglia nor in macrophages, which is in concert with the study performed by Pivovarova and coworkers in hepatocytes, in which they showed that high D-glucose treatment *per se* did not induce IDE mRNA expression but modulated its activity instead (Pivovarova et al., 2009).

A common feature of many neurodegenerative diseases is the excessive production of pro-inflammatory cytokines, mainly by microglia (Heneka et al., 2014). Earlier *in vivo* studies performed in aged NLRP3 deficient mice showed that inflammasome deficiency skewed microglial cells to an “M2-like” phenotype and resulted in the increase of IDE expression (Heneka et al., 2013), linking IDE with an “anti-inflammatory” phenotype (Heneka et al., 2014). We confirmed *in vitro* the direct effect of IL-4+IL-13 stimulation on IDE intracellular protein upregulation. This finding is in line with a previous work which described that the anti-inflammatory effects of the preimplantation factor on monocytes are reversed when IDE is knocked down (Chih Chen et al., 2016). In addition, we described a decrease in IDE intracellular protein upon LPS treatment and, conversely, intracellular

IDE protein was increased after PQ-induced oxidative stress. The overexpression of IDE under oxidative conditions might be a compensatory mechanism to overcome its oxidative-triggered impaired enzymatic activity (De Dios et al., 2019). Collectively, our results support a link between IDE expression and microglial activation states.

IDE molecular evolution and subcellular localization

IDE is an ubiquitous protease that belongs to the M16A family of peptidases, found in both prokaryotic and eukaryotic organisms (Rawlings et al., 2014). As detailed in Chapter 2, an extensive search retrieved homologs of IDE in all kingdoms. The evolutionary conservation of IDE proteins supports the notion of a more general role of IDE in cellular physiology, and/or the acquisition of diverse functions not restricted to proteolysis. In fact, IDE function does not always require the catalytic activity of the enzyme, as evident from studies on the IDE-related *Axl1* gene in yeast, which showed that the budding defect of the *axl1* yeast mutant could be complemented by a catalytically inactive AXL1 protein (Adames et al., 1995). The identification of several molecular interacting partners of IDE (Leissring et al., 2021) also supports its multifunctionality. Indeed, functional explorations during evolution of IDE proteins can be appreciated in the global IDE phylogeny, especially in bacteria and protists.

Although IDE was described more than seven decades ago, there is still much to know about its cellular biology, which remains controversial. Our *in silico* studies on IDE's homologous proteins revealed that a N-terminal signal peptide is mainly present in extant prokaryotes and unicellular eukaryotes, while this sequence secretory motif is absent in multicellular organisms. This finding strongly supports that this trait got lost during the evolution of IDE's ancestors, which tallies with the fact that signal peptides get lost more often in the course of evolution than they are gained, with these events preferentially occurring in the transition from free-living bacteria to endosymbionts (Hönigschmid et al., 2018). The location of clan ME metalloproteases further supports this hypothesis: bacterial pitrilysin is periplasmic (Roth, 2013), while eupitrilysin and MPPs are found in mitochondria (Mzhavia and Devi, 2013; Kutejová et al., 2013), SPP in the stroma of chloroplasts (Lamppa and Zhong, 2013) and PreP1 in both mitochondria and chloroplasts (Glaser et al., 2013). The predicted subcellular localization for IDE's homologs across evolution revealed that IDE is mostly cytosolic in all kingdoms, with the highest variety of predicted sites being found in protists, which agrees with the exploratory changes on IDE sequence in this kingdom.

A discomfiting reality for the IDE field is the uncertainty about its subcellular localization. As recently reviewed by Leissring, the vast majority of IDE is present in the cytosol, and there is also definitive evidence for the presence of IDE within mitochondria, while other proposed localizations are quite controversial, since their underlying evidence is decades old and of mixed quality (Leissring, 2021), for example in some cases only relies on cell transfections. In agreement with Leissring, our results of immunofluorescence and electron-microscopy concurred to the

demonstration that IDE is mostly cytosolic in microglia, but IDE was not found inside any organelle, except for an occasional signal in mitochondria. Given that IDE has a great variety of biological functions in diverse cell types (González-Casimiro et al., 2021), some contradictory evidence about its localization might be explained if the subcellular localization of IDE was cell-type specific.

Since IDE is mostly cytosolic, the mechanisms by which IDE accesses each substrate are still poorly understood. IDE association with plasma membrane has already been described by others in hepatocytes (Duckworth, 1979), skeletal muscle (Yokono et al., 1979) and neurons (Bulloj et al., 2008; Vekrellis et al., 2000). As presented in Chapter 2, we confirmed that IDE partitions between soluble and membrane fractions in both cell lines and primary glial cultures, which is in accordance with the existence of at least two pools of cellular IDE: the cytosolic one, with a longer half-life, and the membrane-associated, with a faster turnover (Bulloj et al., 2008). Nevertheless, contrary to previous works that detected IDE on the cell surface (Bulloj et al., 2008; Goldfine et al., 1984; Yokono et al., 1982), in our studies IDE was associated with membranes at the cytosolic side, but never on the cell surface. Our results make sense with our bioinformatic analyses, since the fact of not having a signal peptide is an argument against IDE being able to reach the cell surface.

As detailed in Chapter 2, we confirmed the presence of IDE in Triton-X100-resistant membrane domains, with only one antecedent in the literature in neurons (Bulloj et al., 2008). Some studies suggest that the different composition of lipid rafts obtained by using different detergents reflects the existence of biochemically distinct lipid membrane domains within the plasma membrane of the same cell (Grassi et al., 2021). Therefore, we explored other methods for lipid rafts isolation. We detected for the first time IDE in sonication-resistant membrane domains. This finding using a detergent-free method, which eliminates possible artifacts introduced by detergents, strongly supports the interaction of IDE with lipid rafts. Conversely, IDE was not found in Triton-X114-resistant membrane domains. We provide compelling evidence that a small proportion of IDE is present in particular types of membrane micro-domains, indicating that IDE association to lipid rafts is not universal but specific to the physicochemical properties of membranes. Also, our results support a scenario in which IDE can switch from non-raft to raft membrane domains.

IDE exportation from microglial cells

The high degree of conservation of the signal peptide in bacteria suggests that IDE protein has relevant extracellular functions and, in this case, the loss of signal peptide during evolution might have been replaced by other “non-canonical” secretory mechanism. Nevertheless, the secretion of IDE from cultured cells remains controversial. Since Qiu and colleagues initially described that microglial BV-2 cell line released IDE to the extracellular space (Qiu et al., 1997), there have been a few studies reporting the secretion of IDE from neurons (Bulloj et al., 2010; De Dios et al., 2019; Vekrellis et al., 2000), T-cells (Miller et al., 1996) and astrocytes (Son et al., 2016), and it was proposed that IDE is exported via an unconventional secretory pathway (Zhao et al., 2009).

Our experiments showed that IDE secretion from microglia depends on the activation state of the cells, being increased upon pro-inflammatory and oxidative stimulation, and reduced in control and anti-inflammatory treatments. Interestingly, IDE exportation outside the cells was increased in parallel with exposure time to A β , which is compatible with an extracellular location of A β degradation by IDE. Our results tally with a recent paper which describes that microglia partially clear soluble A β peptides by secreting IDE, rather than transporting amyloidogenic peptides to the lysosomes (Fu et al., 2020). This modulation of IDE exportation upon A β exposure was reduced under high D-glucose conditions, suggesting an interaction between nutrient managing and amyloid managing, which deserves further research.

However, it was recently called into question the secretion of IDE, arguing that extracellular IDE in conditioned media could result from loss of cell integrity rather than specific protein secretion (Song et al., 2018). To rule out the detection of IDE released from dying cells, and based on some antecedents that described IDE in exosomes (Bulloj et al., 2010; Glebov et al., 2015; Tamboli et al., 2010), we isolated extracellular vesicles (EVs) from primary microglial cultures treated with different stimuli. We showed, for the first time, that the amount of IDE released in EVs is regulated by the activation state of microglial cells, with more IDE being secreted upon LPS and A β treatments. Moreover, we found a prominent IDE presence in MVBs of highly secretory microglial cells, which is in agreement with the increased secretion upon inflammatory, oxidative and amyloid stimuli. Our results, together with previous antecedents, confirmed that IDE is exported in extracellular vesicles, that are therefore probable exosomes (MVB-derived) and not ectosomes (derived by plasma membrane), and this IDE exportation from microglial cells is modulated by stimuli, which again links IDE function and traffic with particular phenotypic states.

One question that remains to be resolved is where IDE meets A β , since IDE is inside extracellular vesicles, while extracellular A β would be outside these vesicles. A plausible hypothesis, proposed some years ago by Glebov and Walter, is that IDE might be released upon breakage of exosomes, allowing the degradation of extracellular A β (Glebov and Walter, 2012). One possible mechanism triggering exosomes rupture would be oxidative stress, a hallmark of AD which has been described to alter biological membranes by phospholipid oxidation (Reis and Spickett, 2012; Wang et al., 2017).

An EV-associated shorter IDE “isoform”

As detailed in Chapter 2, a 60 kDa “isoform” of IDE was detected in EVs preparations. The origin of this shortened IDE is unclear, although a possible explanation would be IDE breakage by its hinge region. In concordance with our hypothesis, *in vitro* experiments using limited proteolysis described that trypsin digestion of human IDE resulted in two proteolytic fragments, corresponding to a 57.5 kDa IDE-N (domains 1-2, amino acids 42-451) and a 55.8 kDa IDE-C (domains 3-4, amino acids 541-1019) (Li et al., 2006). A relevant question is whether this IDE-N “isoform”, which contains the

insulinase domain and the catalytic site, has catalytic activity or not. On the one hand, Li and colleagues reported that IDE-N only has about 2% of the activity of wild-type, full length IDE (Li et al., 2006). On the other hand, the same authors described that the mixing of IDE-N with IDE-C *in vitro* resulted in the reassembly of both parts to make a full IDE protein (Li et al., 2006). These data support that EV-associated shortened IDE, which is found constitutively in EVs, could be functional after reassembly with the IDE-C half. More studies are needed to further assess the biological meaning and potential functionality of this EV-associated IDE-N “isoform”.

The role of IDE in metabolism: an unresolved question

The physiological role of IDE is not as clear as the name would suggest. The evolutionary conservation of IDE proteins and their widespread distribution in different tissues and subcellular compartments suggest a more general function for IDE, and/or the acquisition of diverse roles not restricted to the degradation of insulin and A β peptides. Therefore, we studied the role of IDE *in vivo* in a whole-body constitutive knockout mouse model.

The metabolic effects observed under partial deletion or total IDE ablation were sex-dependent (only observed in males) and quite subtle, with a decrease in body weight of IDE-KO mice, reduced glycemia in IDE-HET mice and no changes in plasma insulin after 6-hour fasting. The literature about the total IDE-KO model agrees on the diabetic phenotype, with all studies describing glucose intolerance (Abdul-Hay et al., 2011; Farris et al., 2003; Steneberg et al., 2013). However, the results about insulin levels are highly contradictory. Some authors showed that total IDE ablation triggers hyperinsulinemia and insulin resistance (Abdul-Hay et al., 2011; Farris et al., 2003), while others reported an opposite phenotype in which total IDE-KO mice showed decreased plasma insulin levels (Steneberg et al., 2013). In all cases experiments were performed after a prolonged fasting (16 hours) and in 2–6-month-old animals, while our experiments were done with a shorter fasting (6 hours) and in 12-month-old, middle-aged mice. Attending to these antecedents it is plausible that our mice had a diabetic phenotype earlier in their life, but got it lost after compensatory effects during aging. To answer this question, a comprehensive metabolic characterization of our mice would be required.

To shed some light to the contradictory phenotypes described in the total IDE-KO model, new tissue-specific *Ide* knockout mouse models have recently been developed (Villa-Pérez et al., 2018; Fernández-Díaz et al., 2019; Merino et al., 2020). These models revealed that hepatic IDE absence causes a defect in insulin signaling (Merino et al., 2020; Villa-Pérez et al., 2018). The recently described interaction of IDE with the insulin receptor (Merino et al., 2020) might explain why insulin signaling is destabilized when IDE is absent. Strikingly, hepatic IDE absence does not increase circulating insulin levels, which calls into question the role of IDE in insulin clearance (Villa-Pérez et al., 2018). Conversely, IDE absence in pancreatic β -cells, which produce insulin, triggers an impairment in insulin secretion, and therefore a decrease in circulating insulin levels (Fernández-Díaz et al., 2019). Overall, these studies indicate that the metabolic phenotype of the total IDE-KO

mouse is difficult to interpret from the metabolic point of view, but the effect of IDE absence is different in each metabolic tissue and, in some cases, opposed.

Brain insulin signaling in middle-aged mice

In this study, two main problems arose. The first one was the constitutive activation of the insulin signaling, probably due to aging. In this regard, it has been proposed that the association of neurodegenerative diseases with advanced age might be related to progressive metabolic stress of aging, where the overactivation of the insulin signaling pathway in the CNS might contribute to exacerbate oxidative stress and the accumulation of damaged proteins (Sadagurski and White, 2013). The second problem was that, contrary to our preliminary tests in young mice, we could not observe the effects of intra-peritoneal administered insulin in middle-aged mice. Our results might be explained by the work from Sartorius *et al.*, who described that the permeability of the BBB for insulin declines with age (Sartorius *et al.*, 2015). Other delivery methods, such as intracerebroventricular injection or intranasal administration, should be explored to address the study of brain insulin signaling in middle-aged mice.

Sexual dimorphism in insulin signaling proteins and gliosis markers

Our molecular biology study in the olfactory bulb did not reveal significant differences between genotypes but, strikingly, great differences were found between sexes.

We reported for the first time a sex-dependent differential expression of IDE protein in the olfactory bulb of middle-aged mice, with males expressing almost twice as much IDE as females. The only antecedent was a previous study conducted in a 9-month-old mouse model of AD found no differences between WT mice, but described a significant reduction in IDE mRNA expression in the hippocampi of transgenic females, compared with mutant males (Gallagher *et al.*, 2013). As regards the insulin signaling pathway, male mice showed higher levels of insulin receptor and AKT1 than females, which agrees with a work that described the same sex differences in the expression of insulin receptors in developing rat hippocampus at post-natal day 14 (Hami *et al.*, 2012).

The overexpression of gliosis markers CD11b and GFAP in females confirms the sexual dimorphism of astrocytes and microglial cells, largely recognized and recently demonstrated (Johnson *et al.*, 2008; Villa *et al.*, 2018). Interestingly, several neurological disorders have been reported to have a sex difference in the incidence, severity and/or progression of the disease (Villa *et al.*, 2016). For instance, AD has a higher prevalence in women above 65 years old (1.6-3:1 ratio compared to men) and also progresses with a greater cognitive deterioration (Plassman *et al.*, 2011; Seshadri *et al.*, 1997), which accords with our results of exacerbated gliosis in females. In addition, our results are in agreement with a work in aged mice, which described a higher pro-inflammatory response to acute LPS challenge in female brains (Murtaf *et al.*, 2019).

Taken together, our results indicate an earlier onset and/or a higher glioinflammatory response in middle-aged females than in males.

General results from multivariate analysis

The multivariate analysis revealed some interesting patterns that validate that our study had enough depth. Some examples are the opposite relationship between “inflammaging” markers and locomotor activity (Mannix et al., 2014), or the inverse weight of the two different forms of memory, OLT and NORT, which was expected since they are mediated by different mechanisms (Denninger et al., 2018). Thus, our new discoveries are of interest and worth to keep studying, especially the sex-dependent effects, from the differential behavior and the contribution of ApoD and CD11b, to specific changes in certain proteins from the insulin pathway, as detailed in Chapter 3. Our *in vivo* data do not fully support our initial hypothesis of IDE being a link between AD and DM, *via* its effects in mediating brain insulin resistance, since partial or total IDE absence did not affect neither metabolic parameters nor insulin signaling proteins in the brain. Instead, multivariate analysis revealed interesting relationships between IDE, glial responses and A β managing.

IDE does not regulate insulin signaling in microglial cells

There are no data in the literature demonstrating the relationship between IDE absence and brain insulin resistance, postulated by the hypothesis of type 3 diabetes. A recent work, studying an intracerebroventricular-streptozotocin rat model of AD, described an impairment in brain insulin signaling accompanied by a decrease in IDE protein expression (Akhtar et al., 2020). These authors proposed that restoration of IDE protein levels by orthovanadate treatment was able to reverse brain insulin resistance. However, the main limitation of this study was that the insulin signaling was studied at the gene expression level, without considering phosphorylated forms of the insulin signaling components (Akhtar et al., 2020).

The vast majority of insulin receptors are localized on neurons (Unger et al., 1989), therefore the study of insulin signaling in the brain has been traditionally focused in neurons. Nevertheless, it was recently demonstrated that insulin receptor and downstream proteins are expressed in microglia, suggesting that insulin might influence microglia activity via the insulin pathway (Spielman et al., 2015). A recent paper proposed that microglia are sensitive to insulin stimulation via AKT signaling (Haas et al., 2020). However, AKT might be activated by different pathways aside from the insulin signaling. As shown in Chapter 4, we found for the first time that insulin stimulation specifically triggers the phosphorylation of the insulin receptor in microglial cells. These results demonstrate that insulin stimulates the insulin signaling pathway in microglia. Notwithstanding, neither IDE expression was regulated by insulin exposure, nor IDE absence impaired the insulin signaling, which indicates that IDE is not involved in microglial insulin signaling.

Although we focused on the study of microglial cells, the role of IDE in astrocytes also deserves further research. On this subject, a recent paper described that insulin signaling pathway regulates

the degradation of A β in cultured astrocytes (Yamamoto et al., 2018), supporting a link between insulin signaling and amyloid degradation via IDE and neprilysin.

IDE absence impairs microglial proliferation

IDE has been typically studied because of its proteolytic functions on insulin and A β peptides. However, its conservation across evolution and its ubiquitous expression in terms of both organisms and cell types suggests that this protease might perform other non-proteolytic functions. For this reason, we delved for the first time into the functions that IDE performs specifically in microglial cells by comparing primary microglial cultures prepared from WT and IDE-KO mice.

The proliferation of microglial cells, regulated by the activation of CSF1R pathway, is a hallmark of many neurodegenerative conditions (Olmos-Alonso et al., 2016). In addition, albeit microglia were believed to be long-lived cells, it has been recently demonstrated that the turnover of the microglial population is a highly dynamic process that happens several times during a lifetime (Askew et al., 2017). These are two examples in which microglial proliferation is a crucial physiological process. We observed that IDE-KO microglia proliferate less than WT cells and also have a delayed response to M-CSF. Our data align with a work in which IDE knockdown in the HepG2 (human hepatoma) cell line produced a decrease in cell proliferation that was attributed to the dysregulation of p53 pathway (Pivovarova et al., 2015), and also with a previous work in which IDE downregulation impaired SH-SY5Y (human neuroblastoma) proliferation (Tundo et al., 2013).

IDE is involved in microglial polarization

Cytokine profiling experiments, presented in Chapter 4, suggest that microglial polarization is impaired in the absence of IDE, with IL-4+IL-13 treatment triggering the production of less IL-4 in IDE-KO microglia and, conversely, PQ treatment producing both an increase in TNF- α and a decrease in TFG- β protein in both male and female microglia. These results tally with the work of Heneka and coworkers performed in *Nlrp3* deficient mice, whose microglia exhibited an “M2-like” phenotype (overexpressing anti-inflammatory markers such as Arg-1, Fizz-1 and IL-4) in parallel with an increase in IDE protein expression (Heneka et al., 2013). Taken together, our results indicate that IDE plays an important role in microglial activation and reveal a previously unknown function for IDE in microglial cell polarization. However, the most striking result is the sex- and genotype-dependent response to A β oligomers, with only male IDE-KO microglial cells synthesizing both TNF- α and IL-6. Sex differences in the neuroimmune system, including glial activation and associated cytokine production in the brain, is a recently emerging field (Osborne et al., 2018).

Although quite promising, these results must be taken with caution since they involve many simplifications of the complex microglial activation responses, with a few stimuli and a small set of cytokines analyzed. Ideally, our results should be complemented by microglia-specific gene signatures in different contexts (Dubbelaar et al., 2018).

Sex-specific effects of IDE in myelin phagocytosis by microglia

Since the anti-inflammatory activation of microglia is linked with an enhanced phagocytic activity (Heneka et al., 2014), and IDE-KO microglia showed an impaired anti-inflammatory polarization, we hypothesized that IDE absence might trigger impaired phagocytosis. As detailed in Chapter 4, we found sex-dependent differences in myelin phagocytosis by microglial cells. Contrary to recent evidence that suggests that female microglia have a higher phagocytic ability (Yanguas-Casás et al., 2018), in our hands male microglia phagocytosed more myelin than female cells. However, this disagreement might be explained by the fact that our experiments were performed *in vitro*, while the previous evidence was achieved *in vivo*. In any case, we found that IDE absence affects myelin phagocytosis in a sex-dependent manner, decreasing myelin uptake in males and increasing it in females.

IDE involvement in A β oligomers managing

Microglial cells play a prominent role in degradation of extracellular A β , but they also phagocytose A β for lysosome-mediated degradation. Since extracellular A β degradation by secreting IDE has already been characterized (Qiu et al., 1998; Mandrekar et al., 2009), we focused on the internalization and intracellular A β degradation. Contrary to the results reported by Fu and colleagues (Fu et al., 2020), we did find microglial uptake of A β oligomers. The main cause for this disagreement could be the different A β oligomer concentrations used, with their experiments being conducted in the nanomolar range (Fu et al., 2020), which could be below detection levels.

As detailed in Chapter 4, IDE absence in microglia resulted in an alteration of A β oligomers internalization dynamics, with a transitory accelerated A β internalization. This increased internalization might be caused by the specific pro-inflammatory activation of IDE-KO cells, in comparison with WT microglia. Although phagocytosis is believed to be enhanced in anti-inflammatory phenotypes (Heneka et al., 2014), A β internalization can occur by other mechanisms besides phagocytosis, such as endocytosis and pinocytosis (Ries and Sastre, 2016), which could explain these apparently contradictory results. Therefore, we should conduct a more in-depth study to assess which internalization pathways are increased when IDE is not present.

The role of IDE in A β oligomers degradation was clearer, with a consistent decrease of A β degradation in all times analyzed when IDE is not present. This impairment of A β oligomers degradation in IDE-KO microglia might involve less A β clearance, not only by direct IDE degradation, but also by other intracellular mechanisms such as intracellular proteases, the ubiquitin proteasome system or the autophagy pathway (Ries and Sastre, 2016).

IDE affects specific “crystals” of the microglial “kaleidoscope”

The kaleidoscope proposed as a description of the functional states of microglia is a good framework to encompass the physiological roles of IDE in microglia. We observed that lack of IDE does not affect the activity of the insulin pathway in microglia, but does affect another relevant functional aspect, its proliferation. On the other hand, specific aspects in the cytokine profile in response to the different stimuli, and the microglial processes of myelin or A β clearance, are added to the “IDE-dependent microglia kaleidoscope crystals”.

Leptolide as a candidate for a new therapeutic approach to tackle type 3 diabetes

As detailed in Chapter 5, the *in vitro* screening of natural compounds in microglial cells revealed interesting immunomodulatory properties for some of the new furanocembranolides and leptolide (Corraliza-Gómez et al., 2020). Previous studies reported anti-inflammatory activity of other furanocembranolides in Raw264.7 macrophages (Chao et al., 2011; Cheng et al., 2009; Lin et al., 2015), but we reported for the first time the anti-inflammatory effects of furanocembranolides in microglial cells. Our results, supported by the background mentioned above, propose furanocembranolides as potential modulators of microglial inflammatory activity and reinforce the suitability of natural products as alternative therapeutic targets to address neuroinflammation.

Besides anti-inflammatory properties, leptolide was shown to be the only compound that increases microglial cell viability. In addition, it had been previously demonstrated that leptolide has protective effects on systemic insulin resistance *in vivo* (Villa-Pérez et al., 2017). For these reasons, we chose leptolide to analyze its potential anti-inflammatory effects *in vivo*, in a mouse model of obesity and insulin resistance. We demonstrated a prominent anti-inflammatory activity for leptolide *in vivo* in both microgliosis and astrogliosis. Although gliosis amelioration may be, at least in part, attributed to the decrease in blood levels of inflammatory molecules associated with leptolide treatment (Villa-Pérez et al., 2017), our *in vitro* results support a direct anti-inflammatory effect of leptolide on microglial cells. It is well known that obesity triggers low-grade chronic inflammation, and this compound could partially revert this status, rendering a less inflammatory body environment and a switch towards a lower inflammatory state of the brain. Altogether, our results postulate leptolide as a promising drug to simultaneously treat insulin resistance and neuroinflammation due to its pleiotropic effects on metabolism and gliosis, constituting a hopeful therapeutic approach viable for treating neuroinflammation concomitant with metabolic impairment.

Limitations

The main limitation of this work is that we have not reached yet a full understanding of the molecular mechanisms underlying the main findings. Since the antecedents on this topic were either scarce or contradictory, the question pursued in this Thesis required first to accomplish a thorough analysis of variables affecting IDE and affected by IDE. A set of functional experiments such as measuring IDE activity under relevant stimuli could be an added value to this knowledge.

Regarding to the *in vivo* study, high variability between individuals from the same group was found, which is attributable to the aging process contributing to life-history dependent variation. In this regard, it would be worth doing a longitudinal study, as initially planned, to collect data on individuals throughout their lives. Unfortunately, it was not possible in the present work due to the difficulty to obtain *knockout* mice. In addition, increasing group sizes to augment the statistical power would be another improvement for this study.

Contribution and future perspectives

More than seven decades have passed since the discovery of IDE. However, there are still many fundamental questions that remain to be elucidated. This PhD thesis has contributed to expand the knowledge about IDE subcellular localization and exportation mechanisms. Although our data do not provide a direct support our initial hypothesis about IDE as a link between AD and DM, we have unveiled previously unknown IDE biological properties and functions in the nervous system, and particularly in microglial cells. Our data make IDE, and the modulation of its expression and traffic, potential therapeutic targets for neurodegenerative processes.

One fundamental remaining question is where IDE meets A β . Although we have not fully addressed this topic, our results support the hypothesis that EVs-associated IDE might meet A β extracellularly, but also suggest a role for IDE in intracellular A β oligomers degradation. Colocalization experiments are required to precisely elucidate where IDE can meet and interact with A β .

Other relevant aspects to be further investigated are the biological meaning of the 60 kDa- “half IDE isoform”, the role of IDE in astrocytes and the insulin signaling pathway activity in the brain of IDE-deficient mice.

CONCLUSIONS

1. High D-glucose activates microglial metabolic activity, promotes a mild pro-inflammatory state and increases sialic acid exposure on microglial cell surface.
2. The phylogenetic tree for IDE reveals that a shift in IDE subcellular localization took place between prokaryotic (with signal peptides) and eukaryotic cells (without it).
3. IDE is mostly cytosolic, not found inside any membranous organelle, and partitions between soluble and membrane fractions. IDE's association to membranes only occurs at the cytosolic side. Moreover, IDE associates with lipid rafts with specific physicochemical properties.
4. IDE is exported from microglial cells inside extracellular vesicles arisen from multivesicular bodies. This exportation is modulated by the activation state of microglia.
5. Insulin signaling related proteins, such as the insulin receptor, AKT and IDE present a sexual dimorphism in the olfactory bulb of middle-aged mice, being significantly decreased in females in comparison with males. Conversely, gliosis markers CD11b and GFAP are significantly increased in females.
6. IDE absence impairs microglial proliferation and delays its response to M-CSF.
7. Lack of IDE alters microglial activation states, making them less responsive to IL-4+IL-13 induced anti-inflammatory polarization, and more pro-inflammatory upon PQ-induced oxidative stress.
8. IDE absence shows sex-specific responses to A β oligomers and myelin phagocytosis, but has no effect in myelin degradation.
9. IDE is involved in A β oligomers managing: lack of IDE alters A β oligomers internalization dynamics and impairs A β oligomers degradation in male microglia.
10. Leptolide is a promising therapeutic approach to simultaneously target systemic insulin resistance and neuroinflammation due to its pleiotropic effects on metabolism and gliosis.

REFERENCES

- Abdul-Hay, S.O., Kang, D., McBride, M., Li, L., Zhao, J., Leissring, M.A., 2011. Deletion of Insulin-Degrading Enzyme Elicits Antipodal, Age-Dependent Effects on Glucose and Insulin Tolerance. *PLoS ONE* 6, e20818. <https://doi.org/10.1371/journal.pone.0020818>
- Adames, N., Blundell, K., Ashby, M.N., Boone, C., 1995. Role of Yeast Insulin-Degrading Enzyme Homologs in Pheromone Processing and Bud Site Selection. *Science* 270, 464–467. <https://doi.org/10.1126/science.270.5235.464>
- Affholter, J.A., Fried, V.A., Roth, R.A., 1988. Human insulin-degrading enzyme shares structural and functional homologies with *E. coli* protease III. *Science*. <https://doi.org/10.1126/science.3059494>.
- Affholter, J.A., Hsieh, C.-L., Francke, U., Roth, R.A., 1990. Insulin-Degrading Enzyme: Stable Expression of the Human Complementary DNA, Characterization of its Protein Product, and Chromosomal Mapping of the Human and Mouse Genes. *Molecular Endocrinology* 4, 1125–1135. <https://doi.org/10.1210/mend-4-8-1125>
- Ahuja, N., Schwer, B., Carobbio, S., Waltregny, D., North, B.J., Castronovo, V., Maechler, P., Verdin, E., 2007. Regulation of Insulin Secretion by SIRT4, a Mitochondrial ADP-ribosyltransferase. *Journal of Biological Chemistry* 282, 33583–33592. <https://doi.org/10.1074/jbc.M705488200>
- Akhtar, A., Bishnoi, M., Sah, S.P., 2020. Sodium orthovanadate improves learning and memory in intracerebroventricular-streptozotocin rat model of Alzheimer's disease through modulation of brain insulin resistance induced tau pathology. *Brain Research Bulletin* 164, 83–97. <https://doi.org/10.1016/j.brainresbull.2020.08.001>
- Akiyama, H., Shii, K., Yokono, K., Yonezawa, K., Sato, S., Watanabe, K., Baba, S., 1988. Cellular localization of insulin-degrading enzyme in rat liver using monoclonal antibodies specific for this enzyme. *Biochemical and Biophysical Research Communications* 155, 914–922. [https://doi.org/10.1016/S0006-291X\(88\)80583-7](https://doi.org/10.1016/S0006-291X(88)80583-7)
- Al-Lamki, R.S., Mayadas, T.N., 2015. TNF receptors: signaling pathways and contribution to renal dysfunction. *Kidney International* 87, 281–296. <https://doi.org/10.1038/ki.2014.285>
- Almagro Armenteros, J.J., Sønderby, C.K., Sønderby, S.K., Nielsen, H., Winther, O., 2017. DeepLoc: prediction of protein subcellular localization using deep learning. *Bioinformatics* 33, 3387–3395. <https://doi.org/10.1093/bioinformatics/btx431>
- Almagro Armenteros, J.J., Tsirigos, K.D., Sønderby, C.K., Petersen, T.N., Winther, O., Brunak, S., von Heijne, G., Nielsen, H., 2019. SignalP 5.0 improves signal peptide predictions using deep neural networks. *Nature Biotechnology* 37, 420–423. <https://doi.org/10.1038/s41587-019-0036-z>
- Altschul, S., 1997. Gapped BLAST and PSI-BLAST: a new generation of protein database search programs. *Nucleic Acids Research* 25, 3389–3402. <https://doi.org/10.1093/nar/25.17.3389>
- Alzheimer, A., 1907. About a peculiar disease of the cerebral cortex. *Centralblatt für Nervenheilkunde Psychiatrie* 30, 177–179.
- Amor, S., Puentes, F., Baker, D., van der Valk, P., 2010. Inflammation in neurodegenerative diseases. *Immunology* 129, 154–169. <https://doi.org/10.1111/j.1365-2567.2009.03225.x>
- Andrews, S., 2010. FastQC: A Quality Control Tool for High Throughput Sequence Data. *Babraham Bioinformatics*.

- Antunes, M., Biala, G., 2012. The novel object recognition memory: neurobiology, test procedure, and its modifications. *Cognitive Processing* 13, 93–110. <https://doi.org/10.1007/s10339-011-0430-z>
- Arnold, S.E., Arvanitakis, Z., Macauley-Rambach, S.L., Koenig, A.M., Wang, H.-Y., Ahima, R.S., Craft, S., Gandy, S., Buettner, C., Stoeckel, L.E., Holtzman, D.M., Nathan, D.M., 2018. Brain insulin resistance in type 2 diabetes and Alzheimer disease: concepts and conundrums. *Nature Reviews Neurology* 14, 168–181. <https://doi.org/10.1038/nrneurol.2017.185>
- Arvanitakis, Z., Wilson, R.S., Bienias, J.L., Evans, D.A., Bennett, D.A., 2004. Diabetes Mellitus and Risk of Alzheimer Disease and Decline in Cognitive Function. *Archives of Neurology* 61, 661. <https://doi.org/10.1001/archneur.61.5.661>
- Askew, K., Gomez-Nicola, D., 2018. A story of birth and death: Insights into the formation and dynamics of the microglial population. *Brain, Behavior, and Immunity* 69, 9–17. <https://doi.org/10.1016/j.bbi.2017.03.009>
- Askew, K., Li, K., Olmos-Alonso, A., Garcia-Moreno, F., Liang, Y., Richardson, P., Tipton, T., Chapman, M.A., Riecken, K., Beccari, S., Sierra, A., Molnár, Z., Cragg, M.S., Garaschuk, O., Perry, V.H., Gomez-Nicola, D., 2017. Coupled Proliferation and Apoptosis Maintain the Rapid Turnover of Microglia in the Adult Brain. *Cell Reports* 18, 391–405. <https://doi.org/10.1016/j.celrep.2016.12.041>
- Authier, F., Bergeron, J.J., Ou, W.J., Rachubinski, R.A., Posner, B.I., Walton, P.A., 1995. Degradation of the cleaved leader peptide of thiolase by a peroxisomal proteinase. *Proceedings of the National Academy of Sciences* 92, 3859–3863. <https://doi.org/10.1073/pnas.92.9.3859>
- Ayala, J.E., Samuel, V.T., Morton, G.J., Obici, S., Croniger, C.M., Shulman, G.I., Wasserman, D.H., McGuinness, O.P., for the NIH Mouse Metabolic Phenotyping Center Consortium, 2010. Standard operating procedures for describing and performing metabolic tests of glucose homeostasis in mice. *Disease Models & Mechanisms* 3, 525–534. <https://doi.org/10.1242/dmm.006239>
- Bach, J.-F., 1994. Insulin-Dependent Diabetes Mellitus as an Autoimmune Disease. *Endocrine Reviews* 15, 27. <https://doi.org/10.1210/edrv-15-4-516>.
- Banks, W.A., Owen, J.B., Erickson, M.A., 2012. Insulin in the brain: There and back again. *Pharmacology & Therapeutics* 136, 82–93. <https://doi.org/10.1016/j.pharmthera.2012.07.006>
- Bartzokis, G., Lu, P.H., Mintz, J., 2007. Human brain myelination and amyloid beta deposition in Alzheimer's disease. *Alzheimer's & Dementia* 3, 122–125. <https://doi.org/10.1016/j.jalz.2007.01.019>
- Baud, V., Karin, M., 2001. Signal transduction by tumor necrosis factor and its relatives. *Trends in Cell Biology* 11, 372–377. [https://doi.org/10.1016/S0962-8924\(01\)02064-5](https://doi.org/10.1016/S0962-8924(01)02064-5)
- Baxevanis, A.D., Bader, G.D., Wishart, D.S. (Eds.), 2020. *Bioinformatics: a practical guide to the analysis of genes and proteins*, Fourth edition. ed. Wiley, Hoboken, NJ, USA.
- Becker, A.B., Roth, R.A., 1992. An unusual active site identified in a family of zinc metalloendopeptidases. *Proceedings of the National Academy of Sciences* 89, 3835–3839. <https://doi.org/10.1073/pnas.89.9.3835>
- Benveniste, E.N., 1992. Inflammatory cytokines within the central nervous system: sources, function, and mechanism of action. *American Journal of Physiology-Cell Physiology* 263, C1–C16. <https://doi.org/10.1152/ajpcell.1992.263.1.C1>

- Benveniste, H., Liu, X., Koundal, S., Sanggaard, S., Lee, H., Wardlaw, J., 2019. The Glymphatic System and Waste Clearance with Brain Aging: A Review. *Gerontology* 65, 106–119. <https://doi.org/10.1159/000490349>
- Bernaus, A., Blanco, S., Sevilla, A., 2020. Glia Crosstalk in Neuroinflammatory Diseases. *Frontiers in Cellular Neuroscience* 14, 209. <https://doi.org/10.3389/fncel.2020.00209>
- Bertram, L., 2000. Evidence for Genetic Linkage of Alzheimer's Disease to Chromosome 10q. *Science* 290, 2302–2303. <https://doi.org/10.1126/science.290.5500.2302>
- Beynon, S.B., Walker, F.R., 2012. Microglial activation in the injured and healthy brain: What are we really talking about? Practical and theoretical issues associated with the measurement of changes in microglial morphology. *Neuroscience* 225, 162–171. <https://doi.org/10.1016/j.neuroscience.2012.07.029>
- Bian, L., Yang, J.D., Guo, T.W., Sun, Y., Duan, S.W., Chen, W.Y., Pan, Y.X., Feng, G.Y., He, L., 2004. Insulin-degrading enzyme and Alzheimer disease: A genetic association study in the Han Chinese. *Neurology* 63, 241–245. <https://doi.org/10.1212/01.WNL.0000129987.70037.DB>
- Biber, K., Neumann, H., Inoue, K., Boddeke, H.W.G.M., 2007. Neuronal 'On' and 'Off' signals control microglia. *Trends in Neurosciences* 30, 596–602. <https://doi.org/10.1016/j.tins.2007.08.007>
- Bickel, P.E., 2002. Lipid rafts and insulin signaling. *American Journal of Physiology-Endocrinology and Metabolism* 282, E1–E10. <https://doi.org/10.1152/ajpendo.2002.282.1.E1>
- Bjerknes, R., Bassoe, C.-F., 1984. Phagocyte C3-mediated attachment and internalization: Flow cytometric studies using a fluorescence quenching technique. *Blut* 49, 315–323. <https://doi.org/10.1007/BF00320205>
- Björk, B.F., Katzov, H., Kehoe, P., Fratiglioni, L., Winblad, B., Prince, J.A., Graff, C., 2007. Positive association between risk for late-onset Alzheimer disease and genetic variation in IDE. *Neurobiology of Aging* 28, 1374–1380. <https://doi.org/10.1016/j.neurobiolaging.2006.06.017>
- Blasi, E., Barluzzi, R., Bocchini, V., Mazzolla, R., Bistoni, F., 1990. Immortalization of murine microglial cells by a v-raf / v-myc carrying retrovirus. *Journal of Neuroimmunology* 27, 229–237. [https://doi.org/10.1016/0165-5728\(90\)90073-V](https://doi.org/10.1016/0165-5728(90)90073-V)
- Bolós, M., Perea, J.R., Avila, J., 2017. Alzheimer's disease as an inflammatory disease. *Biomolecular Concepts* 8. <https://doi.org/10.1515/bmc-2016-0029>
- Bomfim, T.R., Forny-Germano, L., Sathler, L.B., Brito-Moreira, J., Houzel, J.-C., Decker, H., Silverman, M.A., Kazi, H., Melo, H.M., McClean, P.L., Holscher, C., Arnold, S.E., Talbot, K., Klein, W.L., Munoz, D.P., Ferreira, S.T., De Felice, F.G., 2012. An anti-diabetes agent protects the mouse brain from defective insulin signaling caused by Alzheimer's disease-associated A β oligomers. *Journal of Clinical Investigation* 122, 1339–1353. <https://doi.org/10.1172/JCI57256>
- Boucher, J., Kleinridders, A., Kahn, C.R., 2014. Insulin Receptor Signaling in Normal and Insulin-Resistant States. *Cold Spring Harbor Perspectives in Biology* 6, a009191–a009191. <https://doi.org/10.1101/cshperspect.a009191>
- Brocker, C., Thompson, D., Matsumoto, A., Nebert, D.W., Vasiliou, V., 2010. Evolutionary divergence and functions of the human interleukin (IL) gene family. *Human Genomics* 5, 30. <https://doi.org/10.1186/1479-7364-5-1-30>
- Broh-Kahn, R., Mirsky, I., 1949. The inactivation of insulin by tissue extracts; the effect of fasting on the insulinase

- content of rat liver. *Archives of Biochemistry* 20, 10–4.
- Bronzuoli, M.R., Iacomino, A., Steardo, L., Scuderi, C., 2016. Targeting neuroinflammation in Alzheimer's disease. *JIR Volume 9*, 199–208. <https://doi.org/10.2147/JIR.S86958>
- Brown, D.A., Rose, J.K., 1992. Sorting of GPI-anchored proteins to glycolipid-enriched membrane subdomains during transport to the apical cell surface. *Cell* 68, 533–544. [https://doi.org/10.1016/0092-8674\(92\)90189-J](https://doi.org/10.1016/0092-8674(92)90189-J)
- Brown, G.C., Neher, J.J., 2012. Eaten alive! Cell death by primary phagocytosis: 'phagoptosis.' *Trends in Biochemical Sciences* 37, 325–332. <https://doi.org/10.1016/j.tibs.2012.05.002>
- Bulloj, A., Leal, M.C., Surace, E.I., Zhang, X., Xu, H., Ledesma, M.D., Castaño, E.M., Morelli, L., 2008. Detergent resistant membrane-associated IDE in brain tissue and cultured cells: Relevance to A β and insulin degradation. *Molecular Neurodegeneration* 3, 22. <https://doi.org/10.1186/1750-1326-3-22>
- Bulloj, A., Leal, M.C., Xu, H., Castaño, E.M., Morelli, L., 2010. Insulin-Degrading Enzyme Sorting in Exosomes: A Secretory Pathway for a Key Brain Amyloid- β Degrading Protease. *Journal of Alzheimer's Disease* 19, 79–95. <https://doi.org/10.3233/JAD-2010-1206>
- Butterfield, D.A., Halliwell, B., 2019. Oxidative stress, dysfunctional glucose metabolism and Alzheimer disease. *Nature Reviews Neuroscience* 20, 148–160. <https://doi.org/10.1038/s41583-019-0132-6>
- Buttini, M., 2005. -Amyloid Immunotherapy Prevents Synaptic Degeneration in a Mouse Model of Alzheimer's Disease. *Journal of Neuroscience* 25, 9096–9101. <https://doi.org/10.1523/JNEUROSCI.1697-05.2005>
- Caballero, E., Calvo-Rodríguez, M., Gonzalo-Ruiz, A., Villalobos, C., Núñez, L., 2016. A new procedure for amyloid β oligomers preparation enables the unambiguous testing of their effects on cytosolic and mitochondrial Ca²⁺ entry and cell death in primary neurons. *Neuroscience Letters* 612, 66–73. <https://doi.org/10.1016/j.neulet.2015.11.041>
- Caccamo, A., Oddo, S., Sugarman, M.C., Akbari, Y., LaFerla, F.M., 2005. Age- and region-dependent alterations in A β -degrading enzymes: implications for A β -induced disorders. *Neurobiology of Aging* 26, 645–654. <https://doi.org/10.1016/j.neurobiolaging.2004.06.013>
- Caño Espinel, M. del, 2014. Relación de la apolipoproteína D y sus homólogos en *Drosophila* con las membranas biológicas: Estudio de su función en diferentes procesos celulares y de su localización y efectos sobre las balsas lipídicas. Universidad de Valladolid. <https://doi.org/10.35376/10324/7752>
- Caravaggio, J.W., Hasu, M., MacLaren, R., Thabet, M., Raizman, J.E., Veinot, J.P., Marcel, Y.L., Milne, R.W., Whitman, S.C., 2013. Insulin-degrading enzyme deficiency in bone marrow cells increases atherosclerosis in LDL receptor-deficient mice. *Cardiovascular Pathology* 22, 458–464. <https://doi.org/10.1016/j.carpath.2013.03.006>
- Carrasquillo, M.M., Belbin, O., Zou, F., Allen, M., Ertekin-Taner, N., Ansari, M., Wilcox, S.L., Kashino, M.R., Ma, L., Younkin, L.H., Younkin, Samuel G., Younkin, C.S., Dincman, T.A., Howard, M.E., Howell, C.C., Stanton, C.M., Watson, C.M., Crump, M., Vitart, V., Hayward, C., Hastie, N.D., Rudan, I., Campbell, H., Polasek, O., Brown, K., Passmore, P., Craig, D., McGuinness, B., Todd, S., Kehoe, P.G., Mann, D.M., Smith, A.D., Beaumont, H., Warden, D., Holmes, C., Heun, R., Kölsch, H., Kalsheker, N., Pankratz, V.S., Dickson, D.W., Graff-Radford, N.R., Petersen, R.C., Wright, A.F., Younkin, Steven G., Morgan, K., 2010. Concordant

- Association of Insulin Degrading Enzyme Gene (IDE) Variants with IDE mRNA, A β , and Alzheimer's Disease. *PLoS ONE* 5, e8764. <https://doi.org/10.1371/journal.pone.0008764>
- Chan, S.J., Steiner, D.F., 2000. Insulin Through the Ages: Phylogeny of a Growth Promoting and Metabolic Regulatory Hormone. *American Zoologist* 40, 213–222. <https://doi.org/10.1093/icb/40.2.213>
- Chao, C.-H., Chou, K.-J., Huang, C.-Y., Wen, Z.-H., Hsu, C.-H., Wu, Y.-C., Dai, C.-F., Sheu, J.-H., 2011. Bioactive Cembranoids from the Soft Coral *Sinularia crassa*. *Marine Drugs* 9, 1955–1968. <https://doi.org/10.3390/md9101955>
- Cheng, S.-Y., Wen, Z.-H., Wang, S.-K., Chiou, S.-F., Hsu, C.-H., Dai, C.-F., Duh, C.-Y., 2009. Anti-inflammatory cembranolides from the soft coral *Lobophytum durum*. *Bioorganic & Medicinal Chemistry* 17, 3763–3769. <https://doi.org/10.1016/j.bmc.2009.04.053>
- Cherry, J.D., Olschowka, J.A., O'Banion, M., 2014. Neuroinflammation and M2 microglia: the good, the bad, and the inflamed. *Journal of Neuroinflammation* 11, 98. <https://doi.org/10.1186/1742-2094-11-98>
- Chih Chen, Y., Rivera, J., Fitzgerald, M., Hausding, C., Ying, Y.-L., Wang, X., Todorova, K., Hayrabyan, S., Barnea, E.R., Peter, K., 2016. PreImplantation factor prevents atherosclerosis via its immunomodulatory effects without affecting serum lipids. *Thrombosis and Haemostasis* 115, 1010–1024. <https://doi.org/10.1160/TH15-08-0640>
- Chou, Y.-H., Kuo, W.-L., Rosner, M.R., Tang, W.-J., Goldman, R.D., 2009. Structural changes in intermediate filament networks alter the activity of insulin- degrading enzyme. *The FASEB Journal* 23, 3734–3742. <https://doi.org/10.1096/fj.09-137455>
- Cisbani, G., Rivest, S., 2021. Targeting innate immunity to protect and cure Alzheimer's disease: opportunities and pitfalls. *Molecular Psychiatry*. <https://doi.org/10.1038/s41380-021-01083-4>
- Cline, E.N., Bicca, M.A., Viola, K.L., Klein, W.L., 2018. The Amyloid- β Oligomer Hypothesis: Beginning of the Third Decade. *Journal of Alzheimer's Disease* 64, S567–S610. <https://doi.org/10.3233/JAD-179941>
- Cook, D.G., Leverenz, J.B., McMillan, P.J., Kulstad, J.J., Ericksen, S., Roth, R.A., Schellenberg, G.D., Jin, L.-W., Kovacina, K.S., Craft, S., 2003. Reduced Hippocampal Insulin-Degrading Enzyme in Late-Onset Alzheimer's Disease Is Associated with the Apolipoprotein E- ϵ 4 Allele. *The American Journal of Pathology* 162, 313–319. [https://doi.org/10.1016/S0002-9440\(10\)63822-9](https://doi.org/10.1016/S0002-9440(10)63822-9)
- Corraliza-Gómez, M., Gallardo, A.B., Díaz-Marrero, A.R., de la Rosa, J.M., D'Croz, L., Darías, J., Arranz, E., Cózar-Castellano, I., Ganfornina, M.D., Cueto, M., 2020. Modulation of Glial Responses by Furanocembranoides: Leptolide Diminishes Microglial Inflammation in Vitro and Ameliorates Gliosis In Vivo in a Mouse Model of Obesity and Insulin Resistance. *Marine Drugs* 18, 378. <https://doi.org/10.3390/md18080378>
- Corraliza-Gomez, M., Sanchez, D., Ganfornina, M.D., 2019. Lipid-Binding Proteins in Brain Health and Disease. *Frontiers in Neurology* 10, 1152. <https://doi.org/10.3389/fneur.2019.01152>
- Couturier, J., Stancu, I.-C., Schakman, O., Pierrot, N., Huaux, F., Kienlen-Campard, P., Dewachter, I., Octave, J.-N., 2016. Activation of phagocytic activity in astrocytes by reduced expression of the inflammasome component ASC and its implication in a mouse model of Alzheimer disease. *Journal of Neuroinflammation* 13, 20.

<https://doi.org/10.1186/s12974-016-0477-y>

- Cummings, B.J., Su, J.H., Cotman, C.W., 1993. Neuritic Involvement within bFGF Immunopositive Plaques of Alzheimer's Disease. *Experimental Neurology* 124, 315–325. <https://doi.org/10.1006/exnr.1993.1202>
- Davalos, D., Grutzendler, J., Yang, G., Kim, J.V., Zuo, Y., Jung, S., Littman, D.R., Dustin, M.L., Gan, W.-B., 2005. ATP mediates rapid microglial response to local brain injury in vivo. *Nature Neuroscience* 8, 752–758. <https://doi.org/10.1038/nn1472>
- Davidson, M.B., 1979. The effect of aging on carbohydrate metabolism: A review of the English literature and a practical approach to the diagnosis of diabetes mellitus in the elderly. *Metabolism* 28, 688–705. [https://doi.org/10.1016/0026-0495\(79\)90024-6](https://doi.org/10.1016/0026-0495(79)90024-6)
- De Dios, C., Bartolessis, I., Roca-Agüjetas, V., Barbero-Camps, E., Mari, M., Morales, A., Colell, A., 2019. Oxidative inactivation of amyloid beta-degrading proteases by cholesterol-enhanced mitochondrial stress. *Redox Biology* 26, 101283. <https://doi.org/10.1016/j.redox.2019.101283>
- De la Monte, S.M., 2019. The Full Spectrum of Alzheimer's Disease Is Rooted in Metabolic Derangements That Drive Type 3 Diabetes, in: Nakabeppu, Y., Ninomiya, T. (Eds.), *Diabetes Mellitus, Advances in Experimental Medicine and Biology*. Springer Singapore, Singapore, pp. 45–83. https://doi.org/10.1007/978-981-13-3540-2_4
- De la Monte, S.M., 2014. Type 3 diabetes is sporadic Alzheimer's disease: Mini-review. *European Neuropsychopharmacology* 24, 1954–1960. <https://doi.org/10.1016/j.euroneuro.2014.06.008>
- De la Monte, S.M., Tong, M., Wands, J.R., 2018. The 20-Year Voyage Aboard the Journal of Alzheimer's Disease: Docking at 'Type 3 Diabetes', Environmental/Exposure Factors, Pathogenic Mechanisms, and Potential Treatments. *Journal of Alzheimer's Disease* 62, 1381–1390. <https://doi.org/10.3233/JAD-170829>
- De la Monte, S.M., Wands, J.R., 2005. Review of insulin and insulin-like growth factor expression, signaling, and malfunction in the central nervous system: Relevance to Alzheimer's disease. *JAD* 7, 45–61. <https://doi.org/10.3233/JAD-2005-7106>
- de Matos, A.M., de Macedo, M.P., Rauter, A.P., 2018. Bridging Type 2 Diabetes and Alzheimer's Disease: Assembling the Puzzle Pieces in the Quest for the Molecules With Therapeutic and Preventive Potential. *Medicinal Research Reviews* 38, 261–324. <https://doi.org/10.1002/med.21440>
- Denninger, J.K., Smith, B.M., Kirby, E.D., 2018. Novel Object Recognition and Object Location Behavioral Testing in Mice on a Budget. *Journal of Visualized Experiments* 58593. <https://doi.org/10.3791/58593>
- Devanney, N.A., Stewart, A.N., Gensel, J.C., 2020. Microglia and macrophage metabolism in CNS injury and disease: The role of immunometabolism in neurodegeneration and neurotrauma. *Experimental Neurology* 329, 113310. <https://doi.org/10.1016/j.expneurol.2020.113310>
- Di Domenico, F., Tramutola, A., Foppoli, C., Head, E., Perluigi, M., Butterfield, D.A., 2018. mTOR in Down syndrome: Role in A β and tau neuropathology and transition to Alzheimer disease-like dementia. *Free Radical Biology and Medicine* 114, 94–101. <https://doi.org/10.1016/j.freeradbiomed.2017.08.009>
- Dinarello, C.A., 2009. Immunological and Inflammatory Functions of the Interleukin-1 Family. *Annual Review of Immunology* 27, 519–550. <https://doi.org/10.1146/annurev.immunol.021908.132612>
- Dobin, A., Davis, C.A., Schlesinger, F., Drenkow, J., Zaleski, C., Jha, S., Batut, P., Chaisson, M., Gingeras, T.R.,

2013. STAR: ultrafast universal RNA-seq aligner. *Bioinformatics* 29, 15–21. <https://doi.org/10.1093/bioinformatics/bts635>
- Domingues, R., Pereira, C., Cruz, M.T., Silva, A., 2021. Therapies for Alzheimer's disease: a metabolic perspective. *Molecular Genetics and Metabolism* 132, 162–172. <https://doi.org/10.1016/j.ymgme.2021.01.011>
- Domínguez, R.O., Marschoff, E.R., González, S.E., Repetto, M.G., Serra, J.A., 2012. Type 2 diabetes and/or its treatment leads to less cognitive impairment in Alzheimer's disease patients. *Diabetes Research and Clinical Practice* 98, 68–74. <https://doi.org/10.1016/j.diabres.2012.05.013>
- Dubbelaar, M.L., Kracht, L., Eggen, B.J.L., Boddeke, E.W.G.M., 2018. The Kaleidoscope of Microglial Phenotypes. *Frontiers in Immunology* 9, 1753. <https://doi.org/10.3389/fimmu.2018.01753>
- Duckworth, W.C., 1988. Insulin Degradation: Mechanisms, Products, and Significance. *Endocrine Reviews* 9, 319–345. <https://doi.org/10.1210/edrv-9-3-319>
- Duckworth, W.C., 1979. Insulin Degradation by Liver Cell Membranes. *Endocrinology* 104, 1758–1764. <https://doi.org/10.1210/endo-104-6-1758>
- Duggirala, R., Blangero, J., Almasy, L., Dyer, T.D., Williams, K.L., Leach, R.J., O'Connell, P., Stern, M.P., 1999. Linkage of Type 2 Diabetes Mellitus and of Age at Onset to a Genetic Location on Chromosome 10q in Mexican Americans. *The American Journal of Human Genetics* 64, 1127–1140. <https://doi.org/10.1086/302316>
- Eleuteri, S., Di Giovanni, S., Rockenstein, E., Mante, M., Adame, A., Trejo, M., Wrasidlo, W., Wu, F., Fraering, P.C., Masliah, E., Lashuel, H.A., 2015. Novel therapeutic strategy for neurodegeneration by blocking A β seeding mediated aggregation in models of Alzheimer's disease. *Neurobiology of Disease* 74, 144–157. <https://doi.org/10.1016/j.nbd.2014.08.017>
- Ennaceur, A., Delacour, J., 1988. A new one-trial test for neurobiological studies of memory in rats. 1: Behavioral data. *Behavioural Brain Research* 31, 47–59. [https://doi.org/10.1016/0166-4328\(88\)90157-X](https://doi.org/10.1016/0166-4328(88)90157-X)
- Farris, W., Mansourian, S., Chang, Y., Lindsley, L., Eckman, E.A., Frosch, M.P., Eckman, C.B., Tanzi, R.E., Selkoe, D.J., Guenette, S., 2003. Insulin-degrading enzyme regulates the levels of insulin, amyloid β -protein, and the β -amyloid precursor protein intracellular domain in vivo. *Proceedings of the National Academy of Sciences* 100, 4162–4167. <https://doi.org/10.1073/pnas.0230450100>
- Fensterl, V., Sen, G.C., 2009. Interferons and viral infections. *BioFactors* 35, 14–20. <https://doi.org/10.1002/biof.6>
- Fernández Díaz, C., Escobar-Curbelo, L., López-Acosta, J., Lobatón, C.D., Moreno, A., Sanz-Ortega, J., Perdomo, G., Cózar-Castellano, I., 2018. Insulin degrading enzyme is up-regulated in pancreatic β -cells by insulin treatment. *Histology and Histopathology* 33, 1167–1180. <https://doi.org/10.14670/HH-11-997>
- Fernández-Díaz, C.M., Merino, B., López-Acosta, J.F., Ciudad, P., de la Fuente, M.A., Lobatón, C.D., Moreno, A., Leissring, M.A., Perdomo, G., Cózar-Castellano, I., 2019. Pancreatic β -cell-specific deletion of insulin-degrading enzyme leads to dysregulated insulin secretion and β -cell functional immaturity. *American Journal of Physiology-Endocrinology and Metabolism* 317, E805–E819. <https://doi.org/10.1152/ajpendo.00040.2019>
- Ferrero-Miliani, L., Nielsen, O.H., Andersen, P.S., Girardin, S.E., 2006. Chronic inflammation: importance of NOD2 and NALP3 in interleukin-1 β generation. *Clinical and Experimental Immunology* 0, 061127015327006-???. <https://doi.org/10.1111/j.1365-2249.2006.03261.x>

- Fourgeaud, L., Través, P.G., Tufail, Y., Leal-Bailey, H., Lew, E.D., Burrola, P.G., Callaway, P., Zagórska, A., Rothlin, C.V., Nimmerjahn, A., Lemke, G., 2016. TAM receptors regulate multiple features of microglial physiology. *Nature* 532, 240–244. <https://doi.org/10.1038/nature17630>
- Fu, H., Liu, B., Li, L., Lemere, C.A., 2020. Microglia Do Not Take Up Soluble Amyloid-beta Peptides, But Partially Degrade Them by Secreting Insulin-degrading Enzyme. *Neuroscience* 443, 30–43. <https://doi.org/10.1016/j.neuroscience.2020.07.020>
- Fujita, A., Oka, C., Arikawa, Y., Katagai, T., Tonouchi, A., Kuhara, S., Misumi, Y., 1994. A yeast gene necessary for bud-site selection encodes a protein similar to insulin-degrading enzymes. *Nature* 372, 567–570. <https://doi.org/10.1038/372567a0>
- Furukawa, Y., Shimada, T., Furuta, H., Matsuno, S., Kusuyama, A., Doi, A., Nishi, M., Sasaki, H., Sanke, T., Nanjo, K., 2008. Polymorphisms in the IDE-KIF11-HHEX Gene Locus Are Reproducibly Associated with Type 2 Diabetes in a Japanese Population. *The Journal of Clinical Endocrinology & Metabolism* 93, 310–314. <https://doi.org/10.1210/jc.2007-1029>
- Gallagher, J.J., Minogue, A.M., Lynch, M.A., 2013. Impaired Performance of Female APP/PS1 Mice in the Morris Water Maze Is Coupled with Increased A β Accumulation and Microglial Activation. *Neurodegenerative Diseases* 11, 33–41. <https://doi.org/10.1159/000337458>
- Gandy, S., 2005. The role of cerebral amyloid β accumulation in common forms of Alzheimer disease. *Journal of Clinical Investigation* 115, 1121–1129. <https://doi.org/10.1172/JCI25100>
- Gandy, S., Huffman, D.M., 2019. Unexpected systemic phenotypes result from focal combined deficiencies of forebrain insulin receptor/IGF-1 receptor signaling. *Proceedings of the National Academy of Sciences* 116, 5852–5854. <https://doi.org/10.1073/pnas.1901970116>
- García-Mateo, N., Pascua-Maestro, R., Pérez-Castellanos, A., Lillo, C., Sanchez, D., Ganfornina, M.D., 2018. Myelin extracellular leaflet compaction requires apolipoprotein D membrane management to optimize lysosomal-dependent recycling and glycocalyx removal. *Glia* 66, 670–687. <https://doi.org/10.1002/glia.23274>
- Garden, G.A., Möller, T., 2006. Microglia Biology in Health and Disease. *Journal of Neuroimmune Pharmacology* 1, 127–137. <https://doi.org/10.1007/s11481-006-9015-5>
- Gaskin, S., Tardif, M., Cole, E., Piterkin, P., Kayello, L., Mumby, D.G., 2010. Object familiarization and novel-object preference in rats. *Behavioural Processes* 83, 61–71. <https://doi.org/10.1016/j.beproc.2009.10.003>
- Gasparini, L., Gouras, G.K., Wang, R., Gross, R.S., Beal, M.F., Greengard, P., Xu, H., 2001. Stimulation of β -Amyloid Precursor Protein Trafficking by Insulin Reduces Intraneuronal β -Amyloid and Requires Mitogen-Activated Protein Kinase Signaling. *The Journal of Neuroscience* 21, 2561–2570. <https://doi.org/10.1523/JNEUROSCI.21-08-02561.2001>
- Geijselaers, S.L.C., Aalten, P., Ramakers, I.H.G.B., De Deyn, P.P., Heijboer, A.C., Koek, H.L., OldeRikkert, M.G.M., Papma, J.M., Reesink, F.E., Smits, L.L., Stehouwer, C.D.A., Teunissen, C.E., Verhey, F.R.J., van der Flier, W.M., Biessels, G.J., 2017. Association of Cerebrospinal Fluid (CSF) Insulin with Cognitive Performance and CSF Biomarkers of Alzheimer's Disease. *Journal of Alzheimer's Disease* 61, 309–320. <https://doi.org/10.3233/JAD-170522>

- Geneva: World Health Organization, 2019. Classification of diabetes mellitus. Licence: CC BY-NC-SA 3.0 IGO.
- Ginhoux, F., Greter, M., Leboeuf, M., Nandi, S., See, P., Gokhan, S., Mehler, M.F., Conway, S.J., Ng, L.G., Stanley, E.R., Samokhvalov, I.M., Merad, M., 2010. Fate Mapping Analysis Reveals That Adult Microglia Derive from Primitive Macrophages. *Science* 330, 841–845. <https://doi.org/10.1126/science.1194637>
- Ginhoux, F., Lim, S., Hoeffel, G., Low, D., Huber, T., 2013. Origin and differentiation of microglia. *Frontiers in Cellular Neuroscience* 7. <https://doi.org/10.3389/fncel.2013.00045>
- Ginhoux, F., Prinz, M., 2015. Origin of Microglia: Current Concepts and Past Controversies. *Cold Spring Harbor Perspectives in Biology* 7, a020537. <https://doi.org/10.1101/cshperspect.a020537>
- Glaser, E., Kmiec, B., Teixeira, P.F., 2013. Mitochondrial and Chloroplastic Targeting Peptides Peptidase, PreP, in: *Handbook of Proteolytic Enzymes*. Elsevier, pp. 1426–1430. <https://doi.org/10.1016/B978-0-12-382219-2.00321-5>
- Glebov, K., Löchner, M., Jabs, R., Lau, T., Merkel, O., Schloss, P., Steinhäuser, C., Walter, J., 2015. Serotonin stimulates secretion of exosomes from microglia cells: Serotonin Stimulates Microglial Exosome Release. *Glia* 63, 626–634. <https://doi.org/10.1002/glia.22772>
- Glebov, K., Walter, J., 2012. Statins in Unconventional Secretion of Insulin-Degrading Enzyme and Degradation of the Amyloid- β Peptide. *Neurodegenerative Diseases* 10, 309–312. <https://doi.org/10.1159/000332595>
- Gold, M., Alderton, C., Zvartau-Hind, M., Egginton, S., Saunders, A.M., Irizarry, M., Craft, S., Landreth, G., Linnamägi, Ü., Sawchak, S., 2010. Rosiglitazone Monotherapy in Mild-to-Moderate Alzheimer's Disease: Results from a Randomized, Double-Blind, Placebo-Controlled Phase III Study. *Dementia and Geriatric Cognitive Disorders* 30, 131–146. <https://doi.org/10.1159/000318845>
- Goldfine, I.D., Williams, J.A., Bailey, A.C., Wong, K.Y., Iwamoto, Y., Yokono, K., Baba, S., Roth, R.A., 1984. Degradation of Insulin by Isolated Mouse Pancreatic Acini: Evidence for Cell Surface Protease Activity. *Diabetes* 33, 64–72. <https://doi.org/10.2337/diab.33.1.64>
- Gomez-Nicola, D., Perry, V.H., 2015. Microglial Dynamics and Role in the Healthy and Diseased Brain: A Paradigm of Functional Plasticity. *The Neuroscientist* 21, 169–184. <https://doi.org/10.1177/1073858414530512>
- Gong, C.-X., Liu, F., Iqbal, K., 2018. Multifactorial Hypothesis and Multi-Targets for Alzheimer's Disease. *Journal of Alzheimer's Disease* 64, S107–S117. <https://doi.org/10.3233/JAD-179921>
- González-Casimiro, C.M., Merino, B., Casanueva-Álvarez, E., Postigo-Casado, T., Cámara-Torres, P., Fernández-Díaz, C.M., Leissring, M.A., Cózar-Castellano, I., Perdomo, G., 2021. Modulation of Insulin Sensitivity by Insulin-Degrading Enzyme. *Biomedicines* 9, 86. <https://doi.org/10.3390/biomedicines9010086>
- Grassi, S., Giussani, P., Mauri, L., Prioni, S., Prinetti, A., 2021. Isolation and Analysis of Lipid Rafts from Neural Cells and Tissues, in: Bieberich, E. (Ed.), *Lipid Rafts, Methods in Molecular Biology*. Springer US, New York, NY, USA, pp. 1–25. https://doi.org/10.1007/978-1-0716-0814-2_1
- Gray, S.M., Barrett, E.J., 2018. Insulin transport into the brain. *American Journal of Physiology-Cell Physiology* 315, C125–C136. <https://doi.org/10.1152/ajpcell.00240.2017>
- Grodstein, F., Chen, J., Wilson, R.S., Manson, J.E., 2001. Type 2 Diabetes and Cognitive Function in Community-Dwelling Elderly Women. *Diabetes Care* 24, 1060–1065. <https://doi.org/10.2337/diacare.24.6.1060>

- Gu, H.F., Efendic, S., Nordman, S., Ostenson, C.-G., Brismar, K., Brookes, A.J., Prince, J.A., 2004. Quantitative Trait Loci Near the Insulin-Degrading Enzyme (IDE) Gene Contribute to Variation in Plasma Insulin Levels. *Diabetes* 53, 2137–2142. <https://doi.org/10.2337/diabetes.53.8.2137>
- Haas, C.B., de Carvalho, A.K., Muller, A.P., Eggen, B.J.L., Portela, L.V., 2020. Insulin activates microglia and increases COX-2/IL-1 β expression in young but not in aged hippocampus. *Brain Research* 1741, 146884. <https://doi.org/10.1016/j.brainres.2020.146884>
- Habib, P., Beyer, C., 2015. Regulation of brain microglia by female gonadal steroids. *The Journal of Steroid Biochemistry and Molecular Biology* 146, 3–14. <https://doi.org/10.1016/j.jsbmb.2014.02.018>
- Halle, A., Hornung, V., Petzold, G.C., Stewart, C.R., Monks, B.G., Reinheckel, T., Fitzgerald, K.A., Latz, E., Moore, K.J., Golenbock, D.T., 2008. The NALP3 inflammasome is involved in the innate immune response to amyloid- β . *Nature Immunology* 9, 857–865. <https://doi.org/10.1038/ni.1636>
- Hamel, F.G., Mahoney, M.J., Duckworth, W.C., 1991. Degradation of Intraendosomal Insulin by Insulin-Degrading Enzyme Without Acidification. *Diabetes* 40, 436–443. <https://doi.org/10.2337/diab.40.4.436>
- Hami, J., Sadr-Nabavi, A., Sankian, M., Haghiri, H., 2012. Sex differences and left–right asymmetries in expression of insulin and insulin-like growth factor-1 receptors in developing rat hippocampus. *Brain Structure and Function* 217, 293–302. <https://doi.org/10.1007/s00429-011-0358-1>
- Hammond, R., 2004. On the delay-dependent involvement of the hippocampus in object recognition memory. *Neurobiology of Learning and Memory* 82, 26–34. <https://doi.org/10.1016/j.nlm.2004.03.005>
- Hamshere, M.L., Holmans, P.A., Avramopoulos, D., Bassett, S.S., Blacker, D., Bertram, L., Wiener, H., Rochberg, N., Tanzi, R.E., Myers, A., Wavrant-De Vrièze, F., Go, R., Fallin, D., Lovestone, S., Hardy, J., Goate, A., O'Donovan, M., Williams, J., Owen, M.J., 2007. Genome-wide linkage analysis of 723 affected relative pairs with late-onset Alzheimer's disease. *Human Molecular Genetics* 16, 2703–2712. <https://doi.org/10.1093/hmg/ddm224>
- Hanahan, D., Weinberg, R.A., 2011. Hallmarks of Cancer: The Next Generation. *Cell* 144, 646–674. <https://doi.org/10.1016/j.cell.2011.02.013>
- Hanamsagar, R., Bilbo, S.D., 2016. Sex differences in neurodevelopmental and neurodegenerative disorders: Focus on microglial function and neuroinflammation during development. *The Journal of Steroid Biochemistry and Molecular Biology* 160, 127–133. <https://doi.org/10.1016/j.jsbmb.2015.09.039>
- Hansson Petersen, C.A., Alikhani, N., Behbahani, H., Wiehager, B., Pavlov, P.F., Alafuzoff, I., Leinonen, V., Ito, A., Winblad, B., Glaser, E., Ankarcrona, M., 2008. The amyloid β -peptide is imported into mitochondria via the TOM import machinery and localized to mitochondrial cristae. *Proceedings of the National Academy of Sciences* 105, 13145–13150. <https://doi.org/10.1073/pnas.0806192105>
- Hardy, J., Higgins, G., 1992. Alzheimer's disease: the amyloid cascade hypothesis. *Science* 256, 184–185. <https://doi.org/10.1126/science.1566067>
- Hartley, D.M., Walsh, D.M., Ye, C.P., Diehl, T., Vasquez, S., Vassilev, P.M., Teplow, D.B., Selkoe, D.J., 1999. Protofibrillar Intermediates of Amyloid β -Protein Induce Acute Electrophysiological Changes and Progressive Neurotoxicity in Cortical Neurons. *The Journal of Neuroscience* 19, 8876–8884.

- <https://doi.org/10.1523/JNEUROSCI.19-20-08876.1999>
- Hellwig, S., Brioschi, S., Dieni, S., Frings, L., Masuch, A., Blank, T., Biber, K., 2016. Altered microglia morphology and higher resilience to stress-induced depression-like behavior in CX3CR1-deficient mice. *Brain, Behavior, and Immunity* 55, 126–137. <https://doi.org/10.1016/j.bbi.2015.11.008>
- Heneka, M.T., Kummer, M.P., Latz, E., 2014. Innate immune activation in neurodegenerative disease. *Nature Reviews Immunology* 14, 463–477. <https://doi.org/10.1038/nri3705>
- Heneka, M.T., Kummer, M.P., Stutz, A., Delekate, A., Schwartz, S., Vieira-Saecker, A., Griep, A., Axt, D., Remus, A., Tzeng, T.-C., Gelpi, E., Halle, A., Korte, M., Latz, E., Golenbock, D.T., 2013. NLRP3 is activated in Alzheimer's disease and contributes to pathology in APP/PS1 mice. *Nature* 493, 674–678. <https://doi.org/10.1038/nature11729>
- Hicks, D.A., Nalivaeva, N.N., Turner, A.J., 2012. Lipid Rafts and Alzheimer's Disease: Protein-Lipid Interactions and Perturbation of Signaling. *Frontiers in Physiology* 3. <https://doi.org/10.3389/fphys.2012.00189>
- Hoang, D.T., Chernomor, O., von Haeseler, A., Minh, B.Q., Vinh, L.S., 2018. UFBoot2: Improving the Ultrafast Bootstrap Approximation. *Molecular Biology and Evolution* 35, 518–522. <https://doi.org/10.1093/molbev/msx281>
- Hong, M.-G., Reynolds, C., Gatz, M., Johansson, B., Palmer, J.C., Gu, H.F., Blennow, K., Kehoe, P.G., de Faire, U., Pedersen, N.L., Prince, J.A., 2008. Evidence that the gene encoding insulin degrading enzyme influences human lifespan. *Human Molecular Genetics* 17, 2370–2378. <https://doi.org/10.1093/hmg/ddn137>
- Hönigschmid, P., Bykova, N., Schneider, R., Ivankov, D., Frishman, D., 2018. Evolutionary Interplay between Symbiotic Relationships and Patterns of Signal Peptide Gain and Loss. *Genome Biology and Evolution* 10, 928–938. <https://doi.org/10.1093/gbe/evy049>
- Hooper, N.M., 1994. Families of zinc metalloproteases. *FEBS Letters* 354, 1–6. [https://doi.org/10.1016/0014-5793\(94\)01079-X](https://doi.org/10.1016/0014-5793(94)01079-X)
- Hoyer, S., 2006. The aging brain-The risk factor for sporadic Alzheimers disease (SAD). Cellular and molecular aspects., in: *Frontiers in Alzheimer's Disease Research*. Nova Science Publishers, New York, USA.
- Hsu, C.-C., Wahlqvist, M.L., Lee, M.-S., Tsai, H.-N., 2011. Incidence of Dementia is Increased in Type 2 Diabetes and Reduced by the Use of Sulfonylureas and Metformin. *Journal of Alzheimer's Disease* 24, 485–493. <https://doi.org/10.3233/JAD-2011-101524>
- Hughes, C.E., Nibbs, R.J.B., 2018. A guide to chemokines and their receptors. *The FEBS Journal* 285, 2944–2971. <https://doi.org/10.1111/febs.14466>
- Hulse, R.E., Ralat, L.A., Wei- Jen, T., 2009. Chapter 22 Structure, Function, and Regulation of Insulin-Degrading Enzyme, in: *Vitamins & Hormones*. Elsevier, pp. 635–648. [https://doi.org/10.1016/S0083-6729\(08\)00622-5](https://doi.org/10.1016/S0083-6729(08)00622-5)
- Imfeld, P., Bodmer, M., Jick, S.S., Meier, C.R., 2012. Metformin, Other Antidiabetic Drugs, and Risk of Alzheimer's Disease: A Population-Based Case-Control Study. *Journal of the American Geriatrics Society* 60, 916–921. <https://doi.org/10.1111/j.1532-5415.2012.03916.x>
- International Diabetes Federation, 2019. *IDF Diabetes Atlas*. Ninth Edition.

- Iwama, S., Sugimura, Y., Suzuki, Haruyuki, Suzuki, Hiromi, Murase, T., Ozaki, N., Nagasaki, H., Arima, H., Murata, Y., Sawada, M., Oiso, Y., 2011. Time-dependent changes in proinflammatory and neurotrophic responses of microglia and astrocytes in a rat model of osmotic demyelination syndrome. *Glia* 59, 452–462. <https://doi.org/10.1002/glia.21114>
- Iwata, H., Soga, Y., Meguro, M., Yoshizawa, S., Okada, Y., Iwamoto, Y., Yamashita, A., Takashiba, S., Nishimura, F., 2007. High glucose up-regulates lipopolysaccharide-stimulated inflammatory cytokine production via c-jun N-terminal kinase in the monocytic cell line THP-1. *Journal of Endotoxin Research* 13, 227–234. <https://doi.org/10.1177/0968051907082608>
- Janson, J., Laedtke, T., Parisi, J.E., O'Brien, P., Petersen, R.C., Butler, P.C., 2004. Increased Risk of Type 2 Diabetes in Alzheimer Disease. *Diabetes* 53, 474–481. <https://doi.org/10.2337/diabetes.53.2.474>
- Jeannin, P., Paolini, L., Adam, C., Delneste, Y., 2018. The roles of CSFs on the functional polarization of tumor-associated macrophages. *The FEBS Journal* 285, 680–699. <https://doi.org/10.1111/febs.14343>
- Jessen, N.A., Munk, A.S.F., Lundgaard, I., Nedergaard, M., 2015. The Glymphatic System: A Beginner's Guide. *Neurochemical Research* 40, 2583–2599. <https://doi.org/10.1007/s11064-015-1581-6>
- Ji, X., Cheng, K., Chen, Y., Lin, T., Cheung, C.H.A., Wu, C., Chiang, H., 2018. Dysfunction of different cellular degradation pathways contributes to specific β -amyloid₄₂-induced pathologies. *The FASEB Journal* 32, 1375–1387. <https://doi.org/10.1096/fj.201700199RR>
- Jin, X., Yamashita, T., 2016. Microglia in central nervous system repair after injury. *Journal of Biochemistry* 159, 491–496. <https://doi.org/10.1093/jb/mvw009>
- Joachim, C.L., Selkoe, D.J., 1992. The Seminal Role of β -Amyloid in the Pathogenesis of Alzheimer Disease. *Alzheimer Disease & Associated Disorders* 6, 7–34. <https://doi.org/10.1097/00002093-199205000-00003>
- Johnson, R.T., Breedlove, S.M., Jordan, C.L., 2008. Sex differences and laterality in astrocyte number and complexity in the adult rat medial amygdala. *The Journal of Comparative Neurology* 511, 599–609. <https://doi.org/10.1002/cne.21859>
- Junttila, I.S., 2018. Tuning the Cytokine Responses: An Update on Interleukin (IL)-4 and IL-13 Receptor Complexes. *Frontiers in Immunology* 9, 888. <https://doi.org/10.3389/fimmu.2018.00888>
- Kahn, S.E., Cooper, M.E., Del Prato, S., 2014. Pathophysiology and treatment of type 2 diabetes: perspectives on the past, present, and future. *The Lancet* 383, 1068–1083. [https://doi.org/10.1016/S0140-6736\(13\)62154-6](https://doi.org/10.1016/S0140-6736(13)62154-6)
- Kalyaanamoorthy, S., Minh, B.Q., Wong, T.K.F., von Haeseler, A., Jermin, L.S., 2017. ModelFinder: fast model selection for accurate phylogenetic estimates. *Nature Methods* 14, 587–589. <https://doi.org/10.1038/nmeth.4285>
- Karamohamed, S., Demissie, S., Volcjak, J., Liu, C., Heard-Costa, N., Liu, J., Shoemaker, C.M., Panhuysen, C.I., Meigs, J.B., Wilson, P., Atwood, L.D., Cupples, L.A., Herbert, A., 2003. Polymorphisms in the Insulin-Degrading Enzyme Gene Are Associated With Type 2 Diabetes in Men From the NHLBI Framingham Heart Study. *Diabetes* 52, 1562–1567. <https://doi.org/10.2337/diabetes.52.6.1562>
- Karran, E., Mercken, M., Strooper, B.D., 2011. The amyloid cascade hypothesis for Alzheimer's disease: an appraisal for the development of therapeutics. *Nature Reviews Drug Discovery* 10, 698–712. <https://doi.org/10.1038/nrd3505>

- Katoh, K., Rozewicki, J., Yamada, K.D., 2019. MAFFT online service: multiple sequence alignment, interactive sequence choice and visualization. *Briefings in Bioinformatics* 7.
- Katz, L.C., Shatz, C.J., 1996. Synaptic Activity and the Construction of Cortical Circuits. *Science* 274, 1133–1138. <https://doi.org/10.1126/science.274.5290.1133>
- Kehoe, P., Vrieze, F.W.-D., Crook, R., Wu, W.S., Holmans, P., Fenton, I., Spurlock, G., Norton, N., Williams, H., Williams, N., Lovestone, S., Perez-Tur, J., Hutton, M., Chartier-Harlin, M.-C., Shears, S., Roehl, K., Booth, J., Voorst, W.V., Ramic, D., Williams, J., Goate, A., Hardy, J., Owen, M.J., 1999. A full genome scan for late onset Alzheimer's disease. *Human Molecular Genetics* 8, 237–245.
- Kettenmann, H., Hanisch, U.-K., Noda, M., Verkhratsky, A., 2011. Physiology of Microglia. *Physiological Reviews* 91, 461–553. <https://doi.org/10.1152/physrev.00011.2010>
- Kettenmann, H., Kirchhoff, F., Verkhratsky, A., 2013. Microglia: New Roles for the Synaptic Stripper. *Neuron* 77, 10–18. <https://doi.org/10.1016/j.neuron.2012.12.023>
- Kim, S.-K., 2019. *Essentials of Marine Biotechnology*. Springer International Publishing, Cham, Switzerland. <https://doi.org/10.1007/978-3-030-20944-5>
- Kim, S.-K. (Ed.), 2015. *Springer Handbook of Marine Biotechnology*. Springer, Heidelberg, Germany. <https://doi.org/10.1007/978-3-642-53971-8>
- Kolberg, L., Raudvere, U., Kuzmin, I., Vilo, J., Peterson, H., 2020. gprofiler2 -- an R package for gene list functional enrichment analysis and namespace conversion toolset g:Profiler. *F1000Research* 9, 709. <https://doi.org/10.12688/f1000research.24956.2>
- Komleva, Y., Chernykh, A., Lopatina, O., Gorina, Y., Lokteva, I., Salmina, A., Gollasch, M., 2021. Inflamm-Aging and Brain Insulin Resistance: New Insights and Role of Life-style Strategies on Cognitive and Social Determinants in Aging and Neurodegeneration. *Frontiers in Neuroscience* 14, 618395. <https://doi.org/10.3389/fnins.2020.618395>
- Kono, R., Ikegaya, Y., Koyama, R., 2021. Phagocytic Glial Cells in Brain Homeostasis. *Cells* 10, 1348. <https://doi.org/10.3390/cells10061348>
- Kotter, M.R., 2006. Myelin Impairs CNS Remyelination by Inhibiting Oligodendrocyte Precursor Cell Differentiation. *Journal of Neuroscience* 26, 328–332. <https://doi.org/10.1523/JNEUROSCI.2615-05.2006>
- Kubota, Y., Takubo, K., Shimizu, T., Ohno, H., Kishi, K., Shibuya, M., Saya, H., Suda, T., 2009. M-CSF inhibition selectively targets pathological angiogenesis and lymphangiogenesis. *Journal of Experimental Medicine* 206, 1089–1102. <https://doi.org/10.1084/jem.20081605>
- Kulstad, J.J., McMillan, P.J., Leverenz, J.B., Cook, D.G., Green, P.S., Peskind, E.R., Wilkinson, C.W., Farris, W., Mehta, P.D., Craft, S., 2005. Effects of Chronic Glucocorticoid Administration on Insulin-Degrading Enzyme and Amyloid-Beta Peptide in the Aged Macaque. *Journal of Neuropathology & Experimental Neurology* 64, 139–146. <https://doi.org/10.1093/jnen/64.2.139>
- Kumar, S., Stecher, G., Suleski, M., Hedges, S.B., 2017. TimeTree: A Resource for Timelines, Timetrees, and Divergence Times. *Molecular Biology and Evolution* 34, 1812–1819. <https://doi.org/10.1093/molbev/msx116>
- Kuo, W.-L., Gehm, B.D., Rosner, M.R., 1990. Cloning and Expression of the cDNA for a Drosophila Insulin-

- Degrading Enzyme. *Molecular Endocrinology* 4, 1580–1591. <https://doi.org/10.1210/mend-4-10-1580>
- Kuo, W.L., Montag, A.G., Rosner, M.R., 1993. Insulin-degrading enzyme is differentially expressed and developmentally regulated in various rat tissues. *Endocrinology* 132, 604–611. <https://doi.org/10.1210/endo.132.2.7678795>
- Kupfer, S.R., Wilson, E.M., French, F.S., 1994. Androgen and glucocorticoid receptors interact with insulin degrading enzyme. *Journal of Biological Chemistry* 269, 20622–20628. [https://doi.org/10.1016/S0021-9258\(17\)32038-0](https://doi.org/10.1016/S0021-9258(17)32038-0)
- Kurochkin, I.V., 2001. Insulin-degrading enzyme: embarking on amyloid destruction. *Trends in Biochemical Sciences* 26, 421–425. [https://doi.org/10.1016/S0968-0004\(01\)01876-X](https://doi.org/10.1016/S0968-0004(01)01876-X)
- Kurochkin, I.V., Goto, S., 1994. Alzheimer's β -amyloid peptide specifically interacts with and is degraded by insulin degrading enzyme. *FEBS Letters* 345, 33–37. [https://doi.org/10.1016/0014-5793\(94\)00387-4](https://doi.org/10.1016/0014-5793(94)00387-4)
- Kutejová, E., Kučera, T., Matušková, A., Janata, J., 2013. Mitochondrial Processing Peptidase, in: *Handbook of Proteolytic Enzymes*. Elsevier, pp. 1435–1442. <https://doi.org/10.1016/B978-0-12-382219-2.00323-9>
- Kuusisto, J., Koivisto, K., Mykkanen, L., Helkala, E.-L., Vanhanen, M., Hanninen, T., Kervinen, K., Kesaniemi, Y.A., Riekkinen, P.J., Laakso, M., 1997. Association between features of the insulin resistance syndrome and alzheimer's disease independently of apolipoprotein e4 phenotype: cross sectional population based study. *BMJ* 315, 1045–1049. <https://doi.org/10.1136/bmj.315.7115.1045>
- Lamppa, G., Zhong, R., 2013. Chloroplast Stromal Processing Peptidase, in: *Handbook of Proteolytic Enzymes*. Elsevier, pp. 1442–1447. <https://doi.org/10.1016/B978-0-12-382219-2.00324-0>
- Lee, C.Y.D., Landreth, G.E., 2010. The role of microglia in amyloid clearance from the AD brain. *Journal of Neural Transmission* 117, 949–960. <https://doi.org/10.1007/s00702-010-0433-4>
- Lee, S.C., Liu, W., Roth, P., Dickson, D.W., Berman, J.W., Brosnan, C.F., 1993. Macrophage colony-stimulating factor in human fetal astrocytes and microglia. Differential regulation by cytokines and lipopolysaccharide, and modulation of class II MHC on microglia. *Journal of Immunology (Baltimore, Md.: 1950)* 150, 594–604.
- Lehnardt, S., 2009. Innate immunity and neuroinflammation in the CNS: The role of microglia in Toll-like receptor-mediated neuronal injury. *Glia* 58, 253–263. <https://doi.org/10.1002/glia.20928>
- Leibson, C.L., Rocca, W.A., Hanson, V.A., Cha, R., Kokmen, E., O'Brien, P.C., Palumbo, P.J., 1997. Risk of Dementia among Persons with Diabetes Mellitus: A Population-based Cohort Study. *American Journal of Epidemiology* 145, 301–308. <https://doi.org/10.1093/oxfordjournals.aje.a009106>
- Leissring, M.A., 2021. Insulin-Degrading Enzyme: Paradoxes and Possibilities. *Cells* 10, 2445. <https://doi.org/10.3390/cells10092445>
- Leissring, M.A., Farris, W., Chang, A.Y., Walsh, D.M., Wu, X., Sun, X., Frosch, M.P., Selkoe, D.J., 2003. Enhanced Proteolysis of β -Amyloid in APP Transgenic Mice Prevents Plaque Formation, Secondary Pathology, and Premature Death. *Neuron* 40, 1087–1093. [https://doi.org/10.1016/S0896-6273\(03\)00787-6](https://doi.org/10.1016/S0896-6273(03)00787-6)
- Leissring, M.A., Farris, W., Wu, X., Christodoulou, D.C., Haigis, M.C., Guarente, L., Selkoe, D.J., 2004. Alternative translation initiation generates a novel isoform of insulin-degrading enzyme targeted to mitochondria. *Biochemical Journal* 383, 439–446. <https://doi.org/10.1042/BJ20041081>

- Leissring, M.A., González-Casimiro, C.M., Merino, B., Suire, C.N., Perdomo, G., 2021. Targeting Insulin-Degrading Enzyme in Insulin Clearance. *International Journal of Molecular Sciences* 22, 2235. <https://doi.org/10.3390/ijms22052235>
- Lenz, K.M., McCarthy, M.M., 2015. A Starring Role for Microglia in Brain Sex Differences. *The Neuroscientist* 21, 306–321. <https://doi.org/10.1177/1073858414536468>
- Li, H.-Q., Chen, C., Dou, Y., Wu, H.-J., Liu, Y. -j., Lou, H.-F., Zhang, J.-M., Li, X.-M., Wang, H., Duan, S., 2013. P2Y4 Receptor-Mediated Pinocytosis Contributes to Amyloid Beta-Induced Self-Uptake by Microglia. *Molecular and Cellular Biology* 33, 4282–4293. <https://doi.org/10.1128/MCB.00544-13>
- Li, M.-F., Zhang, R., Li, T.-T., Chen, M.-Y., Li, L.-X., Lu, J.-X., Jia, W.-P., 2016. High Glucose Increases the Expression of Inflammatory Cytokine Genes in Macrophages Through H3K9 Methyltransferase Mechanism. *Journal of Interferon & Cytokine Research* 36, 48–61. <https://doi.org/10.1089/jir.2014.0172>
- Li, P., Kuo, W.-L., Yousef, M., Rosner, M.R., Tang, W.-J., 2006. The C-terminal domain of human insulin degrading enzyme is required for dimerization and substrate recognition. *Biochemical and Biophysical Research Communications* 343, 1032–1037. <https://doi.org/10.1016/j.bbrc.2006.03.083>
- Li, X., Leng, S., Song, D., 2015. Link between type 2 diabetes and Alzheimer's disease: from epidemiology to mechanism and treatment. *Clinical Interventions in Aging* 549. <https://doi.org/10.2147/CIA.S74042>
- Liao, Y., Smyth, G.K., Shi, W., 2014. featureCounts: an efficient general purpose program for assigning sequence reads to genomic features. *Bioinformatics* 30, 923–930. <https://doi.org/10.1093/bioinformatics/btt656>
- Limanaqi, F., Biagioni, F., Gambardella, S., Familiari, P., Frati, A., Fornai, F., 2020. Promiscuous Roles of Autophagy and Proteasome in Neurodegenerative Proteinopathies. *International Journal of Molecular Sciences* 21, 3028. <https://doi.org/10.3390/ijms21083028>
- Lin, J., Kong, Q., Hao, W., Hu, W., 2020. High glucose contributes to the polarization of peritoneal macrophages to the M2 phenotype in vivo and in vitro. *Molecular Medicine Reports* 22, 127–134. <https://doi.org/10.3892/mmr.2020.11130>
- Lin, W.-J., Wu, T.-Y., Su, T.-R., Wen, Z.-H., Chen, J.-J., Fang, L.-S., Wu, Y.-C., Sung, P.-J., 2015. Terpenoids from the Octocoral *Sinularia gaweli*. *International Journal of Molecular Sciences* 16, 19508–19517. <https://doi.org/10.3390/ijms160819508>
- Linnartz-Gerlach, B., Mathews, M., Neumann, H., 2014. Sensing the neuronal glycocalyx by glial sialic acid binding immunoglobulin-like lectins. *Neuroscience* 275, 113–124. <https://doi.org/10.1016/j.neuroscience.2014.05.061>
- Liu, F., Arias-Vásquez, A., Slegers, K., Aulchenko, Y.S., Kayser, M., Sanchez-Juan, P., Feng, B.-J., Bertoli-Avella, A.M., van Swieten, J., Axenovich, T.I., Heutink, P., van Broeckhoven, C., Oostra, B.A., van Duijn, C.M., 2007. A Genomewide Screen for Late-Onset Alzheimer Disease in a Genetically Isolated Dutch Population. *The American Journal of Human Genetics* 81, 17–31. <https://doi.org/10.1086/518720>
- Liu, M., Wang, Z., Ren, M., Yang, X., Liu, B., Qi, H., Yu, M., Song, S., Chen, S., Liu, L., Zhang, Y., Zou, J., Zhu, W., Yin, Y., Luo, J., 2019. SIRT4 regulates PTEN stability through IDE in response to cellular stresses. *The FASEB Journal* 33, 5535–5547. <https://doi.org/10.1096/fj.201801987R>

- Liu, Y., Li, M., Zhang, Z., Ye, Y., Zhou, J., 2018. Role of microglia-neuron interactions in diabetic encephalopathy. *Ageing Research Reviews* 42, 28–39. <https://doi.org/10.1016/j.arr.2017.12.005>
- Livak, K.J., Schmittgen, T.D., 2001. Analysis of Relative Gene Expression Data Using Real-Time Quantitative PCR and the $2^{-\Delta\Delta CT}$ Method. *Methods* 25, 402–408. <https://doi.org/10.1006/meth.2001.1262>
- López-Acosta, J.F., Moreno-Amador, J.L., Jiménez-Palomares, M., Díaz-Marrero, A.R., Cueto, M., Perdomo, G., Cózar-Castellano, I., 2013. Epoxypukalide Induces Proliferation and Protects against Cytokine-Mediated Apoptosis in Primary Cultures of Pancreatic β -Cells. *PLoS ONE* 8, e52862. <https://doi.org/10.1371/journal.pone.0052862>
- López-Acosta, J.F., Villa-Pérez, P., Fernández-Díaz, C.M., Román, D. de L., Díaz-Marrero, A.R., Cueto, M., Perdomo, G., Cózar-Castellano, I., 2015. Protective effects of epoxypukalide on pancreatic β -cells and glucose metabolism in STZ-induced diabetic mice. *Islets* 7, e1078053. <https://doi.org/10.1080/19382014.2015.1078053>
- Love, M.I., Huber, W., Anders, S., 2014. Moderated estimation of fold change and dispersion for RNA-seq data with DESeq2. *Genome Biology* 15, 550. <https://doi.org/10.1186/s13059-014-0550-8>
- Lu, J., Wu, T., Zhang, B., Liu, S., Song, W., Qiao, J., Ruan, H., 2021. Types of nuclear localization signals and mechanisms of protein import into the nucleus. *Cell Communication and Signaling* 19, 60. <https://doi.org/10.1186/s12964-021-00741-y>
- Macauley, S.L., Stanley, M., Caesar, E.E., Yamada, S.A., Raichle, M.E., Perez, R., Mahan, T.E., Sutphen, C.L., Holtzman, D.M., 2015. Hyperglycemia modulates extracellular amyloid- β concentrations and neuronal activity in vivo. *Journal of Clinical Investigation* 125, 2463–2467. <https://doi.org/10.1172/JCI79742>
- Malito, E., Ralat, L.A., Manolopoulou, M., Tsay, J.L., Wadlington, N.L., Tang, W.-J., 2008. Molecular Bases for the Recognition of Short Peptide Substrates and Cysteine-Directed Modifications of Human Insulin-Degrading Enzyme. *Biochemistry* 47, 12822–12834. <https://doi.org/10.1021/bi801192h>
- Mandrekar, S., Jiang, Q., Lee, C.Y.D., Koenigsnecht-Talboo, J., Holtzman, D.M., Landreth, G.E., 2009. Microglia Mediate the Clearance of Soluble A through Fluid Phase Macropinocytosis. *Journal of Neuroscience* 29, 4252–4262. <https://doi.org/10.1523/JNEUROSCI.5572-08.2009>
- Mannix, R., Berglass, J., Berkner, J., Moleus, P., Qiu, J., Andrews, N., Gunner, G., Berglass, L., Jantzie, L.L., Robinson, S., Meehan, W.P., 2014. Chronic gliosis and behavioral deficits in mice following repetitive mild traumatic brain injury: Laboratory investigation. *Journal of Neurosurgery* 121, 1342–1350. <https://doi.org/10.3171/2014.7.JNS14272>
- Marlowe, L., Peila, R., Benke, K.S., Hardy, J., White, L.R., Launer, L.J., Myers, A., 2006. Insulin-Degrading Enzyme Haplotypes Affect Insulin Levels but Not Dementia Risk. *Neurodegenerative Diseases* 3, 320–326. <https://doi.org/10.1159/000097300>
- Masters, C.L., Multhaup, G., Simms, G., Martins, R.N., Beyreuther, K., 1985. Neuronal origin of a cerebral amyloid: neurofibrillary tangles of Alzheimer's disease contain the same protein as the amyloid of plaque cores and blood vessels. *The EMBO Journal* 4, 2757–2763.
- Matejuk, A., Vandenbark, A.A., Offner, H., 2021. Cross-Talk of the CNS With Immune Cells and Functions in Health and Disease. *Frontiers in Neurology* 12, 672455. <https://doi.org/10.3389/fneur.2021.672455>

- Mawuenyega, K.G., Sigurdson, W., Ovod, V., Munsell, L., Kasten, T., Morris, J.C., Yarasheski, K.E., Bateman, R.J., 2010. Decreased Clearance of CNS β -Amyloid in Alzheimer's Disease. *Science* 330, 1774–1774. <https://doi.org/10.1126/science.1197623>
- McClellan, P.L., Parthasarathy, V., Faivre, E., Holscher, C., 2011. The Diabetes Drug Liraglutide Prevents Degenerative Processes in a Mouse Model of Alzheimer's Disease. *Journal of Neuroscience* 31, 6587–6594. <https://doi.org/10.1523/JNEUROSCI.0529-11.2011>
- Meigs, J.B., Panhuysen, C.I.M., Myers, R.H., Wilson, P.W.F., Cupples, L.A., 2002. A Genome-Wide Scan for Loci Linked to Plasma Levels of Glucose and HbA1c in a Community-Based Sample of Caucasian Pedigrees: The Framingham Offspring Study. *Diabetes* 51, 833–840. <https://doi.org/10.2337/diabetes.51.3.833>
- Meldolesi, J., 2018. Exosomes and Ectosomes in Intercellular Communication. *Current Biology* 28, R435–R444. <https://doi.org/10.1016/j.cub.2018.01.059>
- Mendiola, A.S., Cardona, A.E., 2018. The IL-1 β phenomena in neuroinflammatory diseases. *Journal of Neural Transmission* 125, 781–795. <https://doi.org/10.1007/s00702-017-1732-9>
- Merino, B., Fernández-Díaz, C.M., Parrado-Fernández, C., González-Casimiro, C.M., Postigo-Casado, T., Lobatón, C.D., Leissring, M.A., Cózar-Castellano, I., Perdomo, G., 2020. Hepatic insulin-degrading enzyme regulates glucose and insulin homeostasis in diet-induced obese mice. *Metabolism* 113, 154352. <https://doi.org/10.1016/j.metabol.2020.154352>
- Miller, B.C., Eckman, E.A., Sambamurti, K., Dobbs, N., Chow, K.M., Eckman, C.B., Hersh, L.B., Thiele, D.L., 2003. Amyloid- β peptide levels in brain are inversely correlated with insulin activity levels in vivo. *Proceedings of the National Academy of Sciences* 100, 6221–6226. <https://doi.org/10.1073/pnas.1031520100>
- Miller, B.C., Thiele, D., Hersh, L.B., Cottam, G.L., 1996. A secreted peptidase involved in T cell β -endorphin metabolism. *Immunopharmacology* 31, 151–161. [https://doi.org/10.1016/0162-3109\(95\)00046-1](https://doi.org/10.1016/0162-3109(95)00046-1)
- Mills, C.D., Kincaid, K., Alt, J.M., Heilman, M.J., Hill, A.M., 2000. M-1/M-2 Macrophages and the Th1/Th2 Paradigm. *The Journal of Immunology* 164, 6166–6173. <https://doi.org/10.4049/jimmunol.164.12.6166>
- Miners, J.S., Barua, N., Kehoe, P.G., Gill, S., Love, S., 2011. β -Degradation Enzymes: Potential for Treatment of Alzheimer Disease. *Journal of Neuropathology & Experimental Neurology* 70, 16.
- Mizutani, T., Amano, N., Sasaki, H., Morimatsu, Y., Mori, H., Yoshimura, M., Yamanouchi, H., Hayakawa, K., Shimada, H., 1990. Senile dementia of Alzheimer type characterized by laminar neuronal loss exclusively in the hippocampus, parahippocampus and medial occipitotemporal cortex. *Acta Neuropathologica* 80, 575–580. <https://doi.org/10.1007/BF00307623>
- Moreno-Navarrete, J.M., Blasco, G., Puig, J., Biarnés, C., Rivero, M., Gich, J., Fernández-Aranda, F., Garre-Olmo, J., Ramió-Torrentà, L., Alberich-Bayarri, Á., García-Castro, F., Pedraza, S., Ricart, W., Fernández-Real, J.M., 2017. Neuroinflammation in obesity: circulating lipopolysaccharide-binding protein associates with brain structure and cognitive performance. *International Journal of Obesity* 41, 1627–1635. <https://doi.org/10.1038/ijo.2017.162>
- Mosher, K.I., Wyss-Coray, T., 2014. Microglial dysfunction in brain aging and Alzheimer's disease. *Biochemical Pharmacology* 88, 594–604. <https://doi.org/10.1016/j.bcp.2014.01.008>

- Mosmann, T., 1983. Rapid colorimetric assay for cellular growth and survival: Application to proliferation and cytotoxicity assays. *Journal of Immunological Methods* 65, 55–63. [https://doi.org/10.1016/0022-1759\(83\)90303-4](https://doi.org/10.1016/0022-1759(83)90303-4)
- Muller, M., Tang, M.-X., Schupf, N., Manly, J.J., Mayeux, R., Luchsinger, J.A., 2007. Metabolic Syndrome and Dementia Risk in a Multiethnic Elderly Cohort. *Dementia and Geriatric Cognitive Disorders* 24, 185–192. <https://doi.org/10.1159/000105927>
- Murtaj, V., Belloli, S., Di Grigoli, G., Pannese, M., Ballarini, E., Rodriguez-Menendez, V., Marmioli, P., Cappelli, A., Masiello, V., Monterisi, C., Bellelli, G., Panina-Bordignon, P., Moresco, R.M., 2019. Age and Sex Influence the Neuro-inflammatory Response to a Peripheral Acute LPS Challenge. *Frontiers in Aging Neuroscience* 11. <https://doi.org/10.3389/fnagi.2019.00299>
- Myers, A., 2000. Susceptibility Locus for Alzheimer's Disease on Chromosome 10. *Science* 290, 2304–2305. <https://doi.org/10.1126/science.290.5500.2304>
- Mzhavia, N., Devi, L.A., 2013. Eupitirylisin, in: *Handbook of Proteolytic Enzymes*. Elsevier, pp. 1457–1459. <https://doi.org/10.1016/B978-0-12-382219-2.00327-6>
- Nakabeppu, Y., Ninomiya, T. (Eds.), 2019. Diabetes Mellitus: A risk factor for Alzheimer's Disease, *Advances in Experimental Medicine and Biology*. Springer Singapore, Singapore. <https://doi.org/10.1007/978-981-13-3540-2>
- Naslund, J., Haroutunian, V., Mohs, R., Davis, K.L., Davies, P., Greengard, P., Buxbaum, J.D., 2000. Correlation between elevated levels of amyloid β -peptide in the brain and cognitive decline. *JAMA* 283, 1571–7. <https://doi.org/10.1001/jama.283.12.1571>
- Nasrabad, S.E., Rizvi, B., Goldman, J.E., Brickman, A.M., 2018. White matter changes in Alzheimer's disease: a focus on myelin and oligodendrocytes. *Acta Neuropathologica Communications* 6, 22. <https://doi.org/10.1186/s40478-018-0515-3>
- Nayak, D., Roth, T.L., McGavern, D.B., 2014. Microglia Development and Function. *Annual Review of Immunology* 32, 367–402. <https://doi.org/10.1146/annurev-immunol-032713-120240>
- Neher, J.J., Neniskyte, U., Zhao, J.-W., Bal-Price, A., Tolkovsky, A.M., Brown, G.C., 2011. Inhibition of Microglial Phagocytosis Is Sufficient To Prevent Inflammatory Neuronal Death. *The Journal of Immunology* 186, 4973–4983. <https://doi.org/10.4049/jimmunol.1003600>
- Neniskyte, U., Neher, J.J., Brown, G.C., 2011. Neuronal Death Induced by Nanomolar Amyloid β Is Mediated by Primary Phagocytosis of Neurons by Microglia. *Journal of Biological Chemistry* 286, 39904–39913. <https://doi.org/10.1074/jbc.M111.267583>
- Neth, B.J., Craft, S., 2017. Insulin Resistance and Alzheimer's Disease: Bioenergetic Linkages. *Frontiers in Aging Neuroscience* 9. <https://doi.org/10.3389/fnagi.2017.00345>
- Nguyen, L.-T., Schmidt, H.A., von Haeseler, A., Minh, B.Q., 2015. IQ-TREE: A Fast and Effective Stochastic Algorithm for Estimating Maximum-Likelihood Phylogenies. *Molecular Biology and Evolution* 32, 268–274. <https://doi.org/10.1093/molbev/msu300>
- NIH's National Institute on Aging, 2015. Alzheimer's disease Summit 2015.

- Nimmerjahn, A., Kirchhoff, F., Helmchen, F., 2005. Resting Microglial Cells Are Highly Dynamic Surveillants of Brain Parenchyma in Vivo. *Science* 308, 1314–8. <https://doi.org/10.1126/science.1110647>.
- Nixon, R.A., 2017. Amyloid precursor protein and endosomal- lysosomal dysfunction in Alzheimer's disease: inseparable partners in a multifactorial disease. *The FASEB Journal* 31, 2729–2743. <https://doi.org/10.1096/fj.201700359>
- Núñez, L., Calvo-Rodríguez, M., Caballero, E., García-Durillo, M., Villalobos, C., 2018. Neurotoxic Ca²⁺ Signaling Induced by Amyloid- β Oligomers in Aged Hippocampal Neurons In Vitro, in: Sigurdsson, E.M., Calero, M., Gasset, M. (Eds.), *Amyloid Proteins, Methods in Molecular Biology*. Springer New York, New York, NY, pp. 341–354. https://doi.org/10.1007/978-1-4939-7816-8_20
- Ohyagi, Y., Miyoshi, K., Nakamura, N., 2019. Therapeutic Strategies for Alzheimer's Disease in the View of Diabetes Mellitus, in: Nakabeppu, Y., Ninomiya, T. (Eds.), *Diabetes Mellitus, Advances in Experimental Medicine and Biology*. Springer Singapore, Singapore, pp. 227–248. https://doi.org/10.1007/978-981-13-3540-2_11
- Okonechnikov, K., Conesa, A., García-Alcalde, F., 2015. Qualimap 2: advanced multi-sample quality control for high-throughput sequencing data. *Bioinformatics* 31, 566–571. <https://doi.org/10.1093/bioinformatics/btv566>
- Olmos-Alonso, A., Schettters, S.T.T., Sri, S., Askew, K., Mancuso, R., Vargas-Caballero, M., Holscher, C., Perry, V.H., Gomez-Nicola, D., 2016. Pharmacological targeting of CSF1R inhibits microglial proliferation and prevents the progression of Alzheimer's-like pathology. *Brain* 139, 891–907. <https://doi.org/10.1093/brain/awv379>
- Orihuela, R., McPherson, C.A., Harry, G.J., 2016. Microglial M1/M2 polarization and metabolic states. *British Journal of Pharmacology* 173, 649–665. <https://doi.org/10.1111/bph.13139>
- Osborne, B.F., Turano, A., Schwarz, J.M., 2018. Sex differences in the neuroimmune system. *Current Opinion in Behavioral Sciences* 23, 118–123. <https://doi.org/10.1016/j.cobeha.2018.05.007>
- Ott, A., Stolk, R.P., Hofman, A., van Harskamp, F., Grobbee, D.E., Breteler, M.M.B., 1996. Association of diabetes mellitus and dementia: The Rotterdam Study. *Diabetologia* 39, 1392–1397. <https://doi.org/10.1007/s001250050588>
- Ott, A., Stolk, R.P., van Harskamp, F., Pols, H.A.P., Hofman, A., Breteler, M.M.B., 1999. Diabetes mellitus and the risk of dementia: The Rotterdam Study. *Neurology* 53, 1937–1937. <https://doi.org/10.1212/WNL.53.9.1937>
- Pan, X., Zhu, Y., Lin, N., Zhang, J., Ye, Q., Huang, H., Chen, X., 2011. Microglial phagocytosis induced by fibrillar β -amyloid is attenuated by oligomeric β -amyloid: implications for Alzheimer's disease. *Molecular Neurodegeneration* 6, 45. <https://doi.org/10.1186/1750-1326-6-45>
- Paolicelli, R.C., Bolasco, G., Pagani, F., Maggi, L., Scianni, M., Panzanelli, P., Giustetto, M., Ferreira, T.A., Guiducci, E., Dumas, L., Ragozzino, D., Gross, C.T., 2011. Synaptic Pruning by Microglia Is Necessary for Normal Brain Development. *Science* 333, 1456–1458. <https://doi.org/10.1126/science.1202529>
- Park, S.-K., Solomon, D., Vartanian, T., 2001. Growth Factor Control of CNS Myelination. *Developmental Neuroscience* 23, 327–337. <https://doi.org/10.1159/000048716>
- Pascua-Maestro, R., Corraliza-Gomez, M., Diez-Hermano, S., Perez-Segurado, C., Ganfornina, M.D., Sanchez,

- D., 2018. The MTT-formazan assay: Complementary technical approaches and in vivo validation in *Drosophila* larvae. *Acta Histochemica* 120, 179–186. <https://doi.org/10.1016/j.acthis.2018.01.006>
- Pérez, A., Morelli, L., Cresto, J.C., Castaño, E.M., 2000. Degradation of Soluble Amyloid β -Peptides 1-40, 1-42, and the Dutch Variant 1-40Q by Insulin Degrading Enzyme from Alzheimer Disease and Control Brains. *Neurochemical Research* 9.
- Pflanzner, T., Janko, M.C., André-Dohmen, B., Reuss, S., Weggen, S., Roebroek, A.J.M., Kuhlmann, C.R.W., Pietrzik, C.U., 2011. LRP1 mediates bidirectional transcytosis of amyloid- β across the blood-brain barrier. *Neurobiology of Aging* 32, 2323.e1-2323.e11. <https://doi.org/10.1016/j.neurobiolaging.2010.05.025>
- Picone, P., Nuzzo, D., Caruana, L., Scafidi, V., Di Carlo, M., 2014. Mitochondrial Dysfunction: Different Routes to Alzheimer's Disease Therapy. *Oxidative Medicine and Cellular Longevity* 2014, 1–11. <https://doi.org/10.1155/2014/780179>
- Pike, C.J., Walencewicz, A.J., Glabe, C.G., Cotman, C.W., 1991. In vitro aging of β -amyloid protein causes peptide aggregation and neurotoxicity. *Brain Research* 563, 311–314.
- Pike, J., Burdick, D., Walencewicz, J., Glabe, G., Cotman, C.W., Research, I., 1993. Neurodegeneration Induced by β -Amyloid Peptides in vitro: The Role of Peptide Assembly State. *The Journal of Neuroscience* 13, 1676–1687.
- Pivovarova, O., Gögebakan, Ö., Pfeiffer, A.F.H., Rudovich, N., 2009. Glucose inhibits the insulin-induced activation of the insulin-degrading enzyme in HepG2 cells. *Diabetologia* 52, 1656–1664. <https://doi.org/10.1007/s00125-009-1350-7>
- Pivovarova, O., Höhn, A., Grune, T., Pfeiffer, A.F.H., Rudovich, N., 2016. Insulin-degrading enzyme: new therapeutic target for diabetes and Alzheimer's disease? *Annals of Medicine* 48, 614–624. <https://doi.org/10.1080/07853890.2016.1197416>
- Pivovarova, O., von Loeffelholz, C., Ilkavets, I., Sticht, C., Zhuk, S., Murahovschi, V., Lukowski, S., Döcke, S., Kriebel, J., de las Heras Gala, T., Malashicheva, A., Kostareva, A., Lock, J.F., Stockmann, M., Grallert, H., Gretz, N., Dooley, S., Pfeiffer, A.F., Rudovich, N., 2015. Modulation of insulin degrading enzyme activity and liver cell proliferation. *Cell Cycle* 14, 2293–2300. <https://doi.org/10.1080/15384101.2015.1046647>
- Pizzino, G., Irrera, N., Cucinotta, M., Pallio, G., Mannino, F., Arcoraci, V., Squadrito, F., Altavilla, D., Bitto, A., 2017. Oxidative Stress: Harms and Benefits for Human Health. *Oxidative Medicine and Cellular Longevity* 2017, 1–13. <https://doi.org/10.1155/2017/8416763>
- Plassman, B.L., Langa, K.M., McCammon, R.J., Fisher, G.G., Potter, G.G., Burke, J.R., Steffens, D.C., Foster, N.L., Giordani, B., Unverzagt, F.W., Welsh-Bohmer, K.A., Heeringa, S.G., Weir, D.R., Wallace, R.B., 2011. Incidence of dementia and cognitive impairment, not dementia in the united states. *Annals of Neurology* 70, 418–426. <https://doi.org/10.1002/ana.22362>
- Pons, V., Rivest, S., 2018. New Therapeutic Avenues of mCSF for Brain Diseases and Injuries. *Frontiers in Cellular Neuroscience* 12, 499. <https://doi.org/10.3389/fncel.2018.00499>
- Porro, C., Cianciulli, A., Panaro, M.A., 2020. The Regulatory Role of IL-10 in Neurodegenerative Diseases. *Biomolecules* 10, 1017. <https://doi.org/10.3390/biom10071017>

- Prince, J.A., Feuk, L., Gu, H.F., Johansson, B., Gatz, M., Blennow, K., Brookes, A.J., 2003. Genetic variation in a haplotype block spanning IDE influences Alzheimer disease. *Human Mutation* 22, 363–371. <https://doi.org/10.1002/humu.10282>
- Prinz, M., Priller, J., 2014. Microglia and brain macrophages in the molecular age: from origin to neuropsychiatric disease. *Nature Reviews Neuroscience* 15, 300–312. <https://doi.org/10.1038/nrn3722>
- Qiu, W., Folstein, M., 2006. Insulin, insulin-degrading enzyme and amyloid- β peptide in Alzheimer's disease: review and hypothesis. *Neurobiology of Aging* 27, 190–198. <https://doi.org/10.1016/j.neurobiolaging.2005.01.004>
- Qiu, W.Q., Walsh, D.M., Ye, Z., Vekrellis, K., Zhang, J., Podlisny, M.B., Rosner, M.R., Safavi, A., Hersh, L.B., Selkoe, D.J., 1998. Insulin-degrading Enzyme Regulates Extracellular Levels of Amyloid β -Protein by Degradation. *Journal of Biological Chemistry* 273, 32730–32738. <https://doi.org/10.1074/jbc.273.49.32730>
- Qiu, W.Q., Ye, Z., Kholodenko, D., Seubert, P., Selkoe, D.J., 1997. Degradation of Amyloid β -Protein by a Metalloprotease Secreted by Microglia and Other Neural and Non-neural Cells. *The Journal of Biological Chemistry* 272, 6641–6646.
- Quan, Y., Jiang, C., Xue, B., Zhu, S., Wang, X., 2011. High glucose stimulates TNF α and MCP-1 expression in rat microglia via ROS and NF- κ B pathways. *Acta Pharmacologica Sinica* 32, 188–193. <https://doi.org/10.1038/aps.2010.174>
- Quarta, A., Berneman, Z., Ponsaerts, P., 2020. Neuroprotective modulation of microglia effector functions following priming with interleukin 4 and 13: current limitations in understanding their mode-of-action. *Brain, Behavior, and Immunity* 88, 856–866. <https://doi.org/10.1016/j.bbi.2020.03.023>
- Raj, D.D.A., Jaarsma, D., Holtman, I.R., Olah, M., Ferreira, F.M., Schaafsma, W., Brouwer, N., Meijer, M.M., de Waard, M.C., van der Pluijm, I., Brandt, R., Kreft, K.L., Laman, J.D., de Haan, G., Biber, K.P.H., Hoeijmakers, J.H.J., Eggen, B.J.L., Boddeke, H.W.G.M., 2014. Priming of microglia in a DNA-repair deficient model of accelerated aging. *Neurobiology of Aging* 35, 2147–2160. <https://doi.org/10.1016/j.neurobiolaging.2014.03.025>
- Ransohoff, R.M., 2016. A polarizing question: do M1 and M2 microglia exist? *Nature Neuroscience* 19, 987–991. <https://doi.org/10.1038/nn.4338>
- Raschke, W.C., Baird, S., Ralph, P., Nakoinz, I., 1978. Functional macrophage cell lines transformed by abelson leukemia virus. *Cell* 15, 261–267. [https://doi.org/10.1016/0092-8674\(78\)90101-0](https://doi.org/10.1016/0092-8674(78)90101-0)
- Rawlings, N.D., Salvesen, G. (Eds.), 2013. *Handbook of proteolytic enzymes*, Third edition. ed. Elsevier/AP, Amsterdam.
- Rawlings, N.D., Waller, M., Barrett, A.J., Bateman, A., 2014. MEROPS : the database of proteolytic enzymes, their substrates and inhibitors. *Nucleic Acids Research* 42, D503–D509. <https://doi.org/10.1093/nar/gkt953>
- Reis, A., Spickett, C.M., 2012. Chemistry of phospholipid oxidation. *Biochimica et Biophysica Acta (BBA) - Biomembranes* 1818, 2374–2387. <https://doi.org/10.1016/j.bbamem.2012.02.002>
- Rezaie, P., Dean, A., Male, D., Ulfig, N., 2005. Microglia in the Cerebral Wall of the Human Telencephalon at Second Trimester. *Cerebral Cortex* 15, 938–949. <https://doi.org/10.1093/cercor/bhh194>
- Ries, M., Sastre, M., 2016. Mechanisms of A β Clearance and Degradation by Glial Cells. *Frontiers in Aging*

- Neuroscience 8. <https://doi.org/10.3389/fnagi.2016.00160>
- Rio-Hortega, P., 1919a. El “‘Tercer Elemento’” de los Centros Nerviosos. I. La Microglía en Estado Normal. *Boletín de la Sociedad Española de Biología VIII*, 67–82.
- Rio-Hortega, P., 1919b. El “‘Tercer Elemento de los Centros Nerviosos’”. III. Naturaleza Probable de la Microglía. *Boletín de la Sociedad Española de Biología VIII*, 108–121.
- Risner, M., Saunders, A., Altman, J., Ormandy, G., Craft, S., Foley, I., Zvartau-Hind, M., Hosford, D., Roses, A., 2006. Efficacy of rosiglitazone in a genetically defined population with mild-to-moderate Alzheimer’s disease. *Pharmacogenomics J* 6, 246–254. <https://doi.org/10.1038/sj.tpj.6500369>
- Robinson, J.T., 2011. Integrative genomics viewer. *Nature Biotechnology* 29, 24–6. <https://doi.org/10.1038/nbt.1754>.
- Roth, M., Tomlinson, B.E., Blessed, G., 1966. Correlation between Scores for Dementia and Counts of ‘Senile Plaques’ in Cerebral Grey Matter of Elderly Subjects. *Nature* 209, 109–110. <https://doi.org/10.1038/209109a0>
- Roth, R.A., 2013. Pitrilysin, in: *Handbook of Proteolytic Enzymes*. Elsevier, pp. 1412–1414. <https://doi.org/10.1016/B978-0-12-382219-2.00318-5>
- Rothaug, M., Becker-Pauly, C., Rose-John, S., 2016. The role of interleukin-6 signaling in nervous tissue. *Biochimica et Biophysica Acta (BBA) - Molecular Cell Research* 1863, 1218–1227. <https://doi.org/10.1016/j.bbamcr.2016.03.018>
- Runyan, K., Duckworth, W.C., Kitabchi, A.E., Huff, G., 1979. The Effect of Age on Insulin-degrading Activity in Rat Tissue. *Diabetes* 28, 324–5. <https://doi.org/10.2337/diab.28.4.324>
- Sadagurski, M., White, M.F., 2013. Integrating Metabolism and Longevity Through Insulin and IGF1 Signaling. *Endocrinology and Metabolism Clinics of North America* 42, 127–148. <https://doi.org/10.1016/j.ecl.2012.11.008>
- Sadeghi, A., Hami, J., Razavi, S., Esfandiary, E., Hejazi, Z., 2016. The effect of diabetes mellitus on apoptosis in hippocampus: Cellular and molecular aspects. *International Journal of Preventive Medicine* 7, 57. <https://doi.org/10.4103/2008-7802.178531>
- Safaiyan, S., Kannaiyan, N., Snaidero, N., Brioschi, S., Biber, K., Yona, S., Edinger, A.L., Jung, S., Rossner, M.J., Simons, M., 2016. Age-related myelin degradation burdens the clearance function of microglia during aging. *Nature Neuroscience* 19, 995–998. <https://doi.org/10.1038/nn.4325>
- Sagare, A., Deane, R., Bell, R.D., Johnson, B., Hamm, K., Pendu, R., Marky, A., Lenting, P.J., Wu, Z., Zarcone, T., Goate, A., Mayo, K., Perlmutter, D., Coma, M., Zhong, Z., Zlokovic, B.V., 2007. Clearance of amyloid- β by circulating lipoprotein receptors. *Nature Medicine* 13, 1029–1031. <https://doi.org/10.1038/nm1635>
- Sartorius, T., Peter, A., Heni, M., Maetzler, W., Fritsche, A., Häring, H.-U., Hennige, A.M., 2015. The Brain Response to Peripheral Insulin Declines with Age: A Contribution of the Blood-Brain Barrier? *PLoS ONE* 10, e0126804. <https://doi.org/10.1371/journal.pone.0126804>
- Sastre, M., Klockgether, T., Heneka, M.T., 2006. Contribution of inflammatory processes to Alzheimer’s disease: molecular mechanisms. *International Journal of Developmental Neuroscience* 24, 167–176. <https://doi.org/10.1016/j.ijdevneu.2005.11.014>

- Saura, J., Tusell, J.M., Serratos, J., 2003. High-yield isolation of murine microglia by mild trypsinization. *Glia* 44, 183–189. <https://doi.org/10.1002/glia.10274>
- Savage, M.J., Trusko, S.P., Howland, D.S., Pinsker, L.R., Mistretta, S., Reaume, A.G., Greenberg, B.D., Siman, R., Scott, R.W., 1998. Turnover of Amyloid β -Protein in Mouse Brain and Acute Reduction of Its Level by Phorbol Ester. *The Journal of Neuroscience* 18, 1743–1752. <https://doi.org/10.1523/JNEUROSCI.18-05-01743.1998>.
- Schafer, D.P., Lehrman, E.K., Kautzman, A.G., Koyama, R., Mardinly, A.R., Yamasaki, R., Ransohoff, R.M., Greenberg, M.E., Barres, B.A., Stevens, B., 2012. Microglia Sculpt Postnatal Neural Circuits in an Activity and Complement-Dependent Manner. *Neuron* 74, 691–705. <https://doi.org/10.1016/j.neuron.2012.03.026>
- Scheibel, A.B., Duong, T., Jacobs, R., 1989. Alzheimer's Disease as a Capillary Dementia. *Annals of Medicine* 21, 103–107. <https://doi.org/10.3109/07853898909149194>
- Scheltens, P., Blennow, K., Breteler, M.M.B., de Strooper, B., Frisoni, G.B., Salloway, S., Van der Flier, W.M., 2016. Alzheimer's disease. *The Lancet* 388, 505–517. [https://doi.org/10.1016/S0140-6736\(15\)01124-1](https://doi.org/10.1016/S0140-6736(15)01124-1)
- Schroeder, A., Mueller, O., Stocker, S., Salowsky, R., Leiber, M., Gassmann, M., Lightfoot, S., Menzel, W., Granzow, M., Ragg, T., 2006. The RIN: an RNA integrity number for assigning integrity values to RNA measurements. *BMC Molecular Biology* 7, 3. <https://doi.org/10.1186/1471-2199-7-3>
- Schubert, M., Gautam, D., Surjo, D., Ueki, K., Baudler, S., Schubert, D., Kondo, T., Alber, J., Galldiks, N., Kustermann, E., Arndt, S., Jacobs, A.H., Krone, W., Kahn, C.R., Bruning, J.C., 2004. Role for neuronal insulin resistance in neurodegenerative diseases. *Proceedings of the National Academy of Sciences* 101, 3100–3105. <https://doi.org/10.1073/pnas.0308724101>
- Seabright, P.J., Smith, G.D., 1996. The characterization of endosomal insulin degradation intermediates and their sequence of production. *Biochemical Journal* 320, 947–956. <https://doi.org/10.1042/bj3200947>
- Selkoe, D.J., 2001. Clearing the Brain's Amyloid Cobwebs. *Neuron* 32, 177–180. [https://doi.org/10.1016/S0896-6273\(01\)00475-5](https://doi.org/10.1016/S0896-6273(01)00475-5)
- Selkoe, D.J., Hardy, J., 2016. The amyloid hypothesis of Alzheimer's disease at 25 years. *EMBO Molecular Medicine* 8, 595–608. <https://doi.org/10.15252/emmm.201606210>
- Seshadri, S., Wolf, P.A., Beiser, A., Au, R., McNulty, K., White, R., D'Agostino, R.B., 1997. Lifetime risk of dementia and Alzheimer's disease: The impact of mortality on risk estimates in the Framingham Study. *Neurology* 49, 1498–1504. <https://doi.org/10.1212/WNL.49.6.1498>
- Seubert, P., Vigo-Pelfrey, C., Esch, F., Lee, M., Dovey, H., Davis, D., Sinha, S., Schioesmacher, M., Whaley, J., Swindlehurst, C., McCormack, R., Wolfert, R., Selkoe, D., Lieberburg, I., Schenk, D., 1992. Isolation and quantification of soluble Alzheimer's β -peptide from biological fluids. *Nature* 359, 325–327. <https://doi.org/10.1038/359325a0>
- Shanmugam, N., Reddy, M.A., Guha, M., Natarajan, R., 2003. High Glucose-Induced Expression of Proinflammatory Cytokine and Chemokine Genes in Monocytic Cells. *Diabetes* 52, 1256–1264. <https://doi.org/10.2337/diabetes.52.5.1256>
- Sharifi-Rad, M., Anil Kumar, N.V., Zucca, P., Varoni, E.M., Dini, L., Panzarini, E., Rajkovic, J., Tsouh Fokou,

- P.V., Azzini, E., Peluso, I., Prakash Mishra, A., Nigam, M., El Rayess, Y., Beyrouthy, M.E., Polito, L., Iriti, M., Martins, N., Martorell, M., Docea, A.O., Setzer, W.N., Calina, D., Cho, W.C., Sharifi-Rad, J., 2020. Lifestyle, Oxidative Stress, and Antioxidants: Back and Forth in the Pathophysiology of Chronic Diseases. *Frontiers in Physiology* 11, 694. <https://doi.org/10.3389/fphys.2020.00694>
- Shen, Y., Joachimiak, A., Rich Rosner, M., Tang, W.-J., 2006. Structures of human insulin-degrading enzyme reveal a new substrate recognition mechanism. *Nature* 443, 870–874. <https://doi.org/10.1038/nature05143>
- Sheng, J., Chen, W., Zhu, H.-J., 2015. The immune suppressive function of transforming growth factor- β (TGF- β) in human diseases. *Growth Factors* 33, 92–101. <https://doi.org/10.3109/08977194.2015.1010645>
- Shibata, M., Yamada, S., Kumar, S.R., Calero, M., Bading, J., Frangione, B., Holtzman, D.M., Miller, C.A., Strickland, D.K., Ghiso, J., Zlokovic, B.V., 2000. Clearance of Alzheimer's amyloid- β 1-40 peptide from brain by LDL receptor-related protein-1 at the blood-brain barrier. *Journal of Clinical Investigation* 106, 1489–1499. <https://doi.org/10.1172/JCI10498>
- Sierra, A., Abiega, O., Shahraz, A., Neumann, H., 2013. Janus-faced microglia: beneficial and detrimental consequences of microglial phagocytosis. *Frontiers in Cellular Neuroscience* 7. <https://doi.org/10.3389/fncel.2013.00006>
- Sierra, A., Encinas, J.M., Deudero, J.J.P., Chancey, J.H., Enikolopov, G., Overstreet-Wadiche, L.S., Tsirka, S.E., Maletic-Savatic, M., 2010. Microglia Shape Adult Hippocampal Neurogenesis through Apoptosis-Coupled Phagocytosis. *Cell Stem Cell* 7, 483–495. <https://doi.org/10.1016/j.stem.2010.08.014>
- Sierra, A., Paolicelli, R.C., Kettenmann, H., 2019. Cien Años de Microglía: Milestones in a Century of Microglial Research. *Trends in Neurosciences* 42, 778–792. <https://doi.org/10.1016/j.tins.2019.09.004>
- Sierra, A., Tremblay, M.-Å., Wake, H., 2014. Never-resting microglia: physiological roles in the healthy brain and pathological implications. *Frontiers in Cellular Neuroscience* 8. <https://doi.org/10.3389/fncel.2014.00240>
- Sinclair, A.J., Girling, A.J., Bayer, A.J., 2000. Cognitive dysfunction in older subjects with diabetes mellitus: impact on diabetes self-management and use of care services. *Diabetes Research and Clinical Practice* 50, 203–212. [https://doi.org/10.1016/S0168-8227\(00\)00195-9](https://doi.org/10.1016/S0168-8227(00)00195-9)
- Smith, J.A., Das, A., Ray, S.K., Banik, N.L., 2012. Role of pro-inflammatory cytokines released from microglia in neurodegenerative diseases. *Brain Research Bulletin* 87, 10–20. <https://doi.org/10.1016/j.brainresbull.2011.10.004>
- Sociedad Española de Diabetes, 2017. *Tratado de Diabetes Mellitus*, 2^a. ed.
- Son, S.M., Cha, M.-Y., Choi, Heesun, Kang, S., Choi, Hyunjung, Lee, M.-S., Park, S.A., Mook-Jung, I., 2016. Insulin-degrading enzyme secretion from astrocytes is mediated by an autophagy-based unconventional secretory pathway in Alzheimer disease. *Autophagy* 12, 784–800. <https://doi.org/10.1080/15548627.2016.1159375>
- Song, E.S., Jang, H., Guo, H.-F., Juliano, M.A., Juliano, L., Morris, A.J., Galperin, E., Rodgers, D.W., Hersh, L.B., 2017. Inositol phosphates and phosphoinositides activate insulin-degrading enzyme, while phosphoinositides also mediate binding to endosomes. *Proceedings of the National Academy of Sciences* 114, E2826–E2835. <https://doi.org/10.1073/pnas.1613447114>

- Song, E.-S., Juliano, M.A., Juliano, L., Hersh, L.B., 2003. Substrate Activation of Insulin-degrading Enzyme (Insulysin). *Journal of Biological Chemistry* 278, 49789–49794. <https://doi.org/10.1074/jbc.M308983200>
- Song, E.S., Rodgers, D.W., Hersh, L.B., 2018. Insulin-degrading enzyme is not secreted from cultured cells. *Scientific Reports* 8, 2335. <https://doi.org/10.1038/s41598-018-20597-6>
- Spielman, L., Bahniwal, M., Little, J., Walker, D., Klegeris, A., 2015. Insulin Modulates *In Vitro Secretion* of Cytokines and Cytotoxins by Human Glial Cells. *Current Alzheimer Research* 12, 684–693. <https://doi.org/10.2174/1567205012666150710104428>
- Spittau, B., 2017. Aging Microglia—Phenotypes, Functions and Implications for Age-Related Neurodegenerative Diseases. *Frontiers in Aging Neuroscience* 9, 194. <https://doi.org/10.3389/fnagi.2017.00194>
- Spittau, B., Dokalis, N., Prinz, M., 2020. The Role of TGF β Signaling in Microglia Maturation and Activation. *Trends in Immunology* 41, 836–848. <https://doi.org/10.1016/j.it.2020.07.003>
- Steen, E., Terry, B.M., J. Rivera, E., Cannon, J.L., Neely, T.R., Tavares, R., Xu, X.J., Wands, J.R., de la Monte, S.M., 2005. Impaired insulin and insulin-like growth factor expression and signaling mechanisms in Alzheimer’s disease – is this type 3 diabetes? *Journal of Alzheimer’s Disease* 7, 63–80. <https://doi.org/10.3233/JAD-2005-7107>
- Steneberg, P., Bernardo, L., Edfalk, S., Lundberg, L., Backlund, F., Östenson, C.-G., Edlund, H., 2013. The Type 2 Diabetes–Associated Gene *Irf1* Is Required for Insulin Secretion and Suppression of α -Synuclein Levels in β -Cells. *Diabetes* 62, 2004–14. <https://doi.org/10.2337/db12-1045>
- Stewart, R., Liolitsa, D., 1999. Type 2 diabetes mellitus, cognitive impairment and dementia. *Diabetic Medicine* 16, 93–112. <https://doi.org/10.1046/j.1464-5491.1999.00027.x>
- Stine, W.B., Dahlgren, K.N., Krafft, G.A., LaDu, M.J., 2003. In Vitro Characterization of Conditions for Amyloid- β Peptide Oligomerization and Fibrillogenesis. *Journal of Biological Chemistry* 278, 11612–11622. <https://doi.org/10.1074/jbc.M210207200>
- Sun, M., Fink, P.J., 2007. A New Class of Reverse Signaling Costimulators Belongs to the TNF Family. *The Journal of Immunology* 179, 4307–4312. <https://doi.org/10.4049/jimmunol.179.7.4307>
- Suzuki, N., Cheung, T.T., Cai, X.-D., Odaka, A., Jr, L.O., Eckman, C., Golde, T.E., Younkin, S.G., 1994. An Increased Percentage of Long Amyloid P3 Protein Secreted by Familial Amyloid IP Protein Precursor (PAPP717) Mutants. *Science* 264, 1336–40. <https://doi.org/10.1126/science.8191290>
- Sweeney, M.D., Sagare, A.P., Zlokovic, B.V., 2018. Blood–brain barrier breakdown in Alzheimer disease and other neurodegenerative disorders. *Nature Reviews Neurology* 14, 133–150. <https://doi.org/10.1038/nrneurol.2017.188>
- Takata, K., Hirata-Fukae, C., Becker, A.G., Chishiro, S., Gray, A.J., Nishitomi, K., Franz, A.H., Sakaguchi, G., Kato, A., Mattson, M.P., LaFerla, F.M., Aisen, P.S., Kitamura, Y., Matsuoka, Y., 2007. Deglycosylated anti-amyloid beta antibodies reduce microglial phagocytosis and cytokine production while retaining the capacity to induce amyloid beta sequestration: Deglycosylated antibody for A β sequestration. *European Journal of Neuroscience* 26, 2458–2468. <https://doi.org/10.1111/j.1460-9568.2007.05852.x>
- Tamboli, I.Y., Barth, E., Christian, L., Siepmann, M., Kumar, S., Singh, S., Tolksdorf, K., Heneka, M.T.,

- Lütjohann, D., Wunderlich, P., Walter, J., 2010. Statins Promote the Degradation of Extracellular Amyloid β -Peptide by Microglia via Stimulation of Exosome-associated Insulin-degrading Enzyme (IDE) Secretion. *Journal of Biological Chemistry* 285, 37405–37414. <https://doi.org/10.1074/jbc.M110.149468>
- Taniguchi, C.M., Emanuelli, B., Kahn, C.R., 2006. Critical nodes in signalling pathways: insights into insulin action. *Nature Reviews Molecular Cell Biology* 7, 85–96. <https://doi.org/10.1038/nrm1837>
- Taylor, R.C., Cullen, S.P., Martin, S.J., 2008. Apoptosis: controlled demolition at the cellular level. *Nature Reviews Molecular Cell Biology* 9, 231–241. <https://doi.org/10.1038/nrm2312>
- Thal, D.R., Griffin, W.S.T., Braak, H., 2008. Parenchymal and vascular A β -deposition and its effects on the degeneration of neurons and cognition in Alzheimer's disease. *Journal of Cellular and Molecular Medicine* 12, 1848–1862. <https://doi.org/10.1111/j.1582-4934.2008.00411.x>
- Tohidpour, A., Morgun, A.V., Boitsova, E.B., Malinovskaya, N.A., Martynova, G.P., Khilazheva, E.D., Kopylevich, N.V., Gertsog, G.E., Salmina, A.B., 2017. Neuroinflammation and Infection: Molecular Mechanisms Associated with Dysfunction of Neurovascular Unit. *Frontiers in Cellular and Infection Microbiology* 7, 276. <https://doi.org/10.3389/fcimb.2017.00276>
- Town, T., Nikolic, V., Tan, J., 2005. The microglial “activation” continuum: from innate to adaptive responses. *Journal of Neuroinflammation* 2, 24. <https://doi.org/10.1186/1742-2094-2-24>
- Travis, M.A., Sheppard, D., 2014. TGF- β Activation and Function in Immunity. *Annual Review of Immunology* 32, 51–82. <https://doi.org/10.1146/annurev-immunol-032713-120257>
- Tundo, G.R., Sbardella, D., Ciaccio, C., Bianculli, A., Orlandi, A., Desimio, M.G., Arcuri, G., Coletta, M., Marini, S., 2013. Insulin-degrading Enzyme (IDE). *Journal of Biological Chemistry* 288, 2281–2289. <https://doi.org/10.1074/jbc.M112.393108>
- Unger, J., McNeill, T.H., Moxley, R.T., White, M., Moss, A., Livingston, J.N., 1989. Distribution of insulin receptor-like immunoreactivity in the rat forebrain. *Neuroscience* 31, 143–157. [https://doi.org/10.1016/0306-4522\(89\)90036-5](https://doi.org/10.1016/0306-4522(89)90036-5)
- Vekrellis, K., Ye, Z., Qiu, W.Q., Walsh, D., Hartley, D., Chesneau, V., Rosner, M.R., Selkoe, D.J., 2000. Neurons Regulate Extracellular Levels of Amyloid β -Protein via Proteolysis by Insulin-Degrading Enzyme. *The Journal of Neuroscience* 20, 1657–1665. <https://doi.org/10.1523/JNEUROSCI.20-05-01657.2000>
- Vepsäläinen, S., Parkinson, M., Helisalmi, S., Mannermaa, A., Soininen, H., Tanzi, R.E., Bertram, L., Hiltunen, M., 2007. Insulin-degrading enzyme is genetically associated with Alzheimer's disease in the Finnish population. *Journal of Medical Genetics* 44, 606–608. <https://doi.org/10.1136/jmg.2006.048470>
- Vezzani, A., Friedman, A., Dingledine, R.J., 2013. The role of inflammation in epileptogenesis. *Neuropharmacology* 69, 16–24. <https://doi.org/10.1016/j.neuropharm.2012.04.004>
- Vilalta, A., Brown, G.C., 2018. Neurophagy, the phagocytosis of live neurons and synapses by glia, contributes to brain development and disease. *The FEBS Journal* 285, 3566–3575. <https://doi.org/10.1111/febs.14323>
- Villa, A., Gelosa, P., Castiglioni, L., Cimino, M., Rizzi, N., Pepe, G., Lolli, F., Marcello, E., Sironi, L., Vegeto, E., Maggi, A., 2018. Sex-Specific Features of Microglia from Adult Mice. *Cell Reports* 23, 3501–3511. <https://doi.org/10.1016/j.celrep.2018.05.048>

- Villa, A., Vegeto, E., Poletti, A., Maggi, A., 2016. Estrogens, Neuroinflammation, and Neurodegeneration. *Endocrine Reviews* 37, 372–402. <https://doi.org/10.1210/er.2016-1007>
- Villa-Pérez, P., Cueto, M., Díaz-Marrero, A.R., Lobatón, C.D., Moreno, A., Perdomo, G., Cózar-Castellano, I., 2017. Leptolide Improves Insulin Resistance in Diet-Induced Obese Mice. *Marine Drugs* 15. <https://doi.org/10.3390/md15090289>
- Villa-Pérez, P., Merino, B., Fernández-Díaz, C.M., Ciudad, P., Lobatón, C.D., Moreno, A., Muturi, H.T., Ghadieh, H.E., Najjar, S.M., Leissring, M.A., Cózar-Castellano, I., Perdomo, G., 2018. Liver-specific ablation of insulin-degrading enzyme causes hepatic insulin resistance and glucose intolerance, without affecting insulin clearance in mice. *Metabolism* 88, 1–11. <https://doi.org/10.1016/j.metabol.2018.08.001>
- Vinters, H.V., 2015. Emerging Concepts in Alzheimer's Disease. *Annual Review of Pathology: Mechanisms of Disease* 10, 291–319. <https://doi.org/10.1146/annurev-pathol-020712-163927>
- Vinters, H.V., Secor, D.L., Pardridge, W.M., Gray, F., 1990. Immunohistochemical study of cerebral amyloid angiopathy. III. Widespread alzheimer A4 peptide in cerebral microvessel walls colocalizes with gamma trace in patients with leukoencephalopathy. *Ann Neurol*. 28, 34–42. <https://doi.org/10.1002/ana.410280108>
- Von Strauss, E., Viitanen, M., De Ronchi, D., Winblad, B., Fratiglioni, L., 1999. Aging and the Occurrence of Dementia: Findings From a Population-Based Cohort With a Large Sample of Nonagenarians. *Archives of Neurology* 56, 587. <https://doi.org/10.1001/archneur.56.5.587>
- Waldron, A.-M., Wintolders, C., Bottelbergs, A., Kelley, J.B., Schmidt, M.E., Stroobants, S., Langlois, X., Staelens, S., 2015. In vivo molecular neuroimaging of glucose utilization and its association with fibrillar amyloid- β load in aged APPS1-21 mice. *Alzheimer's Research & Therapy* 7, 76. <https://doi.org/10.1186/s13195-015-0158-6>
- Walker, F.R., Beynon, S.B., Jones, K.A., Zhao, Z., Kongsui, R., Cairns, M., Nilsson, M., 2014. Dynamic structural remodelling of microglia in health and disease: A review of the models, the signals and the mechanisms. *Brain, Behavior, and Immunity* 37, 1–14. <https://doi.org/10.1016/j.bbi.2013.12.010>
- Walsh, D.M., Selkoe, D.J., 2007. A β Oligomers – a decade of discovery. *Journal of Neurochemistry* 101, 1172–1184. <https://doi.org/10.1111/j.1471-4159.2006.04426.x>
- Wang, D.-S., Dickson, D.W., Malter, J.S., 2006. β -Amyloid Degradation and Alzheimer's Disease. *Journal of Biomedicine and Biotechnology* 2006, 1–12. <https://doi.org/10.1155/JBB/2006/58406>
- Wang, T.-Y., Libardo, M.D.J., Angeles-Boza, A.M., Pellois, J.-P., 2017. Membrane Oxidation in Cell Delivery and Cell Killing Applications. *ACS Chemical Biology* 12, 1170–1182. <https://doi.org/10.1021/acscchembio.7b00237>
- Watson, G.S., Cholerton, B.A., Reger, M.A., Baker, L.D., Plymate, S.R., Asthana, S., Fishel, M.A., Kulstad, J.J., Green, P.S., Cook, D.G., Kahn, S.E., Keeling, M.L., Craft, S., 2005. Preserved Cognition in Patients With Early Alzheimer Disease and Amnesic Mild Cognitive Impairment During Treatment With Rosiglitazone. *The American Journal of Geriatric Psychiatry* 13, 950–958. <https://doi.org/10.1097/00019442-200511000-00005>
- Weinhard, L., di Bartolomei, G., Bolasco, G., Machado, P., Schieber, N.L., Neniskyte, U., Exiga, M., Vadasiute, A., Raggioli, A., Schertel, A., Schwab, Y., Gross, C.T., 2018. Microglia remodel synapses by presynaptic

- trogocytosis and spine head filopodia induction. *Nature Communications* 9, 1228. <https://doi.org/10.1038/s41467-018-03566-5>
- West, P.K., Viengkhou, B., Campbell, I.L., Hofer, M.J., 2019. Microglia responses to interleukin- 6 and type I interferons in neuroinflammatory disease. *Glia* 67, 1821–1841. <https://doi.org/10.1002/glia.23634>
- Wiltshire, S., Hattersley, A.T., Hitman, G.A., Walker, M., Levy, J.C., Sampson, M., O’Rahilly, S., Frayling, T.M., Bell, J.I., Lathrop, G.M., Bennett, A., Dhillon, R., Fletcher, C., Groves, C.J., Jones, E., Prestwich, P., Simecek, N., Rao, P.V.S., Wishart, M., Foxon, R., Howell, S., Smedley, D., Cardon, L.R., Menzel, S., McCarthy, M.I., 2001. A Genomewide Scan for Loci Predisposing to Type 2 Diabetes in a U.K. Population (The Diabetes UK Warren 2 Repository): Analysis of 573 Pedigrees Provides Independent Replication of a Susceptibility Locus on Chromosome 1q. *The American Journal of Human Genetics* 69, 553–569. <https://doi.org/10.1086/323249>
- Witting, A., Möller, T., 2011. Microglia Cell Culture: A Primer for the Novice, in: Costa, L.G., Giordano, G., Guizzetti, M. (Eds.), *In Vitro Neurotoxicology, Methods in Molecular Biology*. Humana Press, Totowa, NJ, pp. 49–66. https://doi.org/10.1007/978-1-61779-170-3_4
- Wolf, S.A., Boddeke, H.W.G.M., Kettenmann, H., 2017. Microglia in Physiology and Disease. *Annual Review of Physiology* 79, 619–643. <https://doi.org/10.1146/annurev-physiol-022516-034406>
- Wolterink-Donselaar, I.G., Meerding, J.M., Fernandes, C., 2009. A method for gender determination in newborn dark pigmented mice. *Lab Animal* 38, 35–38. <https://doi.org/10.1038/labani0109-35>
- Wurtman, R., 2015. Biomarkers in the diagnosis and management of Alzheimer’s disease. *Metabolism* 64, S47–S50. <https://doi.org/10.1016/j.metabol.2014.10.034>
- Xu, W.L., Qiu, C.X., Wahlin, A., Winblad, B., Fratiglioni, L., 2004. Diabetes mellitus and risk of dementia in the Kungsholmen project: A 6-year follow-up study. *Neurology* 63, 1181–1186. <https://doi.org/10.1212/01.WNL.0000140291.86406.D1>
- Xue, J., Schmidt, S.V., Sander, J., Draffehn, A., Krebs, W., Quester, I., De Nardo, D., Gohel, T.D., Emde, M., Schmidleithner, L., Ganesan, H., Nino-Castro, A., Mallmann, M.R., Labzin, L., Theis, H., Kraut, M., Beyer, M., Latz, E., Freeman, T.C., Ulas, T., Schultze, J.L., 2014. Transcriptome-Based Network Analysis Reveals a Spectrum Model of Human Macrophage Activation. *Immunity* 40, 274–288. <https://doi.org/10.1016/j.immuni.2014.01.006>
- Yamamoto, N., Ishikuro, R., Tanida, M., Suzuki, K., Ikeda-Matsuo, Y., Sobue, K., 2018. Insulin-signaling Pathway Regulates the Degradation of Amyloid β -protein via Astrocytes. *Neuroscience* 385, 227–236. <https://doi.org/10.1016/j.neuroscience.2018.06.018>
- Yang, Y., Wu, Y., Zhang, S., Song, W., 2013. High Glucose Promotes A β Production by Inhibiting APP Degradation. *PLoS ONE* 8, e69824. <https://doi.org/10.1371/journal.pone.0069824>
- Yanguas-Casás, N., Crespo-Castrillo, A., de Ceballos, M.L., Chowen, J.A., Azcoitia, I., Arevalo, M.A., Garcia-Segura, L.M., 2018. Sex differences in the phagocytic and migratory activity of microglia and their impairment by palmitic acid. *Glia* 66, 522–537. <https://doi.org/10.1002/glia.23263>
- Yankner, B., Duffy, L., Kirschner, D., 1990. Neurotrophic and neurotoxic effects of amyloid beta protein: reversal by tachykinin neuropeptides. *Science* 250, 279–282. <https://doi.org/10.1126/science.2218531>

- Yankner, B.A., Lu, T., 2009. Amyloid β -Protein Toxicity and the Pathogenesis of Alzheimer Disease. *Journal of Biological Chemistry* 284, 4755–4759. <https://doi.org/10.1074/jbc.R800018200>
- Yokono, K., Imamura, Y., Sakai, H., Baba, S., 1979. Insulin-degrading Activity of Plasma Membranes from Rat Skeletal Muscle: Its Isolation, Characterization, and Biologic Significance. *Diabetes* 28, 810–817. <https://doi.org/10.2337/diab.28.9.810>
- Yokono, K., Roth, R.A., Baba, S., 1982. Identification of Insulin-Degrading Enzyme on the Surface of Cultured Human Lymphocytes, Rat Hepatoma Cells, and Primary Cultures of Rat Hepatocytes. *Endocrinology* 111, 1102–1108. <https://doi.org/10.1210/endo-111-4-1102>
- Zelová, H., Hošek, J., 2013. TNF- α signalling and inflammation: interactions between old acquaintances. *Inflammation Research* 62, 641–651. <https://doi.org/10.1007/s00011-013-0633-0>
- Zhang, J., Xiao, X., Liu, W., Demirci, G., Li, X.C., 2009. Inhibitory Receptors of the Immune System: Functions and Therapeutic Implications. *Cellular & Molecular Immunology* 6, 407–414. <https://doi.org/10.1038/cmi.2009.52>
- Zhao, J., Li, L., Leissring, M.A., 2009. Insulin-degrading enzyme is exported via an unconventional protein secretion pathway. *Molecular Neurodegeneration* 4, 4. <https://doi.org/10.1186/1750-1326-4-4>
- Zhao, L., 2004. Insulin-Degrading Enzyme as a Downstream Target of Insulin Receptor Signaling Cascade: Implications for Alzheimer's Disease Intervention. *Journal of Neuroscience* 24, 11120–11126. <https://doi.org/10.1523/JNEUROSCI.2860-04.2004>
- Zhao, X., Eyo, U.B., Murugan, M., Wu, L.-J., 2018. Microglial interactions with the neurovascular system in physiology and pathology: Microglia-Vascular Communication. *Devel Neurobio* 78, 604–617. <https://doi.org/10.1002/dneu.22576>
- Zhu, S.-H., Liu, B.-Q., Hao, M.-J., Fan, Y.-X., Qian, C., Teng, P., Zhou, X.-W., Hu, L., Liu, W.-T., Yuan, Z.-L., Li, Q.-P., 2017. Paeoniflorin Suppressed High Glucose-Induced Retinal Microglia MMP-9 Expression and Inflammatory Response via Inhibition of TLR4/NF- κ B Pathway Through Upregulation of SOCS3 in Diabetic Retinopathy. *Inflammation* 40, 1475–1486. <https://doi.org/10.1007/s10753-017-0571-z>
- Zuo, X., Jia, J., 2009. Promoter polymorphisms which modulate insulin degrading enzyme expression may increase susceptibility to Alzheimer's disease. *Brain Research* 1249, 1–8. <https://doi.org/10.1016/j.brainres.2008.10.034>

ANNEX

Table A1. Sequences used for global IDE phylogeny. Percentage identity with human IDE.

Abbreviation	Phylum/Clade	Species	Description	% Identity
M16_EurArc	Euryarchaeota	Euryarchaeota archaeon	Peptidase M16	32.2
M16_ChIBac	Chlamydiae	Chlamydiales bacterium 38-26	Peptidase M16	30.9
IDE_ParAca	Chlamydiae	Parachlamydia acanthamoebae	Insulin-degrading enzyme	31.9
PR3_ChIBac	Chlamydiae	Chlamydiae bacterium	Protease 3	30.5
IDEf_LenBac	Lentisphaerae	Lentisphaeria bacterium	Insulinase family protein	33.1
IDEf_PlaBac	Planctomycetes	Planctomycetes bacterium	Insulinase family protein	32.9
M16_RhoBac	Proteobacteria	Rhodobacterales bacterium	Peptidase M16	35.6
IDEf_BurBac	Proteobacteria	Burkholderiales bacterium	Insulinase family protein	31.1
IDEf_Sar324	Proteobacteria	SAR324 cluster bacterium	Insulinase family protein	41.1
M16_DelBac	Proteobacteria	Deltaproteobacteria bacterium	Peptidase M16	35.8
M16_AciBac	Proteobacteria	Acidiferrobacteraceae bacterium	Peptidase M16	34.4
IDEf_AerVer	Proteobacteria	Aeromonas veronii	Insulinase family protein	35.6
IDEf_PseHs1	Proteobacteria	Pseudomonas curvulus sp. HS19	Insulinase family protein	34.8
IDEf_ParF74	Proteobacteria	Parahaliaea sp. F7430	Insulinase family protein	35.7
M16_SpoSp	Proteobacteria	Spongibacter sp.	Peptidase M16	34.1
IDEf_EscCol	Proteobacteria	Escherichia coli	Insulinase family protein	34.9
IDEf_MetSed	Proteobacteria	Methyloprofundus sedimenti	Insulinase family protein	34.2
M16_MetSp	Proteobacteria	Methyloprofundus sp.	Peptidase M16	34.5
IDEf_HahCeb	Proteobacteria	Hahella sp. CCB-MM4	Insulinase family protein	34.5
M16_AmpJap	Proteobacteria	Amphritea japonica	Peptidase M16	34.9
IDEf_Phopro	Proteobacteria	Photobacterium profundum	Insulinase family protein	33.7
IDEf_EreLut	Verrucomicrobia	Ereboglobus luteus	Insulinase family protein	32.2
M16_MacPha	Ascomycota	Macrophomina phaseolina	Peptidase M16	40.3
LuxS_PolCit	Ascomycota	Polychaeton citri CBS 116435	LuxS/MPP-like metallohydrolase	37.7
Ste231_DelStr	Ascomycota	Delphinella strobiligena	Ste23-like protein	38.1
Ste23_ZymBre	Ascomycota	Zymoseptoria brevis	Ste23 like protein	39.1
FLC2_VenNas	Ascomycota	Venturia nashicola	Flavin carrier protein 2	39.5
MEN_PenCam	Ascomycota	Penicillium camemberti	Metalloenzyme	38.4
IDE_BlaDer	Ascomycota	Blastomyces dermatitidis ER-3	Insulysin	36.0
Ste23_LasPus	Ascomycota	Lasallia pustulata	Ste23	39.3
pMUG_GolCic	Ascomycota	Golovinomyces cichoracearum	putative zinc protease mug138	38.0
LuxS_AceMac	Ascomycota	Acephala macrosclerotiorum	LuxS/MPP-like metallohydrolase	36.2
NRD_ArtEnt	Ascomycota	Arthrotrichum entomopaga	Nardilysin	39.5
MEN_TryHyb	Ascomycota	Trichophaea hybrida	Metalloenzyme	40.4
IDE_WicCif	Ascomycota	Wickerhamomyces ciferrii	Insulysin	40.9
MTP_SchCry	Ascomycota	Schizosaccharomyces cryophilus	Metallopeptidase	37.8
ZNP_ColTru	Ascomycota	Colletotrichum truncatum	zinc protease	38.2
IDE_FusCir	Ascomycota	Fusarium circinatum	Insulysin	38.7
Ste23_NeuCra	Ascomycota	Neurospora crassa OR74A	Ste23	40.1
MEN_ProLac	Ascomycota	Protomyces lactucaedebilis	Metalloenzyme	41.7
Ste23_MonRor	Basidiomycota	Moniliophthora roreri	Ste23	36.4
IDE_MycKen	Basidiomycota	Mycena kentingensis	Insulin-degrading enzyme	33.0
LuxS_GauMor	Basidiomycota	Gautieria morchelliformis	LuxS/M16 peptidase-like protein	33.2
IDE_DacPri	Basidiomycota	Dacryopinax primogenitus	insulin-degrading enzyme	36.4
Ste23_MalPac	Basidiomycota	Malassezia pachydermatis	Ste23-metalloprotease	42.4
LuxS_LeuCre	Basidiomycota	Leucosporidium creatinivorum	LuxS/M16 peptidase-like protein	41.2
IDE_RhoMuc	Basidiomycota	Rhodotorula mucilaginosa	Insulinase (Peptidase M16)	39.3
IDE_PucGra	Basidiomycota	Puccinia graminis f. sp. tritici	Insulinase (Peptidase M16)	39.3
IDE_CryDep	Basidiomycota	Cryptococcus depauperatus	Insulysin	36.8
AFA_TriAsa	Basidiomycota	Trichosporon asahii var. asahii	a-factor processing enzyme	35.4
NRD1_MoeAnt	Basidiomycota	Moesziomyces antarcticus T-34	NRD1	42.0
IDE_WalIch	Basidiomycota	Wallemia ichthyophaga	Insulin-degrading enzyme	39.0
IDE_RhiGlo	Chytridiomycota	Rhizoclostridium globosum	Insulin-degrading enzyme	40.0
LuxS_GonPro	Chytridiomycota	Gonapodya prolifera JEL478	LuxS/MPP-like metallohydrolase	38.5
Ste23_NeoCal	Chytridiomycota	Neocallimastix californiae	Metallopeptidase-like protein Ste23	37.0
MTE_GigMar	Mucoromycota	Gigaspora margarita	Metalloenzyme	48.4
Ste23_RhiIrr	Mucoromycota	Rhizophagus irregularis	Ste23p	47.0
MTE_JimFla	Mucoromycota	Jimgerdemannia flammicorona	Metalloenzyme	46.7
IDE_ChoCuc	Mucoromycota	Choanephora cucurbitarum	Insulin-degrading enzyme	48.2
MTE_AbsRep	Mucoromycota	Absidia repens	Metalloenzyme	42.2
Ste23_LicCor	Mucoromycota	Lichtheimia corymbifera	Ste23	44.5
IDE_ApoOss	Mucoromycota	Apophysomyces ossiformis	Insulinase (Peptidase M16)	44.3
UCC_PhyBla	Mucoromycota	Phycomyces blakesleeanae	Ubiquinol-cytochrome c reductase	46.4
IDE1_CryUbi	Apicomplexa	Cryptosporidium ubiquitum	Insulinase-like peptidase	29.3
SDP_EimBov	Apicomplexa	Euryarchaeota archaeon	Peptidase M16	29.6
IDE_EimBru	Apicomplexa	Chlamydiales bacterium 38-26	Peptidase M16	41.7
TLN1_BesBes	Apicomplexa	Parachlamydia acanthamoebae	Insulin-degrading enzyme	30.9
M16_NeoCan	Apicomplexa	Chlamydiae bacterium	Protease 3	30.6
IDE_TetThe	Ciliophora	Lentisphaeria bacterium	Insulinase family protein	39.2
Unn_ParTet	Ciliophora	Planctomycetes bacterium	Insulinase family protein	33.8
LuxS_PsePer	Ciliophora	Rhodobacterales bacterium	Peptidase M16	32.9
IDE_StyLem	Ciliophora	Burkholderiales bacterium	Insulinase family protein	32.6

Prokarya
 Fungi
 Protists
 Metazoa
 Viridiplantae
 Viruses

Table A1. Sequences used for global IDE phylogeny. Percentage identity with human IDE (continued)

Abbreviation	Phylum/Clade	Species	Description	% Identity
IDE_SymMic	Alveolata	SAR324 cluster bacterium	Insulinase family protein	34.6
NRD_SymMic	Alveolata	Symbiodinium microadriaticum	Nardilysin	30.3
Unn_VitBra	Alveolata	Vitrella brassicaformis	Unnamed protein product	32.0
PEP_AcaCas	Discosea	Acanthamoeba castellanii	Peptidase	39.1
IDE_CavFas	Evosea	Cavenderia fasciculata	Insulin-degrading enzyme	31.2
IDE_PlaFun	Evosea	Planoprotostelium fungivorum	Insulin-degrading enzyme	33.7
IDE_StrCul	Euglenozoa	Strigomonas culicis	Insulysin	32.8
SCG5_TryCru	Euglenozoa	Trypanosoma cruzi	Galactosyltransferase 5 (SCG5)	31.7
pUnn_MonBre	Opisthokonta	Monosiga brevicollis MX1	Predicted protein	34.3
M16_FraCyl	Bacillariophyta	Fragilariopsis cylindrus	Peptidase M16	33.1
IDE_FisSol	Bacillariophyta	Fistulifera solaris	Insulysin	33.3
PR3_FisSol	Bacillariophyta	Fistulifera solaris	Protease III	30.4
IDE_HonFer	Bigyra	Hondaea fermentalgiana	Insulin-degrading enzyme	43.8
pIDE_AlbcCan	Oomycota	Albugo laibachii Nc14	insulindegradinglike enzyme putative	35.8
IDE_PhyNic	Oomycota	Phytophthora nicotianae	Insulin-degrading enzyme	34.7
M16_PhyInf	Oomycota	Phytophthora infestans	Peptidase M16 inactive domain	39.7
MMS19_PhyNic	Oomycota	Phytophthora nicotianae	MMS19 nucleotide excision repair	31.1
NRD_PhyPal	Oomycota	Phytophthora palmivora	Nardilysin	32.8
M16A_ThrCla	Oomycota	Thraustotheca clavata	IDE-like enzyme (M16A)	40.5
NRD_ThrCla	Oomycota	Thraustotheca clavata	Nardilysin	31.8
IDE_NanGad	Stramenopiles	Nannochloropsis gaditana	Insulin-degrading enzyme	32.9
NRD_NanGad	Stramenopiles	Nannochloropsis gaditana	N-arginine dibasic convertase	30.6
IDEI_EctSil	Stramenopiles	Ectocarpus siliculosus	Similar to insulin-degrading enzyme	30.5
M16_EmiHux	Haptista	Emiliana huxleyi CCMP1516	Peptidase M16	30.5
IDE_ChrTob	Haptista	Chrysochromulina tobini	Insulin degrading enzyme	42.2
Ste23_ChrTob	Haptista	Chrysochromulina tobini	Ste23p	35.0
IDE_GalSul	Rhodophyta	Galdieria sulphuraria	Insulysin	35.5
IDE_PorPur	Rhodophyta	Porphyridium purpureum	Insulin-degrading enzyme	38.3
IDE_GraCho	Rhodophyta	Gracilariopsis chorda	Insulin-degrading enzyme	36.4
IDEI_DimGyr	Annelida	Dimorphilus gyrocolliatus	DgyrCDS1510 NRD like	32.3
NRD1_DimGyr	Annelida	Dimorphilus gyrocolliatus	DgyrCDS4521 IDE like	55.4
IDE_ArgBru	Arthropoda	Argiope bruennichi	Insulin-degrading enzyme	54.4
IDEI_DapMag	Arthropoda	Daphnia magna	Uncharacterized protein	54.0
IDE_OrcCin	Arthropoda	Orchesella cincta	Insulin-degrading enzyme	45.5
IDE_TigJap	Arthropoda	Tigriopus japonicus	Insulin-degrading enzyme	50.0
IDE_ZooNev	Arthropoda	Zootermopsis nevadensis	Insulin-degrading enzyme	57.7
IDE_TriCas	Arthropoda	Tribolium castaneum	Insulin-degrading enzyme-like	55.5
IDE_DroMel	Arthropoda	Drosophila melanogaster	Insulin-degrading enzyme	46.5
IDEX1_AphCra	Arthropoda	Aphis craccivora	insulin-degrading enzyme isoform X1	44.0
IDE_OocBir	Arthropoda	Ooceraea biro	Insulin-degrading enzyme	50.8
IDE_PapXut	Arthropoda	Papilio xuthus	Insulin-degrading enzyme	53.9
IDEI_TimBar	Arthropoda	Timema bartmani	unnamed protein product	55.9
IDEp_PedHum	Arthropoda	Pediculus humanus corporis	Insulin-degRading enzyme, putative	50.1
NRD1_FraOcc	Arthropoda	Frankliniella occidentalis	Nardilysin-like	31.9
M16_TriLon	Arthropoda	Trinorchestia longiramus	Peptidase M16 N-terminal	50.0
NRD_PenVan	Arthropoda	Penaeus vannamei	Nardilysin	30.8
IDE_ArmVul	Arthropoda	Armadillidium vulgare	Insulin-degrading enzyme	55.1
IDEI_DarSte	Arthropoda	Darwinula stevensoni	unnamed protein product	46.2
NRD1_BugNer	Bryozoa	Bugula neritina	NRD1	33.6
IDE_BugNer	Bryozoa	Bugula neritina	IDE	44.8
IDE_AciRut	Chordata	Acipenser ruthenus	Insulin-degrading enzyme	87.5
IDE_OryMel	Chordata	Oryzias melastigma	Insulin-degrading enzyme	87.5
IDE_DanRer	Chordata	Danio rerio	Insulin-degrading enzyme	89.0
NRDb_DanRer	Chordata	Danio rerio	Nardilysin b	31.3
NRD_NotFur	Chordata	Nothobranchius furzeri	Transcript variant X1	31.2
NRD_SclFor	Chordata	Scleropages formosus	Nardilysin-like	31.8
NRD_ColLuc	Chordata	Collichthys lucidus	Nardilysin	31.1
IDE_ScoMax	Chordata	Scophthalmus maximus	putative insulin-degrading enzyme	89.1
IDE_XenTro	Chordata	Xenopus tropicalis	XENTR_v10018032	91.7
NRD_XenLae	Chordata	Xenopus laevis	XELAEV_18023170mg	33.7
IDE_PhaMam	Chordata	Phallusia mammillata	Insulin-degrading enzyme	54.8
NRD_PhaMam	Chordata	Phallusia mammillata	IDE (NRD-like)	30.1
IDE_AsaScu	Chordata	Asarcornis scutulata	IDE enzyme	94.3
IDE_AegBen	Chordata	Aegotheles bennettii	IDE enzyme	94.6
IDE_PatFas	Chordata	Patagioenas fasciata monilis	insulin-degrading enzyme	92.3
NRD_PatFas	Chordata	Patagioenas fasciata monilis	nardilysin	31.6
IDE_ChIAen	Chordata	Chloroceryle aenea	IDE enzyme	94.7
NRD_LepDis	Chordata	Leptosomus discolor	Nardilysin	32.1
IDE_CeuAer	Chordata	Ceuthmochares aereus	IDE enzyme	94.1
NRD_GalGal	Chordata	Gallus gallus	nardilysin	31.6
IDE_ArdKor	Chordata	Ardeotis kori	IDE enzyme	94.7
IDE_EryMcc	Chordata	Erythrocerus mcallii	IDE enzyme	92.7

Prokarya
 Fungi
 Protists
 Metazoa
 Viridiplantae
 Viruses

Table A1. Sequences used for global IDE phylogeny. Percentage identity with human IDE (continued)

Abbreviation	Phylum/Clade	Species	Description	% Identity
NRD_LonStr	Chordata	Lonchura striata domestica	Nardilysin	32.7
IDE_CrySou	Chordata	Crypturellus soui	IDE enzyme	94.7
hIDE_ChiPun	Chordata	Chiloscyllium punctatum	Hypothetical protein (IDE like)	80.7
hNRD_ChiPun	Chordata	Chiloscyllium punctatum	Hypothetical protein (NRD like)	29.1
IDE_PolSen	Chordata	Polypterus senegalus	IDE enzyme	84.0
NRD_PolSen	Chordata	Polypterus senegalus	NRDC protein	31.6
IDE_VarKom	Chordata	Varanus komodoensis	Insulin-degrading enzyme	90.4
IDE_BosTau	Chordata	Bos taurus	Insulin-degrading enzyme precursor	98.8
NRD_CamDro	Chordata	Camelus dromedarius	Nardilysin	31.5
IDE_CanLup	Chordata	Canis lupus familiaris	Insulin-degrading enzyme isoform 15a	98.7
NRD2_LynPar	Chordata	Lynx pardinus	Nardilysin isoform 2	33.2
IDE_PteAle	Chordata	Pteropus alecto	Insulin-degrading enzyme	98.0
NRD_RhiFer	Chordata	Rhinolophus ferrumequinum	Nardilysin convertase	33.5
IDE1_HomSap	Chordata	Homo sapiens	Insulin-degrading enzyme isoform 1	100.0
NRDb_HomSap	Chordata	Homo sapiens	Nardilysin isoform b precursor	33.7
IDE_MusMus	Chordata	Mus musculus	Insulin-degrading enzyme	95.2
NRD1_MusMus	Chordata	Mus musculus	Nardilysin	33.6
IDE_TupChi	Chordata	Tupaia chinensis	Insulin-degrading enzyme	91.8
IDEa_AllMis	Chordata	Alligator mississippiensis	Insulin-degrading enzyme isoform A	91.8
NRD_AllMis	Chordata	Alligator mississippiensis	Nardilysin	32.5
IDE_PlaMeg	Chordata	Platysternon megacephalum	Insulin-degrading enzyme	92.3
RhoG_PlaMeg	Chordata	Platysternon megacephalum	Rho GTPase-activating protein 24-like	33.3
IDE_ExaDia	Cnidaria	Exaiptasia diaphana	Insulin-degrading enzyme	56.3
IDEp_ApoJap	Echinodermata	Apostichopus japonicus	Putative insulin-degrading enzyme	57.0
IDE_HypDuj	Eutardigrada	Hypsibius dujardini	Insulin-degrading enzyme	45.2
IDE_MytCor	Mollusca	Mytilus coruscus	IDE	57.9
IDE1_OctVul	Mollusca	Octopus vulgaris	Insulin-degrading enzyme-like	53.5
IDE_HalDiv	Mollusca	Haliotis diversicolor	Insulin-degrading enzyme-like	52.2
IDE_ToxCan	Nematoda	Toxocara canis	Insulin-degrading enzyme	41.9
IDE1_AngCos	Nematoda	Angiostrongylus costaricensis	Unnamed protein product	53.2
M16_HaeCon	Nematoda	Haemonchus contortus	Peptidase M16	42.8
IDE_TriPse	Nematoda	Trichinella pseudospiralis	Insulin-degrading enzyme	46.2
IDE_EchGra	Platyhelminthes	Echinococcus granulosus	Insulin degrading enzyme	37.0
M16_OpiViv	Platyhelminthes	Opisthorchis viverrini	Peptidase, M16 family	39.2
IDE_FasHep	Platyhelminthes	Fasciola hepatica	Insulin degrading enzyme	39.7
IDE_BraPli	Rotifera	Brachionus plicatilis	Insulin-degrading enzyme isoform X1	44.6
LuxS_DunSal	Chlorophyta	Dunaliella salina	LuxS/M16 peptidase-like protein	37.8
NRD1_ScePab	Chlorophyta	Scenedesmus sp. PABB004	Nardilysin-like protein	39.9
ZNP_RapSub	Chlorophyta	Raphidocelis subcapitata	Zinc protease	42.7
IDE1_ChlPri	Chlorophyta	Chloropicon primus	Insulinase-like metalloprotease	35.7
IDE_TreA12	Chlorophyta	Trebouxia sp. A1-2	Insulin-degrading enzyme-like	39.0
pIDE_ZosMar	Streptophyta	Zostera marina	Putative Insulin-degrading enzyme	39.6
NRD_CocNuc	Streptophyta	Cocos nucifera	Nardilysin-like	30.9
ZNP_ApoShe	Streptophyta	Apostasia shenzhenica	Zinc-metallopeptidase	40.8
IDEf_ArtAnn	Streptophyta	Artemisia annua	Insulinase (Peptidase family M16)	39.9
IDEf_AraTha	Streptophyta	Arabidopsis thaliana	Insulinase (Peptidase family M16)	38.1
ZNP_TriWil	Streptophyta	Tripterygium wilfordii	Zinc-metallopeptidase peroxisomal-like	38.5
IDE1_CucMel	Streptophyta	Cucumis melo var. makuwa	insulin-degrading enzyme-like 1	39.8
IDE1_ActChi	Streptophyta	Actinidia chinensis var. chinensis	Insulin-degrading enzyme-like 1	40.2
ZNP_GlySoj	Streptophyta	Glycine soja	Zinc-metallopeptidase	40.1
ZNP_MorRub	Streptophyta	Morella rubra	Zinc-metallopeptidase	34.7
Unn_CofCan	Streptophyta	Coffea canephora	Unnamed protein product	39.8
NRD1_DorHyg	Streptophyta	Dorcoceras hygrometricum	Nardilysin-like	33.6
NRD_SalSpl	Streptophyta	Salvia splendens	Nardilysin	34.7
IDE1_OleEur	Streptophyta	Olea europaea subsp. europaea	Insulin-degrading enzyme-like 1	39.9
IDE_StrAsi	Streptophyta	Striga asiatica	Insulin-degrading enzyme	39.4
M16_CinMic	Streptophyta	Cinnamomum micranthum	Peptidase M16	39.9
NRD_PopAlb	Streptophyta	Populus alba	Nardilysin	33.7
IDE_TheCac	Streptophyta	Theobroma cacao	Insulinase (Peptidase family M16)	40.1
M16_CepFol	Streptophyta	Cephalotus follicularis	Peptidase M16	34.7
IDE_AnaCom	Streptophyta	Ananas comosus	Insulin-degrading enzyme	35.7
ZNP_CarLit	Streptophyta	Carex littledalei	Zinc-metallopeptidase	39.8
M16_MacCor	Streptophyta	Macleaya cordata	Peptidase M16	40.4
IDE_ThaTha	Streptophyta	Thalictrum thalictroides	Insulin-degrading enzyme	36.7
PQQ_TreOri	Streptophyta	Trema orientale	Coenzyme PQQ biosynthesis protein	40.1
IDE_MorNot	Streptophyta	Morus notabilis	Insulin-degrading enzyme	35.0
ZNP_PyrUss	Streptophyta	Pyrus ussuriensis	Zinc-metallopeptidase	38.8
IDE1_NicAtt	Streptophyta	Nicotiana attenuata	Insulin-degrading enzyme-like 1	39.3
ZNP_HomVir	Bamfordvirae	Homavirus sp.	Zn-dependent peptidase	31.0
IDE_MimVir	Bamfordvirae	Mimivirus LCMiAC01	Insulinase	31.6
ZNP_IndVir	Bamfordvirae	Indivirus ILV1	Zn-dependent peptidase	30.3
IDE_YasVir	Unclassified	Yasminevirus sp. GU-2018	Insulin-degrading enzyme	30.1

Prokarya
 Fungi
 Protists
 Metazoa
 Viridiplantae
 Viruses

Table A2. Genes upregulated in IDE-KO microglia vs WT microglia.

Gene	Description	Fold change	FDR p-value
Slfn1	Schlafen 1	32.56	2.76E-09
Ccl7	Chemokine (C-C motif) ligand 7	12.95	4.03E-138
Ms4a4c	Membrane-spanning 4-domains, subfamily A, member 4C	11.69	3.89E-19
Ccl5	Chemokine (C-C motif) ligand 5	9.38	5.97E-105
Lcn2	Lipocalin 2	9.28	9.89E-05
Il1b	Interleukin 1 beta	7.77	7.97E-11
Gm6545	Predicted gene 6545	7.53	4.53E-15
Ccl8	Chemokine (C-C motif) ligand 8	6.80	4.65E-34
Iigp1	Interferon inducible GTPase 1	5.82	9.46E-12
H2-Q7	Histocompatibility 2, Q region locus 7	5.50	5.37E-23
Slc13a3	Solute carrier family 13 (sodium-dependent dicarboxylate transporter), member 3	5.39	6.60E-09
Ifi208	Interferon activated gene 208	4.75	2.22E-16
Fgl2	Fibrinogen-like protein 2	4.57	8.38E-17
Oas11	2'-5' oligoadenylate synthetase-like 1	4.09	1.87E-08
BC147527	cDNA sequence BC147527	4.03	1.15E-03
Gm1966	Predicted gene 1966	3.90	1.92E-04
Clec4a1	C-type lectin domain family 4, member a1	3.67	1.63E-40
Fcrls	Fc receptor-like S, scavenger receptor	3.45	4.28E-34
Slco2b1	Solute carrier organic anion transporter family, member 2b1	3.43	7.58E-18
Gbp5	Guanylate binding protein 5	3.34	1.08E-02
Ifi205	Interferon activated gene 205	3.32	6.15E-07
Irf7	Interferon regulatory factor 7	3.30	1.25E-37
Nav3	Neuron navigator 3	3.11	1.15E-03
Ifi209	Interferon activated gene 209	2.96	3.76E-23
Ifi206	Interferon activated gene 206	2.90	5.93E-13
Ifi213	Interferon activated gene 213	2.90	2.41E-09
Slamf7	SLAM family member 7	2.84	4.10E-08
Atf5	Activating transcription factor 5	2.77	1.57E-15
G530011O06Rik	RIKEN cDNA G530011O06 gene	2.74	1.81E-12
Ccr5	Chemokine (C-C motif) receptor 5	2.68	2.78E-20
Mx1	MX dynamin-like GTPase 1	2.67	1.81E-12
Ifi44	Interferon-induced protein 44	2.66	5.21E-05
Ccl12	chemokine (C-C motif) ligand 12	2.66	5.11E-31
Zbp1	Z-DNA binding protein 1	2.57	1.30E-15
Phf11a	PHD finger protein 11A	2.52	4.16E-20
Ifi211	Interferon activated gene 211	2.51	3.44E-07
Phf11b	PHD finger protein 11B	2.45	3.07E-22
Socs3	Suppressor of cytokine signaling 3	2.40	2.11E-04
Phf11d	PHD finger protein 11D	2.39	8.72E-17
Ifi2	Interferon-induced protein with tetratricopeptide repeats 2	2.37	2.53E-10
Ifi3	Interferon-induced protein with tetratricopeptide repeats 3	2.35	1.99E-13
Bcl3	B cell leukemia/lymphoma 3	2.35	1.52E-05
Clec4a3	C-type lectin domain family 4, member a3	2.33	1.75E-09
AW112010	Expressed sequence AW112010	2.32	5.26E-04
Ms4a6b	Membrane-spanning 4-domains, subfamily A, member 6B	2.25	1.65E-17
Tap1	Transporter 1, ATP-binding cassette, sub-family B (MDR/TAP)	2.18	3.62E-04
Egr1	Early growth response 1	2.18	6.09E-09
Zfp36	Zinc finger protein 36	2.16	4.39E-10
Ly6e	Lymphocyte antigen 6 complex, locus E	2.15	7.51E-16
Ifi47	Interferon gamma inducible protein 47	2.15	4.81E-10
Ifi204	Interferon activated gene 204	2.10	1.97E-14
Ptger4	Prostaglandin E receptor 4 (subtype EP4)	2.07	4.07E-07
Isg20	Interferon-stimulated protein	2.07	2.28E-03
Gbp7	Guanylate binding protein 7	2.06	2.99E-04
Nfkbiz	Nuclear factor of kappa light polypeptide gene enhancer in B cells inhibitor, zeta	2.06	7.67E-06
Oas3	2'-5' oligoadenylate synthetase 3	2.06	1.01E-08
Eps8	Epidermal growth factor receptor pathway substrate 8	2.05	3.75E-02
Traf1	TNF receptor-associated factor 1	2.04	8.57E-03
Fcgr1	Fc receptor, IgG, high affinity I	2.03	8.99E-14
Asb2	Ankyrin repeat and SOCS box-containing 2	2.00	6.46E-03
Ms4a6c	Membrane-spanning 4-domains, subfamily A, member 6C	1.99	2.60E-05
Sdc4	Syndecan 4	1.98	6.57E-09
Noval	Neuro-oncological ventral antigen 1	1.98	5.19E-03
Isg15	ISG15 ubiquitin-like modifier	1.97	1.43E-14

Table A2. Genes upregulated in IDE-KO microglia vs WT microglia (continued)

Gene	Description	Fold change	FDR p-value
Igtp	Interferon gamma induced GTPase	1.97	4.01E-06
St3gal6	ST3 beta-galactoside alpha-2,3-sialyltransferase 6	1.95	3.08E-06
BC051226	cDNA sequence BC051226	1.95	5.64E-04
Oasl2	2'-5' oligoadenylate synthetase-like 2	1.94	1.81E-12
Dusp1	Dual specificity phosphatase 1	1.94	4.25E-05
Rsad2	Radical S-adenosyl methionine domain containing 2	1.93	3.31E-09
Pim1	Proviral integration site 1	1.88	3.86E-05
Tmem176a	Transmembrane protein 176A	1.88	6.56E-10
Elavl4	ELAV like RNA binding protein 4	1.87	1.94E-02
Gatm	Glycine amidinotransferase (L-arginine:glycine amidinotransferase)	1.86	1.93E-05
Ifit3b	Interferon-induced protein with tetratricopeptide repeats 3B	1.86	7.55E-03
Tlr1	Toll-like receptor 1	1.85	7.24E-03
Rgl1	Ral guanine nucleotide dissociation stimulator,-like 1	1.84	9.56E-03
Cp	Ceruloplasmin [1.83	1.08E-02
Xaf1	XIAP associated factor 1	1.81	1.45E-06
Gbp2	Guanylate binding protein 2	1.79	1.99E-02
Pml	Promyelocytic leukemia	1.76	4.98E-05
Oas2	2'-5' oligoadenylate synthetase 2	1.75	2.53E-04
Stat2	Signal transducer and activator of transcription 2	1.75	4.10E-08
Ifit1	Interferon-induced protein with tetratricopeptide repeats 1	1.73	1.59E-06
Zfp3611	Zinc finger protein 36, C3H type-like 1	1.73	8.78E-10
Trib3	Tribbles pseudokinase 3	1.73	1.51E-02
Fos	FBJ osteosarcoma oncogene	1.72	7.37E-07
Vmp1	Vacuole membrane protein 1	1.72	4.12E-05
Mthfr	Methylenetetrahydrofolate reductase	1.72	7.23E-06
Ccl2	Chemokine (C-C motif) ligand 2	1.71	1.60E-08
Gm46224	Predicted gene, 46224	1.71	3.94E-02
Dhx58	DEXH (Asp-Glu-X-His) box polypeptide 58	1.70	7.90E-05
Fcgr4	Fc receptor, IgG, low affinity IV	1.70	2.44E-04
Helz2	Helicase with zinc finger 2, transcriptional coactivator	1.69	1.85E-03
H2-K1	Histocompatibility 2, K1, K region	1.68	2.82E-10
Dck	Deoxycytidine kinase	1.68	9.92E-06
Pgap2	Post-GPI attachment to proteins 2	1.68	9.92E-06
Trim30d	Tripartite motif-containing 30D	1.68	4.31E-02
Fcrl1	Fc receptor-like 1	1.68	1.40E-05
Adgre1	Adhesion G protein-coupled receptor E1	1.66	3.84E-10
Slc39a14	Solute carrier family 39 (zinc transporter), member 14	1.66	3.29E-02
Mx2	MX dynamin-like GTPase 2	1.66	1.16E-02
Glrx	Glutaredoxin	1.66	3.94E-02
Sgce	Sarcoglycan, epsilon	1.66	3.31E-08
Ms4a6d	Membrane-spanning 4-domains, subfamily A, member 6D	1.63	1.40E-07
Psmb9	Proteasome (prosome, macropain) subunit, beta type 9	1.63	3.29E-02
H2-T22	Histocompatibility 2, T region locus 22	1.63	1.35E-04
Pou2f2	POU domain, class 2, transcription factor 2	1.62	4.55E-09
Gtpbp2	GTP binding protein 2	1.62	1.63E-04
Epsti1	Epithelial stromal interaction 1 (breast)	1.61	5.15E-06
Cmpk2	Cytidine monophosphate (UMP-CMP) kinase 2, mitochondrial	1.61	1.64E-04
Gm4951	Predicted gene 4951	1.61	2.86E-02
Ctsc	cathepsin C	1.60	6.91E-07
Rtp4	Receptor transporter protein 4	1.60	7.35E-03
Herc6	Hect domain and RLD 6	1.60	4.05E-03
Sfxn5	Sideroflexin 5	1.60	7.64E-09
Klf7	Kruppel-like factor 7 (ubiquitous)	1.59	1.18E-05
Parp11	Poly (ADP-ribose) polymerase family, member 11	1.59	7.50E-03
Ddx60	DEAD (Asp-Glu-Ala-Asp) box polypeptide 60	1.58	8.26E-03
C3	Complement component 3	1.58	1.74E-03
Ifih1	Interferon induced with helicase C domain 1	1.58	1.16E-05
Rnf213	Ring finger protein 213	1.58	2.99E-04
Clec4a2	C-type lectin domain family 4, member a2	1.57	3.80E-02
Aoah	Acyloxyacyl hydrolase	1.57	8.85E-04
Sorl1	Sortilin-related receptor, LDLR class A repeats-containing	1.56	2.66E-02
Sp100	Nuclear antigen Sp100	1.55	8.41E-06
Ly86	Lymphocyte antigen 86	1.55	3.13E-04
Ptafr	Platelet-activating factor receptor	1.55	1.63E-02

Table A2. Genes upregulated in IDE-KO microglia vs WT microglia (continued)

Gene	Description	Fold change	FDR p-value
Tmcc3	Transmembrane and coiled coil domains 3	1.54	4.89E-04
Nfx11	Nuclear transcription factor, X-box binding-like 1	1.54	1.58E-03
Mthfd2	Methylenetetrahydrofolate dehydrogenase (NAD ⁺ dependent)	1.54	1.10E-05
Cmtm6	CKLF-like MARVEL transmembrane domain containing 6	1.54	8.39E-05
BE692007	Expressed sequence BE692007	1.54	3.52E-02
Gm12250	Predicted gene 12250	1.54	4.93E-02
Pde4b	Phosphodiesterase 4B, cAMP specific	1.52	5.98E-03
Usp18	Ubiquitin specific peptidase 18	1.52	1.83E-02
Marcks	Myristoylated alanine rich protein kinase C substrate	1.51	1.62E-06
Stat1	Signal transducer and activator of transcription 1	1.51	3.26E-03
Ube216	Ubiquitin-conjugating enzyme E2L 6	1.51	2.27E-05
Abca1	ATP-binding cassette, sub-family A (ABC1), member 1	1.50	1.68E-03
Nlrp3	NLR family, pyrin domain containing 3	1.50	7.56E-03
Lgals3bp	Lectin, galactoside-binding, soluble, 3 binding protein	1.50	1.40E-05
Unc93b1	Unc-93 homolog B1, TLR signaling regulator	1.49	1.46E-05
Klf2	Kruppel-like factor 2 (lung)	1.49	8.19E-03
ApoE	Apolipoprotein E	1.48	2.74E-02
Chst1	Carbohydrate sulfotransferase 1	1.48	9.72E-07
Ntpr	Nucleoside-triphosphatase, cancer-related	1.47	9.36E-03
Rassf2	Ras association (RalGDS/AF-6) domain family member 2	1.46	3.96E-03
Lst1	Leukocyte specific transcript 1	1.46	1.34E-04
Smim3	Small integral membrane protein 3	1.46	3.50E-02
Uba7	Ubiquitin-like modifier activating enzyme 7	1.45	9.10E-04
Tmem8	Transmembrane protein 8	1.45	1.85E-02
Ap1b1	Adaptor protein complex AP-1, beta 1 subunit	1.45	1.96E-04
Smad3	SMAD family member 3	1.45	3.55E-03
Trafd1	TRAF type zinc finger domain containing 1	1.45	2.26E-04
Gm8995	Predicted gene 8995	1.45	9.87E-04
Plxna4os1	Plexin A4, opposite strand 1	1.45	2.78E-02
Pttg1	Pituitary tumor-transforming gene 1	1.44	1.69E-03
Rnf114	Ring finger protein 114	1.44	3.56E-03
Tspo	Translocator protein	1.43	2.96E-02
Slamf9	SLAM family member 9	1.43	1.28E-04
Limd2	LIM domain containing 2	1.43	3.14E-05
Dtx3l	Deltex 3-like, E3 ubiquitin ligase	1.43	4.73E-03
Cx3cr1	Chemokine (C-X3-C motif) receptor 1	1.43	2.59E-03
Samhd1	SAM domain and HD domain, 1	1.42	3.26E-03
Parp9	Poly (ADP-ribose) polymerase family, member 9	1.42	1.73E-04
Pxn	Paxillin	1.42	1.02E-02
Flt1	FMS-like tyrosine kinase 1	1.42	4.88E-02
Znfx1	Zinc finger, NFX1-type containing 1	1.41	4.82E-04
Fcgrt	Fc receptor, IgG, alpha chain transporter	1.41	2.24E-02
H2-D1	Histocompatibility 2, D region locus 1	1.40	3.09E-04
ApoBec3	Apolipoprotein B mRNA editing enzyme, catalytic polypeptide 3	1.40	7.02E-04
Sbf2	SET binding factor 2	1.40	2.62E-03
Pik3ap1	Phosphoinositide-3-kinase adaptor protein 1	1.40	9.01E-03
Trim30a	Tripartite motif-containing 30A	1.40	2.62E-03
Lgals9	Lectin, galactose binding, soluble 9	1.39	3.80E-03
B2m	Beta-2 microglobulin	1.39	2.33E-02
Rapgef2	Rap guanine nucleotide exchange factor (GEF) 2	1.39	2.51E-04
Cxcl16	Chemokine (C-X-C motif) ligand 16	1.39	6.39E-03
Sf3b4	Splicing factor 3b, subunit 4	1.39	3.12E-02
Adar	Adenosine deaminase, RNA-specific	1.38	4.10E-02
Stard3	START domain containing 3	1.38	6.08E-03
Ifnar2	Interferon (alpha and beta) receptor 2	1.38	1.72E-02
Rassf5	Ras association (RalGDS/AF-6) domain family member 5	1.37	2.20E-02
Skil	SKI-like	1.37	2.95E-02
Chmp4b	Charged multivesicular body protein 4B	1.37	1.15E-04
Il10ra	Interleukin 10 receptor, alpha	1.37	2.95E-02
Slc9a9	Solute carrier family 9 (sodium/hydrogen exchanger), member 9	1.37	1.23E-02
Elk3	ELK3, member of ETS oncogene family	1.36	4.98E-02
Serp1	Stress-associated endoplasmic reticulum protein 1	1.36	4.81E-02
Aftph	Aftiphilin	1.36	8.00E-04
Ddx58	DEAD (Asp-Glu-Ala-Asp) box polypeptide 58	1.36	6.46E-03

Table A2. Genes upregulated in IDE-KO microglia vs WT microglia (continued)

Gene	Description	Fold change	FDR p-value
Gas7	Growth arrest specific 7	1.36	6.51E-03
Bin2	Bridging integrator 2	1.36	1.34E-02
Ccl4	Chemokine (C-C motif) ligand 4	1.36	2.79E-02
Susd6	Sushi domain containing 6	1.36	2.50E-04
Abcg1	ATP binding cassette subfamily G member 1	1.36	7.13E-03
Ifi2712a	Interferon, alpha-inducible protein 27 like 2A	1.35	4.60E-03
Lmo4	LIM domain only 4	1.35	1.22E-02
Adam9	A disintegrin and metallopeptidase domain 9 (meltrin gamma)	1.35	4.25E-02
Ell2	Elongation factor RNA polymerase II 2	1.35	1.51E-02
Parp14	Poly (ADP-ribose) polymerase family, member 14	1.34	4.42E-02
Ms4a7	Membrane-spanning 4-domains, subfamily A, member 7	1.34	6.88E-03
Lbh	Limb-bud and heart	1.34	1.89E-03
Itpkb	Inositol 1,4,5-trisphosphate 3-kinase B	1.34	3.06E-02
Lgmn	Legumain	1.34	1.00E-03
Picalm	Phosphatidylinositol binding clathrin assembly protein	1.34	1.92E-03
Ppp1r18	Protein phosphatase 1, regulatory subunit 18	1.34	3.74E-03
Dpp8	Dipeptidylpeptidase 8	1.34	4.02E-02
Daxx	Fas death domain-associated protein	1.33	2.86E-02
Tmem176b	Transmembrane protein 176B	1.33	6.38E-03
Pld4	Phospholipase D family, member 4	1.33	1.15E-02
Ninj1	Ninjurin 1	1.33	2.86E-02
2410006H16Rik	RIKEN cDNA 2410006H16 gene	1.33	2.27E-02
Ctsh	Cathepsin H	1.33	9.04E-03
Dpysl2	Dihydropyrimidinase-like 2	1.33	1.49E-02
Slc25a45	Solute carrier family 25, member 45	1.33	7.29E-03
Cd47	CD47 antigen (Rh-related antigen, integrin-associated signal transducer)	1.33	1.34E-02
Twf1	Twinfilin actin binding protein 1	1.32	3.06E-02
Evi2a	Ecotropic viral integration site 2a	1.32	9.74E-03
Lpl	Lipoprotein lipase	1.32	2.65E-02
Ogfr	Opioid growth factor receptor	1.32	3.46E-02
N4bp1	NEDD4 binding protein 1	1.32	3.87E-02
Rap2c	RAP2C, member of RAS oncogene family	1.32	4.70E-02
Tmem171	Transmembrane protein 171	1.31	4.91E-02
Fndc3a	Fibronectin type III domain containing 3A	1.31	1.83E-02
Itm2b	Integral membrane protein 2B	1.31	2.76E-02
Arid1a	AT rich interactive domain 1A (SWI-like)	1.31	3.00E-02
Rbpj	Recombination signal binding protein for immunoglobulin kappa J region	1.31	8.65E-03
Actr3	ARP3 actin-related protein 3	1.31	4.20E-02
C1qa	Complement component 1, q subcomponent, alpha polypeptide	1.30	9.74E-03
Ifitm2	Interferon induced transmembrane protein 2	1.30	4.80E-03
Tapbp	TAP binding protein	1.30	7.57E-03
Serinc3	Serine incorporator 3	1.29	5.98E-03
Dazap2	DAZ associated protein 2	1.28	6.28E-03
Tgfb2	Transforming growth factor, beta receptor II	1.28	2.23E-02
Sbno2	Strawberry notch 2	1.28	4.02E-02
Ppp1r9b	Protein phosphatase 1, regulatory subunit 9B	1.28	4.76E-02
Slc31a2	Solute carrier family 31, member 2	1.28	4.98E-02
Ctss	Cathepsin S	1.27	4.54E-02
Riok3	RIO kinase 3	1.27	1.18E-02
Rab5c	RAB5C, member RAS oncogene family	1.26	1.64E-02
Ubb	Ubiquitin B	1.25	1.60E-02
Trim25	Tripartite motif-containing 25	1.25	4.95E-02
Cd14	CD14 antigen	1.24	2.20E-02
Tubb5	Tubulin, beta 5 class I	1.23	4.42E-02
Ubc	Ubiquitin C	1.23	4.73E-02
Ptpn6	Protein tyrosine phosphatase, non-receptor type 6	1.23	2.98E-02
Efhd2	EF hand domain containing 2	1.22	4.68E-02

Table A3. Genes downregulated in IDE-KO microglia vs WT microglia.

Gene	Description	Fold change	FDR p-value
Rps19	Ribosomal protein S19	0.17	9.46E-12
Atp6v1d	ATPase, H ⁺ transporting, lysosomal V1 subunit D	0.18	3.61E-20
Chchd2	Coiled-coil-helix-coiled-coil-helix domain containing 2	0.19	1.79E-18
Gusb	Glucuronidase, beta	0.21	2.71E-04
Cd68	CD68 antigen	0.24	3.71E-08
Atp6v1f	ATPase, H ⁺ transporting, lysosomal V1 subunit F	0.24	5.88E-03
Npm1	Nucleophosmin 1	0.25	1.64E-02
Plin2	Perilipin 2	0.29	3.26E-03
Fuca1	Fucosidase, alpha-L- 1, tissue	0.29	3.92E-27
Zbtb7a	Zinc finger and BTB domain containing 7a	0.32	2.78E-03
Msr1	Macrophage scavenger receptor 1	0.33	4.20E-02
Rnh1	Ribonuclease/angiogenin inhibitor 1	0.35	3.66E-02
1810058I24Rik	RIKEN cDNA 1810058I24 gene	0.35	2.60E-31
Glmp	Glycosylated lysosomal membrane protein	0.36	2.16E-03
Mdm2	Transformed mouse 3T3 cell double minute 2	0.37	1.55E-19
Ldlrap1	Low density lipoprotein receptor adaptor protein 1	0.37	2.38E-07
Ftl1	Ferritin light polypeptide 1	0.38	6.78E-03
Rnf128	Ring finger protein 128	0.38	5.56E-12
Psmc8	Proteasome (prosome, macropain) 26S subunit, non-ATPase, 8	0.38	1.96E-04
Pomp	Proteasome maturation protein	0.38	1.27E-08
Lrrfip1	Leucine rich repeat (in FLII) interacting protein 1	0.39	1.72E-02
Rplp2	Ribosomal protein, large P2	0.39	3.09E-04
Anxa2	Annexin A2	0.39	1.72E-05
Rnase4	Ribonuclease, RNase A family 4	0.40	9.64E-03
Slc25a4	Solute carrier family 25 (mitochondrial carrier, adenine nucleotide translocator), 4	0.41	7.60E-03
Atp6v1b2	ATPase, H ⁺ transporting, lysosomal V1 subunit B2	0.41	1.99E-13
Gpx1	Glutathione peroxidase 1	0.42	1.37E-06
Paics	Phosphoribosylaminoimidazole carboxylase, succinocarboxamide synthetase	0.44	1.87E-11
Frrs1	Ferric-chelate reductase 1	0.44	6.16E-06
Cmas	Cytidine monophospho-N-acetylneuraminic acid synthetase	0.44	3.96E-05
Apb2	Amyloid beta (A4) precursor protein-binding, family B, member 2	0.45	2.05E-09
Eif3a	Eukaryotic translation initiation factor 3, subunit A	0.45	4.42E-16
Tmem14c	Transmembrane protein 14C	0.45	1.30E-03
Vma21	VMA21 vacuolar H ⁺ -ATPase homolog (<i>S. cerevisiae</i>)	0.46	1.30E-05
Srpk2	Serine/arginine-rich protein specific kinase 2	0.47	1.39E-05
Lgals1	Lectin, galactose binding, soluble 1	0.47	4.97E-07
Lima1	LIM domain and actin binding 1	0.47	1.82E-02
Snx8	Sorting nexin 8	0.48	5.36E-03
Gnl3	Guanine nucleotide binding protein-like 3 (nucleolar)	0.48	2.38E-05
Tnip1	TNFAIP3 interacting protein 1	0.49	1.61E-11
Sgta	Small glutamine-rich tetratricopeptide repeat (TPR)-containing, alpha	0.50	8.85E-04
Hspa4	Heat shock protein 4	0.50	9.02E-11
Mt1	Metallothionein 1	0.50	4.54E-13
Msrb1	Methionine sulfoxide reductase B1	0.50	3.57E-03
Tm2d3	TM2 domain containing 3	0.50	1.94E-03
Slc25a24	Solute carrier family 25 (mitochondrial carrier, phosphate carrier), member 24	0.51	3.96E-08
Dusp3	Dual specificity phosphatase 3 (vaccinia virus phosphatase VH1-related)	0.51	3.03E-04
Arhgap25	Rho GTPase activating protein 25	0.51	3.55E-04
Ccnd2	Cyclin D2	0.52	5.18E-03
Sec11c	SEC11 homolog C, signal peptidase complex subunit	0.52	3.59E-06
Pgd	Phosphogluconate dehydrogenase	0.52	2.60E-09
Atad2	ATPase family, AAA domain containing 2	0.53	2.97E-03
Zranb3	Zinc finger, RAN-binding domain containing 3	0.53	7.41E-05
Rgs2	Regulator of G-protein signaling 2	0.54	8.38E-05
Plec	Plectin	0.54	2.17E-04
Cd300ld	CD300 molecule like family member d	0.55	7.04E-07
Rragc	Ras-related GTP binding C	0.55	3.80E-08
Degs1	Delta(4)-desaturase, sphingolipid 1	0.56	3.55E-04
Ucp2	Uncoupling protein 2 (mitochondrial, proton carrier)	0.56	1.85E-05
Pdap1	PDGFA associated protein 1	0.56	6.73E-03
Slc20a1	Solute carrier family 20, member 1	0.57	1.77E-02
Sh3bgrl3	SH3 domain binding glutamic acid-rich protein-like 3	0.57	1.86E-02
Ptgs1	Prostaglandin-endoperoxide synthase 1	0.57	9.36E-03
Rpl23	Ribosomal protein L23	0.58	8.59E-05

Table A3. Genes downregulated in IDE-KO microglia vs WT microglia (continued)

Gene	Description	Fold change	FDR p-value
Tspan14	Tetraspanin 14	0.58	4.10E-08
Smpd13a	Sphingomyelin phosphodiesterase, acid-like 3A	0.58	3.04E-06
Agap1	ArfGAP with GTPase domain, ankyrin repeat and PH domain 1	0.58	9.66E-11
Pdlim5	PDZ and LIM domain 5	0.58	1.22E-03
Syng1	Synaptogyrin 1	0.59	1.70E-03
Rps26	Ribosomal protein S26	0.59	5.10E-09
Spag7	Sperm associated antigen 7	0.60	4.31E-02
Rassf3	Ras association (RalGDS/AF-6) domain family member 3	0.60	1.83E-08
Actn4	Actinin alpha 4	0.60	4.26E-02
Psap	Prosaposin	0.60	4.34E-02
Plaur	Plasminogen activator, urokinase receptor	0.61	5.98E-03
Tecpr1	Tectonin beta-propeller repeat containing 1	0.61	2.83E-04
Clec7a	C-type lectin domain family 7, member a	0.61	6.69E-05
Slc41a2	Solute carrier family 41, member 2	0.62	1.39E-03
Aldh2	Aldehyde dehydrogenase 2, mitochondrial	0.62	1.11E-02
Pgm211	Phosphoglucomutase 2-like 1	0.62	1.60E-06
Plxna2	Plexin A2	0.62	1.16E-05
Dpp7	Dipeptidylpeptidase 7	0.62	2.96E-11
Ttyh2	Tweety family member 2	0.62	4.69E-07
Aplp2	Amyloid beta (A4) precursor-like protein 2	0.63	2.59E-03
mt-Tp	Mitochondrially encoded tRNA proline	0.63	1.03E-02
Colec12	Collectin sub-family member 12	0.63	1.55E-02
Ulk1	Unc-51 like kinase 1	0.64	2.87E-02
Lmna	Lamin A	0.65	2.76E-03
Cyb5r1	Cytochrome b5 reductase 1	0.65	5.76E-03
Inpp1	Inositol polyphosphate phosphatase-like 1	0.65	6.42E-05
Higd1a	HIG1 domain family, member 1A	0.66	1.60E-02
Bhlhe41	Basic helix-loop-helix family, member e41	0.66	1.17E-03
Amdhd2	Amidohydrolase domain containing 2	0.66	3.09E-04
Cd33	CD33 antigen	0.66	1.15E-03
Ttl	Tubulin tyrosine ligase	0.66	1.97E-02
Mfge8	Milk fat globule-EGF factor 8 protein	0.66	1.68E-03
Lyz2	Lysozyme 2	0.67	7.34E-04
Myo10	Myosin X	0.67	2.51E-04
Crip1	Cysteine-rich protein 1 (intestinal)	0.67	1.02E-02
Ifi30	Interferon gamma inducible protein 30	0.67	4.52E-03
Lgals3	Lectin, galactose binding, soluble 3	0.67	4.37E-02
Rap2a	RAS related protein 2a	0.68	3.32E-02
Gm38248	Predicted gene, 38248	0.68	4.72E-04
Fam20c	Family with sequence similarity 20, member C	0.68	2.73E-02
Itga4	Integrin alpha 4	0.69	1.14E-05
Plxna1	Plexin A1	0.69	7.99E-04
Tuba4a	Tubulin, alpha 4A	0.69	2.54E-02
Zfp503	Zinc finger protein 503	0.69	2.26E-04
Piezo1	Piezo-type mechanosensitive ion channel component 1	0.69	7.50E-04
Plau	Plasminogen activator, urokinase	0.69	1.74E-03
Vim	Vimentin	0.70	7.13E-03
Aifm2	Apoptosis-inducing factor, mitochondrion-associated 2	0.70	1.78E-05
Ifi27	Interferon, alpha-inducible protein 27	0.70	8.85E-04
Ptpn7	Protein tyrosine phosphatase, non-receptor type 7	0.70	3.43E-02
Usf2	Upstream transcription factor 2	0.70	4.95E-02
Tox2	TOX high mobility group box family member 2	0.70	1.15E-02
Alcam	Activated leukocyte cell adhesion molecule	0.70	5.87E-03
Kcnab2	Potassium voltage-gated channel, shaker-related subfamily, beta member 2	0.72	1.51E-04
Kcnn4	Potassium intermediate/small conductance calcium-activated channel, N 4	0.72	2.84E-02
Tnfrsf26	Tumor necrosis factor receptor superfamily, member 26	0.72	5.68E-03
Inf2	Inverted formin, FH2 and WH2 domain containing	0.72	3.81E-03
Ephx1	Epoxide hydrolase 1, microsomal	0.72	1.24E-02
Tmem273	Transmembrane protein 273	0.72	5.23E-03
Nav2	Neuron navigator 2	0.73	1.81E-03
Csf2ra	Colony stimulating factor 2 receptor, alpha, low-affinity (granulocyte-macrophage)	0.73	1.05E-03
Lrpprc	Leucine-rich PPR-motif containing	0.73	3.89E-03
Sh3bgrl2	SH3 domain binding glutamic acid-rich protein like 2	0.73	1.53E-02
Stx3	Syntaxin 3	0.73	4.58E-04

Table A3. Genes downregulated in IDE-KO microglia vs WT microglia (continued)

Gene	Description	Fold change	FDR p-value
Pygl	Liver glycogen phosphorylase	0.73	9.36E-03
Bc1	Brain cytoplasmic RNA 1	0.73	2.27E-02
Mmp12	Matrix metalloproteinase 12	0.74	4.76E-04
Iqgap2	IQ motif containing GTPase activating protein 2	0.74	2.36E-02
Cpeb1	Cytoplasmic polyadenylation element binding protein 1	0.74	3.79E-03
Dmpk	Dystrophia myotonica-protein kinase	0.74	1.16E-02
Zfp618	Zinc finger protein 618	0.74	2.99E-02
Pilra	Paired immunoglobulin-like type 2 receptor alpha	0.74	4.37E-02
S100a10	S100 calcium binding protein A10 (calpactin)	0.75	3.71E-02
Lrrc27	Leucine rich repeat containing 27	0.75	2.22E-03
Cdkn2a	Cyclin dependent kinase inhibitor 2A	0.76	4.07E-02
Rraga	Ras-related GTP binding A	0.76	7.13E-03
Tgm2	Transglutaminase 2, C polypeptide	0.76	2.10E-02
St3gal5	ST3 beta-galactoside alpha-2,3-sialyltransferase 5	0.76	4.86E-02
Ralgapa2	Ral GTPase activating protein, alpha subunit 2 (catalytic)	0.76	5.38E-03
Emp1	Epithelial membrane protein 1	0.76	4.86E-02
L1cam	L1 cell adhesion molecule	0.76	3.78E-02
Pdxk	Pyridoxal (pyridoxine, vitamin B6) kinase	0.76	2.01E-03
Pls3	Plastin 3 (T-isoform)	0.76	3.94E-02
Sgsh	N-sulfoglucosamine sulfohydrolase (sulfamidase)	0.77	1.16E-02
Cd28	CD28 antigen	0.77	4.87E-02
Cd9	CD9 antigen	0.77	1.85E-02
Anxa1	Annexin A1	0.77	4.39E-02
Anpep	Alanyl (membrane) aminopeptidase	0.77	1.69E-02
Alox5	Arachidonate 5-lipoxygenase	0.77	3.28E-02
Lrrc17	Leucine rich repeat containing 17	0.77	1.01E-02
Ahnak	AHNAK nucleoprotein (desmoyokin)	0.77	9.36E-03
Il1rn	Interleukin 1 receptor antagonist	0.77	4.37E-03
Slc7a2	Solute carrier family 7 (cationic amino acid transporter, y+ system), member 2	0.77	3.06E-02
Fabp4	Fatty acid binding protein 4, adipocyte	0.77	1.64E-02
Bhlhe40	Basic helix-loop-helix family, member e40	0.78	1.49E-02
Marveld1	MARVEL (membrane-associating) domain containing 1	0.78	3.65E-03
Ldlrad3	Low density lipoprotein receptor class A domain containing 3	0.78	4.10E-02
Emilin2	Elastin microfibril interfacier 2	0.78	7.30E-03
Chchd10	Coiled-coil-helix-coiled-coil-helix domain containing 10	0.78	7.53E-03
Abcb4	ATP-binding cassette, sub-family B (MDR/TAP), member 4	0.78	2.87E-02
Gask1b	Golgi associated kinase 1B	0.79	1.34E-02
Atp8b4	ATPase, class I, type 8B, member 4	0.79	3.07E-02
Hgsnat	Heparan-alpha-glucosaminide N-acetyltransferase	0.79	4.31E-02
Gm14221	Predicted gene 14221	0.79	3.94E-02
Gpnmb	Glycoprotein (transmembrane) nmb	0.79	4.91E-02
Tmem158	Transmembrane protein 158	0.79	2.29E-02
Gcm2	Glial cells missing homolog 2	0.79	9.64E-03
Alox15	Arachidonate 15-lipoxygenase	0.80	2.51E-02
S100a6	S100 calcium binding protein A6 (calcyclin)	0.80	4.98E-02
Dab2ip	Disabled 2 interacting protein	0.80	3.44E-02
Tnfsf8	Tumor necrosis factor (ligand) superfamily, member 8	0.80	1.16E-02
Adgre5	Adhesion G protein-coupled receptor E5	0.80	4.92E-02
S100a4	S100 calcium binding protein A4	0.80	1.16E-02
Timd4	T cell immunoglobulin and mucin domain containing 4	0.80	2.87E-02
Ide*	Insulin degrading enzyme	0.80	1.82E-02
Csta2	Cystatin A family member 2	0.81	3.94E-02
Fcna	Ficolin A	0.81	2.70E-02
Serpinb10	Serine (or cysteine) peptidase inhibitor, clade B (ovalbumin), member 10	0.96	2.26E-02

* Due to the knockout system, IDE-KO microglia have two stop codons in exon 4 of *Ide* gene, but exons 1-3 are still expressed (see **Figure 13**), resulting in damaged mRNA. Although *Ide* mRNA (exons 1-3) is still produced, cell quality control will quickly degrade it due to the presence of the stop codons. Samples were genotyped, and protein was not detectable at all in IDE-KO microglia.

ACKNOWLEDGEMENTS

“El agradecimiento es la memoria del corazón”

Muchas veces había oído que lo importante de llegar a la meta es lo que aprendes por el camino, y ahora que estoy llegando al final parece que empiezo a entender qué significa. Ninguna tesis se escribe en total soledad, ni es fruto de un solo par de manos, ni de una sola mente. Por eso, quiero agradecer a todas las personas que han recorrido junto a mí parte de este camino y me han ayudado a llegar hasta aquí.

En primer lugar, gracias a mis directores de tesis por darme la oportunidad de llevar a cabo este trabajo. Gracias por darme libertad para desarrollar mis propias ideas y por dirigirme sabiamente, cada uno con vuestro estilo, durante toda mi Tesis. Gracias **Lola** por transmitirme tu entusiasmo por la ciencia y tus infinitas ganas de aprender, y por enseñarme a confiar en mí misma. Gracias **Irene** por tu paciencia conmigo y por ofrecerme siempre tu ayuda y tus ánimos. Gracias **Eduardo** por tu guía tranquila, y por enseñarme con tanta humildad y sencillez. Y gracias a los tres por dar lo mejor de vosotros para cuadrar este triángulo irrepetible. Sin vuestra ayuda durante todo este tiempo, este doctorado nunca habría sido posible. Ha sido un honor trabajar con vosotros.

Gracias a **Lola y Diego**, mis “padres científicos”, por acogerme en vuestro laboratorio y permitirme formar parte de la superfamilia Lazarillo. Gracias a los dos por toda la confianza que habéis depositado en mí, por tener siempre un buen consejo que darme, y por enseñarme todo lo que sé. Por ser un ejemplo no sólo científico sino también personal. Gracias **Diego** por ser mi cuarto director, por poner un poco de cordura cuando Lola y yo nos volvíamos maximalistas, y por enseñarme a desdramatizar las situaciones y preocuparme por lo que de verdad importa.

Gracias a todos mis compañeros del Laz C5: a **Raquel**, por enseñarme a dar mis primeros pasos en cultivos; a **Sergio**, por convencerme de que “la estadística puede ser mi amiga”; a **Cándido**, el apuntador de las mejores frases, por tener siempre alguna historia divertida que contar (con cotas de malla incluidas); a **Elisa**, por tu energía contagiosa y por descubrirme los temazos que se han convertido en mi banda sonora estos años; a **Bea**, por tu ejemplo de vocación, estoy segura de que algún día serás doble doctora; a **Cristian**, por tu entusiasmo en todo lo que haces. Gracias a mis niños de TFG, **Marta y Miguel**, por los buenos ratos que pasamos haciendo experimentos con la multicanal y por lo orgullosa que estoy del trabajo que hicieron. A **Teresa**, gracias por acompañarme en la etapa más difícil del camino, el final de la tesis, por entenderme y saber cómo ayudarme en cada momento, por haber compartido conmigo el día a día codo con codo, ya fuera pipeta en mano, en el animalario o con un café. Gracias a la nueva generación del Lazlab por permitirme enseñaros algo de lo que he aprendido y, sobre todo, por enseñarme vosotros a mí. Gracias a **David**, quien más entiende mi fanatismo por BioRender (aunque me critique por no ser moderna y usar un cuaderno de verdad...); a **Luz**, la persona más hiperactiva que he conocido, y la única capaz de quedarse en el lab hasta las tantas hablando de modelos logísticos; a **Cecilia y Alejandro**, por vuestra curiosidad y ganas de aprender; a **Laura**, la raft queen y experta en sacar cajas del nitrógeno líquido; y a **Jorge**, por traer nueva energía al lab y darme tan buenas ideas para la portada. Dicen que cuando te dedicas a la investigación es muy importante trabajar en algo que te guste de verdad, pero yo añadiría que es incluso más importante contar con un buen grupo de trabajo, y gracias a vosotros yo he contado con el mejor.

Gracias a todos los miembros del Diabetes Lab. A **Cristina**, por ejercer de mi doctoranda mayor y enseñarme tantísimas cosas en mis primeros años, fue una suerte poder aprender contigo. A **Virginia** y **Tamara**, gracias por estar siempre dispuestas a echarme una mano. A **Carlos, Bea, Elena, Patri, Alba** y **Germán**, con los que comparto proteína favorita, gracias por compartir vuestras ideas conmigo.

Gracias al IBGM, y sobre todo a la gente de la primera planta. Gracias **Laura** por venir todos los días al lab con tan buen ánimo. Gracias a **Bea**, una de las científicas que más admiro, por nuestras tertulias de pasillo a altas horas, por contarme tu experiencia y animarme a seguir en este camino. Gracias a **Alba** por nuestras charlas en cultivos y por aconsejarme siempre que lo he necesitado; a **Patry**, por llevar tu alegría allá donde vas; a **Karla, Espe, Pili, Marycarmen, Nuria, Aida** y todos los demás, por los ratos que hemos compartido.

Una de las cosas más bonitas de la Ciencia es la oportunidad que te da de conocer y poder interactuar con gente de diversos lugares y ámbitos. Gracias a la Dra. **Mercedes Cueto** por nuestra colaboración y por darme a conocer el campo de los compuestos naturales. Gracias a la Dra. **Conchi Lillo** por la fantástica microscopía electrónica de IDE, que ha acabado siendo fundamental. Gracias a las chicas del Achúcarro, **Noelia, Virginia** y **Eneritz**, por acogerme tan bien en vuestra tierra (sigo esperando vuestra visita a Pucela para tomarnos unos Ylleras). Gracias **Jorge** por ser un mentor desde el inicio de mi tesis. 謝謝 **Tao** for giving me the opportunity to get started in the fascinating world of bioinformatics and for your valuable teaching. Muito obrigado **Antonio** for teaching me all the secrets of RNA-seq analysis and for our conversations about soccer, science and life. Thanks, Dr. **Malcolm Leissring**, for your generosity, for sharing your knowledge about IDE with me, for guiding me during my first steps and helping me to improve the final manuscript of this Thesis.

Gracias a mis amigos de toda la vida por aceptarme como soy y por preocuparse por mí todos estos años. En especial a **Laura** y **Fer**, por estar siempre ahí y sacar un rato para ponernos al día, y a **Ana**, por no descambiarme y estar siempre lista para acompañarme a la llorería.

Gracias a mi familia, a la que va dedicada esta tesis. A mis abuelos, espero que estén orgullosos de mí desde allí arriba. A **Carlos**, por ser un verdadero hermano mayor y estar siempre dispuesto a ayudar. A mis padres, **Carlos y Loli**, porque todo lo que soy hoy se lo debo a ellos: gracias por educarme, por hacerme crecer en todos los sentidos, por enseñarme el valor del esfuerzo y la constancia, por vuestro cariño incondicional y vuestra comprensión, y por tener una cita literaria adecuada para cada ocasión. Gracias a vosotros, lo hemos conseguido (esta vez no es plural mayestático, este logro también es vuestro). Y por último, y no menos importante, gracias a **Kike**, mi ser multicelular preferido, por ser mi apoyo incondicional durante todos estos años, por aguantarme cuando ni yo misma lo hacía y por confiar en mí antes que nadie. Gracias por poder contar contigo siempre, por darme fuerzas en los momentos difíciles y apoyarme en los importantes, por tener más paciencia que un santo y animarme a ir donde haga falta para perseguir mis sueños. Gracias, en definitiva, por ser mi binomio de la vida.

NOTES

